Defining and targeting combination immunotherapies in mouse models of cancer

Dafne Sofía Franz Demané

Supervisors: Prof. Sergio A. Quezada and Prof. Karl Peggs

A dissertation submitted in partial fulfilment of
the requirements for the degree of

DOCTOR OF PHILOSOPHY

of

UNIVERSITY COLLEGE LONDON

Cancer Institute

University College London

March 2019

I, Dafne Sofía Franz Demané, confirm that the work presented in this thesis is my own. Where information has been derived from other sources, I confirm that this has been indicated in the thesis.

Abstract

Checkpoint blockade has achieved long-lasting anti-tumour responses, unfortunately this is limited to a fraction of patients, highlighting the need for more effective therapies.

This thesis focuses on the rational proposal and design of new cancer immunotherapies through: (1) proposing a novel immunomodulatory-target for cancer-immunotherapy, Inducible T-cell co-stimulator (ICOS), and studying its efficacy in murine models of cancer; and (2) the description of the immune tumour-microenvironment (TME) of mouse models of lung cancer, to propose strategies that promote increased immunogenicity and tumour rejection.

In models of melanoma, the absence of ICOS/ICOSL pathway in $ICOS^{-/-}$ mice, impaired the efficacy of anti-CTLA-4 (Cytotoxic T-lymphocyte antigen-4) therapy. Additionally, patients that received ipilimumab (anti-CTLA-4) monoclonal antibody (mAb) had an increase in the frequency of $ICOS^{+}$ T-cells.

We hypothesised that an agonistic non-depleting anti-ICOS mAb will promote the function of activated T-cells in the TME. Here we show that an agonistic anti-ICOS mAb, with either mIgG1 (non-depleting) or mIgG2a (depleting) isotype, does not promote survival, either as a monotherapy or in combination with other antibody therapies. We also showed that both anti-ICOS isotypes eliminated T-cells in the TME and that anti-ICOS mIgG1 T-cell elimination was Fc-engagement independent. These results were replicated using mice expressing human Fcγ receptors (FcγRs) and anti-ICOS mAb with human (h)IgGs, demonstrating that anti-cancer therapy with anti-ICOS mAbs should be carefully evaluated before use in clinical trials.

To design and test new combination therapies, we described the immune-TME of mouse models of lung cancer. Currently, lung cancer has the highest mortality among cancers, with immunotherapy-benefit limited to some patients. Here we described the TME of two mouse models of lung cancer: KPB6.F1 and CMT-167. We did not find significant differences in the TME of the KPB6.F1 model after radiotherapy and chemotherapy. To promote immunogenicity, combination therapy with anti-

CD25 mAb and anti-4-1BB mAb was evaluated in both the KPB6.F1 and CMT-167 models. Anti-4-1BB promoted proliferation, granzyme B production and expression of activation markers on effector $CD4^+$ and $CD8^+$ T-cells. Whilst this combination reduced the tumour-burden of the CMT-167 model, no differences were observed in the KPB6.F1 model, suggesting intrinsic differences between them. Further work describing the differential response of both models to specific therapies could provide important information regarding resistant tumours in patients, together with strategies to overcome those resistances.

The work presented in this thesis describes variations in the immune-TME following different therapies, suggesting that further investigation is crucial for understanding the biology of the mechanism of action of cancer immunotherapies and to improve their efficacy.

Impact statement

An understanding of the role played by inhibitory immune checkpoints in the survival of cancer cells, has allowed the development of novel immunotherapies that can achieve significant and durable clinical responses. However, only a fraction of patients benefits from a long-lasting response by immunological memory, highlighting the need to develop new and more effective therapies.

Currently, three clinical trials are in development, testing three different anti-ICOS mAbs for anti-cancer therapy. Anti-ICOS (clone 37A10) mAb is a cross-reactive mouse and human antibody developed by Jounce Therapeutics. Jounce is currently developing a phase I clinical trial combining JTX-2011, an agonistic anti-ICOS mAb with depleting activity, with nivolumab (anti-PD-1 mAb), pembrolizumab (anti-PD-1 mAb) or ipilimumab (anti-CTLA-4 mAb). The preliminary results of their clinical trial indicated low efficacy of JTX-2011 mAb as monotherapy and in combination with nivolumab.

In this thesis we demonstrated that, in contradiction to Jounce's pre-clinical data, anti-ICOS 37A10 mAb therapy failed in improving survival in mouse models of cancer, regardless the function of the isotype chosen for the therapy. We also demonstrated that anti-ICOS 37A10 mAb therapy promoted the elimination of activated $ICOS^{hi}$ effector T-cells in the tumour, independently of Fc-engagement to Fcγ receptors (FcγR), which has not been described previously for antibodies targeting co-stimulatory molecules of the immunoglobulin superfamily. We corroborated this detrimental effect using the anti-ICOS 37A10 mAb with human IgG isotypes in mice expressing human FcγR. The anti-ICOS 37A10-mediated T-cell elimination described in this project clearly indicates that precautions should be taken in targeting ICOS as an anti-tumour immunotherapy.

We showed a mechanism that explains the ineffective anti-tumour response driven by JTX-2011, suggesting that this trial should be re-evaluated in order to protect patients. This unexpected mechanism of anti-ICOS mAb raises concerns in the way antibodies are tested in pre-clinical models. We hope that for the benefit of cancer patients, these results can provide more tools and considerations in the way

immunotherapeutic antibodies are pre-clinically tested. Further work needs to be done to dissect the underlying mechanism in anti-ICOS 37A10-mediated T-cell elimination.

By using mouse models, we also described and tested potential combination immunotherapies for the treatment of lung cancer. Currently, lung cancer has the highest mortality among cancers. It is responsible of 1.71 million deaths in 2016 alone, with a predicted increase driven by a rise of smoking habits in developing countries. Therefore, more therapies are urgently needed. We proposed and tested anti-41BB mAb combined with anti-CD25 mAb as a rationally designed therapy for lung cancer treatment of patients with a PD-1^{+} $CD8^{+}$ infiltrating T-cells. We think the mouse models generated in this project will help to better understand the mechanisms defining the success (or failure) of different therapies in lung cancer, to rationally develop combination therapies that promote tumour control in cancer patients. The models developed and described in this project will also provide meaningful information about the biology of the interaction between the immune system and malignant cells in lung cancer, which could lead to improvements in currently tested therapies.

Acknowledgements

I would like to thank to all the people that supported me during these four years of PhD. Firstly I would like to thank to my supervisors, Sergio Quezada and Karl Peggs. Sergio, thank you so much for giving me the opportunity to work in your laboratory and introducing me to cancer immunotherapy, a subject that I feel I can contribute in a meaningful way. Thank you for receiving me in your office and discuss with me when I had questions or doubts about my projects.

Karl, thank you so much for your challenging observations that always helped me to have a fresh vision of my results, especially when research paths were no so straightforward, and you gave me scientific reassurance.

Many thanks also to the 404 lab and all the people that I have met during this time: I have learned a lot from all of you and I am very grateful for the shared time.

I would like to thank Marta for teaching me molecular biology in the lab and teaching me how to live-in-London when I was disorientated and alone; you are great. Thank you also to Laurie and Kate for all their comments about my work, and for all the support in the moments of struggle. Thank you Fred for all the training and patience, I could always ask you anything when in doubt. Thanks to Anna for always find the time to discuss results, protocols and science, and also life. Thanks to Isabelle, Mariana, Dimitris and Cristobal for the help gave in a lot of the experiments in this work. Thank you again Mariana, Isabelle, Anna and Emine for all those lunches, coffees, cookies, some dinners and talks that keep me going when the energy and enthusiasm was low, you are all amazing guys.

Thank you to all my friends (overseas) for the support you gave in all these years (and before), I could not be the person I am without you. Especially to Daniela, Amanda, Sarah and Yessia for sharing this PhD-process (we did it!). Benja, Javi, Francisco SM, Camilo, Marcelo, Alan, Ely, Danny, Olga, Eli, Roberto and Mayito, Pancho O, Caro and Camilo, Xime and Alvaro, thanks, you are great.

Thank you to my family, for being there and supporting. Weli Meche, I miss you deeply. Abuelo Sergio and abueli Betty, thanks for being around and remember me. Mom, dad, Ely, Nicole, and Klaus thanks for your help and caring love.

And finally, thanks to David, for being my main support and companion, because your hug is everything I need at the end of the day, because you are always there after a long day, because sharing my time with you just makes sense and at the same time, is the best thing to do. Love you.

Table of Contents

List of figures

List of tables

List of abbreviations

4-1BBL: 4-1BB ligand

Ab: Antibody

ADCC: Antibody-dependent cell-mediated cytotoxicity

ADCP: Antibody-dependent cellular phagocytosis

APC: Antigen presenting cell

ATP: Adenosine triphosphate

CRC: Colorectal cancer

CTL: Cytotoxic T lymphocyte

CTLA-4: Cytotoxic T lymphocyte antigen-4

DAMP: Damage-associated molecular pattern

DC: Dendritic cell

dMMR: Mismatch repair deficient

EAE: Experimental autoimmune encephalomyelitis

EGFR: Epidermal growth factor receptor

Fab: Fragment, antibody binding

Fc: Fragment, crystallizable

FcγR: Fc gamma (γ) receptor

FcγR$^{-/-}$: FcγR *knock-out* mice (other names: *Fcer1g$^{-/-}$* or *Fcer1g^{tm1Rav}* mice). Mice that lack the three activating Fcγ receptors (FcγRI, FcγRIII, FcγRIV)

FcγRIIb$^{-/-}$: FcγRIIb *knock-out* mice (other names: *Fcgr2b$^{-/-}$* or *Fcgr2b^{tm1Ttk}* mice) Mice that lack the inhibitory FcγRIIb.

FGFR: Fibroblast growth factor receptor

GITR: Glucocorticoid-induced tumour necrosis factor receptor [TNFR] family related protein

GITRL: GITR ligand

GM-CSF: Granulocyte-Macrophage Colony stimulating factor

GVHD: Graft-versus-host disease

GzmB: Granzyme B

hFcγR: human Fc gamma (γ) receptor mice (other names: huFcγR or C57BL/6 FcRα$^{-/-}$*Fcgr1*$^{-/-}$*FCGR1*^{tg}*FCGR2A*^{R131tg}*FCGR2B*^{I232tg}*FCGR3A*^{F158tg}*FCGRIIIB*^{tg} mice). Mice that express the human FcγRs (FcγRI, FcγRIIA, FcγRIIB, FcγRIIIA, and FcγRIIIB) without expressing mouse FcγR.

HNSCC: Head and neck squamous cell carcinoma

ICOS: Inducible T-cell Co-stimulator

ICOSL: Inducible T-cell Co-stimulator ligand

IDO: Indoleamine 2,3-dioxygenase

IgG: Immunoglobulin G

IgSF: Immunoglobulin super-family

IFNγ: Interferon γ

IFNGR1: IFNγ receptor 1

IL-1: Interleukin 1

IL-2: Interleukin 2

IL-10: Interleukin 10

IL-17: Interleukin 17

ITAM: Immunereceptor tyrosine-based activating motif

ITIM: Immunereceptor tyrosine-based inhibitory motif

ITSM: Immunereceptor tyrosine-based swtich motif

KO: Knock out

LAG3: Lymphocyte activation gene 3

LN: Lymph node

LPS: Lipopolysaccharide

mAb: Monoclonal antibody

MDSC: Myeloid-derived suppressor cells

MHC-I: Major Histocompatibility complex class I

MHC-II: Major Histocompatibility complex class II

mOS: Median overall survival

MSI-H: Microsatellite instability-high

NK: Natural Killer cell

NKT: Natural Killer T-cell

NOD (mice): Non-obese diabetic (mice)

NSCLC: Non-small cell lung cancer

OVA: Ovalbumin

OS: Overall survival

OX-40L: OX-40 ligand

PBMC: Peripheral blood mononuclear cell

PD-1: Programmed death-1

PD-L1: Programmed death-ligand 1

PD-L2: Programmed death-ligand 2

PFS: Progression free survival

TAM: Tumour-associated macrophages

Tc1: Type 1 T cytotoxic

TCR: T-cell receptor

Teff: Effector T-cell

TGFα: Transforming growth factor-α

TGFβ: Transforming growth factor-β

Th1: Type 1 T helper

Th2: Type 2 T helper

Th17: Type 17 T helper

TIGIT: T cell Immunoglobulin and ITIM (immunoreceptor tyrosine-based inhibitory motif) domain

TIL: Tumour infiltrating lymphocyte

TIM-3: T-cell Immunoglobulin- and mucin-domain-containing 3

TME: Tumour microenvironment

TNFα: Tumour necrosis factor α

TNFR: Tumour necrosis factor receptor

TNFRSF: Tumour necrosis factor receptor superfamily

Treg: Regulatory T-cell

WT: Wild-type

1 Introduction

1.1 Lung cancer

Lung cancer has the highest mortality of all cancers worldwide, responsible for 1.71 million deaths in 2016 alone (Figure 1.1) (Ritchie, 2018). In the United Kingdom (UK), lung cancer is the third most common cancer accounting for 35,620 deaths in 2016, equivalent to 21% of all cancer-related deaths that year. Statistics from Cancer Research UK (CRUK) also indicate that around 46,700 new cases are diagnosed every year (Cancer Research UK, 2018a).

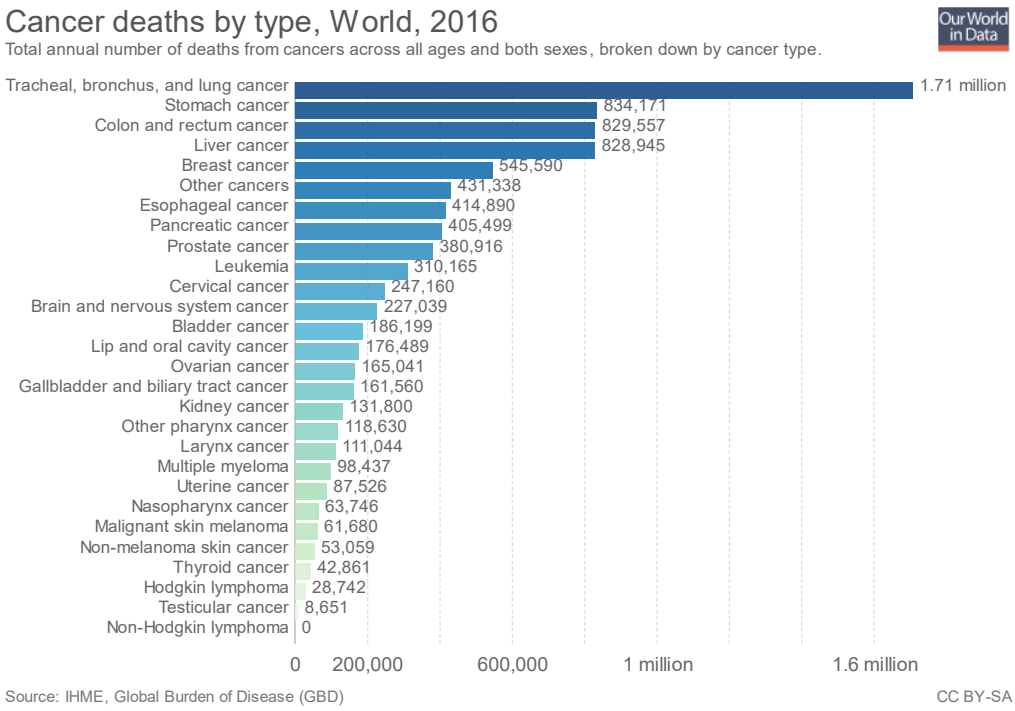

Figure 1.1 Number of cancer-associated deaths worldwide in 2016.

Credit: Hannah Ritchie (2018) - "How many people in the world die from cancer". Published online at OurWorldInData.org. Retrieved from: https://ourworldindata.org/how-many-people-in-the-world-die-from-cancer. Image reproduced with permission of the rights holder, Our World in Data.

Comparable to the UK, reports from the United States (US) estimate that lung cancer accounted for 26% of all cancer-related mortalities in 2017, with 155,870 deaths (Siegel et al., 2017). The same report estimated that lung cancer was also the second most common cancer diagnosed in the US population (Siegel et al., 2017).

Northern America, Europe and Eastern Asia have the highest incidence of lung cancer currently. These trends mainly reflect the peak of tobacco consumption in the last century (Torre et al., 2015). In western countries, including the UK and US, this peak was around the 1950's and has gradually decreased with time. Consequently, a decline in lung cancer rates and mortality has been observed and is expected to continue (Malvezzi et al., 2015; Molina et al., 2008). On the other hand, in countries where tobacco consumption is currently peaking or increasing, like China, Indonesia and some parts of Africa, there is a rise in lung cancer incidence and deaths in their populations. It was estimated that in 2015 in China the cancer with the highest incidence and mortality was lung cancer, with 733,300 new diagnosis and 610,200 deaths (Chen et al., 2016). The high lung cancer rates in these regions continue to drive a global trend of increasing mortality and incidence worldwide, despite an improvement in anti-cancer therapies (Malvezzi et al., 2015; Torre et al., 2015).

Lung cancer continues to carry a high mortality despite improvements in its treatment, which have yet to make substantial clinical difference on a population scale. In the UK, lung cancer 10-year survival has had an slight improvement from 3% to 5% during the last 40 years (Cancer Research UK, 2018a). Currently, 5-year survival rate for lung cancer patients is 10% in the UK, varying between genders with an 8% for men and 10% for women. In Europe, the 5-year survival is 12% for men and 16% for women, whilst in the US the average 5-year survival is 18% (Cancer Research UK, 2018a; Siegel et al., 2017).

Overall, the high incidence and mortality of lung cancer, together with its poor-prognosis and reduced long-term survival make it necessary to develop new and more effective therapies that will finally improve the survival chances of patients.

1.1.1 NSCLC TNM staging

Lung cancer can be separated in two main categories according to its histopathological subtype: small cell lung cancer (SCLC) and non-small cell lung cancer (NSCLC). SCLC accounts for approximately 15% of all lung cancers, whilst the remaining 85% is classified as NSCLC. NSCLC can be further classified as adenocarcinoma (40%), squamous cell carcinoma (30%) and large cell carcinoma (15%) (Bender, 2014; Xia et al., 2017). In general, NSCLC has a better 5-year survival (21%) compared to SCLC (6%) (Bender, 2014), further effected by the disease stage at diagnosis.

The most common staging system used for lung cancer is the tumour, nodules and metastasis (TNM) classification, which has recently been reviewed by the International Association of Study of Lung Cancer (IASLC) in its 8th edition. Its goal is to describe the anatomical extent of a tumour, based on the extent of the primary tumour (T), the involvement of lymph nodes (N) and presence of distal metastases (M) (Detterbeck et al., 2017). NSCLC is therefore divided in stages I through IV, according to its extent of spread measured by T, N and M. The different stages are summarised in tables 1.1 and 1.2.

The standard of care for NSCLC patients varies depending on the histological subtype and stage of the disease. The main treatment for patients with stage I, II and III disease is surgery, which may involve removal of a part of the lung (lobectomy) or the whole lung (pneumonectomy). Patients are also offered adjuvant chemotherapy and/or radiotherapy to reduce the chance of recurrence after surgery. If surgery is not possible, radiotherapy and systemic anti-cancer therapies are the mainstay of treatment. For patients with stage IV disease, with the cancer spread to the other lung or metastasis in other parts of the body, the cancer is currently considered incurable and the treatment focus is in improving longevity but importantly controlling symptoms. For stage IV patients, the standard of care consists of systemic anti-cancer therapies including chemotherapy, immunotherapy or targeted agents depending on the histological and molecular characteristics of the cancer. Furthermore, radiotherapy may play a role in particular circumstances, especially for the control of specific symptoms, in addition to standard best supportive care measures (Cancer Research UK, 2018a; Mozayen et al., 2016; Mountain, 1997).

Table 1.1. Definition of TNM descriptors by the 8th edition cancer stage classification of the IASLC.

Modified from (Detterbeck, 2018). Image reproduced with permission of the rights holder, Elsevier.

T (primary tumor)	
T0	No primary tumor
Tis	Carcinoma in situ (squamous or adenocarcinoma)
T1	Tumor ≤3 cm
T1mi	Minimally invasive adenocarcinoma
T1a	Superficial spreading tumor in central airways*
T1a	Tumor ≤1 cm
T1b	Tumor >1 but ≤2 cm
T1c	Tumor >2 but ≤3 cm
T2	Tumor >3 but ≤5 cm or tumor involving: visceral pleura,† main bronchus (not carina), atelectasis to hilum†
T2a	Tumor >3 but ≤4 cm
T2b	Tumor >4 but ≤5 cm
T3	Tumor >5 but ≤7 cm or invading chest wall, pericardium, phrenic nerve; or separate tumor nodule(s) in the same lobe
T4	Tumor >7 cm or tumor invading: mediastinum, diaphragm, heart, great vessels, recurrent laryngeal nerve, carina, trachea, esophagus, spine; or tumor nodule(s) in a different ipsilateral lobe
N (regional lymph nodes)	
N0	No regional node metastasis
N1	Metastasis in ipsilateral pulmonary or hilar nodes
N2	Metastasis in ipsilateral mediastinal or subcarinal nodes
N3	Metastasis in contralateral mediastinal, hilar, or supraclavicular nodes
M (distant metastasis)	
M0	No distant metastasis
M1a	Malignant pleural or pericardial effusion‡ or pleural or pericardial nodules or separate tumor nodule(s) in a contralateral lobe
M1b	Single extrathoracic metastasis
M1c	Multiple extrathoracic metastases (1 or >1 organ)

*Superficial spreading tumour of any size but confined to the tracheal or bronchial wall. † Atelectasis or obstructive pneumonitis extending to hilum; such tumours are classified as T2a if>3 and ≤4 cm, T2b if>4 and ≤5 cm.

‡Pleural effusions are excluded that are cytologically negative, non-bloody, transudative, and clinically judged not to be due to cancer.

Table 1.2. Lung cancer stage classification by 8th edition.

Modified from (Detterbeck, 2018). Image reproduced with permission of the rights holder, Elsevier.

T/M	Subcategory	N0	N1	N2	N3
T1	T1a	IA1	IIB	IIIA	IIIB
	T1b	IA2	IIB	IIIA	IIIB
	T1c	IA3	IIB	IIIA	IIIB
T2	T2a	IB	IIB	IIIA	IIIB
	T2b	IIA	IIB	IIIA	IIIB
T3	T3	IIB	IIIA	IIIB	IIIC
T4	T4	IIIA	IIIA	IIIB	IIIC
M1	M1a	IVA	IVA	IVA	IVA
	M1b	IVA	IVA	IVA	IVA
	M1c	IVB	IVB	IVB	IVB

In general, the 5-year survival rate decreases the more advanced stage the cancer is. Patients diagnosed with stage IA1, IA2 and IA3 disease have a 5-year survival rate of 92%, 83% and 77% respectively (Table 1.3). On the contrary, for stage IVA NSCLC the 5-year survival rate drops to 10%, reaching less than 1% for patients diagnosed with stage IVB disease (Table 1.3) (Goldstraw et al., 2016).

Table 1.3. Overall 5-year survival rate for the different stages of NSCLC.

Data adapted from (Goldstraw et al., 2016).

Stage	IA1	IA2	IA3	IB	IIA	IIB	IIIA	IIIB	IIIC	IVA	IVB
5-year survival	92%	83%	77%	68%	60%	53%	36%	26%	13%	10%	< 1%

1.1.2 NSCLC current treatment options

As mentioned before, the treatment approach depends entirely on the NSCLC stage. Surgery is the main strategy for patients that can tolerate the surgery and have resectable stage I, II and III tumours. Some patients also undergo adjuvant therapy after surgery, to avoid cancer relapse, usually consisting of chemotherapy or radiotherapy (Zappa and Mousa, 2016; Cancer Research UK, 2018b). Adjuvant chemotherapy has been suggested after surgical resection in patients with high-risk stage IIA, IIB and IIIA disease. In this context, platinum-based chemotherapy treatment provided an improvement of 4.5% in survival in patients with stage I, II and III after resection (Visbal et al., 2005).

Diagnosis of metastatic stage IV NSCLC accounts for 40% of all patients. As surgical resection is not possible, the main purpose of treatment is prolonging survival and improving quality of life through symptom management. Treatment approaches and their outcomes are now dependent upon certain molecular characteristics of the tumour. The approach in the majority of patients is the use of platinum-based chemotherapy (carboplatin or cisplatin) combined with a taxane (paclitaxel or docetaxel), gemcitabine, vinorelbine, irinotecan or pemetrexed. In general, all these regimens provide similar clinical benefit, with a median overall survival (mOS) of 8 to 10 months (Zappa and Mousa, 2016; Spiro et al., 2004; Scagliotti et al., 2008). On the other hand, radiotherapy is the therapy of choice when a localised tumour in the chest cannot be surgically removed. Radiotherapy is also used as a palliative treatment in patients who had no response to surgery or chemotherapy (Zappa and Mousa, 2016).

Immunotherapy is the most recent approach to managing many different malignancies, including NSCLC. It aims to enhance the patient's own anti-tumour immune response, ideally promoting immune memory. Even though checkpoint blockade immunotherapy increases survival and may promote long-lasting response, the therapeutic benefit is limited to a fraction of patients. In the case of NSCLC, patients treated with nivolumab (a monoclonal antibody targeting Programmed cell death protein 1 [anti-PD-1 mAb]) after platinum-based chemotherapy reported 51% 1-year survival, compared with 39% of docetaxel-treated patients (Borghaei et al., 2015). Similar results were obtained in a phase III trial comparing nivolumab and docetaxel in a Chinese population. The median overall survival (mOS) for nivolumab in this study was 12 months, compared to 9.6 months for

docetaxel (Wu et al., 2018). Long-term data of studies evaluating nivolumab in NSCLC are limited, but ≥3 years follow-up of two phase III clinical trials showed that the nivolumab-group had a higher 3-year mOS than docetaxel group, with 17% and 8% respectively (NCT01642004, NCT01673867) (Vokes et al., 2018).

Clinical trials conducted in advanced melanoma, a tumour considered to have high immunogenicity, have shown increased response rates with combination checkpoint blockade. In this study, combination checkpoint blockade correlated with a 10% increase in 2-year OS when compared with nivolumab alone (Hodi et al., 2016). As such, a phase III trial evaluated the efficacy of combination therapy nivolumab plus ipilimumab (an anti-CTLA-4 mAb) compared to chemotherapy in NSCLC patients with high mutational burden. The 1-year progression free survival was 42.6% for nivolumab plus ipilimumab versus 13.2% for standard of care chemotherapy, showing a clear benefit for the combined immunotherapy used as first-line therapy (Hellmann et al., 2018). Importantly, all these treatments have been approved by the US Food and Drug Administration (FDA) for the treatment of advanced NSCLC.

Currently, research is aiming to develop new therapies to improve tumour regression and long-term responses in patients with NSCLC and other malignancies that do not respond to checkpoint blockade. This will be discussed further in this thesis.

1.2 Immune function in the context of cancer

1.2.1 Cancer immunology at a glance

The main function of the immune system is to distinguish self-antigens from danger signals. Tolerance is promoted after recognition of self-antigens, whilst danger signals such as pathogens and malignant cells initiate an immune response.

An effective immune response that promotes tumour rejection involves the interaction of different immune cells and the coordinated orchestration of their function. In general, the immune response is divided into innate and adaptive immunity. Cells from the innate immune response, such as natural killer cells and γδ T-cells are capable of recognising and directly killing tumour cells. B-cells, $CD4^+$ and $CD8^+$ T-cells form the adaptive immune

response, capable of recognising specific tumour antigens, infiltrating the tumour and promoting tumour elimination. B-cells and T-cells can also promote a long-lasting response through tumour-antigen recognition memory.

$CD4^+$ and $CD8^+$ T-cells have the capacity to scan their specific antigen presented by antigen presenting cells (APCs) in a major histocompatibility complex (MHC) class II or class I molecule, respectively. According to the two-signal model, T-cell activation requires both: (a) signal one, consisting of the recognition of the antigen/MHC complex by the T-cell receptor (TCR), which provides the specificity to the response; and (b) signal two, given normally by co-stimulatory molecules from B7/CD28 family like CD80/CD86, normally expressed on APCs and able to engage and deliver positive signals to T-cells upon binding to the co-stimulatory receptor CD28 (Bretscher, 1999). This antigen-driven activation promotes proliferation, differentiation and survival of T-cells.

Once fully activated, T-cells can migrate to the periphery and preferentially to inflamed tissue. In the context of cancer, after recognition of tumour antigens presented upon MHC-I molecules on the surface of tumour cells by $CD8^+$ T-cells, these cells target the malignant cell for elimination through the secretion of granzyme B (GzmB) and perforin. The elimination of the target cell by the killer cell in the immune synapse is triggered by the release of cytotoxic granules containing GzmB and perforin. Perforin, a pore-forming protein, allows GzmB to enter the target cell, cleave and activate caspases and caspase substrates, inducing apoptosis (Barry and Bleackley, 2002).

Activated $CD4^+$ T-cells can also promote tumour elimination and help B-cells to produce anti-tumour antibodies. T-helper 1 (Th1) $CD4^+$ T-cells orchestrate the antitumor response through the secretion of cytokines such as interleukin 2 (IL-2) and interferon-γ (IFNγ), a pro-inflammatory cytokine.

Natural killer (NK) cells, which are part of the innate compartment, are lymphocytes that also have cytotoxic activity. NK cells can promote tumour elimination by secretion of GzmB and perforin like $CD8^+$ T-cells, without antigen recognition. On the contrary, NK cell functions are regulated by a balance between activating and inhibitory signals delivered by receptors on the surface of cells. Malignant cells can be spontaneously killed by NK cells by either the loss of self-identifying molecules (as MHC-I) that triggers inhibitory signals in NK

cells or the upregulation of ligands that trigger activating signals, which overcome inhibitory signals and switch the balance towards cytotoxicity (Morvan and Lanier, 2016).

Despite the existence of these immune mechanisms in preventing tumour growth, tumours can "escape" being eliminated by immune cells by using some of the regulatory mechanisms of the immune system itself. These immune-regulatory mechanisms are important in a healthy person to control an excessive inflammatory response and auto-immunity. Tumours may also utilise these pathways to evade detection by the immune system and subsequent destruction. The immune escape-mechanisms used by cancer cells include:

1. Low immunogenicity due to downregulation of MHC-I, loss of β2-microglobulin (part of the MHC-I), upregulation of inhibitory ligands (i.e. PD-L1, discussed further) in response to IFNγ, increased IFNγ insensitivity by expression of loss-of-function mutations in IFNGR1 (IFNγ receptor 1) and lack of antigens recognised by T-cells. A caveat of MHC-I downregulation may be susceptibility to NK cells, but this is normally overcome by the tumour cells downregulating just one allele.
2. Tumour antigens are seen by T-cells as self-antigen when presented by APCs without co-stimulation (signal two), which results in the induction of tolerance.
3. Antigen loss, by the survival of tumour cells that do not express antigen recognised by T-cells and driven by genomic instability of the tumour.
4. Tumour-induced privileged site, by secretion of molecules such as collagen that creates a physical barrier around the tumour preventing immune cell infiltration.
5. Tumour-induced immune suppression. The tumour can produce soluble factors such as interleukin 10 (IL-10), transforming growth factor-β (TGF-β) and indoleamine 2,3-dioxygenase (IDO) that directly suppress immune response, or it can upregulate the expression of PD-L1 having a deleterious effect on activated T-cells, as explained further. Also, the tumour can recruit regulatory T-cells. $CD4^+FoxP3^+$ regulatory T-cells (Treg) are a subset of $CD3^+CD4^+$ cells with immune-modulatory function, able to inhibit the function

of cytotoxic $CD8^+$ T-cells and $CD4^+$ effector T-cells (Teff) by secretion of immunosuppressive cytokines or by direct contact with other T-cells.

6. Tumour-induced immune privilege. Tumour cells and blood endothelial cells within the tumour can upregulate the expression of CD95L (FasL) inducing apoptosis of cytotoxic T-cells expressing CD95 (Fas). Interestingly, Treg cells are refractory to CD95L-mediated apoptosis, promoting immune-tolerance to the tumour. (Bernal et al., 2012; Murphy and Weaver, 2017; Alspach et al., 2018; Turley et al., 2015).

Other cells capable of strongly suppressing T-cell function recruited within the tumour are myeloid-derived suppressor cells (MDSC). MDSCs are a heterogeneous population of immature myeloid cells accumulated during tumour progression (Umansky et al., 2016). MDSCs are able to inhibit the antitumor response through induction of apoptosis of T-cells and NK cells, impairing T-cell proliferation, antigen-recognition, migration, and production of immune suppressive cytokines like IL-10 and TGFβ (Umansky et al., 2016). Moreover, MDSCs have been described to promote tumour angiogenesis and metastasis (Gabrilovich and Nagaraj, 2009).

In general, several immune cell types can infiltrate the tumour, skewing the immune response towards immunosuppression and promotion of tumour growth. Conversely, tumour rejection may be promoted by enhancing the cytotoxic function of T-cells and NK cells through immunotherapeutic strategies, thereby shifting the balance towards an effective anti-tumour immune response. A summary of the interactions between the tumour and the immune system is shown in Figure 1.2.

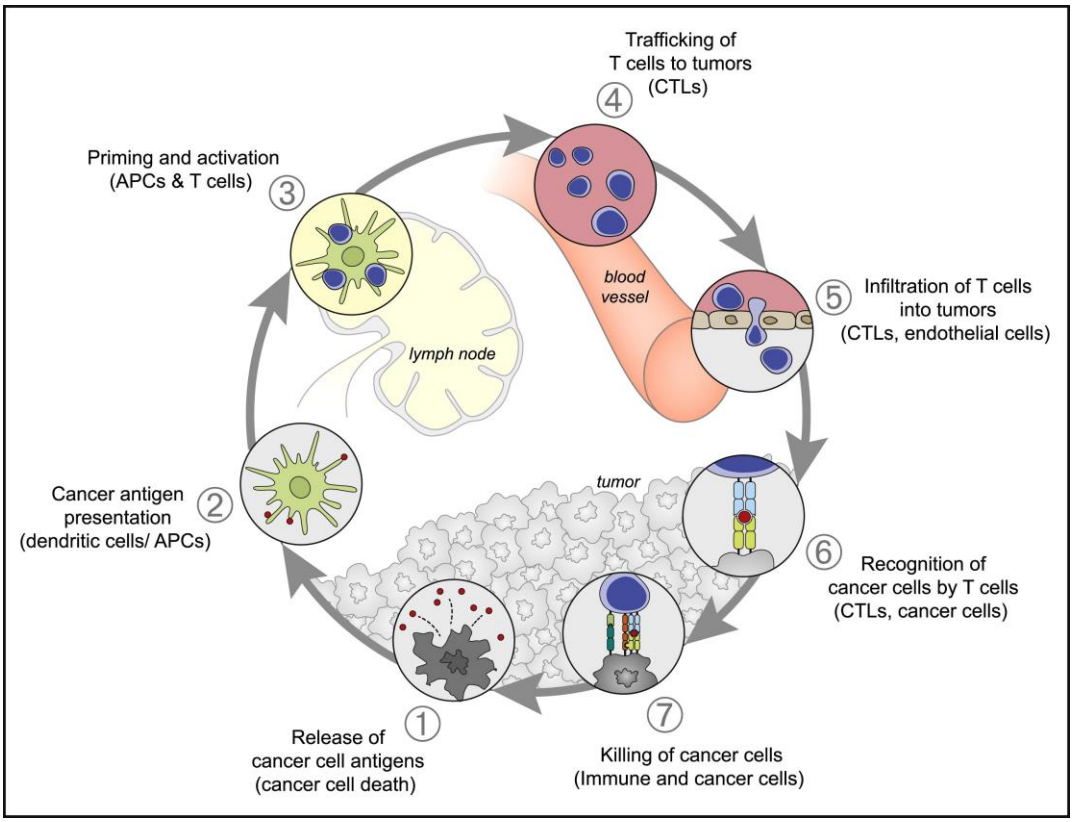

Figure 1.2. The cancer-immunity cycle.

The crosstalk between the immune system and tumour cells is a cyclic process, starting with the recognition of the tumour by immune cells and the subsequent development of inhibitory mechanism by the tumour (Chen and Mellman, 2013). Image reproduced with permission of the rights holder, Elsevier.

1.2.2 Cancer immunoediting

Cancer immunoediting is the process by which the immune system senses and eliminates malignant cells to avoid the development of cancer. However, this process can result in the survival and thus selection of less immunogenic cancer cell variants that may finally develop into a tumour. In other words, it is a balanced process where most malignant cells are continuously eliminated by the immune system, however, unwillingly promote the survival of less immunogenic cancer cells that may avoid the immune response and proliferate (Dunn et al., 2002). Therefore, immunoediting is in itself a mechanism of resistance that is required by malignant tumours to avoid immune detection and promote survival.

Cancer immunosurveillance, defined as the ability of the immune system to recognise and eliminate tumours, is a part of cancer immunoediting. The first unequivocal experimental suggestions of the ability of the immune system to detect and eliminate cancer cells were shown using mouse models. Using tumour-transplantation models of fibrosarcoma and antibodies against IFNγ, it was shown that tumours grow faster in mice treated with anti-IFNγ antibody compared with untreated mice, showing an important role of endogenously produced IFNγ in immune competent mice. Furthermore, when the authors generated an IFNγ-insensitive fibrosarcoma cell line, tumours grew despite the administration of lipopolysaccharide (LPS) injection to reject the tumour as observed in control mice (Dighe et al., 1994; Dunn et al., 2002). The second strong evidence of immunosurveillance in cancer was given by perforin$^{-/-}$ (PKO) mice. Perforin is part of the cytolytic granules in CD8^{+} T-cells and NK cells responsible for perforating the plasma membrane of target cells, which allows the passive diffusion of pro-apoptotic proteases that promote cell death. Wild-type (WT) and PKO mice were injected with different syngeneic tumour cell lines at different concentrations. PKO-mice struggled to control tumour development when injected between 10- to 100-fold less cells than WT mice (van den Broek et al., 1996; Dunn et al., 2002). Similarly, when mice were injected with the chemical carcinogen methylcholanthrene (MCA), the MCA-induced tumours grew rapidly and with a higher incidence in PKO-mice than in *wild-type* mice (van den Broek et al., 1996; Dunn et al., 2002). These results were replicated by other groups, initiating a large amount of research supporting immunosurveillance of cancer in mouse models.

Data from long-term large cohort studies have also provided evidence of cancer immunosurveillance in humans. The knowledge that transplant patients have a higher rate of cancer-incidence than the general population is widely reported and accepted (Penn and Starzl, 1972). As transplant recipients normally receive immunosuppressive medication to reduce the risk of transplant rejection, they become more susceptible to cancers of viral origin (Trofe et al., 2004). Additionally, the frequency of non-viral-derived malignancies is also higher in transplant patients when age-matched to the general population (Ross Sheil, 1986; Dunn et al., 2002). Furthermore, human immunodeficiency virus (HIV)-positive patients exhibit increased risk of viral-derived cancers, driven predominantly by Epstein-Barr virus (lymphoma), human herpes virus 8 (Kaposi's sarcoma) and human papillomavirus (HPV; cervical cancer, rectal cancer and mouth cancer) (Boshoff and Weiss, 2002).

However, the existence of immunosurveillance in non-viral malignancies remained to be confirmed. In fact, higher relative risk ratios have been observed in transplant recipients for tumours without a known viral aetiology (Dunn et al., 2002). For example, assessment of renal transplant patients showed increased standardized cancer-incidence ratios of colon, lung, bladder, larynx, prostate, testis, kidney, non-Hodgkin lymphoma, cervix, ureter and endocrine cancers when compared to the general population (Birkeland et al., 1995; Dunn et al., 2003). Following cardiac transplantation, higher rates of both lung cancer and melanoma was also found (Pham et al., 1995). Other studies showed similar tendencies with *de novo* melanoma and other non-skin malignancies, the incidence ratio increasing 2- to 4-fold in transplant patients when compared to the general population (Ross Sheil, 1986; Penn, 1996). Therefore, immunocompromised patients had a higher probability to develop both viral and non-viral tumours. Moreover, another observation confirming immunosurveillance in human is the correlation between tumour-infiltrating lymphocytes (TILs) and prolonged survival of patients. This correlation has been observed in a variety of malignancies including melanoma, colorectal, oesophageal, gastric and ovarian cancers, indicating the importance of the immune system in controlling and rejecting cancers (Clark Wallace H. et al., 1989; Naito et al., 1998; Schumacher et al., 2001; Ishigami et al., 2000; Mihm et al., 1996; Zhang et al., 2003).

Cancer immunoediting is consequently a process that involves cancer immunosurveillance, but also considers the crosstalk between the initially transformed cells and the immune tumour microenvironment that permits the development of neoplasia. The

steps of immunoediting have been described as the “three Es”: **e**limination, **e**quilibrium and **e**scape (Dunn et al., 2002).

- **Elimination -** depends on cancer immunosurveillance. The majority of premalignant cells are recognised and eradicated before they are able to continue to the next steps of the immunoediting process. The process starts with the invasive growth of the tumour that leads to inflammation signals that recruit IFNγ-producing innate immune cells, such as NK cells, macrophages and dendritic cells (DCs) amongst others. IFNγ induces local tumour cell death, promoting chemokine production and the restriction of blood supply to the tumour, promoting additional cell death. DCs, classic antigen-presenting cells (APCs), digest tumour-debris and migrate to the draining lymph node (LN) to activate $CD4^+$ T-cells. At this point, the increased inflammation recruits more NK cells and macrophages that transactivate each other by production of IFNγ and interleukin 12 (IL-12), resulting in further cell death. The last phase of elimination is the arrival of $CD4^+$ Th1 and $CD8^+$ T-cells to the tumour site, to eradicate any remaining tumour cells.
- **Equilibrium -** is a dynamic balance between the immune cells and any remaining cancer cell population that survived the elimination stage. It is a process of Darwinian selection promoted by the pressure of lymphocytes that eliminates most variants of cancer cells, controlling cancer growth. However, a high mutational burden and genomic instability of the tumour cells can promote the generation of new variants and clones that are essentially sculpted by the immune system to acquire and display immune-resistance. In brief, it is a period of cancer dormancy and selection of low immunogenic variants.
- **Escape -** those tumour cells that survive the equilibrium phase and acquire the ability to avoid detection or elimination by the immune system, start to rapidly divide and expand generating a clinically detectable tumour. The tumour develops extrinsic mechanisms to avoid the immune response like production of immunosuppressive cytokines (e.g. IL-10 and TGF-β) and the recruitment of regulatory T-cells. Tumour-intrinsic mechanism to avoid elimination are related to downregulation of cancer antigens, MHC-I, development of IFNγ-insensitivity, expression of anti-apoptotic signals or disruptions in death-receptor signalling, among other strategies. These

mechanisms finally allow the cancer cells to overcome the immune system and proliferate unchecked (Dunn et al., 2002, 2003; Schreiber et al., 2011).

To summarise, cancer immunoediting explains both the success and failure of the immune system during its interaction with a developing tumour. As long as the cancer cell population is controlled but not eliminated in the equilibrium phase, the sculpting of transformed cells by the pressure imposed by the immune system allows the selection of those features that finally allow the tumour to escape immune detection and expand. Cancer has many strategies to avoid immune-detection, but as advances are made in the basic understanding of tumour/immune-system interactions, the development of novel and potent strategies that overcome tumour-escape will become a reality.

1.2.3 Modifications to the tumour microenvironment

The crosstalk between malignant, immune and non-malignant cells defines the tumour microenvironment (TME) – the cellular environment associated with the tumour (Hui and Chen, 2015). In this thesis, a focus on the immune cells of the TME will drive most of the discussion. The immune TME is defined by a variety of adaptive and innate immune cells that suppress tumour elimination, as described above. The other components of the TME that can also affect the immune-TME include stromal cells, fibroblasts, the extracellular matrix and the vasculature (Hui and Chen, 2015).

An immunosuppressive TME is a key factor for tumour progression and one of the main obstacles that immunotherapy must overcome to promote increased immunogenicity and cancer cell destruction. Immunosuppression is associated with cytokines, chemokines and growth factors produced by malignant and stroma cells in the context of chronic inflammation associated with cancer (Hui and Chen, 2015). Also, the abnormal vasculature in the TME is incapable of meeting the increasing requirements of a growing tumour, leading to hypoxia and acidity (Hui and Chen, 2015). Hypoxia, besides directly promoting tumour growth, recruits and re-educates immune cells towards immunosuppression and inhibits killing functions (Noman et al., 2015).

To overcome the immunosuppressive milieu and promote an effective anti-tumour immune response, one strategy is to target the TME to revert their immunosuppressive

activity. Standard treatments including chemotherapy and radiotherapy, historically described as selective cancer-killing therapies, have been studied in the last decade for their effect on the tumour-infiltrating immune cells and their function.

Radiotherapy is used in up to 50% of patients of all cancers during the course of their treatment, targeting the tumour cells and promoting their elimination (Harrington et al., 2011). However, due to the unspecific nature of irradiation, radiotherapy also affects the TME. Radiation induces endothelial cell dysfunction and apoptosis, promoting inflammation (Paris et al., 2001). Irradiation also damages the vasculature, potentiating hypoxia which increases the production of cytokines and chemokines that can then trigger an effective immune response (Barker et al., 2015). Radiation can also increase the relative number of immune suppressive cells by killing more radiosensitive cells, such as lymphocytes (Barker et al., 2015). However, this increased relative number of suppressive cells can be counterbalanced by the radiotherapy-triggered recruitment of circulating immune cells and increased antigen exposure and presentation, promoting an effective immune response (Barker et al., 2015). Therefore, the effect of radiotherapy on infiltrating immune cell populations should be evaluated case-by-case. Moreover, pro-inflammatory cytokines such as IL-1 and tumour necrosis factor-α (TNF-α) can also recruit more innate immune cells, that in turn can recognise damage-associated molecular patterns (DAMPs) generated by cell stress and death. DAMPs can be divided into (1) molecules exposed on the cell surface like calreticulin, (2) passively released molecules such as high-mobility-group box 1 (HMGB1) and (3) actively released molecules such as ATP (adenosine triphosphate). After irradiation, the DAMP-response may promote immunogenic cell death, potentiating an immune response by inducing the activation and maturation of DCs (Apetoh et al., 2007). Consequently, the overall impact of irradiation on the anti-tumour immune response is difficult to predict.

Chemotherapy, another conventional anti-tumour treatment, can kill tumour cells or stop their growth. Nevertheless, it also has effects on the immune function of the TME. In general, chemotherapy can stimulate the immune function by (1) eliciting cellular rearrangements that make dying cancer cells visible to the immune system (for example, release of calreticulin, ATP and HMGB1) and by (2) transient lymphodepletion, overturning immunosuppression and providing direct or indirect stimulation to immune effector cells (Bracci et al., 2014). In this context, chemotherapy can also promote immune-mediated

cancer cell death. For example, gemcitabine eliminated MDSC in a mouse model of colon cancer, promoting the activity of immunomodulatory antibodies on T-cells for efficient tumour elimination (Ko et al., 2007). Cyclophosphamide, another chemotherapeutic agent, induces the secretion of stress cytokines by cancer cells, promoting the infiltration and phagocytic activity of macrophages in a humanised mouse model of leukaemia (Pallasch et al., 2014). Additionally, cyclophosphamide in combination with oxaliplatin has been shown to increase sensitivity of $CD8^+$ T-cells to checkpoint blockade (Pfirschke et al., 2016). Moreover, it has been described that an increase in the number of $CD8^+$ T-cells relative to Treg cells after chemotherapy predicts a good therapeutic response in breast and colorectal cancer (Kroemer et al., 2013).

On the other hand, chemotherapy, similarly to radiotherapy, can upregulate the production of chemokines, cytokines and growth factors that recruit immunosuppressive cells and inhibit DC activation and $CD8^+$ T-cell function (Wu and Dai, 2017). Additionally, chemotherapy can stimulate the production of tumour-derived factors that promote the expansion of MDSCs, also contributing to immunosuppression (Wu and Dai, 2017). Therefore, as with radiotherapy, a complete understanding of the impact of chemotherapy on the TME is yet to be fully appreciated and requires further investigation.

Both standard therapies can be used as an approach to increase tumour immunogenicity, in addition to their already described direct effect on cancerous cells. This is especially important in the context of combination with antibody immunotherapies and the potentiation of a memory response that can overcome resistance and assures long-lasting tumour-control.

1.3 Antibody-mediated immunotherapy

In recent years, immunotherapy has emerged as a breakthrough in cancer treatment. It works by reactivating and mobilising the immune cells from the patient to promote cancer recognition and immune-mediated cytotoxic response. The modulation of co-inhibitory and co-stimulatory signals through the targeting of immunomodulatory receptors expressed on tumour-reactive lymphocytes has become a promising anti-cancer approach in various

malignancies (Hodi et al., 2010; Larkin et al., 2015). A hallmark of immunotherapy is its ability to induce long-term responses driven by acquisition of immunological memory.

The advances in the hybridoma technology leading to the development of monoclonal antibodies (mAbs) in the last four decades contributed to the approval of the first antibody to be used in humans, the anti-CD3 mAb muromonab (Bournazos and Ravetch, 2017). Since then, more than 65 mAbs have been approved by the Food and Drug Administration (FDA) for the treatment of autoimmune, neoplastic, chronic inflammatory and infectious diseases with hundreds of ongoing clinical trials testing new antibodies (Bournazos and Ravetch, 2017).

The function of a therapeutic antibody (Ab) is defined by the targeted antigen and the desired clinical outcome, which can be achieved through various mechanisms. In the context of cancer therapy, cytotoxic antibodies directly targeting lymphoma and solid tumour cells promote the elimination of transformed cells, whilst traditional immunomodulatory antibodies, targeting molecules on the surface of leucocytes, mediate the anti-tumour response through the regulation of the function of those cells. Depending on the target of the antibody, immunomodulatory antibodies can either activate the function of the molecule by acting as an agonist or suppress its function by blocking the receptor-ligand interaction thereby antagonising it (antagonist antibody).

1.3.1 Role of the Fc:FcγR interaction in cancer antibody therapy

Antibodies currently used in immunotherapy are usually of the immunoglobulin G (IgG) type. Considering their structure, antibodies have two different functional parts: the fragment of antigen binding (Fab) and the fragment crystallizable (Fc). The Fab fraction contains the variable region of the antibody, whilst the Fc provides antibodies with their immune function by interaction with other soluble immune-components (such as complement cascade elements) and with cells expressing specific receptors for the Fc (Fcγ receptors).

In general, mammals have four subclasses of IgG antibodies that can interact with their receptors, Fcγ receptors (FcγRs). The assignment of γ in the FcγR is related to their interaction with Ig**G** and no other classes of antibodies, i.e. Ig**A**, Ig**E** or Ig**M**.

FcγRs are expressed on NK cells, DCs, macrophages, B cells and neutrophils. Depending of their activity, FcγRs are divided into two groups, activating and inhibitory FcγRs (Furness et al., 2014). Activating FcγRs have an immunoreceptor tyrosine-based activation motif (ITAM) that transduces activation signals, whilst inhibitory FcγRs possess an immunoreceptor tyrosine-based inhibition motif (ITIM) delivering inhibitory signals. In general, activating and inhibitory receptors are simultaneously expressed on the same cell and the triggering of activating or inhibitory signals in the cell relies in achieving defined thresholds in a tightly controlled manner (Furness et al., 2014; Weiner et al., 2010).

The only known inhibitory FcγR, in both mouse and human, is the FcγRIIb (or CD32b). It is a single-chain receptor, expressed on all cells of the immune system except NK cells and T-cells. It is also the only FcγR expressed on B-cells, regulating the activation by the B-cell receptor (BCR), promoting tolerance (Bournazos and Ravetch, 2017; Nimmerjahn and Ravetch, 2006).

FcγR from human and mouse have different nomenclature (Table 1.4). In humans, activating receptors include FcγRI (CD64), FcγRIIa (CD32a) and FcγRIIIa (or CD16a). FcγRI and FcγRIIIa also need an ITAM-containing γ chain to initiate signalling. In humans, FcγRI is the high-affinity receptor expressed on macrophages, DCs, neutrophils and eosinophils, whilst FcγRIIIa is the primary FcγR expressed by NK cells, mast cells, macrophages and DC- (Weiner et al., 2010). Importantly, FcγRIIIa is required for depletion of target cells by antibody-dependent cell-mediated cytotoxicity (ADCC) in NK cells (Takai et al., 1994). In mice the activating FcγR orthologues are FcγRIa, FcγRIII and FcγRIV (Furness et al., 2014).

Individuals FcγRs have different affinities to the different isotypes of IgGs and these affinities define the capacity of a monoclonal antibody to induce ADCC. The specific affinity of the antibody to activating and inhibitory FcγRs is used to calculate an activating/inhibitory (A:I) ratio. If the ratio is higher than 1, it indicates that the antibody has more affinity to activating FcγRs and therefore is more likely to promote ADCC. On the contrary, if the A:I ratio is less than 1, the antibody binds with higher affinity to the inhibitory FcγRIIb and triggers inhibitory signals, thus not promoting ADCC (Furness et al., 2014). In case of human IgGs, human IgG1 (hIgG1) and hIgG3 have higher affinities for the activating FcγRs than hIgG2 and hIgG4, suggesting different approach in a clinical setting. In mice, the A:I for IgG1 antibodies is <1, indicating the high affinity for the inhibitory FcγRIIb, and is normally described as a non-

depleting antibody. On the other hand, murine IgG2a and IgG2b have much higher A:I ratios (up to 70) and are therefore normally described as depleting antibodies (Table 1.4) (Hamaguchi et al., 2006; Furness et al., 2014).

Table 1.4. Table 1.4. Mouse and human FcγR homologues.

Modified from (Furness et al., 2014).

Mouse	FcγRI	FcγRIII	FcγRIV	FcγRIIb
Signalling motif	ITAM	ITAM	ITAM	ITIM
Function	Activating	Activating	Activating	Inhibitory
Affinity	High	Low	Low	Low
IgG subclass binding	IgG2a>IgG2b>IgG1	IgG2a>IgG2b>IgG1	IgG2a>IgG2b>IgG1	IgG1>IgG2b>IgG2a
Human	**FcγRI**	**FcγRIIa**	**FcγRIIIa**	**FcγRIIb**
Signalling motif	ITAM	ITAM	ITAM	ITIM
Function	Activating	Activating	Activating	Inhibitory
Affinity	High	Low	Low	Low
IgG subclass binding	IgG1>IgG3>IgG4>IgG2	IgG1>IgG3>IgG2>IgG4	IgG3>IgG1>IgG4>IgG2	IgG3+IgG4>IgG2>IgG1

The first class of antibodies ever used for cancer therapy focused on targeting cancer cells directly. These antibodies acted either by (1) blocking receptors and stopping the interaction with their ligands, binding to antigens on target cells and regulating their signalling or (2) by inducing depletion or phagocytosis of target cells expressing the antigen via ADCC or antibody-dependent cellular phagocytosis (ADCP), respectively (Johnson and Glennie, 2003; Li et al., 2005). As mentioned, for antibodies that directly eliminate cancer cells by depletion or phagocytosis, the selection of adequate IgG isotypes promoting that function is essential. For example, the clinical antibodies rituximab (anti-CD20 mAb, a treatment for lymphoma) and trastuzumab (anti-HER2 mAb, a treatment for breast cancer) were tested in mouse models and their clinical efficacy required the presence of activating FcγR, whilst it was regulated by the inhibitory FcγRIIb. Moreover, in mice lacking the inhibitory FcγRIIb, the ADCC induced by both antibodies was more efficient, promoting increased anti-tumour response in mice (Clynes et al., 2000). The same strategy is used with antibodies targeting epidermal growth factor receptor (EGFR, by cetuximab), fibroblast growth factor receptor (FGFR) and CD52 (Uchida et al., 2004; Barok et al., 2007; Hara et al., 2008; Qing et al., 2009; Golay et al., 2006). This defined the importance of engagement of activating over inhibitory FcγR, promoting higher A:I ratios, and thus the therapeutic function of these antibodies (Beers et al., 2016).

A second class of antibodies are immunomodulatory antibodies which drive anti-tumour immunity, either by providing co-stimulation to immune cells or by blocking co-inhibitory signals repressing the function of effector immune cells. These antibodies are going to be discussed further in this section.

1.3.2 Overview on immunomodulatory antibodies

As discussed before, based upon their structure, antibodies can be divided in two functional components: Fab and Fc. The role of the Fc part was already discussed in the previous section. The role of the Fab, which contains the variable region, is to interact specifically with the antigen. Thereby, immunomodulatory antibodies bind to the antigen and trigger the activation of co-stimulatory receptors or block signalling through co-inhibitory receptors on immune cells (Figure 1.3).

As immunomodulatory antibodies also contain an Fc portion, the design of these antibodies should consider the potential impact of their interaction with different FcγRs *in vivo*. In the beginning, these antibodies were designed to avoid engagement with activating FcγRs and ADCC, therefore only acting through their modulatory function. However, later studies comparing different isotypes of agonistic anti-CD40 mAbs reported that engagement with FcγRIIb promoted increased activity and tumour elimination due to optimal crosslinking of the target driven by FcγRIIb-engagement (White et al., 2011; Li and Ravetch, 2011). It was suggested that this could be a mechanism common to all tumour necrosis factor receptor superfamily (TNFRSF) molecules (Furness et al., 2014). However, further work in mouse models showed that engagement of activating FcγR and the consequent depletion of regulatory T-cells was crucial for the anti-tumour response exerted by checkpoint blockers like anti-CTLA-4 mAb and the co-stimulatory antibodies anti-GITR mAb and anti-OX-40 mAb (Bulliard et al., 2013, 2014; Simpson et al., 2013; Selby et al., 2013). These co-stimulatory antibodies, by eliminating Treg cells in the tumour and providing agonistic signals to effector T-cell subsets, promote an anti-tumour T-cell response by $CD8^+$ T-cells. The preferred elimination of regulatory T-cells in the tumour was associated with the higher level of expression of the target protein on Treg compared to activated $CD8^+$ T-cells (Bulliard et al., 2013).

In the case of human antibodies some evidence indicates a similar role for activating FcγR in their *in vivo* activity. Ipilimumab, a human anti-CTLA-4 IgG1 monoclonal antibody has been shown to promote Treg depletion *ex vivo*. In this study, using matched samples of PBMC (peripheral blood mononuclear cell) and melanoma biopsies after ipilimumab treatment, the investigators demonstrated that ipilimumab engaged FcγRIIIa expressed on non-classical monocytes and, thereby promoted ADCC of Treg cells (Romano et al., 2015). Moreover, *in vivo* data using mice expressing human FcγR showed that mouse anti-CTLA-4 antibodies with Fc portions orthologous to the human isotypes of ipilimumab (IgG1) and tremelimumab (IgG2) depleted Treg cells in the tumour, increasing the $CD8^+$ to Treg cell ratio (Arce Vargas et al., 2018). Additionally, our laboratory demonstrated that anti-CTLA-4 antibodies engineered to enhance their FcγR binding-profile increased the anti-tumour response, whilst the use of isotypes lacking the capacity to evoke ADCC had impaired anti-tumour ability (Arce Vargas et al., 2018). Moreover, a new report showed that the engagement of the Fc of mouse and

human anti-CTLA-4 mAbs with the FcγRs on APCs was important for enhanced antigen-specific T-cell responses and anti-tumour activity (Waight et al., 2018b).

The use of immunomodulatory antibodies for cancer therapy is currently under intensive research, to potentiate an effective immune response in a higher proportion of patients. In this context, a variety of new immunomodulatory targets are being explored and tested in preclinical and clinical studies (Figure 1.3). In the next section some of those targets will be described.

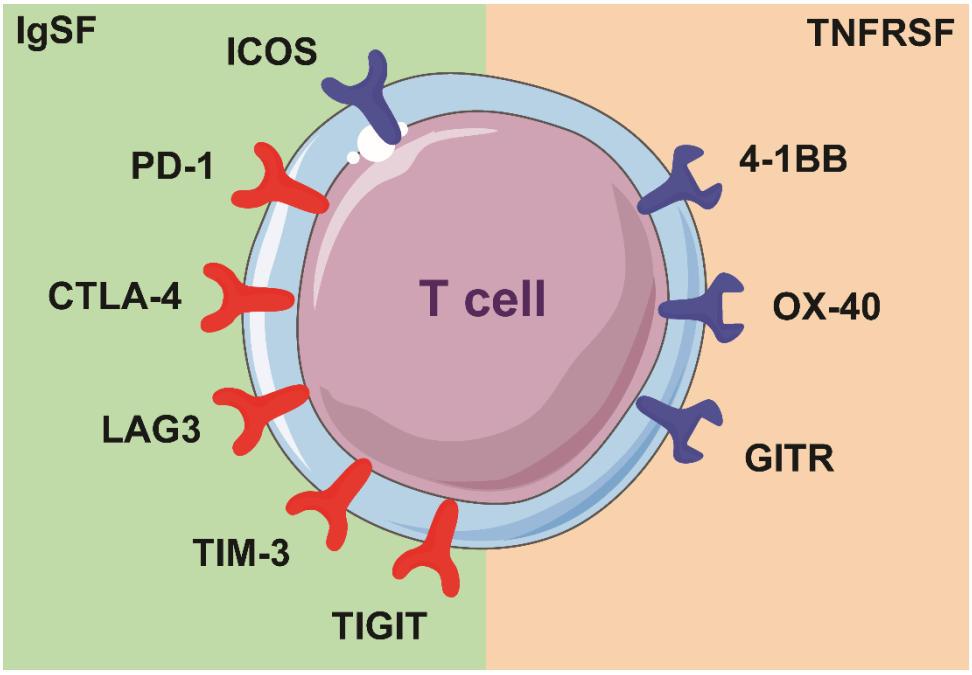

Figure 1.3. Overview of the immune-modulatory receptors.

Immune-modulatory receptors are expressed on the surface of T-cells. They are divided in co-stimulatory (blue) or co-inhibitory (red). ICOS, PD-1, CTLA-4, LAG3, TIM-3 and TIGIT belong to Immunoglobulin super-family (IgSF), whilst GITR, 4-1BB and OX-40 belong to the tumour necrosis factor receptor super-family (TNFRSF). The figure was generated using Servier Medical Art (2018).

1.3.3 Immunomodulatory targets: members of the immunoglobulin super family

1.3.3.1 CTLA-4

Cytotoxic **T** **l**ymphocyte **a**ntigen-4 (CTLA-4, CD152) is an inhibitory receptor member of the CD28-B7 immunoglobulin superfamily (IgSF). CTLA-4 is homologue to CD28, and both genes are encoded in the same chromosome in mouse (chromosome 1) and human (chromosome 2) (Dariavach et al., 2018; Śledzińska et al., 2015).

CTLA-4 is mainly expressed by T-cells upon activation. After T-cell activation, CTLA-4 is translocated to the membrane where it competes with CD28 for the binding of CD80 and CD86 expressed on APCs. CTLA-4 has a 10-fold higher affinity for the binding of CD80 and CD86 than CD28 and can even interfere with their interaction in the immune synapse, regulating the priming of T-cells (Greene et al., 1996; Khalil et al., 2016; Walunas et al., 1994). As with many other co-modulatory receptors, CTLA-4 is constitutively expressed on $CD4^+$ $CD25^+$ Treg cells (Takahashi et al., 2000).

Evidence of the checkpoint function of CTLA-4 controlling T-cell activation and peripheral tolerance has been provided by mouse models. *Ctla4*$^{-/-}$ mice develop a lymphoproliferative autoimmune disorder, multiorgan lymphocytic infiltration and tissue destruction, with death at around 3-4 weeks of age (Waterhouse et al., 1995; Tivol et al., 1995). Later studies showed that CTLA-4 deficiency restricted to $CD4^+$ $FoxP3^+$ Treg cells promoted spontaneous systemic lymphoproliferation and fatal autoimmune disease, associated with impaired suppressive function of *Ctla*$^{-/-}$ Treg *in vitro* and *in vivo* (Wing et al., 2008).

Currently, extensive evidence for the role of CTLA-4 as a negative regulator of anti-tumour response has been produced. One of the first reports showing anti-tumour response in mouse models of colon carcinoma using anti-CTLA-4 antibodies was presented by James Allison's group. In this study, *in vivo* administration of anti-CTLA-4 mAb promoted rejection of pre-stablished tumours and gave protection against a second tumour challenge (Leach et al., 1996). Similar anti-cancer effects were observed in another immunogenic mouse model of prostate cancer after anti-

CTLA-4 mAb administration (Kwon et al., 1997). However, for poorly immunogenic mouse tumours like B16-BL6 melanoma, anti-CTLA-4 mAb alone did not promote significant tumour rejection, however, tumour elimination was observed after combining anti-CTLA-4 mAb therapy with a tumour cell-based vaccine that produces Granulocyte-Macrophage Colony stimulating factor (GM-CSF) (van Elsas et al., 1999; Quezada et al., 2006). Most of these studies hypothesised the anti-tumour response observed after anti-CTLA-4 mAb treatment was mainly driven by its checkpoint blocking activity, "releasing the brakes" restraining T-cell function, promoting the survival and proliferation of T-cells. Thus, increases in the $CD8^+$ T-cell to Treg cell ratios observed in experiments combining anti-CTLA-4 mAb and GM-CSF producing cellular vaccine (GVAX) were attributed to the increase in $CD8^+$ T-cells by the blocking checkpoint activity of the antibody (Quezada et al., 2006).

Consequently to the Fc function of antibodies detailed above, experiments performed in B16-BL6 melanomas combining GVAX with different clones of anti-CTLA-4 mAb showed that the antibody preferentially eliminated Treg cells in the tumour by FcγR-engagement of macrophages in the TME (Simpson et al., 2013). Similar results were obtained in more immunogenic mouse models of colon adenocarcinoma using anti-CTLA-4 mAb as a monotherapy (Selby et al., 2013; Bulliard et al., 2013). Moreover, the study of human anti-CTLA-4 mAbs *in vivo* using transgenic mouse models (mice expressing human FcγR) replicated the importance of Treg cell depletion for tumour elimination, as already described above (Arce Vargas et al., 2018).

Ipilimumab (marketed by Bristol-Myers Squibb) is a fully human IgG1 monoclonal antibody targeting CTLA-4, approved in 2011 by the FDA for the treatment of unresectable or metastatic melanoma following phase III clinical trials demonstrating increased mOS in patients treated with ipilimumab (Hodi et al., 2010; McDermott et al., 2013). Moreover, up to 10 years follow up of patients treated with ipilimumab was performed using pooled analysis, showing that after 3 years a plateau of survival is observed in ipilimumab-treated patients, independent of the dose received or previous treatments (Schadendorf et al., 2015). Ipilimumab has also been tested in melanomas with brain metastasis, metastatic castration-resistant prostate

cancer, and in combination as adjuvant therapy for stage III melanoma (Kwon et al., 2014; Margolin et al., 2012; Eggermont et al., 2016).

A phase II trial testing ipilimumab with standard chemotherapy (paclitaxel plus carboplatin) showed that phased ipilimumab (after two doses of chemotherapy and placebo) increased progression free survival (PFS) of chemotherapy-naïve patients with stage IIIB/IV NSCLC (Lynch et al., 2012). Unfortunately, a double-blinded phase III study comparing chemotherapy plus ipilimumab or placebo did not significantly increase mOS or PFS in advanced squamous NSCLC (Govindan et al., 2017). Ipilimumab is also currently under evaluation for NSCLC treatment in further combination clinical trials with standard chemotherapy and radiotherapy (NCT03573947, NCT03168464) (Monteiro et al., 2016).

Tremelimumab is a human IgG2 anti-CTLA-4 mAb selected in pre-clinical design to reduce ADCC promotion (Hanson et al., 2004). Even though it showed encouraging results in phase I/II trials, a phase III trial evaluating tremelimumab in patients with advanced melanoma indicated no significant survival advantage compared to standard chemotherapy (Ribas et al., 2013).

CTLA-4 as a target for immunotherapy in poor prognosis cancers has promoted a significant increase in research in recent years investigating other possible targets. Problems with its toxicity have encouraged the search of more tolerable agents, such as antibodies targeting PD-1/PD-L1.

1.3.3.2 PD-1/PD-L1

The immune checkpoint **p**rogrammed cell **d**eath-**1** (PD-1, CD279) is an inhibitory surface protein member of the CD28 family and IgSF. PD-1 is expressed on B-cells, NK and activated, but not resting T-cells (Keir et al., 2008). It is upregulated after TCR-driven T-cell activation and by common γ chain cytokines including IL-2, IL-7, IL-15 and IL-21 (Śledzińska et al., 2015). PD-1 was firstly identified in a murine hybridoma cell line after inducing classic programmed cell death and was named accordingly (Ishida et al., 1992).

PD-1 has two known ligands, PD-L1 and PD-L2 which both have co-inhibitory properties (Latchman et al., 2001). Many tumours have infiltrating T-cells that express PD-1, upon binding of PD-1 to its ligands, the signalling pathway results in diminished cytokine production, impaired proliferation and cell lysis (Sundar et al., 2014). PD-1 in its intracellular tail has phosphorylation sites located in the ITIM and in the immunoreceptor tyrosine-based switch motif (ITSM), which is essential for PD-1 function on $CD8^+$ T-cells (He et al., 2015).

Evidence for a role of PD-1 and its ligands in peripheral tolerance has been obtained in transgenic mouse models. For example, aged PD-$1^{-/-}$ mice develop a lupus-like proliferative arthritis together with highly proliferative T-cells *in vitro* (Nishimura H, Nose M, Hiai H, Minato N, 1999). These mice also exhibit dilated cardiomyopathy with high titres of IgG (Nishimura et al., 2001). Another autoimmune disease associated to PD-1 was observed in non-obese diabetic (NOD) mice, in which PD-1 deficiency accelerate the onset of the disease (Wang et al., 2005).

The ligand PD-L1 is normally expressed at low levels and upregulated upon activation on immune cells such as T-cells, B-cells, DCs and myeloid cells. PD-L1 can also be expressed by non-immune cells, such as lung, heart and more importantly on malignant cells promoting T-cell anergy, exhaustion and recruitment of Treg cells (Crespo et al., 2013; Śledzińska et al., 2015; Wang et al., 2008). The expression of the ligand PD-L2 is restricted to macrophages, DCs and some cancer cells, but has also been found on activated $CD4^+$ and $CD8^+$ T-cells, regulating their function (Latchman et al., 2001; Messal et al., 2011). In general, PD-L2 expression is normally more restricted and at lower levels than PD-L1 expression (Śledzińska et al., 2015).

It has been shown that PD-L1 promotes the development and maintenance of induced Treg cells (iTreg), thus PD-$L1^{-/-}$ APCs failed to convert naïve $CD4^+$ T-cells into iTreg (Francisco et al., 2009). Additionally, the important role of the PD-1/PD-L1 axis in peripheral tolerance is shown by the development of fatal inflammation in PD-$L1^{-/-}$ PD-$L2^{-/-}$ $Rag^{-/-}$ recipients after transfer of naïve $CD4^+$ T-cells (Francisco et al., 2009).

In the context of cancer, PD-1 and PD-L1 blockade by antibodies resulted in reduced tumour growth in mouse models (Blank et al., 2004; Strome et al., 2003).

Additionally, it has been associated with the selection of intra-tumoral $CD8^+$ $PD\text{-}1^+$ cells with an enrichment for tumour reactive cells, and the use of anti-PD-1 antibodies as a strategy to rescue those cells from early stage of exhaustion (Inozume et al., 2010; Gros et al., 2014; Ahmadzadeh et al., 2009; Ye et al., 2014). Currently, there are hundreds of ongoing clinical trials using anti-PD-1 or anti-PD-L1 antibodies as an intervention for cancer therapy. The rationale in the design of antibodies targeting PD-1 relies in blocking the interaction with both ligands, PD-L1 and PD-L2. On the contrary, cancer immunotherapy antibodies targeting PD-L1 block the interaction between PD-1/PD-L1, without interfering with the interaction PD-1/PD-L2, which has been associated to reduced toxicity of the treatment due to maintenance of peripheral tolerance (Chinai et al., 2015). Currently, there are not clinical trials evaluating anti-PD-L2 antibodies, because that treatment would not prevent the tumour-induced immune suppression driving by $PD\text{-}L1^+$ tumour cells (NIH - clinicaltrials.gov, 2019). AMP-224 is a PD-L2 IgG2a fusion protein that were tested in different phase I trials (NIH - clinicaltrials.gov, 2019). As a PD-L2-IgG2a fusion protein, it binds preferentially to $PD\text{-}1^{hi}$ T-cells blocking the interaction with PD-L1 (Duffy et al., 2016). The clinical trial showed that AMP-224 is safe, but unfortunately no objective response was observed (Duffy et al., 2016).

Nivolumab is a fully human IgG4 mAb against PD-1. It was initially approved by the FDA for the treatment of advanced melanoma at the end of 2014. Since then, nivolumab has been granted approval by the FDA for the treatment of advanced-stage NSCLC patients, renal cell carcinoma, Hodgkin lymphoma, head and neck cancer, advanced or metastatic urothelial carcinoma, metastatic colorectal cancer, hepatocellular carcinoma, as adjuvant therapy in resected melanoma and SCLC (Robert et al., 2014; FDA website, 2018).

Pembrolizumab, a humanized IgG4 mAb against PD-1, was the first checkpoint inhibitor approved for NSCLC, and is currently used as first line treatment in patients with high expression of PD-L1 (> 50%) in the UK as suggested by National Institute for Health and Care Excellence (NICE) guidelines (NICE, 2017). Pembrolizumab has also been approved by the FDA for the treatment of patients with advanced melanoma, advanced NSCLC, metastatic head and neck squamous cell carcinoma, classical

Hodgkin lymphoma, advanced or metastatic urothelial carcinoma, recurrent advanced or metastatic gastric or gastroesophageal junction cancer expressing PD-L1, recurrent or metastatic cervical cancer expressing PD-L1, refractory or relapsed Primary Mediastinal Large B-cell Lymphoma and metastatic non squamous NSCLC (FDA website, 2018). Pembrolizumab has also been approved for the treatment of unresectable or metastatic, microsatellite instability-high (MSI-H) or mismatch repair deficient (dMMR) solid tumours (FDA website, 2018).

A different approach has been used with atezolizumab. Atezolizumab is an anti-PD-L1 mAb with a human IgG1 (N298A) mutation that eliminates the binding to human FcγR, thereby reducing ADCC. Atezolizumab has been approved by the FDA in the last couple of years for the treatment of urothelial carcinoma, metastatic NSCLC with disease progression after platinum chemotherapy (Rittmeyer et al., 2017) and advanced bladder cancer. Currently, there are around 180 clinical trials recruiting patients evaluating atezolizumab (NIH - clinicaltrials.gov, 2018) .

Avelumab (MSB0010718C) is the only anti-PD-L1 mAb that has an active hIgG1. It is currently being tested in multiple clinical trials as mono- or combination therapy. Avelumab was tested in a phase II trial as a treatment for metastatic Merkel cell carcinoma, showing promising results with 31.8% of patients achieving an objective response (Kaufman et al., 2016). It is yet to be shown whether its unique design promoting ADCC will result in higher efficacy than other anti-PD-(L)1 mAb.

In addition to the numerous investigations and approvals for both anti-CTLA-4 and anti-PD-1/PD-L1 mAbs as monotherapies, many ongoing trials are evaluating the benefits of combination therapy. Supporting this idea, preclinical data showed an increased anti-tumour response after combination therapy targeting both PD-1 and CTLA-4 in mouse models of melanoma (Curran et al., 2010). This resulted in clinical trials investigating the efficacy of the combination of nivolumab (anti-PD-1 mAb) with ipilimumab (anti-CTLA-4 mAb), compared to ipilimumab alone, for the treatment of unresectable or metastatic melanoma. The study showed 2-year OS of 63.8% for the combination group and 53.6% for patients assigned to ipilimumab alone (Hodi et al., 2016). This resulted in the first approval granted for combination checkpoint inhibitor immunotherapies by the FDA (FDA website, 2018).

Combinations anti-CTLA-4 mAb and anti-PD-1 mAb therapies

Since the approval by the FDA of combined nivolumab and ipilimumab for the treatment of late stage melanoma in 2015, this combination has also been investigated and subsequently approved for metastatic colorectal cancer this year (Postow et al., 2015; Overman et al., 2018).

In 2018, the FDA also approved the combination of nivolumab and ipilimumab for the treatment of intermediate/poor risk treatment-naïve advanced renal cell-carcinoma based on the results of the CheckMate 214 study (Tannir et al., 2018). Additionally, the FDA has accepted the application of the same combination for the treatment of NSCLC patients with high mutational burden following the results of the phase III CheckMate 227 study which demonstrated increased progression free survival when compared with chemotherapy (Hellmann et al., 2018).

Despite the advances made in the development and study of checkpoint blockade-based therapies, the percentage of patients with advanced disease benefiting from durable responses remains very low. Therefore, new targets and combination therapies require further investigation.

1.3.3.3 ICOS

Inducible T-cell **Co-s**timulator (ICOS, CD278) is a costimulatory receptor expressed on T-cells. ICOS also belongs to the IgSF and, together with CD28 and CTLA-4, belongs to the CD28 family (Hutloff et al., 1999).

ICOS is normally upregulated after activation through TCR-engagement and co-stimulation of CD28. For this reason, naïve T-cells and resting $CD4^+$ and $CD8^+$ T-cells upregulate ICOS expression after TCR-stimulation. On the contrary, regulatory T-cells express ICOS constitutively to a higher level than naïve subsets of T-cells. The engagement of ICOS by its ligand (ICOSL, CD275) concomitantly with TCR-activation (signal 1) triggers its co-stimulatory function, promoting survival, proliferation and differentiation (Burmeister et al., 2008; Hutloff et al., 1999; Rudd and Schneider,

2003). ICOS is also involved in the secretion of a variety of Th1, Th2 and Th17 cytokines, thus enhancing their function. However, ICOS-mediated co-stimulation tends to be less powerful than CD28-mediated co-stimulation, mainly because CD28, but not ICOS, co-induces IL-2 secretion (Amatore et al., 2018).

ICOS ligand (ICOSL) is expressed mostly by professional APCs such as DCs, B-cells and macrophages, but is also expressed on non-haematopoietic cells such as endothelial cells, providing endothelial co-stimulation to T-cells (Khayyamian et al., 2002).

ICOS is also an important co-stimulatory molecule in the context of cancer and the mounting of an anti-tumour response. High expression of ICOS has been described on regulatory tumour infiltrating lymphocytes (TILs) from melanoma and gastric cancer patients and correlated with enhanced suppressor activity. Moreover $ICOS^+$ Treg cells were preferentially expanded after IL-2 therapy, correlating with a poor prognosis (Strauss et al., 2008; Nagase et al., 2016; Sim et al., 2014). Furthermore, ICOSL expressed on melanoma cells co-stimulated Treg cells (Martin-Orozco et al., 2010). Similarly, in breast cancer, ICOSL expressed by plasmacytoid DC (pDC) promoted the proliferation of Tregs, correlating with a poor prognosis (Faget et al., 2012).

In the context of cancer immunotherapy increased frequency of $CD4^+$ $ICOS^+$ cells after treatment with ipilimumab (anti-CTLA-4 mAb) has been described in bladder cancer, urothelial carcinoma and metastatic melanoma (Liakou et al., 2008; Carthon et al., 2010; Di Giacomo et al., 2013). This higher frequency of $CD4^+$ $ICOS^+$, found in the TILs and peripheral blood, led to an increased $ICOS^+$ Teff:Treg ratio after ipilimumab therapy, which did not correlate with clinical outcome (Liakou et al., 2008).

Similarly, using mouse models of melanoma, it was observed that after anti-CTLA-4 mAb therapy, $ICOS^{-/-}$ mice had worse survival than wild-type counterparts (Fu et al., 2011). Conversely, anti-CTLA-4 mAb combined with ICOS engagement by a cellular vaccine expressing ICOSL, promoted better outcome in mice normally resistant to anti-CTLA-4 therapy alone (Fan et al., 2014).

Considering the data discussed, ICOS appears to be an interesting immunotherapy target. Moreover, three clinical trials using anti-ICOS mAbs as a cancer therapy are currently recruiting patients having presented their preliminary results. The first one is a phase I trial testing MEDI-570, an antagonistic anti-ICOS mAb, in peripheral T-cell Lymphoma patients, sponsored by the US National Cancer Institute (NCI) (NCT02520791). The second one is a phase I/II clinical trial using JTX-2011, an anti-ICOS agonistic mAb, as single agent or in combination with nivolumab, ipilimumab or pembrolizumab for the treatment of advanced solid tumours (NCT02904226). The third one, sponsored by GSK, is a phase I trial evaluating dose escalation of the GSK3359609 anti-ICOS mAb in patients with advanced solid tumours (NCT02723955). All these trials are further discussed in Chapter 3.

1.3.3.4 LAG3

Lymphocyte **a**ctivation **g**ene 3 (LAG3, CD223) is a co-inhibitory immune checkpoint expressed on activated T-cells, regulatory T-cells, B-cells, NK cells and DCs. LAG3 is also member of the IgSF, forming four extracellular Ig domains resembling CD4 (Huang et al., 2004). Both mouse and human LAG3 share structural similarity with CD4 (Miyazaki et al., 1996; Triebel et al., 1990). LAG3 binds to MHC-II with a higher affinity and inhibits activation of effector $CD4^+$ T-cells by a conserved KIEELE motif in its cytoplasmatic tail (Workman et al., 2002; Huard et al., 1995). LAG3 is also expressed by Treg cells, promoting their suppressive activity as shown by the limited suppressive function of Treg derived from $LAG3^{-/-}$ mice (Huang et al., 2004). Importantly, $LAG3^{-/-}$ mice do not develop lymphoproliferative or autoimmune pathologies as other inhibitory molecule-*Knock out* mice, however $LAG3^{-/-}$ mice showed expansion of $CD4^+$ and $CD8^+$ T-cells in the spleen starting at around 16 weeks of age, indicating a modulatory function of LAG3 (Workman and Vignali, 2005). Moreover, the binding of LAG3 expressed by activated human T-cells promoted the secretion of IL-12 and TNFα by autologous monocytes, showing that the roles of LAG3 in homeostasis needs to be carefully evaluated (Avice et al., 1999).

In the context of tumour immunotherapy, LAG3 has been investigated for its role as an immune checkpoint like CTLA-4 and PD-1. Firstly, in models of chronic

infection, LAG3 co-expression with PD-1 and 2B4 (an inhibitory molecule expressed on innate cells and some subsets of T-cells) was defined as a marker of exhausted $CD8^+$ T-cells (Wherry et al., 2007; Assarsson et al., 2005). The same idea has been translated to cancer immunotherapy, where T-cells co-expressing PD-1 and LAG3 are also described as "exhausted", but this definition has been questioned as expression of inhibitory receptors is concomitant to different stages of activation and differentiation (Fuertes Marraco et al., 2015). In this context, combination therapy with anti-PD-1 mAb and anti-LAG3 mAb has shown tumour regression of pre-established tumours in mouse models of fibrosarcoma, colorectal cancer, melanoma and ovarian cancer, consistently with a state of differentiation that can be overcome instead of "exhaustion" (Woo et al., 2012; Huang et al., 2015).

A soluble LAG3 (sLAG3), generated by alternative splicing, can be normally found in healthy patients and high levels of sLAG3 has been described as a good prognosis factor for disease-free and overall survival in breast cancer expressing oestrogen or progesterone receptors (Triebel et al., 2006). The phase I/II trial evaluating IMP321, a fusion LAG3-Ig, combined with paclitaxel has shown clinical benefit in patients with metastatic breast cancer, together with long-term activation of APCs, NK and $CD8^+$ T-cells (Brignone et al., 2010). In another phase I trial evaluating the safety, tolerability and pharmacokinetics of IMP321 in renal carcinoma patients, the study also showed sustained $CD8^+$ T-cell activation, tumour reduction and longer progression free-survival after 3 months in patients receiving doses above 6 mg (Brignone et al., 2009). An active not yet recruiting phase II study (TACTI-002) is aiming to test the combination of IMP321 with pembrolizumab in unresectable or metastatic NSCLC, recurrent PD-1 refractory NSCLC or with recurrent or metastatic head and neck squamous cell carcinoma (HNSSC) (NCT03625323). Additionally, a recent press release confirmed that IMP321 is going to start a new study in combination with avelumab (anti-PD-L1 mAb) (Immutep, 2018).

Antibody therapy targeting LAG3 is also under further development with clinical trials underway. LAG3 expression has been described in renal cell carcinoma, melanoma and lymphoma, mostly restricted to $CD8^+$ T-cells (Demeure et al., 2001). As mentioned before, some tumours can express MHC-II. Considering this, a study using

a mouse model of melanoma showed that MHC-II expression by tumour cells promoted a LAG3-induced protection from apoptosis after binding of LAG3 expressed on TILs, suggesting that blocking antibodies could also promote tumour elimination by cutting survival signals within the tumour (Hemon et al., 2011).

To date there are 17 active clinical trials testing BMS-986016 (anti-LAG3 mAb, by Bristol-Myer Squibb) in phase I, I/II or II investigating the benefit of this checkpoint inhibitor in different malignancies either as a single agent (NCT02061761) or combined with nivolumab, ipilimumab or other therapies (NIH - clinicaltrials.gov, 2018).

1.3.3.5 TIGIT

TIGIT (T cell Immunoglobulin and immunoreceptor tyrosine-based inhibitory motif [ITIM] domain, VSTM3 or WUCAM) is an inhibitory immune checkpoint member of the CD28 family and the IgSF and is expressed on T-cells and NK cells (Levin et al., 2011; Burugu et al., 2017). TIGIT has an extracellular Ig variable domain and its cytoplasmatic tail contains an ITIM and an Ig tail-tyrosine (ITT)-like motif (Yu et al., 2008; Dougall et al., 2017). Similar to the network between CD28/CTLA-4/CD80/CD86, CD266 is a co-stimulatory receptor sharing ligands with the inhibitory receptors TIGIT and CD96 (Levin et al., 2011; Dougall et al., 2017). CD266 and TIGIT share two ligands: CD155, a nectin-like protein also known as PVR, and CD112 also known as nectin-2 or PVRL2 (Yu et al., 2008; Deuss et al., 2017).

In a model of murine autoimmune arthritis (CIA, collagen-induced arthritis), injections with soluble TIGIT-Ig attenuated the CIA score, whilst blocking with an anti-TIGIT mAb accelerated the onset of the disease score (Levin et al., 2011). Moreover, $Tigit^{-/-}$ mice showed an increased disease score in another model of autoimmunity, EAE (experimental autoimmune encephalomyelitis), showing its important role in immune tolerance (Levin et al., 2011).

In mouse models of colon cancer and melanoma, tumour-infiltrating $CD8^{+}$ T-cells expressed high levels of TIGIT and PD-1, marking a dysfunctional subset (Zhang et al., 2018; Johnston et al., 2014; Kurtulus et al., 2015). In a study using mouse models

of colon carcinoma, most of the tumour-bearing mice rejected the tumours after treatment with anti-TIGIT mAb and anti-PD-L1 mAb, but not with each antibody as a monotherapy (Johnston et al., 2014). Moreover, when the mice were re-challenged, none of them developed tumour proving a long-lasting response (Johnston et al., 2014). In other mouse models, anti-TIGIT mAb therapy alone was enough for longer survival (Zhang et al., 2018). Additionally, Tigit$^{-/-}$ mice had longer survival in mouse models of melanoma and colon carcinoma (Kurtulus et al., 2015; Zhang et al., 2018). Also, in mouse models of melanoma TIGIT^{+} Treg TILs showed a more suppressive and activated phenotype (Kurtulus et al., 2015). However, between all these studies the main target for TIGIT's role has been exhausted CD8^{+} T-cells (Johnston et al., 2014), exhausted NK cells (Zhang et al., 2018) or Treg cells (Kurtulus et al., 2015), showing that the exact mechanism of action of this inhibitory molecule remains elusive.

High TIGIT-expression together with high levels of PD-1 on CD8^{+} T-cells has been observed on TILs from NSCLC, oesophageal cancer and melanoma patients, suggesting that both markers defined a tumour-reactive CD8^{+} subpopulation (Johnston et al., 2014; Chauvin et al., 2015; Xie et al., 2016; Tassi et al., 2016). Between studies, the definition of CD8^{+}PD-1^{+}TIGIT^{+} cells as "exhausted" or activated has been observed. TIGIT alone has also been identified as an "exhaustion" marker for tumour-infiltrating NK cells in patients with colon cancer, demonstrating that the mechanism of TIGIT in human malignancies is yet to be fully appreciated (Wang et al., 2015; Zhang et al., 2018).

Although TIGIT has only recently been described as a potential therapeutic target and its mechanism of action is not fully understood, there are currently three clinical trials testing three different anti-TIGIT antibodies. The MTIG7192A/ BMS-986207 antagonistic anti-TIGIT hIgG1 mAb is being tested in combination with atezolizumab for the treatment of advanced or metastatic chemotherapy-naïve NSCLC patients in a phase II trial (NCT03563716). Another antibody, OMP-313M32 is being tested in a phase I trial with nivolumab, recruiting patients with advanced or metastatic cancer (NCT03119428). Another phase I trial is evaluating AB154, a hIgG1 anti-TIGIT mAb in combination with AB122, a hIgG4 anti-PD-1 mAb, for the treatment of advances malignancies (NCT03628677).

1.3.3.6 TIM-3

TIM-3 (T-cell Immunoglobulin- and mucin-domain-containing 3) is a member of the TIM family of which all members form part of the IgSF. TIM-3 is an inhibitory receptor expressed on T-cells and NK cells (Burugu et al., 2017). TIM-3 is a specific Th1/Tc1 molecule that, after engagement by its ligand galectin-9, induces an intracellular calcium flux and subsequent death of Th1 cells *in vitro*, thereby possibly contributing to the control of a Th1 response (Zhu et al., 2005). In mouse models, blocking TIM-3 using antibodies led to accelerated diabetes in NOD mice, showing the role of TIM-3 in Th1-tolerance (Sánchez-Fueyo et al., 2003). Moreover, it has been shown that *in vivo* administration of galectin-9 resulted in the elimination of $IFN\gamma^+$-cells and, consequently, suppression of Th1 autoimmunity (Zhu et al., 2005). TIM-3 is also highly expressed on Treg cells and promotes their suppressive function, which is associated with STAT3 expression (Gautron et al., 2014; Gupta et al., 2012).

Similar to other checkpoint inhibitors, TIM-3 expression has also been associated with exhaustion in chronic infections, including HIV, Hepatitis C and lymphocytic choriomeningitis virus (Jones et al., 2008; Golden-Mason et al., 2009; Jin et al., 2010). In cancer, comparable observations have been made. Exhausted $CD8^+$ $TIM3^+$ $PD\text{-}1^+$ cells with compromised production of pro-inflammatory cytokines have been identified in melanoma, gastric cancer, perineural squamous cell carcinoma, oesophageal cancer, HNSSC, colon cancer, NSCLC and Schwannomas (Fourcade et al., 2010; Lu et al., 2017; Linedale et al., 2017; Shayan et al., 2017; Li et al., 2017b; Zhou et al., 2015; Xie et al., 2016; Tassi et al., 2016). Additionally, IL-12 treatment induced exhaustion and poor prognosis in non-Hodgkin lymphoma patients, associated with increased expression of TIM-3 (Yang et al., 2012). Considering this evidence, studies in a mouse model of colon carcinoma showed that combination therapy anti-PD-L1 mAb plus anti-TIM-3 mAb promoted the rejection of established tumours, without significant rejection demonstrated from giving each therapy alone (Sakuishi et al., 2010).

There are currently six clinical trials testing five different anti-TIM-3 antibodies. MBG453, a humanised anti-TIM-3 hIgG4 mAb, is being tested in a phase I clinical trial

for the treatment of haematologic malignancies combined with chemotherapy (NCT03066648). MBG453 is also being tested in a phase I/II clinical trial in combination with PDR001 (an anti-PD-1 hIgG4 mAb) for the treatment of solid tumours (NCT02608268). The anti-TIM-3 mAbs INCAGN02390 (a fully hIgG1) and Sym023, are currently being evaluated in phase I trials for the treatment of advanced solid tumour or lymphomas as monotherapy (NCT03652077, NCT03489343) (Waight et al., 2018a). Another two phase I clinical trials targeting TIM-3 with two different antibodies, TSR-022 (hIgG4) and LY3321367 (hIgG1 Fc null), are currently active, evaluating the safety of different doses of the antibodies for the treatment of solid tumours in combination with antibodies targeting PD-1/PD-L1 (NCT02817633, NCT03099109).

1.3.4 Immunomodulatory targets: members of the tumour necrosis factor (TNF) receptor super family

1.3.4.1 GITR

GITR (Glucocorticoid-induced tumour necrosis factor receptor [TNFR] family related protein, TNFRSF18, CD357) is a co-stimulatory receptor expressed by T-cells, B-cells and NK cells (Ward-Kavanagh et al., 2016). GITR is constitutively expressed on Treg cells, whilst naïve T-cells have low levels of expression that can be upregulated upon activation (Clouthier and Watts, 2014). On the other hand, GITR ligand (GITRL) is also a member of the TNF superfamily and is mostly expressed by APCs such as DCs, activated B cells and macrophages (Knee et al., 2016).

GITR was first described as a promoter of correct Treg function, as *in vitro* assays with anti-GITR mAb impaired their suppressive function (Shimizu et al., 2002). Moreover, administration of anti-GITR mAb to normal mice induced autoimmune gastritis, highlighting the relevance of the receptor in the maintenance of tolerance (Shimizu et al., 2002).

In mouse models, anti-GITR mAb therapy has shown tumour rejection in bladder carcinoma, colon carcinoma, mammary tumours, lung cancer and peptide-

expressing melanoma and, to a lesser degree, in pancreatic cancer (Coe et al., 2010; Zhou et al., 2007; Aida et al., 2014; Duan et al., 2009; Zhou et al., 2010; Zhu et al., 2015). In an ovarian cancer model, even though anti-GITR mAb or anti-PD-1 mAb monotherapy did not promote tumour rejection, the combination therapy resulted in a significant inhibition of peritoneal tumours (Lu et al., 2014). In a model of liver metastasis by renal cell carcinoma, anti-GITR mAb combined with sunitinib (a tyrosine kinase inhibitor) inhibited metastatic-growth by promoting infiltration and activation of $CD8^+$ T-cells and NK cells together with macrophage activation (Yu et al., 2015). In these models, because tumour-infiltrating Treg cells are the population with the highest expression of GITR, the main function of anti-GITR mAb is Treg depletion, which leads to effector $CD4^+$, $CD8^+$ T-cells and NK activation. Importantly, anti-GITR mAb therapy has shown effectivity in both immunogenic and non-immunogenic models of cancer emerging as a suitable combination with other agents. Interestingly, all these works used a rat IgG2b, which promotes depletion in mice. When the variable region sequence of the anti-GITR antibody was engineered into a mouse IgG2a Fc fraction and tested in a model of colon cancer, it was demonstrated that the depleting function of the antibody by the correct binding to activating FcγR was necessary for the anti-tumour response (Bulliard et al., 2013).

High GITR expression has been described on $CD4^+CD25^+$ TILs from endometrial cancer patients, correlating with poorly infiltrated and dysfunctional $CD8^+$ (Chang et al., 2010). Additionally, high GITR expression has been described on Treg cells from breast cancer, lymph nodes (LN) infiltrated from advanced breast cancer, hepatocellular carcinoma and liver metastases from colorectal cancer (Krausz et al., 2012; Li et al., 2011; Pedroza-Gonzalez et al., 2015).

There are seven clinical trials currently ongoing targeting GITR. OMP-336B11 (GITRL-Fc [hIgG1]) is being tested as monotherapy in a phase I clinical trial (NCT03295942) for advanced or metastatic tumours (Chan et al., 2018). MEDI1873, a hexameric human GITRL-hIgG1 fusion protein, is in an active, non-recruiting phase I trial (NCT02583165). The remaining five clinical trials are evaluating three different anti-GITR mAbs. TRX518 (anti-GITR hIgG1 mAb) is in a phase I trial (NCT01239134) recruiting patients with stage III or IV melanoma and other solid tumours, with

preliminary results confirming safety and tolerability (Koon et al., 2016). GWN323 (anti-GITR hIgG1 mAb) is being evaluated in a phase I/Ib study, alone or combined with PDR001 (anti-PD-1 hIgG4 mAb) in advanced solid tumours and lymphomas (NCT02740270). The anti-GITR mAb INCAGN01876 is currently being investigated in three trials: monotherapy in a phase I/II trial for advanced and metastatic malignancies (NCT02697591), in combination with nivolumab and ipilimumab in a phase I/II clinical trial (NCT03126110) and in combination with pembrolizumab or epacadostat (IDO inhibitor) in another phase I/II trial (NCT03277352).

1.3.4.2 4-1BB

4-1BB (CD137 or TNFRSF9) is another co-stimulatory receptor from the TNFR super family (TNFRSF) and its expression is upregulated upon cell activation. It is expressed on activated T-cells, activated NK cells, Treg cells, DCs and other myeloid cells (Chester et al., 2017). It was first described that the interaction between 4-1BB and its ligand (4-1BBL) induces proliferation of splenic T-cells (Goodwin et al., 1993). 4-1BBL is mostly expressed on APCs like DCs, macrophages and B-cells (Chester et al., 2017). Accordingly, activation, proliferation, differentiation, survival, cytokine production and generation of stable memory have been described after stimulation of T-cells with agonistic anti-4-1BB Abs *in vitro* (Xu et al., 2005; Willoughby et al., 2014; Hernandez-Chacon et al., 2011; Hurtado et al., 1997, 1995).

In mouse models of graft-versus-host disease (GVHD), anti-4-1BB mAb promoted skin rejection that was linked to exacerbated cytotoxic $CD8^+$ (CTL) response *in vivo* (Shuford et al., 1997). Moreover, anti-4-1BB mAb therapy prevented and reversed OVA-induced anergy of cytotoxic $CD8^+$ T-cells in mice, restoring the proliferation and cytokine production of $CD8^+$ cells, indicating a role of 4-1BB in disrupting T-cell dysfunction (Wilcox et al., 2002).

Anti-4-1BB mAb therapy has also shown efficacy as a monotherapy in models of fibrosarcoma, glioma, ovarian tumours, lung carcinoma and myeloma (Vinay and Kwon, 2012). In mouse models of cancer with different levels of immunogenicity, such as sarcoma and mastocytoma, anti-4-1BB mAb therapy effectively prolonged the

survival of the mice (Melero et al., 1997). In less immunogenic models such as melanoma, anti-4-1BB mAb combined with anti-LAG3 mAb promoted rejection of tumours together with a reduced frequency of dysfunctional T-cells, reinforcing the role of 4-1BB in restoring T-cell functionality in cancer (Williams et al., 2017). In other less immunogenic models like colon carcinoma, anti-4-1BB mAb combined with local IL-12 or a tumour antigen-derived peptide rejected tumours (Xu et al., 2005; Wilcox et al., 2002). Additionally, in an OVA-melanoma model, anti-4-1BB mAb therapy promoted the persistence and function of adoptively transferred CTLs (Weigelin et al., 2015).

Infiltration of 4-1BB$^+$ cells has also been described in human malignancies. Houot et al made this observation in human primary lymphoma (Houot et al., 2009). Additionally, 4-1BB has been used as a marker of tumour-reactive T-cells from PBMC of gastric cancer patients and has been used for the selection of tumour-reactive T-cells *in vitro* and *in vivo* from samples of ovarian and melanoma patients (Ye et al., 2014; Choi et al., 2014).

Urelumab (BMS-663513), a fully human non-blocking anti-4-1BB IgG4 mAb, was the first anti-4-1BB mAb entering clinical trials in the last decade. The dose-escalation trials revealed dose-dependent liver toxicity, leading to termination of the trials. Currently, liver toxicity has been described at low dose level (0.3 mg/Kg), resulting in the adoption of a lower flat dose of 8 mg that reduced liver toxicity and is being utilised in new clinical trials testing urelumab in combination with other anti-cancer agents (Chester et al., 2017). There are currently five clinical trials recruiting patients to evaluate urelumab in combination with nivolumab (NCT02253992, NCT02845323, NCT02534506, NCT02658981), cabiralizumab (NCT03431948), BMS 986016 (anti-LAG3 mAb) and anti-PD-1 mAb (NCT02658981). There are another four completed clinical trials in which urelumab (NCT01471210) was evaluated alone or in combination with rituximab (NCT01775631), cetuximab (NCT02110082) and lirilumab (anti- KIR2DL1/2L3 mAb) or elotuzumab (anti- SLAMF7 mAb) (NCT02252263). The study of urelumab dosage (NCT01471210) showed significant transaminitis associated to doses of ≥1 mg/Kg, however, safety was demonstrated for 0.1 mg/Kg doses every 3 weeks, encouraging the evaluation of combination therapies (Segal et al., 2017).

Importantly, a recent study elucidated the mechanism related to anti-4-1BB liver toxicity. According to the authors, the expansion of IL-27-producing cells in the liver triggered by anti-4-1BB mAbs promotes the accumulation and cytotoxicity of $CD8^+$ T-cells and hepatitis (Bartkowiak et al., 2018). Undoubtedly, these results will provide new strategies for safer and more tolerable urelumab therapy in the future.

Utomilumab (PF-05082566) is a fully humanized IgG2 agonistic anti-4-1BB mAb that blocks the interaction 4-1BB/4-1BBL. Interestingly, initial results of a dose-escalation clinical trial (NCT01307267) have shown no sign of liver toxicity, compared to that observed with urelumab (Segal et al., 2014). The same phase I clinical trial is testing utomilumab combined with rituximab in $CD20^+$ non-Hodgkin lymphoma patients, with 2 complete responses reported to date (Gopal et al., 2015). However, the effectivity of utomilumab as an anti-tumour agent remains to be confirmed in further studies.

Currently, there are 12 ongoing clinical trials evaluating the utomilumab in combination with pembrolizumab, rituximab, PF-04518600 (anti-OX-40 mAb), trastuzumab, avelumab, vaccines and chemotherapy for treatment of solid cancer and haematological malignancies (NCT03290937, NCT02315066, NCT03364348, NCT02554812, NCT03318900, NCT03258008, NCT03414658, NCT03217747, NCT03390296, NCT02951156, NCT03440567).

1.3.4.3 OX-40

A member of the TNFRSF, OX-40 (CD134) is another co-stimulatory receptor expressed on activated T-cells and Treg. It is also expressed to a lesser extent on NK and natural killer T-cells (NKT cells). OX-40 is upregulated upon activation and is constitutively expressed on Treg cells (Willoughby et al., 2017). OX-40 is normally transiently expressed after TCR-triggering, promoting proliferation, differentiation and survival of memory subsets (Ward-Kavanagh et al., 2016). OX-40 ligand (OX-40L, CD252) is also induced after stimulation and is expressed on DCs, B-cells, macrophages, NK and mast cells (Willoughby et al., 2017).

The interaction of OX-40 with OX-40L induces T-cell proliferation and cytokine secretion (Godfrey et al., 1994; Baum et al., 1994). Experiments evaluating OX-40$^{-/-}$ mice and OX-40$^{-/-}$ Ag-specific CD8^{+} T-cells showed *in vivo* that deficiency in OX-40 signalling lead to impaired proliferation, decreased survival and lower frequency of memory T-cells, indicating a role for OX-40 in optimal clonal expansion (Gramaglia et al., 2000; Bansal-Pakala et al., 2004).

In mouse models of cancer, OX40$^{-/-}$ mice developed more EG.7 tumours than *wild-type* mice, suggesting an important role of this modulatory molecule (Bansal-Pakala et al., 2004). Accordingly, mice treated with anti-OX-40 mAb rejected tumours in a variety of mouse models of cancer (Piconese et al., 2008; Bansal-Pakala et al., 2004).

Agonistic antibodies against OX-40 have also been studied. In a mouse model of ovarian cancer, anti-OX-40 mAb combined with anti-PD-1 mAb promoted survival in a CD8^{+}-dependent manner, with reduced Treg cells (Guo et al., 2014). Similarly, anti-OX-40 mAb combined with anti-CTLA-4 mAb or radiotherapy also showed tumour elimination (Redmond et al., 2014; Marabelle et al., 2013; Yokouchi et al., 2008). Interestingly, in these experiments the isotypes used were not ADCC-optimised, but retaining ADCC function in tumour context, as demonstrated by Bulliard and collaborators (Bulliard et al., 2014). Remarkably, when the isotype of the antibody was optimised for a depleting function it could be confirmed that anti-OX-40 mAb anti-tumour activity is dependent on Treg depletion in the tumour (Bulliard et al., 2014).

Similarly to mice, high OX-40 expression has been described on Treg cells in gastric cancer patients (Piconese et al., 2014). Expression of OX-40 has also been described on CD4^{+} infiltrating T-cells from melanoma, head and neck and primary breast tumours (Vetto et al., 1997; Ramstad et al., 2000). 9B12, a murine IgG1 anti-OX-40 mAb was shown to have acceptable toxicity and a response rate of 40% in a phase I clinical trial (Curti et al., 2013).

Currently, there are several clinical trials evaluating several different agonistic anti-OX-40 antibodies in various malignancies. Antibodies including MEDI6469, PF-04518600, BMS 986178, MEDI0562, GSK3174998, INCAGN01949 and MOXR0916 are

being evaluated as monotherapy or in combination with ipilimumab, nivolumab, pembrolizumab, atezolizumab, tremelimumab, avelumab, rituximab, axitinib and chemotherapy, among others (Bell et al., 2017; Dempke et al., 2017; NIH - clinicaltrials.gov, 2018).

1.4 Scientific rationale and aims

Checkpoint blockade, one of the immunotherapeutic approaches in anti-cancer therapy, has provided durable remission in some patients with advanced disease. Unfortunately, the fraction of patients benefiting from these therapies remains low. For this reason, it is necessary to rationally design, develop and test new therapies and strategies to promote cancer rejection and immune memory to avoid cancer relapse.

The work undertaken in this thesis focused on two different approaches in the design and proposal of new immunotherapies, as described below.

1.4.1 Selection of ICOS as a target for antibody immunotherapy

ICOS was selected as an interesting target for antibody immunotherapy to study in this project based on ambiguous clinical and preclinical data. ICOS is a co-stimulatory molecule expressed on activated T-cells and Treg cells that after stimulation promotes T-cell proliferation and survival, as discussed above.

Experiments in mouse models of melanoma showed that ICOS-signalling is required for effective tumour rejection with anti-CTLA-4 mAb therapy (Fu et al., 2011; Fan et al., 2014). Moreover, clinical data from patients treated with ipilimumab (an anti-CTLA-4 mAb) has shown increased frequency of $CD4^+$ $ICOS^+$ cells in the blood as a good prognosis indicator in melanoma (Carthon et al., 2010; Di Giacomo et al., 2013). Further preclinical and clinical data will be discussed in Chapter 3.

It was hypothesised that an anti-ICOS agonistic antibody might provide co-stimulatory signals to T-cells in the tumour, promoting T-cell activation and function.

It was expected that this T-cell activation could drive tumour rejection in established mouse models of cancer.

To test this hypothesis, the following aims were set:

1. Produce an agonistic anti-ICOS monoclonal antibody;
2. Test anti-tumour efficacy of anti-ICOS mAb in mouse models of cancer as monotherapy;
3. Test anti-tumour efficacy of anti-ICOS mAb combined with anti-PD-1 mAb or anti-CTLA-4 mAb in mouse models of cancer.

The generals aim of this project will be expanded in Chapter 3.

1.4.2 Deciphering the immune tumour microenvironment of mouse models of lung cancer for the rationale design of therapies.

As mentioned before in this Chapter, lung cancer carries the highest mortality in the UK (Cancer Research UK, 2018a). Immunotherapies have been approved for the treatment of advanced NSCLC and provide significant benefit for patients when compared to traditional chemotherapy.

Nevertheless, as clinical benefit is still restricted to a fraction of the patients, the necessity of new therapies requires suitable preclinical models. In order to develop suitable mouse models, firstly NSCLC samples were evaluated, with their immune landscape previously characterised in the laboratory by Dr Andrew Furness.

It was hypothesised that systematic characterisation of the immune landscape in lung cancer will inform the rational development of improved immune-modulatory antibodies and the evaluation of novel combination immunotherapies. Therefore, the need to characterise this immune landscape in mouse models of cancer and compare it to the TME of human NSCLC was identified.

This project focused on characterising mouse models that resembled the previously described immune landscape in NSCLC, in order to define the most relevant

murine models for the evaluation of novel therapies as single agents and in combination.

The general aims of this part of the project were:

1. To develop mouse models of lung cancer and characterise their immune TME;
2. To evaluate the immune TME of models of lung cancer after traditional treatments as radiotherapy and chemotherapy;
3. To propose, test and evaluate the effect of immunotherapies in the immune TME.

2 Materials and Methods

2.1 Cell lines

The cell lines Jurkat-NFAT.GFP, HEK 293T (human embryonic kidney 293) and CT 26 (mouse colon carcinoma) were kindly donated by Dr Martin Pule.

MCA 205, a mouse chemically induced sarcoma cell line, were kindly donated by Dr Lorenzo Galluzzi.

MC 38 mouse colon adenocarcinoma were kindly donated by Dr Burkhard Becher.

CMT-167, a mouse lung carcinoma cell line, were purchased from Sigma Aldrich (Catalogue number: 10032302, Sigma Aldrich). Briefly, the CMT-167 cell line is a highly metastatic subclone of the murine lung carcinoma cell line CMT-64 that was isolated by subcloning and selected by its metastatic potential.

KPB6.F1 and KPB6.F2, mouse lung adenocarcinoma cell lines, were generated previously in our laboratory by Dr Fred Arce Vargas. Briefly, $Kras^{LSL/G12D}$; $Trp53^{flox/flox}$ C57BL/6 mice developed lung adenocarcinomas after intra nasal administration of adenovirus expressing the protein Cre recombinase (DuPage et al., 2009). After euthanising the mice, lungs were recovered and grown *in vitro* to generate the KPB6.F0 cell line. After the establishment of the KPB6.F0 cell line, *wild-type* (WT) C57BL/6 mice were challenged with the KPB6.F0 cell line and developed lung tumours. Lungs of tumour-bearing mice injected with KPB6.F0 cell line were then recovered and cultured *in vitro* to generate the KPB6.F1 cell line. To favour immunoediting, KPB6.F1 cells were injected intravenously into WT C57BL/6 mice and after the development of lung tumours, the tissue was recovered and cultured *in vitro* to generate the KPB6.F2 cell line. Regarding lung cancer models, the main work in this thesis was done using the KPB6.F1 cell line. KPB6.F2 cell line was later transduced to express GFP (KPB6.F2-GFP^+). KPB6.F2 and KPB6.F2-GFP^+ cell lines were used in experiments referred in the annex of this thesis.

2.2 Cell culture

MCA205 and CMT-167 cell lines were cultured in Dulbecco's Modified Eagle's Medium (DMEM, Sigma Aldrich) supplemented with 10% Foetal Bovine Serum (FBS, Gibco), 2 mM L-Glutamine (Sigma Aldrich) and 100 U/mL penicillin plus 100 µg/mL streptomycin (Sigma Aldrich). HEK 293T, KPB6.F1 and KPB6.F2 cell lines were grown in supplemented Iscove's Modified Eagle's Medium (cIMDM, Sigma Aldrich). Jurkat-NFAT.GFP, CT 26 and MC 38 cell lines were cultured in supplemented Roswell Park Memorial Institute medium 1640 (cRPMI, Sigma Aldrich).

2.3 Mice

Seven- to 8-week-old female C57BL/6 and BALB/c *wild-type* (WT) mice were obtained from Charles River Laboratories.

FcγR$^{-/-}$ (Fc gamma receptor [FcγR] *knock-out*) also known as *Fcer1g*$^{-/-}$ or *Fcer1g*^{tm1Rav} mice, in a C57BL/6 background, are mice that lack the three activating Fcγ receptors (FcγRI, FcγRIII, FcγRIV) (Takai et al., 1994). FcγR$^{-/-}$ mice were kindly donated by Dr Stephen Beers and were bread and housed at UCL Biological Service Unit (BSU).

FcγRIIb$^{-/-}$ (Fc gamma receptor IIb [FcγRIIb] *knock-out*) also known as *Fcgr2b*$^{-/-}$ or *Fcgr2b*^{tm1Ttk} mice in a C57BL/6 background, are mice that lack the inhibitory FcγRIIb (Takai et al., 1996). hFcγR (human Fc gamma receptor) mice, also known as huFcγR or C57BL/6 FcRα$^{-/-}$*Fcgr1*$^{-/-}$ *FCGR1*^{tg}*FCGR2A*^{R131tg}*FCGR2B*^{I232tg}*FCGR3A*^{F158tg}*FCGRIIIB*^{tg} mice, in a C57BL/6 background, are mice that express the human FcγRs FcγRI, FcγRIIA, FcγRIIB, FcγRIIIA, and FcγRIIIB without expressing mouse FcγR. Briefly, mice lacking mouse FcγRIIB, FcγRIII, and FcγRIV (FcγRα$^{-/-}$ mice) were crossed to FcγRI$^{-/-}$ mice generating FcRα null mice, with no detectable murine FcγR expression (Smith et al., 2012). The FcRα null mice were then bred with the strains huFCGR1A, huFCGR2A^{R131}, huFCGR2B^{I232}, huFCRG3A^{F158} and huFCGR3B, leaving the expression of human FcγR under the control of their endogenous human regulatory elements (Smith et al., 2012). Both mice strains, FcγRIIb$^{-/-}$ and hFcγR, were a kind gift by Dr Jeffrey Ravetch. FcγRIIb$^{-/-}$ and hFcγR mice were housed and bred in Charles Rivers Laboratories.

All animals were maintained in individually ventilated cages and pathogen-free conditions at UCL Biological Service Unit (BSU) following arrival, in accordance with Home Office and institutional guidelines. Animal protocols were approved by local institutional research committees and in accordance with the Animal (Scientific Procedures) Act 1986 guidelines by UK Home Office.

2.4 Therapeutic antibodies

The production of anti-ICOS (37A10 clone) mAb with the isotypes mouse IgG1, mouse IgG2a, human IgG1 and human IgG4, anti-CD25 (PC61 clone) mAb mouse IgG2a and anti-4-1BB (3H3 clone) mAb mouse IgG1 was outsourced to Evitria AG (Switzerland).

The antibodies anti-4-1BB mAb (clone LOB12.3) rat IgG1, anti-TIGIT mAb (clone 1G9, mouse IgG1), anti-LAG3 mAb (clone C9B7W, rat IgG1) and anti-CD16/CD32 mAb (clone 2.4G2) rat IgG2b were purchased from BioXcell (US).

The anti-CD25 mAb (TUSKC22) mouse IgG2a was kindly provided by Tusk Therapeutics.

2.5 Tumour models

2.5.1 Subcutaneous tumours

C57BL/6, FcγR$^{-/-}$, FcγRIIb$^{-/-}$ and hFcγR mice were injected subcutaneously with 500,000 MCA205, MC 38 or CMT-167 cells in the right flank. BALBc mice were injected subcutaneously with 500,000 cells CT 26 cells in the right flank.

For survival experiments, mice were treated with therapeutic antibodies at the dose indicated in each figure by intraperitoneal injection on days 6, 9 and 12 after tumour injection, unless indicated otherwise. Tumours were measured three-times-weekly and mice were euthanised when any orthogonal measured reached 150 mm.

For tumour microenvironment evaluation experiments, mice were treated with therapeutic antibodies at the dose indicated in each figure by intraperitoneal injection on days 6 and 9 after tumour injection. 48 hours after the last treatment injection, mice were euthanised and tumours and draining lymph nodes (LN) were collected for further analysis by flow cytometry.

2.5.2 Lung cancer models

2.5.2.1 Titration

C57BL/6 mice were injected intravenously with increasing numbers of KPB6.F2, KPB6.F1 and CMT-167 cells in order to stablish the optimal number of cells to set up the models. After 21 days, mice were culled, and tumour-bearing lungs were collected.

2.5.2.2 Radiotherapy experiment

C57BL/6 mice were injected intravenously with 80,000 KPB6.F1 and were divided in two fractioning schedules in the right lung: one dose of 8 Gy or 3x8Gy fraction. The first dose of irradiation was given 10 days after tumour injection, the second dose at day 12 and the third dose at day 14 post-tumour injection. Mice that received a single dose of irradiation were euthanised at day 13 and 17 post-tumour challenge. Mice that received 3x8Gy fractions were euthanised at day 17 and 21 after tumour challenge. Lungs were collected for further analysis.

Irradiation treatments

Irradiation treatments were done in collaboration with Dr Rebecca Carter and Mr Adam Westhorpe.

An Xstrahl SARRP S/N 525722 irradiator (225kV x-ray tube, dose rate 2.83 Gy/min) with 0.1 mm Be filtration was used.

CBCT was performed before each radiation treatment to confirm target position. Each mouse was anaesthetized with isoflurane on a 3D printed bed and rotated between the X-ray source and a digital flat-panel detector. The images were obtained at 60 kVp and 0.8 mA with 1 mm Al filtration of an uncollimated primary beam. For most mice, 720 projections were acquired (approx. 0.5° increments for each projection, 0.02 Gy total radiation dose). The CBCT slices were rendered into a 3D image reconstruction, using the FDK® algorithm with a voxel size from between .01 to 5 mm.

Muriplan software was used to enable treatment planning to target the right lung individually. Dose calculations used a Monte Carlo simulation superposition-convolution dose algorithm, similar to those used clinically.

Mice received either a single dose of 8 Gy, or 3x 8 Gy fractions delivered with 48 hours between treatments. Each treatment was delivered using 2x 4 Gy, targeted to maximise dose delivery to a single lung, the beam used was 220 kVp and 13 mA, filtered with 0.15 mm Cu, targeted via a 10 mm collimator.

2.5.2.3 Chemotherapy experiment

C57BL/6 mice were injected intravenously with 80,000 KPB6.F1. For the treatments, 10 days after tumour injection, mice were intraperitoneally injected with 1 mg of cyclophosphamide (Sigma Aldrich), 0.05 mg oxaliplatin (Sigma Aldrich) or 200 µg of anti-CD25 (clone PC61) mAb mouse IgG2a. At day 21 after tumour injection, mice were euthanised and tumour-bearing lungs were collected for further analysis.

2.5.2.4 Immunotherapy experiments

C57BL/6 mice were injected intravenously with 80,000 KPB6.F1 cells or 300,000 CMT-167 cells on day 0. KPB6.F1 tumour-bearing mice were treated with therapeutic antibodies at the dose indicated in each figure by intraperitoneal injection on days 6, 7, 10 and 13 after the tumour cell injection. Mice were euthanised 17 days after tumour challenge and tumour bearing-lungs were recovered for further analysis by flow cytometry.

CMT-167 tumour-bearing mice received therapeutic antibodies by intraperitoneal injection on days 5, 6, 9 and 12 post-tumour injection. At day 19 after tumour cell injection, mice were euthanised and tumour-bearing lungs were collected. The right lung was processed and analysed by flow cytometry, whilst the left lung was fixed, and H&E stained.

Haematoxylin and Eosin staining

Haematoxylin and Eosin (H&E) staining of formalin-fixed left lungs was performed by Ms Adriana Resende in the Pathology Core Facility at UCL.

Metastatic index calculation

H&E slides were used to calculate the metastatic index (Qian et al., 2009). Briefly, the area of tumour nodules and total area of the left lung were calculated for three different slides for each mouse to obtain the volume of tumours and total volume of the lung. The metastatic index was then calculated for each mouse with the following formula:

$$Metastatic\ index = \frac{Metastasis\ volumen}{Total\ lung\ volumen}$$

2.5.3 Single cell suspension for flow cytometry analysis

Tumours or tumour-bearing lungs were chopped and digested with a mix of Liberase TL (300 µg/mL, Roche) and DNAse (2 µg/mL, Roche) in RPMI for 30 minutes at 37˚C. A single cell suspension was obtained, resuspended in 3 mL of RPMI and put into a 3 mL single density gradient (Histopaque 1119, Sigma-Aldrich). After centrifugation (700G, 10 minutes, 25˚C) cells were collected from the gradient interface and resuspended in a define volume of FACS buffer (2% FBS, 2mM EDTA in PBS) for further staining.

2.6 Flow cytometry staining and analysis

2.6.1 Surface staining

Samples were resuspended in 50 µl of SuperBlock (2% FBS, 5% rat serum, 5% mouse serum, 5% rabbit serum, 25 µg/mL anti-FcγR mAb in PBS) with a mix of surface antibodies and stained during 30 minutes at 4˚ C in dark. Then, samples were washed twice with FACS buffer (2% FBS, 2mM EDTA in PBS) and either, continue with intracellular staining or fixed in PBS containing 1% paraformaldehyde (PFA). The fluorochrome labelled antibodies used for staining are listed below.

2.6.2 Intracellular staining

Cells were fixed and permeabilized using the Fixation/Permeabilization buffer (Fixation/Permeabilization Concentrate diluted in Fixation/Permeabilization Diluent, both from Thermo Fisher) during 25 minutes at 4˚ C. Samples were washed twice with Permeabilization buffer (Thermo Fisher) and then intracellular stained in a mix of Permeabilization buffer plus 10% SuperBlock with intracellular antibodies for 30 minutes at 4˚C. Cells were then washed twice and resuspended in 150µl of FACS buffer and 10,000 counting beads in 50µl PBS were added prior to data acquisition.

Antigen	Clone	Conjugate	Company	Catalogue number
4-1BB	17B5	Biotin	ThermoFisher	13-1371-82
CD3	17A2	Brilliant™ Ultraviolet 737	BD Bioscience	564380
CD3	17A2	Brilliant™ Violet 785	BioLegend	100232
CD4	GK1.5	Brilliant™ Ultraviolet 496	BD Bioscience	564667
CD4	RM4-5	Brilliant™ Violet 510	BioLegend	100559
CD4	RM4-5	v500	BD Bioscience	560782
CD45	30-F11	Brilliant™ Ultraviolet 563	BD Bioscience	565710
CD8a	53-6.7	Brilliant™ Ultraviolet 805	BD Bioscience	564920
CD8a	53-6.7	Brilliant Violet 650	BioLegend	100742
CD8a	53-6.7	BV 650	BD Bioscience	563234
CD25	7D4	Alexa Fluor 660	ThermoFisher	50-0252-82
CD25	PC61.5	Biotin	ThermoFisher	13-0251-85
CD25	7D4	FITC	BD Bioscience	553071
CD25	PC61.5	Alexa Fluor 488	ThermoFisher	53-0251-82
CD40L	24-31	PE	BioLegend	12-1548-42
CTLA-4	UC10-4B9	Brilliant Violet 605	BioLegend	106323
CTLA-4	UC10-4B9	APC	ThermoFisher	17-1522-82
FoxP3	FJK-16s	Alexa Fluor 700	ThermoFisher	56-5773-82
FoxP3	FJK-16s	eFluor 450	ThermoFisher	48-5773-82

GITR	DTA-1	APC	ThermoFisher	17-5874-81
GITR	DTA-1	BV510	BD Bioscience	740192
Granzyme B	GB12	APC	ThermoFisher	MHGB05
Granzyme B	GB12	PE	ThermoFisher	MHGB04
ICOS	C398.4A	PE-Cy7	BioLegend	313520
Ki67	SolA 15	Alexa Fluor 700	ThermoFisher	56-5698-82
Ki67	SolA 15	eFluor450	ThermoFisher	48-5698-82
LAG3	C9B7W	Brilliant Violet 650	BioLegend	125227
LAG3	C9B7W	PE	ThermoFisher	12-2231-82
NK1.1	PK136	Brilliant™ Ultraviolet 395	BD Bioscience	564144
NK1.1	PK136	Alexa Fluor 488	BioLegend	108718
OX-40	OX-86	PE-Cy7	BioLegend	119415
OX-40	OX-86	BV786	BD Bioscience	740945
PD-1	29F.1A12	PE-Dazzle™ 594	BioLegend	135228
PD-1	RMP1-30	PerCP-eFluor™ 710	ThermoFisher	46-9981-82
Streptavidin	-	Brilliant Violet 605	BioLegend	405229
Streptavidin	-	Brilliant Violet 711	BD Bioscience	563262
TIGIT	GIGD7	PerCP-eFluor™ 710	ThermoFisher	46-9501-82
TIM-3	RMT3-23	PE	BioLegend	119704
Viability Dye	-	eFluor™ 780	ThermoFisher	65-0865-18

2.6.3 Quantification of tumour-infiltrating lymphocytes

The total number of infiltrating lymphocytes was calculated using counting bead as a reference (Cell Sorting Set-up Beads (for UV lasers), by Thermo Fisher). The beads were added prior to acquisition of the sample. The normalised number of lymphocytes per gram of tumour was calculated using the following formula. As an example, the normalised number of $CD4^+$ T-cells would be calculated as follow:

$$Normalised\ number\ CD4 = \left(\frac{Acquired\ number\ CD4 * Beads\ added\ to\ sample}{Acquired\ beads}\right) * {}^{1}/_{Tumour\ mass}$$

2.7 Molecular biology

2.7.1 Anti-ICOS 37A10 mAb and mouse ICOS sequences

The sequences of the variable regions of the heavy chain and light chain of the anti-ICOS 37A10 mAb were obtained from a US patent application from Jounce Therapeutics (US20160304610A1) (Sazinsky et al., 2016). The consensus sequence of mouse ICOS was obtained from NCBI database (NCBI Reference Sequence: NM_017480.2).

The sequences were purchased as a GBlock fragment (Integrated DNA Technologies) with restriction sites for further enzymatic digestion.

The fragments of the heavy and light chain of anti-ICOS 37A10 antibody were amplified by a PCR as explained below.

2.7.2 Fusion PCR

In order to modify the constant region of the antibody to the desire isotype a fusion PCR was done using Phusion High-Fidelity DNA Polymerase and the Phusion HF Buffer (both from New England Biolabs). Firstly, the variable region and the constant region are amplified separately. The size of the fragments was confirmed by an agarose gel, and the DNA was extracted (see section 2.7.3) to be used in the second step of the fusion PCR to generate the complete sequences of the heavy and the light chain of the antibody.

First PCR step: each fragment

35.5 µL	ddH_2O
10 µL	Phusion HF Buffer 5X
1 µL	dNTPs
0.5 µL	Phusion Polymerase
1 µL	Forward primer
1 µL	Reverse primer
1 µL	Template

Second PCR step: fusion of the fragments

120.75 µL	ddH_2O
35 µL	Phusion HF Buffer 5X
3.5 µL	dNTPs
1.75 µL	Phusion Polymerase
3.5 µL	Forward primer
3.5 µL	Reverse primer
3.5 µL	Cleaned up PCR product 1
3.5 µL	Cleaned up PCR product 2

Programme

98 ˚C	2 minutes	
98 ˚C	40 seconds	} 35 cycles
65 ˚C	40 seconds	
72 ˚C	60 seconds/Kb of template	
72 ˚C	10 minutes	
4 ˚C	∞	

2.7.3 DNA gel extraction

DNA was extracted using QIAquick Gel Extraction Kit (Qiagen) according to manufacturer's protocol.

2.7.4 Restriction digestion and ligation

After the fusion PCR, the sequence of anti-ICOS 37A10 variable and constant region (either mouse IgG1 for the heavy chain or kappa for the light chain) were enzymatically digested and ligated into an expression plasmid. In the case of mouse ICOS, after amplification by PCR it was directly digested and ligated into a plasmid.

Restriction enzymes were obtained from New England Biolabs and used according to manufacturer's recommendations.

Diagnostic digestion

2 µL	Buffer (depending of enzymes used)
1 µL	DNA
0.5 µL	Each enzyme
16 µL	ddH_2O

Incubate at 37˚ C for 1 hour.

Complete digestion of plasmid or PCR product

4 µL	Buffer (depending of enzymes used)
30 µL	DNA
1 µL	Each enzyme
4 µL	ddH_2O

Incubate at 37˚ C for 4 hours.

Ligation reactions were done with T4 DNA Ligase and the T4 Ligase Reaction Buffer 10X (both from New England Biolabs).

Ligation

1 µL	T4 Ligase
1 µL	Buffer
4 µL	Plasmid
4 µL	Insert

Incubate at room temperature for 1 hour.

2.7.5 Bacteria transformation

A vial of NEB5α chemically competent *E. coli* bacteria (New England Biolabs) was thawed on ice, and 5 µL of ligation or cloning product was added without pipetting. After 30 minutes incubation on ice, bacteria were heat shocked for 35 seconds at 42 ˚C and left another 30 minutes recovering in SOC medium at 37 ˚C. Bacteria were plated on a LB agar plate with ampicillin (50 µg/mL) and incubated over night at 37˚ C.

2.7.6 DNA purification from bacteria

Single colonies were selected from LB agar plates and grown over night at 37˚ C, either in 3 mL (Minipreps) or 200 mL (Midipreps) of LB broth medium with ampicillin (50 µg/mL). After centrifugation, plasmid DNA was purified using QiaPrep Spin Miniprep kit (Qiagen) or NucleoBond Xtra Midi (Macherey-Nagel) respectively, following manufacturer's protocol.

2.7.7 Transfection and virus production

HEK 293T were transfected using FuGENE 6 Transfection Reagent (Promega). Fugene was added to plain RPMI medium and incubated for 5 minutes. Later DNA was added to Fugene-RPMI mix, incubated another 15 minutes at room temperature and added drop-wise into HEK 293T plate. For anti-ICOS 37A10 heavy chain mIgG1 and anti-ICOS 37A10 light chain, HEK 293T cells were co-transfected with two different plasmids containing either construct (heavy or light chain) to produce a small amount of the antibody and check its binding by flow cytometry, before outsourcing its production to Evitria AG (Switzerland).

For murine ICOS virus production after transfecting HEK293T cells with the plasmid containing murine ICOS sequence, the supernatant was collected 48 and 72 hours after transfection and snap freeze immediately for further use.

470 µL	Plain RPMI
30 µL	Fugene
3.125 µg	Envelope plasmid pMD.G (just for virus production)
4.69 µg	Gag-pol plasmid pPAX2 (just for virus production)
4.69 µg	Retroviral construct

2.7.8 Transduction

For transducing Jurkat-NFAT.GFP cells to make them express murine ICOS, the cells were cultured in a non-tissue culture treated plate previously coated with retronectin 25 µg/mL. The viral supernatant was added to the cells and then were centrifuged without break (1000G, 40 minutes, 25˚C) and incubate at 37˚ C. Cells were checked for transduction 7 days later by flow cytometry. Cells expressing murine ICOS were electronically sorted and named Jurkat-NFAT.GFP/mICOS.

2.8 CD40L assay

Jurkat-NFAT.GFP/mICOS were activated with plate-bound 250 ng of anti-CD3 mAb (clone OKT3) and either plate-bound isotype control, anti-ICOS mAb (clone C398.4A, used as a positive control) or anti-ICOS mAb (clone 37A10). After 72 hours, cells were stained and the levels of CD40L were measured by flow cytometry.

2.9 Data acquisition and analysis

Flow cytometry data was obtained using LSR-Fortessa analyser (BD Biosciences) and BD FACSymphony™ (BD Biosciences). Electronic cell sorting was done with FACS Aria III sorter (BD Biosciences). Flow cytometry data analysis was done with FlowJo v10.5.0. Fusion PCR was designed with SnapGene 3.3.2. Flow cytometry data was also analysed using PhenoGraph clustering using the pipeline Cytofpipev0.2.

Quantification of the area of H&E slides was done using NDP.view 2.3.

Statistical analysis was performed with GraphPad Prism 6.0. Heatmapping was generated using RStudio Desktop 1.0.44.

3 Results: Testing anti-ICOS monoclonal antibody therapy in mouse models of cancer

3.1 Introduction

3.1.1 Evidence for anti-ICOS mAb as a new immunotherapy target

ICOS is a co-stimulatory molecule expressed on the surface of activated T-cells. As a member of the CD28 superfamily, it shares functional homology with CD28 and CTLA-4 (Hutloff et al., 1999). Whilst ICOS is upregulated on effector T-cells ($CD4^+$ $FoxP3^-$and $CD8^+$ T-cells) and Treg cells ($CD4^+$ $FoxP3^+$) after T-cell activation, in the absence of inflammatory stimuli Treg cells express higher levels of ICOS than effector T-cells, which is thought to be driven by chronic (self)-antigen stimulation (Redoglia et al., 2018; Wikenheiser and Stumhofer, 2016).

The different levels of expression of ICOS on effector and Treg cells has generated different views on the role of this co-stimulatory receptor on the immune response to cancer. Data obtained from the analysis of tumour infiltrating lymphocytes (TILs) in melanoma patients clearly shows that ICOS is highly expressed on $CD4^+CD25^+$ Treg cells, and that Treg cells co-expressing ICOS ($CD4^+CD25^+ICOS^{hi}$) have higher suppressive capacity than $CD4^+CD25^+ICOS^{lo}$ regulatory T-cells (Strauss et al., 2008). Additionally, melanoma cells can express ICOSL suggesting that tumours could subvert anti-tumour immunity by directly activating $ICOS^+$ Treg cells, enhancing their suppressive activity (Martin-Orozco et al., 2010). Furthermore, melanoma patients treated with high doses of IL-2 preferentially expanded $ICOS^+$ Treg cells in the blood, which correlated with impaired clinical outcome (Sim et al., 2014). On the other hand, another study identified a positive correlation between high level of ICOS expression and improved survival in colorectal cancer (CRC) patients, unfortunately they just described such population as $CD4^+ICOS^+$, being unable to distinguish between effector or regulatory T-cells (Zhang et al., 2016).

Clinical data from a small pre-operative clinical trial evaluating the safety of ipilimumab (anti-CTLA-4 hIgG1 mAb) showed increased frequency of $CD4^+ICOS^+$ cells in the tumour and peripheral blood from patients with urothelial carcinoma of the bladder (Carthon

et al., 2010). Additionally, in a retrospective study of melanoma patients treated with ipilimumab, the authors found that a persistent population of $CD4^+ICOS^{hi}$ T-cells in the blood correlated with increased overall survival (Di Giacomo et al., 2013). Furthermore, the $CD4^+ICOS^+$ cells obtained from peripheral blood of bladder cancer patients treated with ipilimumab produce IFNγ in recognition of a tumour antigen (NY-ESO-1) presented by APCs (Liakou et al., 2008). Breast cancer patients treated with tremelimumab (another anti-CTLA-4 hIgG2 mAb) and NSCLC patients treated with chemotherapy and ipilimumab showed an increased frequency of $CD4^+ICOS^+$ and $CD8^+ICOS^+$ in the periphery (Vonderheide et al., 2010; Yi et al., 2017). This increase in the frequency of $CD4^+ICOS^+$ has recently been suggested as a potential pharmacodynamic biomarker of ipilimumab treatment (Ng Tang et al., 2013).

Further experiments in mouse models have primarily supported an activator role of ICOS/ICOSL interactions in the context of cancer. Experiments carried out in the mouse B16/BL6 melanoma model, showed that anti-CTLA-4 mAb treatment increased the frequency of $IFNγ^+$ tumour-reactive $CD4^+FoxP3^-ICOS^+$ and $CD8^+ICOS^+$ cells. Accordingly, mice deficient in ICOS ($ICOS^{-/-}$) or ICOSL ($ICOSL^{-/-}$) failed to respond to anti-CTLA-4 mAb and GM-CSF-expressing tumour cell vaccines (GVAX), demonstrating the critical role of the pathway in the context of immunotherapy (Fu et al., 2011). In addition, experiments combining anti-CTLA-4 mAb with tumour cell-based vaccines engineered to express ICOSL (IVAX) in B16.F10 tumours, showed that the combination therapy significantly improved survival and tumour rejection when compared with anti-CTLA-4 mAb monotherapy (Fan et al., 2014).

Together, these data underscore the relevance of the ICOS pathways as a potential target to enhance the activity of the immune response against cancer and highlight the need to develop new means to deliver activating signals via ICOS and to evaluate its potential synergy with other therapeutic modalities

3.1.2 ICOS as a current clinical target

In the context of cancer immunotherapy, ICOS has become an important target to be studied and tested. There are currently three different clinical trials targeting ICOS as a therapy for different types of cancer (NCT02520791, NCT02723955, NCT02904226), and a

fourth trial is soon to begin in a collaboration between Kymab and Roche by 2019 (Kymab News Release, 2018).

The first anti-ICOS monoclonal antibody (mAb) developed as a therapy was MEDI-570 mAb by MedImmune. It was developed as an antagonistic fully human afucosylated IgG1κ monoclonal antibody with enhanced ADCC activity, designed to deplete auto-reactive $ICOS^+$ T-cells found in patients with the autoimmune disease Systemic Lupus Erythematosus (NCT01127321) (Nicholson et al., 2017). Even though that clinical trial was terminated due to business reasons (NCT01127321), MEDI-570 antibody is currently in a new clinical trial sponsored by the NCI (National Cancer Institute, USA). In this new phase I clinical trial (NCT02520791), which is currently recruiting patients, anti-ICOS MEDI-570 mAb is being tested as a treatment for patients with relapsed or refractory Peripheral T-cell Lymphoma and angioimmunoblastic T-cell Lymphoma. The aim of this trial is to target ICOS expressed on T-cells by blocking the interaction with ICOSL expressed by plasmacytoid dendritic cells (pDCs), thereby avoiding the proliferation and accumulation of Tregs in the tumour and the secretion of IL-10 by $CD4^+$ cells, allowing cytotoxic function of T-cells in the absence of Treg suppression, a phenomenon observed in breast cancer (Faget et al., 2013, 2012).

Currently, MEDI-570 is the only anti-ICOS antibody in development that has an antagonistic function and that is being tested in clinical trials. The current consensus in developing an agonistic anti-ICOS mAb relies on the hypothesis that an agonistic antibody may trigger the co-stimulatory activity of ICOS on effector T-cells, promoting T-cell activation and tumour control.

In accordance with this concept, GlaxoSmithKline (GSK) is running an open label clinical trial testing its GSK3359609 anti-ICOS antibody for solid tumours as a monotherapy or in combination with pembrolizumab (anti-PD-1) in the INDUCE-1 trial (NCT02723955). GSK3359609 is a humanised IgG4 non-depleting isotype, selected based on its potent agonistic activity against human ICOS (Angevin et al., 2017). This phase I study which aims to evaluate safety of GSK3359609 is now recruiting patients with relapse or refractory solid tumours. The first dose escalation studies as monotherapy were completed without dose limiting toxicities (Angevin et al., 2017). The hypothesis behind the INDUCE-1 trial is to promote the activity of T-cells associated with clinical benefit, without depleting them. One potential concern with this approach is that Treg cells found in the tumour normally express

high levels of ICOS (Strauss et al., 2008), hence an agonistic anti-ICOS mAb might promote the activation and suppressive function of $ICOS^+$ Treg cells.

A third open label clinical trial testing an anti-ICOS mAb is the ICONIC trial. Lead by Jounce Therapeutics, the ICONIC trial aims to test JTX-2011 mAb, an agonistic human IgG1 anti-ICOS mAb with additional depleting activity, as a monotherapy and in combination with anti-PD-1 mAb in patients with advanced or refractory solid tumours (NCT02904226). Recently, the study added a new treatment arm aiming to test another group of patients with anti-CTLA-4 mAb and JTX-2011 mAb (NCT02904226). The rationale for designing an agonistic anti-ICOS mAb with additional depleting activity is based on prior work on anti-CTLA-4 mAb. Experiments with anti-CTLA-4 mAb demonstrated that, based on the high levels of CTLA-4 on Treg cells and low levels on effector T-cells, the antibody can preferentially deplete Treg cells whilst at the same time block the inhibitory activity of CTLA-4 on effector T-cells (Simpson et al., 2013; Arce Vargas et al., 2018; Bulliard et al., 2013). In the same manner, based on the high levels of ICOS on Treg cells compared to effector $CD4^+$ and $CD8^+$ T-cells, an anti-ICOS human IgG1 mAb should deplete $ICOS^{hi}$ Treg cells (by ADCC) whilst delivering activating signals to effector $CD4^+$ and $CD8^+$ T-cells expressing lower levels of ICOS. The first results of this phase I/II trial were presented recently, leading to the modification of the trial to include another condition evaluating the combination of JTX-2011 with ipilimumab (anti-CTLA-4 mAb) as one of the tested treatments (Yap et al., 2018). The addition of anti-CTLA-4 mAb treatment in combination with JTX-2011 in the trial was motivated by the lack of clinical benefit observed in the trial of the JTX-2011 Ab alone or in combination with nivolumab.

The fourth anti-ICOS antibody is being developed by Kymab, the KY1044 mAb, is yet to be tested in the clinic. Similar to Jounce's JTX-2011, KY1044 is also a hIgG1κ agonistic anti-ICOS mAb with depleting activity. Kymab's pre-clinical data shows promising results of KY1044 in combination with anti-PD-L1 mAb *in vivo* (Sainson et al., 2018a), and a clinical trial in collaboration with Roche is due on 2019, as announced by a recent press release (Kymab News Release, 2018).

3.2 Rationale and aims

Although a lot of clinical and commercial interest has been developed around the ICOS/ICOSL pathway, there is still a lack of understanding on how this pathway affects T-cell function and anti-tumour immunity. Moreover, there is no consensus whether the more appropriate method for targeting this pathway is a depleting or a non-depleting activity, nor if an agonistic or an antagonistic function should be preferred The development of anti-ICOS antibodies that promote ADCC for the elimination of Treg may be risky, because the antibody could also target and eliminate highly activated $CD4^+$ and $CD8^+$ effector T-cells expressing high levels of ICOS on their surface. This observation becomes especially important when trials are starting to recruit patients to be treated with combination anti-CTLA-4 mAb and anti-ICOS mAb, as it has been previously shown that anti-CTLA-4 mAb increases ICOS expression on activated effector T-cells and that the presence of $ICOS^+$ T-cells is associated with clinical benefit in patients treated with anti-CTLA-4 mAb (Vonderheide et al., 2010; Yi et al., 2017).

In order to prevent potential depletion of $ICOS^{hi}$ effector T-cells, we hypothesised that an agonistic non-depleting anti-ICOS mAb would be the best strategy to deliver maximal anti-tumour activity *in vivo*, especially in combination with Treg depleting agents such as anti-CTLA-4 mAb. Therefore, the aims of this project were:

1. To develop an assay to determinate the agonistic function of anti-ICOS antibodies.
2. To characterise the pattern of expression of ICOS on tumour infiltrating lymphocytes in different mouse models of cancer.
3. To test the anti-tumour efficacy of depleting and non-depleting anti-ICOS mAb isotypes.
4. To evaluate the anti-tumour efficacy of different isotypes of anti-ICOS mAb in combination with anti-PD-1 mAb and anti-CTLA-4 mAb.
5. To describe the impact of anti-ICOS mAb in the tumour microenvironment to understand mechanisms underpinning response and resistance.

3.3 Anti-ICOS 37A10 clone has agonistic activity *in vitro*

Since the aim of this work was to test and promote the agonistic function of anti-ICOS mAbs *in vivo*, the first objective was to design an assay to test the agonistic activity driven by ICOS stimulation on T-cells. As ICOS stimulation has been associated with the expression of CD40L on T-cells (McAdam et al., 2001), the expression of CD40L was used as a readout. To generate an assay to evaluate CD40L expression, Jurkat cells (Jurkat-NFAT.GFP cells), used as a reporter for NFAT signalling, were transduced to express mouse ICOS (mICOS) constitutively on their surface. To validate the assay, Jurkat-NFAT.GFP/mICOS cells were activated with plate-bound anti-CD3 (OKT3 clone) mAb and increasing concentrations of plate-bound anti-ICOS mAb as a positive control (C398.4A clone, a commercially available agonistic antibody), or isotype control. After 72 hours of activation, the frequency of $CD40L^+$ was analysed by flow cytometry. The difference in the percentage of $CD40L^+$ cells between the anti-ICOS mAb-treated versus isotype control was plotted for every concentration tested. As shown in Figure 3.1A, plate-bound anti-ICOS mAb increases the frequency of $CD40L^+$ Jurkat cells in a dose-dependent manner, demonstrating that the assay is suitable to measure agonistic activity of unknown anti-ICOS antibodies. The assay was also performed with soluble anti-ICOS mAb, but no $CD40L^+$ upregulation was observed (Supplementary figure 7.1A).

The sequence of the variable region of the cross-reactive mouse and human anti-ICOS mAb (clone 37A10) was obtained from a patent application publicly available (Sazinsky et al., 2016). The variable region of the heavy chain was cloned into a mouse IgG1 and IgG2a backbone, while the variable region of the light chain was cloned into a kappa (κ) chain. Expression plasmids carrying the heavy and light chain of the 37A10 anti-ICOS antibody were used to transfect HEK293T cells and the supernatant containing the anti-ICOS mAb was recovered and concentrated.

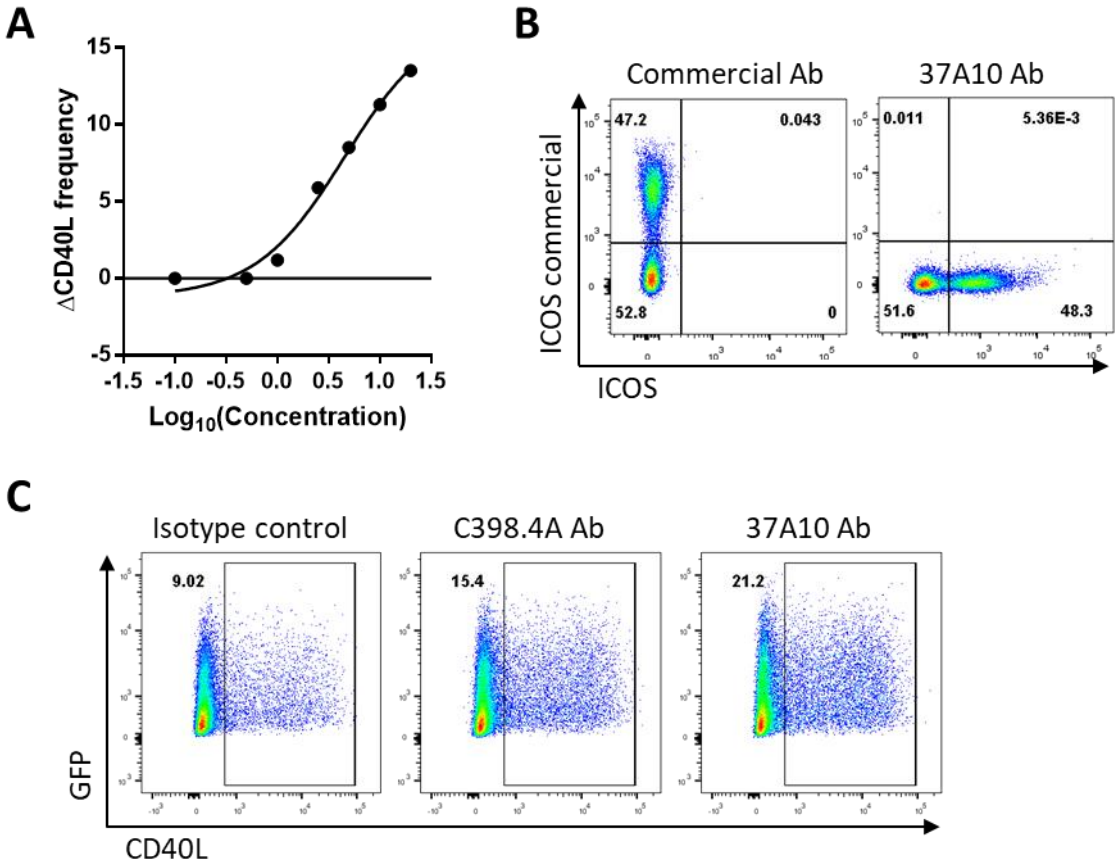

Figure 3.1. Anti-ICOS monoclonal antibody 37A10 exhibits agonistic activity in vitro.

(A) Jurkat cells transduced to constitutively express mouse ICOS and NFAT.GFP reporter were activated with a combination of plate-bound anti-CD3 mAb clone OKT3 (250 ng) and increasing concentrations of isotype control or anti-ICOS (clone C398.4A) mAb. After 72 hours, cells were stained and the levels of CD40L were measured by flow cytometry. The difference in the frequency of $CD40L^+$ cells between the anti-ICOS treatment and the isotype controls versus the logarithm of the concentration are shown. Representative graph of two independent experiments. **(B)** Activated splenocytes were stained with a commercial (clone C398.4A) or the tested (clone 37A10) anti-ICOS antibody to check the binding of the 37A10 clone. **(C)** Jurkat cells, as above, were activated with plate-bound anti-CD3 (OKT3) mAb plus 20μg/mL isotype control, anti-ICOS (clone C398.4A) mAb or anti-ICOS (clone 37A10) mAb. Cells were stained and CD40L frequency was evaluated by flow cytometry. Representative plots from three independent evaluations.

To test the binding of the anti-ICOS mAb, splenocytes were activated for 16 hours with 800 ng/mL of Concanavalin A (ConA) plus 1 pg/mL of IL-7 to increase the expression of ICOS on the cell surface. The 37A10 anti-ICOS mAb binds to ICOS, detecting a similar frequency of $ICOS^+$ cells that the commercial anti-ICOS (clone C398.4A) mAb on activated splenocytes (Figure 3.1B). After confirming the binding of the 37A10 anti-ICOS mAb, the agonistic function was tested with the established assay as outlined above. Plate-bound anti-CD3 mAb together with plate-bound anti-ICOS mAb or isotype control were used as shown in Figure 3.1C. The 37A10 anti-ICOS mAb showed to have an increased agonistic activity when compared with the C398.4A anti-ICOS mAb. On the contrary, when the assay was performed with plate-bound anti-CD3 and soluble anti-ICOS mAb, no upregulation of CD40L was observed compared with the isotype control (Supplementary figure 7.1A). Taken together this data validates the binding and agonistic function of the 37A10 anti-ICOS mAb *in vitro*.

3.4 ICOS is highly expressed on tumour infiltrating regulatory T-cells

To evaluate the expression of ICOS in different murine cancer models, BALBc or C57BL/6 mice were injected in the flank with the tumour cell lines CT-26 (colon carcinoma), MCA-205 (fibrosarcoma) or CMT-167 (lung carcinoma), respectively. After 11 days, the levels of ICOS were evaluated in draining lymph nodes (LNs) and tumour infiltrating lymphocytes (TILs) by flow cytometry. A very small frequency of effector $CD8^+$ and $CD4^+Foxp3^-$ T-cells expressed ICOS in the draining LNs of tumour bearing mice, whereas approximately 30% of regulatory T-cells (Tregs) expressed ICOS (Figure 3.2A). On the contrary, the frequency and level of expression of ICOS was increased for all the infiltrating T-cell subsets in the tumour microenvironment, although at different levels depending on the tumour type. Whilst both frequency and level of ICOS expression where increased in tumour infiltrating T-cells, regulatory T-cells (Tregs) remained as the population expressing the highest levels of this receptor (Figure 3.2A).

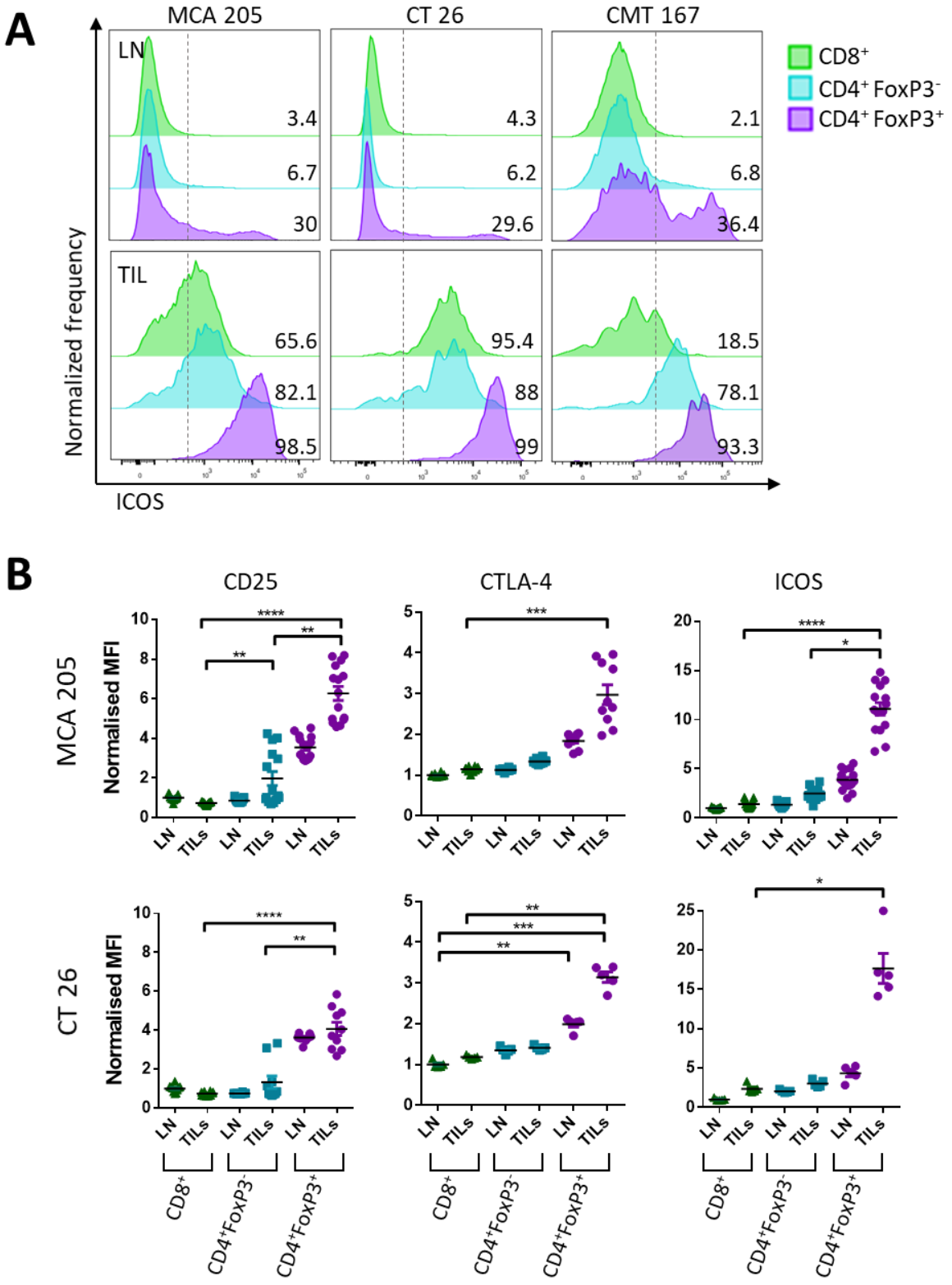
A
MCA 205
CT 26
CMT 167
LN
TIL
3.4
6.7
30
4.3
6.2
29.6
2.1
6.8
36.4
65.6
82.1
98.5
95.4
88
99
18.5
78.1
93.3
CD8+
CD4+ FoxP3-
CD4+ FoxP3+
Normalized frequency
ICOS
B
CD25
CTLA-4
ICOS
MCA 205
CT 26
Normalised MFI
LN
TILs
CD8+
CD4+FoxP3-
CD4+FoxP3+

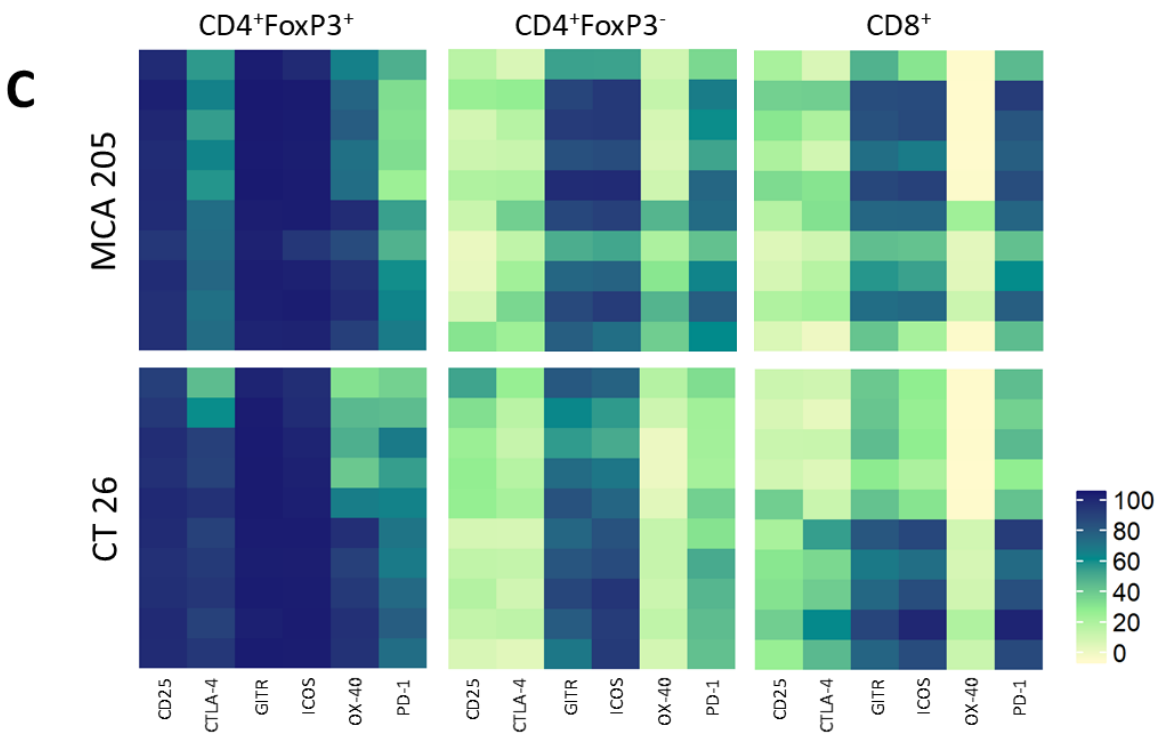

Figure 3.2. CD25, CTLA-4 and ICOS are highly expressed on tumour infiltrating regulatory T-cells.

C57BL/6 and BALBc mice were injected subcutaneously with the tumour cell lines MCA-205 or CMT-167 and CT-26, respectively. After 11 days the tumours and draining LNs were collected and processed into a single cell suspension. Cells from LN and infiltrating T-cells (TILs) were stained and evaluated by flow cytometry. **(A)** Representative histograms showing the expression of ICOS on regulatory, effector $CD4^+$ and $CD8^+$ T-cells found in draining LNs and TILs. The number indicates the frequency of $ICOS^+$ cells. **(B)** MFI (median fluorescence intensity) fold-increase normalised to the MFI of $CD8^+$ from LN of the indicated co-inhibitory or co-stimulatory molecule in the three different T-cell subsets evaluated. **(C)** Heatmap showing the frequency of co-inhibitory and co-stimulatory molecules expressed by three different T-cells subsets in the tumour. Horizontal bars represent the mean, errors bars shown ± standard error of the mean (SEM). p values were calculated using non-parametrical analysis Kruskal-Wallis test. ns = $p > 0.05$, *$p \leq 0.05$, **$p \leq 0.01$, ***$p \leq 0.001$, **** $P \leq 0.0001$.

Of relevance, almost all the Treg cells in the tested tumour models expressed ICOS, but also the frequency of effector $CD4^+$ and $CD8^+$ T-cells expressing ICOS is very high in the tumour. This high ICOS frequency of expression suggests that using anti-ICOS mAb in a depleting isotype to eliminate Treg cells in the tumour may also deplete effector T-cell subsets, given their high frequency and level of expression of ICOS. As Treg depletion in the tumour (by targeting CTLA-4 or CD25 through the use of depleting antibodies) has shown effectivity as a strategy to promote tumour rejection (Arce Vargas et al., 2018, 2017), the level of expression (measured as MFI) of common receptors expressed on Treg cells were compared between the different T-cell subsets in the TILs and draining LN after being normalised as fold-increase relative to the MFI of $CD8^+$ T-cells in the draining LN (Figure 3.2B). The level of expression of CD25 is very low on effector $CD4^+$ and $CD8^+$ cells in draining LN and TILs, whereas on Treg cells the MFI can be up to six times higher than the other T-cell subsets within the tumour. Higher level of expression of CTLA-4 was also observed on Tregs infiltrating the tumour compared with the other T-cell populations. The trend is similar for ICOS in the two evaluated models of cancer, showing the highest MFI in tumour infiltrating Treg cells (Figure 3.2B). However, when comparing the frequency of expression of those markers it becomes clear that using ICOS as a target for Treg depletion may be challenging due to its expression pattern on tumour infiltrating effector T-cells. A heatmap was produced to illustrate the frequency of expression of different immune co-stimulatory and co-inhibitory molecules between the three main T-cell subsets (Figure 3.2C). The frequency and levels of expression of CD25 and CTLA-4 on $CD4^+$ and $CD8^+$ T-cells are very low when compared to Treg, whilst ICOS expression is high in both effector populations. Therefore, it can be hypothesised that using an anti-ICOS mIgG2a mAb in the same manner that anti-CTLA-4 mAb or anti-CD25 mAb has been used by various authors (Arce Vargas et al., 2018, 2017; Simpson et al., 2013; Du et al., 2018; Tang et al., 2018) could lead to depletion of effector T-cells together with Treg cells. For this reason, it was hypothesised that the human IgG1 isotype (with depleting activity) chosen for the clinical anti-ICOS mAb (JTX-2011) from Jounce Therapeutics may not be the best isotype.

3.5 Anti-ICOS and anti-PD-1 combination therapy fails to provide benefit in mouse models of cancer

We next sought to determine whether agonistic anti-ICOS mAb with a depleting mIgG2a isotype were able to drive tumour control as a single agent or in combination with anti-PD-1 blocking antibodies. As the current clinical trial by Jounce is evaluating the combination of anti-ICOS mAb depleting isotype with anti-PD-1 mAb therapy, this combination was the first tested in our different preclinical models. Mice were injected with one of four different cell lines (CMT-167, CT 26, MCA 205 or MC 38) in the flank and after developing palpable tumours, mice were treated with three doses of anti-ICOS mIgG2a mAb (anti-ICOSm2a), anti-PD-1 ratIgG2a mAb (anti-PD-1r2a) or a combination of both antibodies. Individual tumour growth curves were drawn for every treatment tested in all four different models (Figure 3.3A). Anti-ICOS mAb and anti-PD-1 mAb either as single agents or as combination failed to promote tumour control in CMT 167, CT26 and MC38 mouse models (Figure 3.3A). The results with anti-PD-1 were expected as these models are known to be resistant to anti-PD-1 mAb. However, the lack of response of the agonist anti-ICOSm2a contradicts the data presented by Jounce and Kymab with anti-ICOS mAbs of similar isotypes (Sainson et al., 2018a; Yap et al., 2018). In the case of the chemically induced MCA 205 fibrosarcoma model, a partial increase in the survival was observed with anti-PD-1 mAb monotherapy as measured by median overall survival and, although not statistically significant, anti-ICOSm2a mAb tends to revert this response (Figure 3.3B).

Based on the high levels of ICOS expression observed on tumour-infiltrating effector T-cells (Figure 3.2), we hypothesised that the depleting activity of the anti-ICOSm2a mAb is preventing its activity as a single agent and, most importantly, even existing a prohibitive effect on the efficacy of anti-PD-1 mAb therapy.

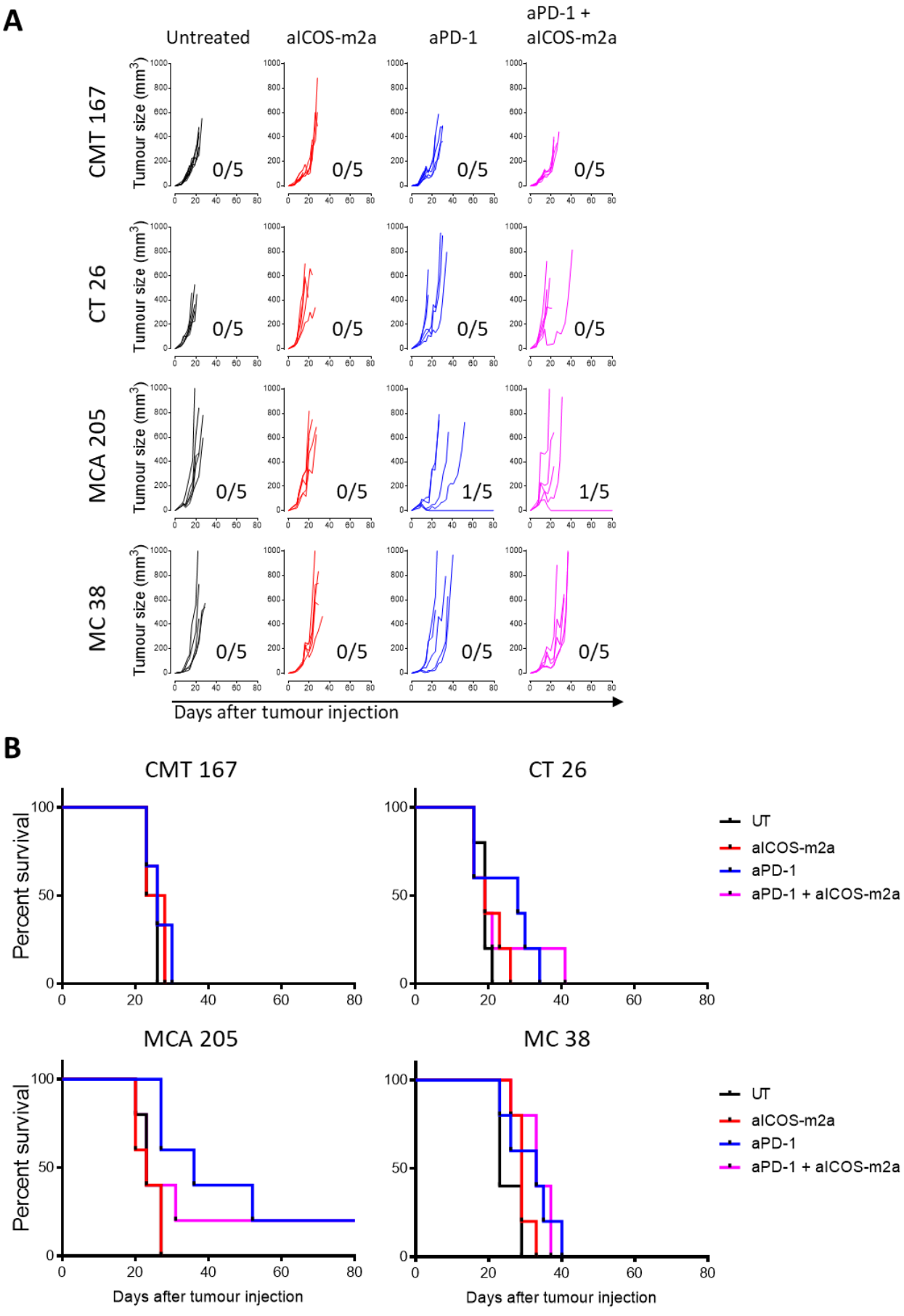
A
Untreated
aICOS-m2a
aPD-1
aPD-1 +
aICOS-m2a
CMT 167
CT 26
MCA 205
MC 38
Tumour size (mm3)
0/5
0/5
0/5
0/5
0/5
0/5
0/5
0/5
0/5
1/5
1/5
0/5
0/5
0/5
0/5
Days after tumour injection
B
CMT 167
CT 26
MCA 205
MC 38
Percent survival
UT
aICOS-m2a
aPD-1
aPD-1 + aICOS-m2a
Days after tumour injection

Figure 3.3. Combination of anti-PD-1 mAb with anti-ICOSm2 mAb does not provide anti-tumour protection.

C57BL/6 and BALBc mice were injected subcutaneously with the tumour cell lines CMT-167, MCA 205 and MC 38 (C57BL/6) or CT-26 (BALBc). Five mice per group were treated on day 6, 9 and 12 with 100 μg of anti-ICOSm2a mAb, 200 μg of anti-PD-1 r2a mAb or a combination of both as indicated. **(A)** Individual tumour growth curves for different mouse models of cancer and treatment conditions. Numbers show the fraction of mice with complete long-term response. **(B)** Kaplan-Meier curves demonstrating survival of mice that were given different treatment regimens, as described above.

Since the MCA 205 sarcoma model showed a partial response to anti-PD-1 mAb, it was used to test and compare the two different isotypes of the 37A10 anti-ICOS mAb. As previously, mice were injected subcutaneously with MCA 205 cells and after the establishment of palpable tumours in the flank, mice were treated with three doses of anti-PD-1 mAb, anti-ICOS mAbs or their combination. Individual tumour growth curves are showed in Figure 3.4A. We observed no differences in tumour growth between untreated mice and mice treated with either anti-ICOSm2a mAb (depleting) and anti-ICOSm1 mAb (non-depleting). The individual curves of tumour growth between mice treated with anti-PD-1 mAb and mice treated with a combination of anti-PD-1 mAb and both anti-ICOS mAb isotypes are similar, showing an initial reduction in the tumour size after the initiation of treatment followed by a subsequent relapse (Figure 3.4A). Overall, there is no benefit in the tumour growth and survival of mice treated with any of the therapies tested (Figure 3.4B). Whilst the lack of synergy with combination of anti-ICOSm2a mAb and anti-PD-1 mAb was expected due to potential depletion of activated $ICOS^{hi}$ effector T-cells, the lack of activity of anti-ICOSm1 mAb with anti-PD-1 mAb was surprising, as we hypothesised that this isotype could drive primary agonistic activity on $ICOS^{+}$ effector T-cells in absence of depletion, hence allowing adequate activation and accumulation of effector T-cells within tumours.

Furthermore, the similar results between the combination of anti-PD-1 mAb with either anti-ICOSm1 mAb or anti-ICOSm2a mAb, highlights the need for further understanding of the impact of these antibodies in the immune TME.

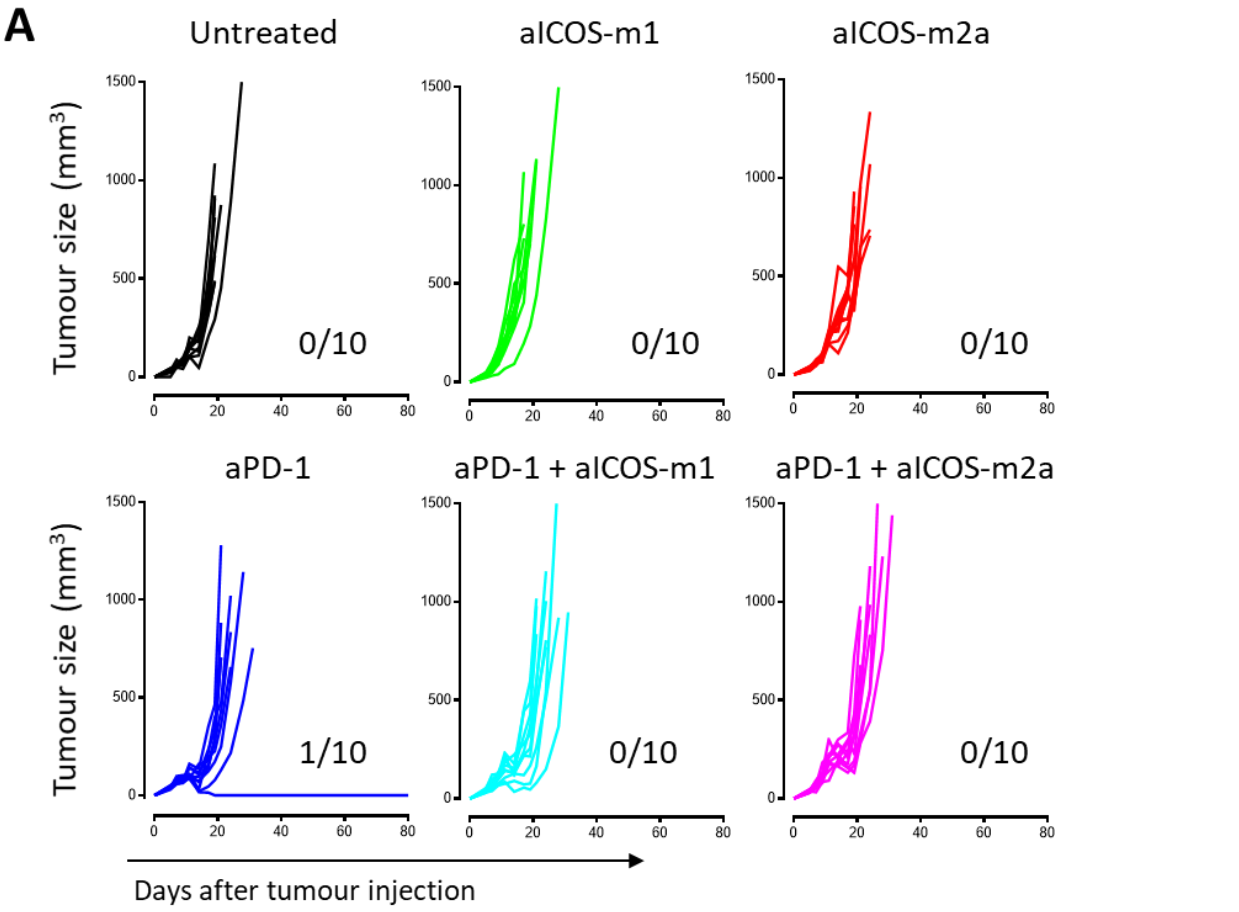
A
Untreated
aICOS-m1
aICOS-m2a
aPD-1
aPD-1 + aICOS-m1
aPD-1 + aICOS-m2a
Tumour size (mm3)
0/10
0/10
0/10
1/10
0/10
0/10
Days after tumour injection

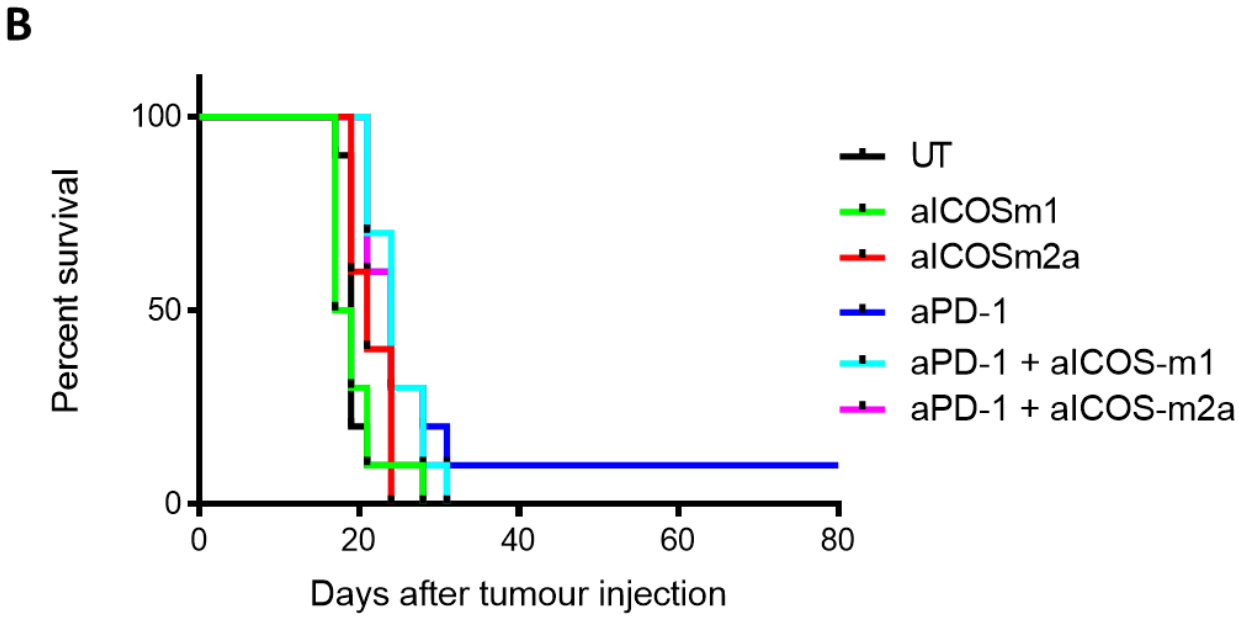
B
Percent survival
Days after tumour injection
UT
aICOSm1
aICOSm2a
aPD-1
aPD-1 + aICOS-m1
aPD-1 + aICOS-m2a

Figure 3.4. Combination of anti-PD-1 mAb with anti-ICOS mAb antibodies does not provide a therapeutic effect.

C57BL/6 mice were injected subcutaneously with 500,000 MCA-205 cells. Mice were treated on day 6, 9 and 12 with 100 µg of anti-ICOSm1 mAb, 100 µg anti-ICOSm2a mAb, 200 µg anti-PD-1 mAb or a combination of treatments as indicated. **(A)** MCA-205 tumour growth in individual C57BL/6 mice in each group. Numbers show the fraction of mice with complete long-term response. **(B)** Kaplan-Meier curves demonstrating survival of mice that were given different treatment regimens, as described above.

3.6 Anti-ICOS antibodies do not synergise with the anti-tumour effect of anti-PD-1

Whilst our data clearly demonstrated a lack of *in vivo* efficacy of anti-ICOS mIgG2a mAb, data from Jounce Therapeutics (US20160304610A1) obtained with the same anti-ICOS (clone 37A10) mAb showed tumour protection in combination with anti-PD-1 mAb (Sazinsky et al., 2016). Hence, we repeated our experiment with exactly the same treatment regimen as reported by Jounce. For this reason, BALBc mice were injected in the flank with the colon carcinoma cell line CT-26 and after 3 days, prior to the tumours being palpable, mice received the first of four doses of antibody treatment. Tumours were measured and mice were sacrificed when the tumour sizes reached the humane endpoint.

The individual tumour growth of each mouse treated with the different therapies tested is presented in Figure 3.5A. Mice treated with monotherapy anti-ICOS mAb isotype mIgG1 or mIgG2a were unable to effectively control tumour growth when compared with untreated mice. Interestingly, unlikely to what was shown in Figure 3.4, anti-PD-1 mAb therapy alone increased survival and tumour control in seven out of 20 mice treated, when the therapy started at an earlier time point (day 3 versus day 6). The partial response to anti-PD-1 mAb therapy in the CT26 model when the therapy started earlier is consistent with the preclinical data from Jounce with the same anti-ICOS (37A10) clone (Sazinsky et al., 2016).

Moreover, mice treated with anti-PD-1 mAb monotherapy or in combination with anti-ICOSm2a mAb showed a similar pattern of control and progression, with tumour size being stable until 28 days after termination of the therapy, followed by a relapse in two mice of each condition (Figure 3.5A). Interestingly, when anti-PD-1 mAb was combined with anti-ICOSm1 mAb, 13 of 20 mice were able to control the tumour growth up to 35 days after tumour injection. Three of those 13 mice had their tumours relapsing. The median survival of untreated, anti-ICOSm1 mAb and anti-ICOSm2a mAb treated mice was 22, 25 and 21 days, respectively; confirming the lack of efficacy of anti-ICOS mAb monotherapy also in an early start treatment set up (Figure 3.5B). On the contrary, the median survival for anti-PD-1 mAb therapy, anti-PD-1 mAb co-therapy with anti-ICOSm1 mAb or anti-ICOSm2a mAb was 44, 82.5 and 29.5 days for each of the conditions, showing that starting anti-PD-1 mAb therapy early in this model promotes a survival benefit (Figure 3.5B).

It is important to note that the benefit obtained upon combination of an anti-PD-1 mAb with anti-ICOSm1 mAb trends towards a synergistic rather than additive effect (as anti-ICOSm1 mAb does not provide protection by itself), even though no significant differences were observed between anti-PD-1 mAb alone and combination of anti-PD-1 mAb plus anti-ICOSm1 mAb. In general, the combination of anti-PD-1 mAb with anti-ICOSm2a mAb appeared to worsen the median survival of mice when compared with anti-PD-1 mAb alone and the survival of mice treated with the combination of anti-PD-1 mAb plus anti-ICOSm2a mAb was significantly worse than combination of anti-PD-1 mAb with anti-ICOSm1 mAb.

These results showed no significant improvement between anti-PD-1 mAb monotherapy and combination of anti-PD-1 mAb with anti-ICOSm1 mAb. Additionally, combination of anti-PD-1 mAb and anti-ICOSm2a mAb worsened the effect of anti-PD-1 mAb monotherapy in a setting previously described as synergistic (Sazinsky et al., 2016).

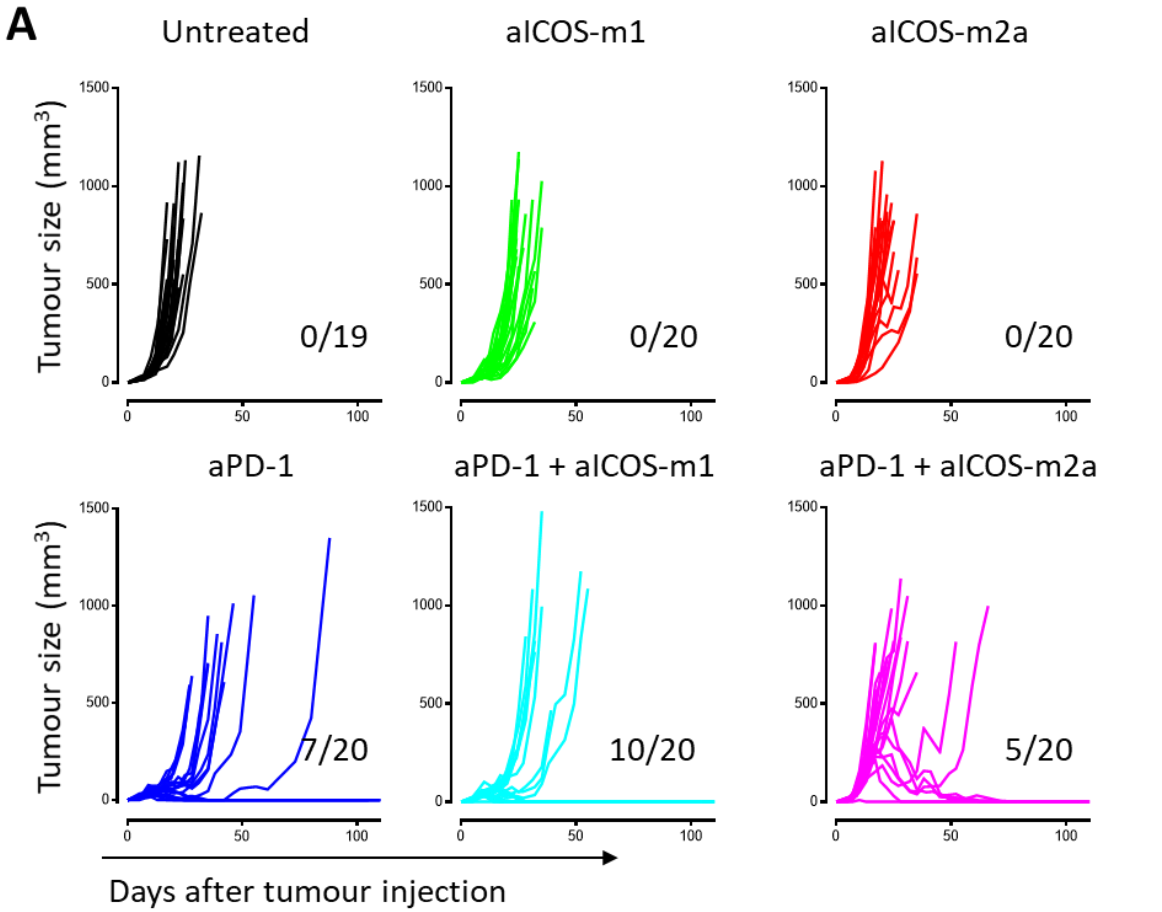
A
Untreated
aICOS-m1
aICOS-m2a
Tumour size (mm3)
0/19
0/20
0/20
aPD-1
aPD-1 + aICOS-m1
aPD-1 + aICOS-m2a
7/20
10/20
5/20
Days after tumour injection

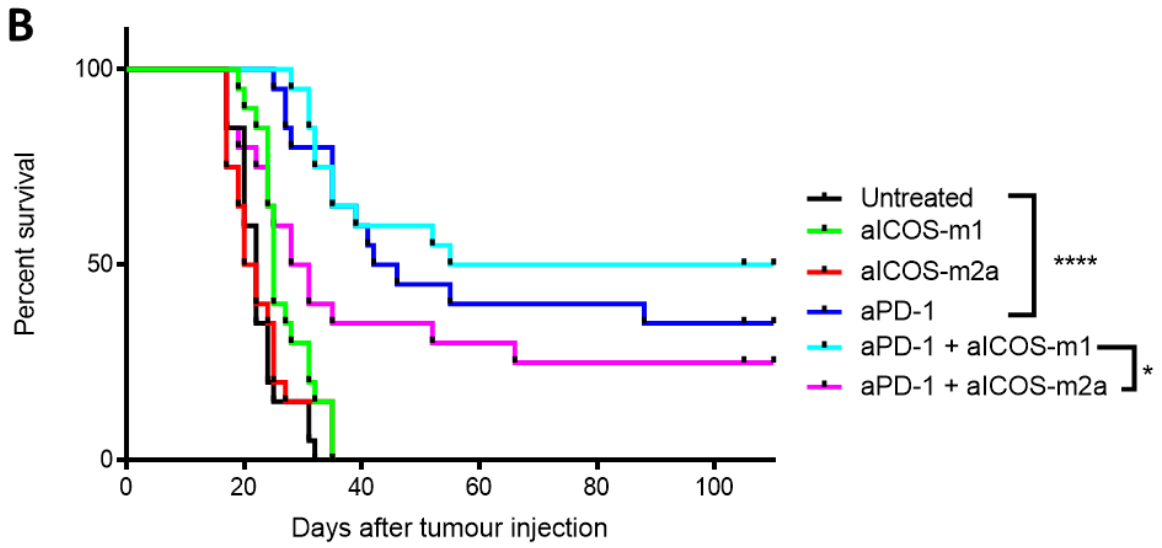
B
Percent survival
Days after tumour injection
Untreated
aICOS-m1
aICOS-m2a
aPD-1
aPD-1 + aICOS-m1
aPD-1 + aICOS-m2a
****
*

Figure 3.5. Combination of anti-PD-1 mAb with anti-ICOS mAb does not improve the therapeutic effect of anti-PD-1 mAb alone.

BALBc mice were injected subcutaneously with the tumour cell CT-26. Mice were treated on day 3, 6, 9 and 12 with 160 µg of anti-ICOSm1 mAb, anti-ICOSm2a mAb, anti-PD-1 mAb or a combination of treatments as indicated. Results of two independent experiments using 10 mice per condition **(A)** CT-26 tumour growth in individual BALBc mice in each group. Numbers show the fraction of mice with complete long-term response. **(B)** Kaplan-Meier curves demonstrating survival of mice that were given different treatment regimens, as described above. ns = $p > 0.05$, *$p \leq 0.05$, **$p \leq 0.01$, ***$p \leq 0.001$, **** $P \leq 0.0001$ log-rank test. Combined result from two independent experiments with 10 mice per condition.

3.7 Anti-ICOS antibodies deplete tumour infiltrating T-cells regardless of isotype

The depleting activity of anti-ICOSm2a mAb was hypothesised to be one of the reasons behind the deleterious effects in survival potentially due to depletion of $ICOS^{hi}$ activated effector T-cell subsets present in the tumour. To test this hypothesis, we evaluated the TME of mice treated with anti-ICOSm1 mAb or anti-ICOSm2a mAb in the CT 26 model. Mice were injected with the CT-26 tumour cell line as before and received two doses of anti-ICOSm1 mAb or anti-ICOSm2a mAb antibody. To evaluate the direct effect of the therapy in the tumour microenvironment, 48 hours after the last dose mice were euthanised and draining LNs and tumour-infiltrating lymphocytes were analysed by flow cytometry. The normalised number of total tumour-infiltrating T-cells to the mass of tumour was evaluated and it was

observed that in anti-ICOSm2a mAb treated mice the number of regulatory T-cells was significantly lower than in untreated mice. Furthermore, as hypothesised, the number of effectors $CD4^+FoxP3^-$ and $CD8^+$ T-cells was also decreased, confirming that a depleting isotype may not be the best approach. Surprisingly, anti-ICOSm1 mAb treatment also promoted both Treg and effector T-cell depletion within the tumour, however, the elimination of Treg and activated T-cells by anti-ICOSm1 mAb isotype was to a lower extent than anti-ICOSm2a mAb isotype (Figure 3.6A). Importantly, when anti-ICOSm2a mAb was used, Treg cells were almost completely eliminated from the tumour, leading to an increased $CD4^+$ effector/Treg and $CD8^+$/Treg ratio in the tumour, but not in draining LNs. Furthermore, anti-ICOSm1 mAb treatment also promoted a partial increase in these ratios in the tumour, albeit not statistically significant (Figure 3.6B). The data showing the elimination of tumour infiltrating $CD4^+$ and $CD8^+$ T-cells without variations in draining LNs by the two anti-ICOS antibodies, is shown by representative dot plots in Figure 3.6C and D.

Even though the depletion of Treg and effector $CD4^+$ and $CD8^+$ cells was hypothesised for anti-ICOSm2a mAb isotype due to the high levels and frequency of expression of ICOS on T-cells in the tumours (Figure 3.1), the reduction in frequency and number of regulatory T-cells and effector T-cells by the non-depleting anti-ICOSm1 mAb antibody was unexpected and needed further investigation. The reduction of the number of infiltrating T-cells in the tumour by both anti-ICOS mAb treatments regardless of the isotype, may explain the lack of therapeutic effect of both anti-ICOS antibodies as monotherapy and the mild benefits in survival when combined with anti-PD-1 mAb as monotherapy, as previously shown.

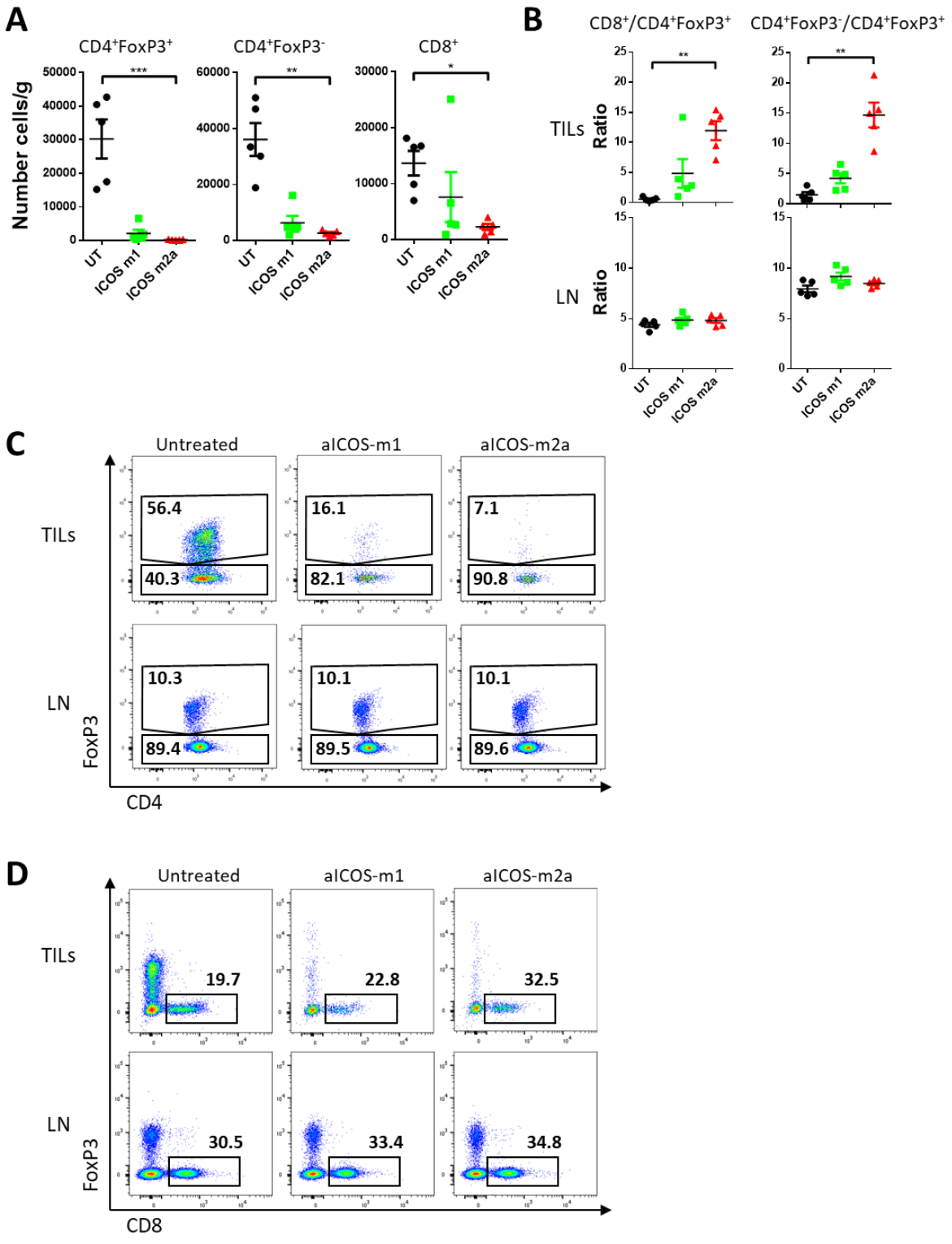
A
CD4+FoxP3+
CD4+FoxP3-
CD8+
Number cells/g
***
**
*
UT
ICOS m1
ICOS m2a
B
CD8+/CD4+FoxP3+
CD4+FoxP3-/CD4+FoxP3+
TILs
LN
Ratio
C
Untreated
aICOS-m1
aICOS-m2a
TILs
LN
56.4
40.3
16.1
82.1
7.1
90.8
10.3
89.4
10.1
89.5
10.1
89.6
FoxP3
CD4
D
Untreated
aICOS-m1
aICOS-m2a
TILs
LN
19.7
22.8
32.5
30.5
33.4
34.8
FoxP3
CD8

Figure 3.6. Anti-ICOS antibodies deplete tumour infiltrating T-cells regardless of the isotype.

BALBc mice were injected subcutaneously with CT-26 cells. Mice were treated on day 6 and 8 with 160 µg of anti-ICOSm1 mAb or anti-ICOSm2a mAb and were euthanized on day 10. Single cell suspension of draining LNs and tumour-infiltrating lymphocytes (TILs) were stained by an optimized panel of monoclonal antibodies and evaluated by flow cytometry. **(A)** Total number of T-cells found in the tumour, normalised to the tumour weight. **(B)** Ratio between $CD8^+$ T-cells or $CD4^+$ effector T-cells relative to regulatory T-cells in the tumour and in the draining LNs. Representative dot plot showing the frequency of **(C)** regulatory T-cells and $CD4^+$ effector T-cells from total $CD3^+$ $CD4^+$ cells in the TILs and draining LNs and **(D)** $CD8^+$ T-cells from total $CD3^+$ cells in the TILs and draining LNs. Horizontal bars represent the mean, errors bars shown ± standard error of the mean (SEM). p values were calculated using non-parametrical analysis Kruskal-Wallis test. ns = $p > 0.05$, *$p \leq 0.05$, **$p \leq 0.01$, ***$p \leq 0.001$, **** $P \leq 0.0001$. Results from one experiment with 5 mice per condition.

3.8 Lower concentrations of anti-ICOS mIgG1 isotype also eliminate regulatory T-cells

A possible mechanism for anti-ICOSm1-mediated elimination of T-cells in the tumour was hypothesised to be due to the fact that mIgG1 of the antibody is also able to bind to activating Fcγ receptors (FcγRs) due to the high amount of antibody being available. To test this hypothesis, mice were injected subcutaneously with CT 26 cells and treated with decreasing doses of anti-ICOSm1 mAb six and nine days after tumour injection, and TILs and draining LN were recovered after 48 hours of the last antibody injection. There was no significant difference in the number of $CD45^+$ cells in the tumour between the three concentrations tested, although the smallest concentration tested (10 μg anti-ICOSm1 mAb) was correlated with a lower number of cells in the tumour.

Importantly, the normalised number of Treg cells was significantly reduced in all the concentrations of anti-ICOSm1 mAb tested in the tumour (Figure 3.7A). Moreover, the normalised number of $CD4^+$ effector ($CD4^+FoxP3^-$) and $CD8^+$ T-cells remained similar between the isotype control and the higher concentrations of anti-ICOSm1 mAb tested (160 μg and 50 μg) but significantly dropped when 10 μg anti-ICOSm1 mAb was used (Figure 3.7A). On the other hand, whilst the total number of Treg in the draining LN was significantly lower just at 10 μg of anti-ICOSm1 mAb, the total number of effector $CD4^+$ or $CD8^+$ T-cells remained without changes (Figure 3.7B). The reduction of total Treg cells led to increased ratios in the tumour and no changes in the draining LNs (Figure 3.7C).

Taken together, these results show that lowering the amount of anti-ICOSm1 mAb therapy does not prevent the elimination of Treg cells in the tumour, whilst it also eliminates activated effector T-cells, although to a lesser extent.

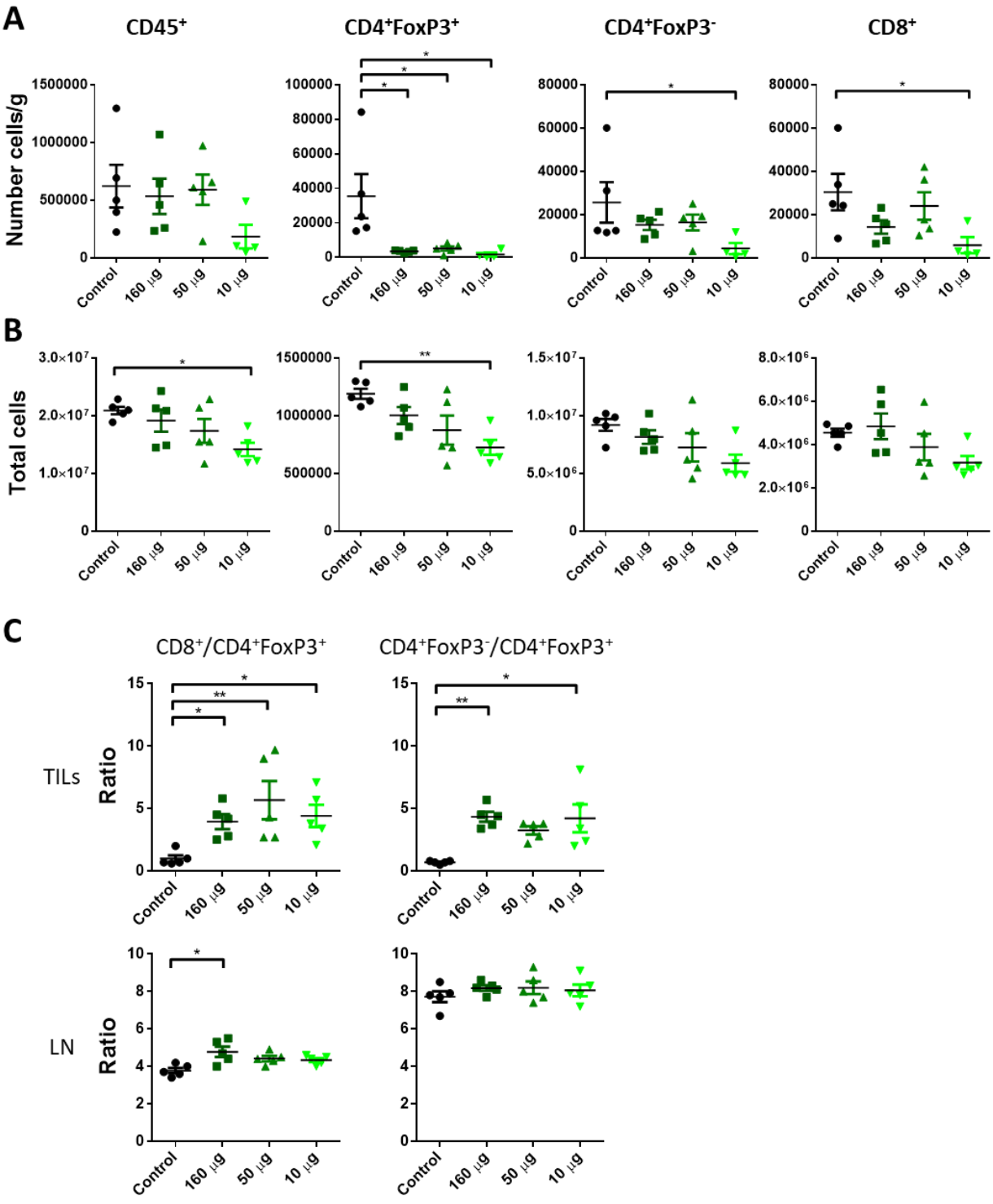
A
CD45+
CD4+FoxP3+
CD4+FoxP3-
CD8+
Number cells/g
1500000
1000000
500000
0
100000
80000
60000
40000
20000
80000
60000
40000
20000
Control
160 µg
50 µg
10 µg
B
Total cells
3.0×10^7
2.0×10^7
1.0×10^7
1500000
1000000
500000
1.5×10^7
1.0×10^7
5.0×10^6
8.0×10^6
6.0×10^6
4.0×10^6
2.0×10^6
C
CD8+/CD4+FoxP3+
CD4+FoxP3-/CD4+FoxP3+
TILs
LN
Ratio
15
10
5
0
8
6
4
2

Figure 3.7 The anti-ICOS-mIgG1 mAb antibody depletes T-cells in the tumour at different concentrations.

BALBc mice were injected subcutaneously with CT-26 cells. Mice were treated on day 6 and 9 with 160 µg of mouse-IgG1 isotype control or different doses of anti-ICOSm1 mAb. On day 11, mice were euthanized, and a single cell suspension was obtained from draining LNs and tumour-infiltrating lymphocytes (TILs). The cells were stained and evaluated by flow cytometry. **(A)** Total number of $CD45^+$ and different subsets of T-cells found in the tumour, normalised to the mass of tumour. **(B)** Total number of $CD45^+$ and different subsets of T-cells found in the draining LNs. **(C)** Ratio between $CD8^+$ T-cells or $CD4^+$ effector T-cells relative to regulatory T-cells in the tumour (TILs) and draining LNs. Horizontal bars represent the mean, errors bars shown ± standard error of the mean (SEM). p values were calculated using non-parametrical analysis Kruskal-Wallis test. ns = $p > 0.05$, *$p \leq 0.05$, **$p \leq 0.01$, ***$p \leq 0.001$, **** $P \leq 0.0001$. Results from one experiment with 5 mice per condition.

3.9 Elimination of T-cells after anti-ICOS mIgG1 treatment persists in the absence of activating FcγR

To test whether the depleting activity observed under anti-ICOSm1 mAb therapy is by a non-canonical activating FcγR engagement, FcγR$^{-/-}$ mice in a C57BL/6 background were used (Takai et al., 1994). FcγR$^{-/-}$ mice, also known as *Fcer1g*$^{-/-}$ mice, do not express activating FcγR (I, III and IV), but maintain the expression of the inhibitory FcγRIIb, which engage preferentially to mouse IgG1. Wild-type (WT) and FcγR$^{-/-}$ mice were injected with MCA 205 cells in the flank and received two doses of anti-ICOSm1 mAb. Additionally, one group of FcγR$^{-/-}$ mice received concomitantly with anti-ICOSm1 mAb two doses of the blocking anti-CD16/CD32 mAb, to avoid the interaction within immunoglobulin mIgG1 and the FcγRIIb (CD32), the only FcγR expressed by FcγR$^{-/-}$ mice.

As previously shown, anti-ICOSm1 mAb treatment increased CD8^{+}/Treg ratio and CD4^{+}effector/Treg ratio in the tumour compared to the untreated condition in WT mice. When the same therapy was given to FcγR$^{-/-}$ mice the ratios remained comparable to WT untreated condition. Importantly, there was no change observed in the ratios in the draining LNs, as showed before in this work (Figure 3.8A). Also, the frequency of regulatory T-cells from total CD3^{+} TILs significantly decreased in mice treated with anti-ICOSm1 mAb, and the reduced frequency was reverted in FcγR$^{-/-}$ mice (Figure 3.8B).

No changes in the frequency of effector CD4^{+} or CD8^{+} T-cells from total CD3^{+} were observed in the tumour, and accordingly to previous data in this thesis (Figure 3.6C and D), no changes in the frequency of T-cell populations were detected in the draining LNs for any of the three T-cell subsets evaluated (Figure 3.8).

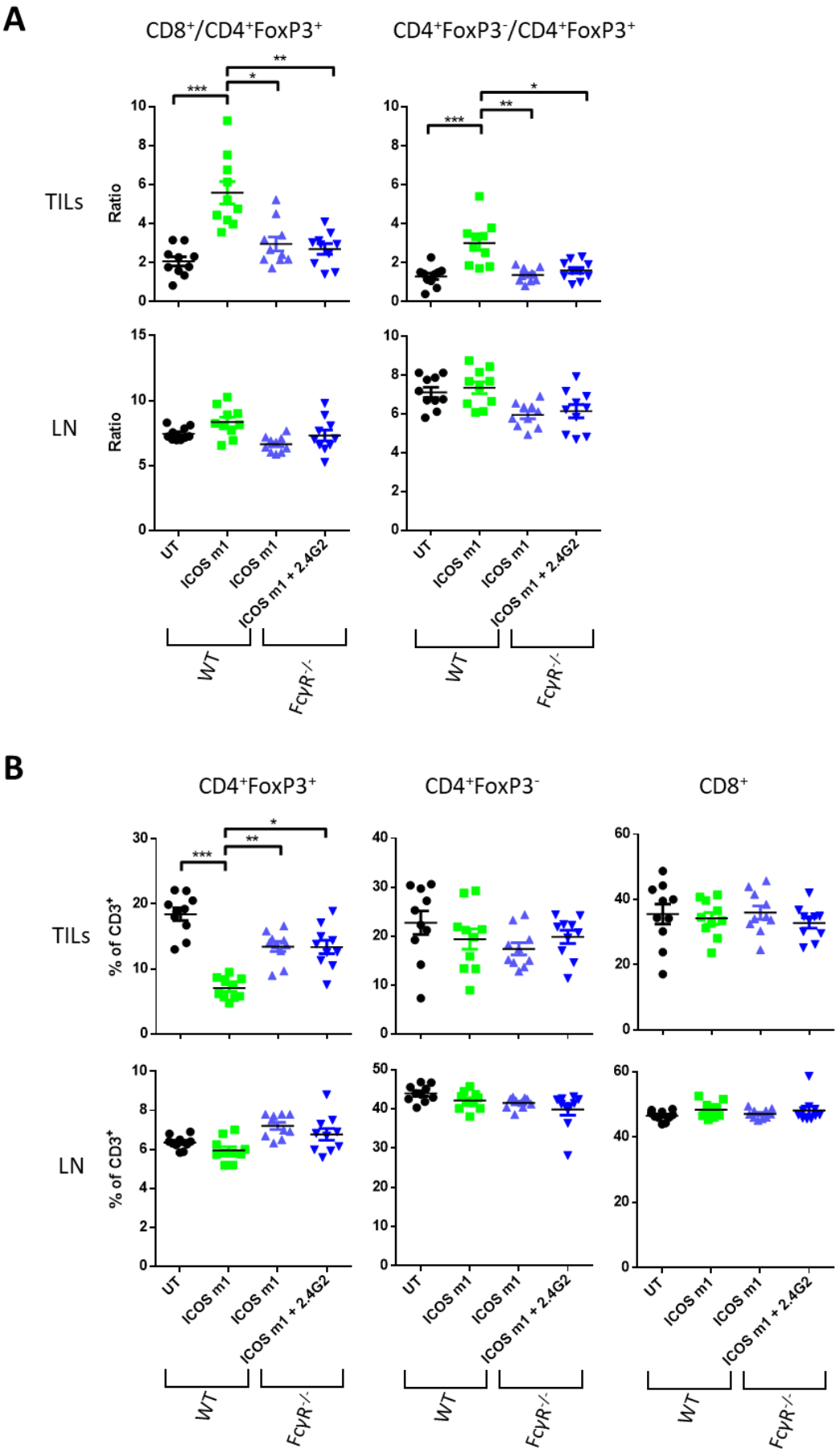
A
CD8+/CD4+FoxP3+
CD4+FoxP3-/CD4+FoxP3+
TILs
LN
Ratio
UT
ICOS m1
ICOS m1
ICOS m1 + 2.4G2
WT
FcγR-/-
B
CD4+FoxP3+
CD4+FoxP3-
CD8+
% of CD3+

Figure 3.8. Reduced frequency of regulatory T-cells after anti-ICOS-mIgG1 antibody treatment in the tumour is partially reverted in the absence of FcγR.

C57BL/6 and FcγR$^{-/-}$ mice were injected subcutaneously with MCA 205 cells. Mice were treated on day 6 and 9 with 160 µg anti-ICOS mIgG1 mAb or with a combination of 160 µg anti-ICOS mIgG1 mAb plus 200 µg anti-mCD16/CD32-rIgG2b mAb (clone 2.4G2). On day 11, mice were euthanized, and a single cell suspension was obtained from draining LNs and tumour-infiltrating lymphocytes (TILs). The cells were stained and evaluated by flow cytometry. **(A)** Ratio between CD8$^+$ T-cells or CD4$^+$ effector T-cells relative to regulatory T-cells in the tumour (TILs) and draining LNs. **(B)** Frequency of CD4$^+$FoxP3$^+$, CD4$^+$FoxP3$^+$ and CD8$^+$ T-cells from total CD3$^+$ cells. Horizontal bars represent the mean, errors bars shown ± standard error of the mean (SEM). p values were calculated using non-parametrical analysis Kruskal-Wallis test. ns = $p > 0.05$, *$p \leq 0.05$, **$p \leq 0.01$, ***$p \leq 0.001$, **** $P \leq 0.0001$. Results from two independent experiments using 5 mice per condition.

However, when the total normalised number of TILs was evaluated, we observed that the reduction on the number of Treg, CD4$^+$ effector and CD8$^+$ T-cells driven by anti-ICOSm1 mAb treatment in WT mice is maintained in FcγR$^{-/-}$ mice even in the presence of anti-CD16/CD32 blocking antibody used to prevent the crosslinking of the anti-ICOSm1 mAb *in vivo* (Figure 3.9A). Whilst the total number of CD45$^+$ remained with no significant difference between untreated WT mice, anti-ICOSm1 mAb treated WT mice and anti-ICOSm1 mAb treated FcγR$^{-/-}$ mice, a reduction was observed in FcγR$^{-/-}$ mice treated with anti-ICOSm1 and anti-CD16/CD32 mAb (Figure 3.9A). On the other hand, no significant difference was obtained in the total number of CD45$^+$ cells and the three populations of T-cells between the groups in draining LNs (Figure 3.9B).

Altogether, our data suggests that anti-ICOS mIgG1 isotype promotes elimination of tumour infiltrating T-cells in an FcγR-independent manner. The partial recovery in the frequency of tumour infiltrating Treg cells suggests that the anti-ICOS mIgG1 isotype is able to engage with activating FcγR and drive ADCC of ICOS^{hi} Treg and effector T-cells to some

extent, but the main effect in total numbers of TILs appears to be independent of activating FcγR.

These findings are critical to the development of agonistic anti-ICOS antibodies, as the initial hypothesis of this project, in consensus with part of the field, was that to avoid effector T-cell depletion an anti-ICOS mIgG1 isotype was needed. Instead it appears that a partially detrimental effect could also be mediated by this isotype. The potential mechanism underpinning this effect is discussed further in this work.

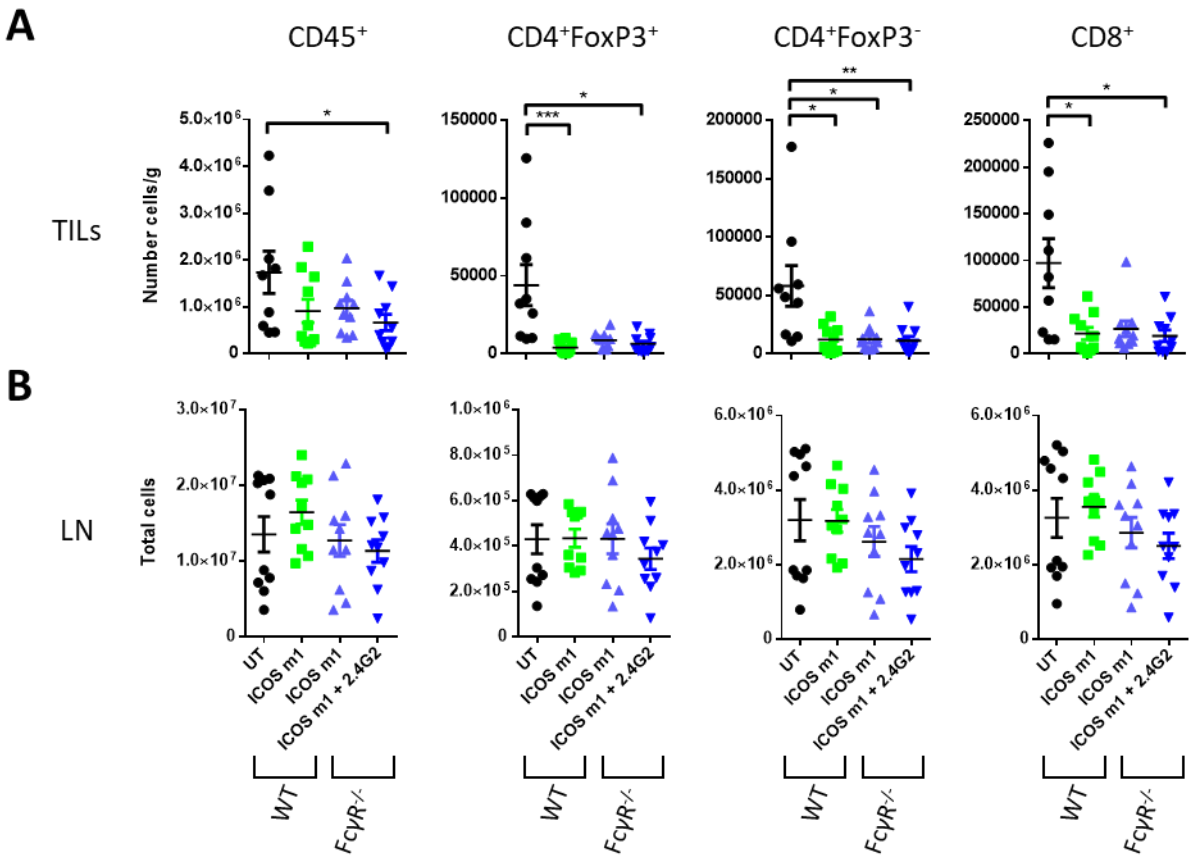

Figure 3.9 Elimination of different T-cell subsets driven by anti-ICOS-mIgG1 treatment is slightly reversed in the absence of FcγR.

C57BL/6 and FcγR$^{-/-}$ mice were injected subcutaneously with MCA 205 cells. Mice were treated on day 6 and 9 with 160 µg anti-ICOS mIgG1 mAb or with a combination of 160 µg anti-ICOS mIgG1 mAb plus 200 µg anti-mCD16/CD32-rIgG2b mAb (clone 2.4G2). On day 11 mice were euthanized, and a single cell suspension was obtained from draining LNs and tumour-infiltrating lymphocytes (TILs). The cells were stained and evaluated by flow cytometry. Total number of CD45^{+} and different subsets of T-cells found in **(A)** the tumour (TILs) and **(B)** draining LN. Horizontal bars represent the mean, errors bars shown ± standard error of the mean (SEM). p values were calculated using non-parametrical analysis Kruskal-Wallis test. ns = $p > 0.05$, *$p \leq 0.05$, **$p \leq 0.01$, ***$p \leq 0.001$, **** $P \leq 0.0001$. Results from two independent experiments using 5 mice per condition.

3.10 The absence of FcγRIIb promotes further elimination of regulatory T-cells by anti-ICOS mIgG1 mAb therapy

To continue elucidating the mechanism of action of the anti-ICOSm1 (37A10) mAb in the tumour microenvironment, WT and FcγRIIb$^{-/-}$ mice (mice lacking the inhibitory FcγRIIb whilst retaining expression of activating FcγRs) were injected subcutaneously with MCA 205 cells and treated with anti-ICOSm1 mAb as in previous experiments. 48 hours after the last dose of treatment, mice were euthanised and TILs and draining LN were analysed by flow cytometry.

Therapy with anti-ICOSm1 mAb produced a slight increase of CD8$^+$/Treg ratio and CD4$^+$effector/Treg ratio in WT mice as described before. Interestingly, when the same treatment was given to FcγRIIb$^{-/-}$ mice both ratios increased dramatically from around 2 to ~22 for CD8$^+$/Treg ratio and increased from ~2 to ~14 for CD4$^+$effector/Treg ratio. Consistently with previous data of this work, no changes in the ratios were observed in draining LNs of these mice (Figure 3.10A).

The frequency of Treg, CD4$^+$effector and CD8$^+$ T-cells were also evaluated from total CD3$^+$ in the TILs and LNs. The frequency of regulatory T-cells from total CD3$^+$ significantly dropped in FcγRIIb$^{-/-}$ mice treated with anti-ICOSm1 mAb when compared with untreated WT mice (from 16% to 2%). Consistently with the previous data, a lower frequency of regulatory T-cells from CD3$^+$ gated cells was also observed in WT mice treated with anti-ICOSm1 (from 16% to 6%), showing a trend towards fewer Treg cells available in the tumour after anti-ICOSm1 mAb therapy. The frequency was even lower in the absence of the inhibitory FcγRIIb in FcγRIIb$^{-/-}$ mice (Figure 3.10B). Interestingly, the frequency of CD4$^+$ effector and CD8$^+$ T-cells remained similar for all the conditions in the tumour and no changes were observed in the frequency of T-cell populations in the LN (Figure 3.10B).

Similar observations were made when the normalised total number of CD45$^+$ and T-cells was also evaluated. Fewer Treg cells in the tumour were observed with anti-ICOSm1 mAb treatment in WT mice, and this Treg-reduction was accentuated in the absence in FcγRIIb$^{-/-}$ mice (Figure 3.11A). A trend towards lower numbers of CD4$^+$ effector and CD8$^+$ T-cells TILs after the treatment with an anti-ICOSm1 mAb was observed, without differences between the two genotypes, suggesting that expression of FcγRIIb is not preventing these

phenomena. On the other hand, the number of $CD45^+$ TILs normalised to the tumour weight remained similar in all the tested conditions. Increased total number of $CD45^+$, $CD4^+$ effector and $CD8^+$ cells were observed in the LN of anti-ICOSm1-treated WT and $FcγRIIb^{-/-}$ mice (Figure 3.11B). This may be attributed to a decreased total number of cells from LN of untreated WT mice when compared with other experiments, rather than an increment related to anti-ICOSm1 treatment. In accordance to all the work presented in this thesis, no difference in the frequency of T-cells were observed after anti-ICOSm1 mAb treatment in LN from WT mice.

Taken together, the above data suggests that anti-ICOSm1 mAb is effectively binding its preferred FcγR, the inhibitory FcγRIIb, because the lack of this interaction leads to increased reduction in the frequency of regulatory T-cells in the tumour.

Importantly, this suggest that the preferential elimination of regulatory T-cells in the tumour by anti-ICOSm1 mAb might be due the levels of expression (MFI) of ICOS on Treg in the MCA 205 and CT 26 model (Figure 3.2). We hypothesised that anti-ICOSm2a mAb, the antibody that binds with high affinity to the activating FcγRs, mediates the elimination of regulatory T-cells, effector $CD4^+$ and $CD8^+$ T-cells by ADCC and by a Fcγ-independent mechanism. Whilst the mIgG1 fraction of the anti-ICOSm1 mAb binds preferentially to the inhibitory FcγRIIb not promoting ADCC, we still observe T-cell elimination driven mostly by a Fcγ-independent mechanism.

Even though this seems like a plausible hypothesis for the mechanism of action behind the observed results with $FcγRIIb^{-/-}$ mice, further experiments are needed to clarify the effects FcγR-independent observed before (Figure 3.9).

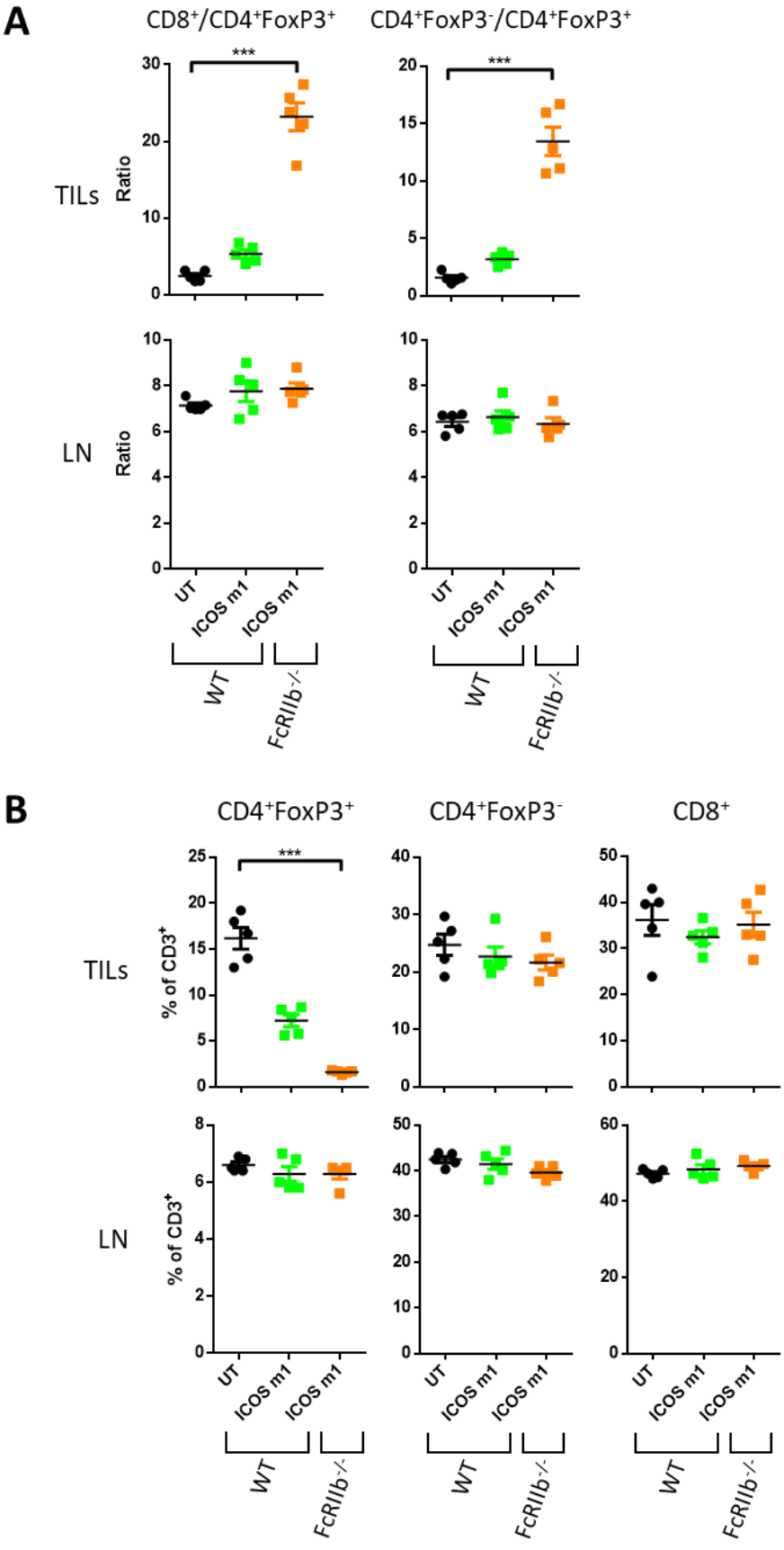
A
CD8+/CD4+FoxP3+
CD4+FoxP3-/CD4+FoxP3+
***
***
TILs
LN
Ratio
UT
ICOS m1
ICOS m1
WT
FcRIIb-/-
B
CD4+FoxP3+
CD4+FoxP3-
CD8+
% of CD3+

Figure 3.10. The anti-ICOS-mIgG1 antibody effectively binds to the inhibitory FcγRIIb, preventing efficient regulatory T-cells depletion.

C57BL/6 and FcγRIIb$^{-/-}$ mice were injected subcutaneously with 500,000 MCA 205 cells. Mice were treated on day 6 and 9 with 160 µg anti-ICOS mIgG1 mAb and on day 11 tumour-infiltrating lymphocytes (TILs) and draining LN were collected. The cells were stained and evaluated by flow cytometry. **(A)** Ratio between CD8^{+} T-cells or CD4^{+} effector T-cells relative to regulatory T-cells in the tumour (TILs) and draining LNs. **(B)** Frequency of regulatory CD4^{+}FoxP3^{+} T-cells, CD4^{+}FoxP3^{-} effector T-cells and CD8^{+} T-cells from total CD3^{+} cells in TILs and draining LN is shown. Horizontal bars represent the mean, errors bars shown ± standard error of the mean (SEM). p values were calculated using non-parametrical analysis Kruskal-Wallis test. ns = $p > 0.05$, *$p \leq 0.05$, **$p \leq 0.01$, ***$p \leq 0.001$, **** $P \leq 0.0001$. Results from one experiment with 5 mice per condition.

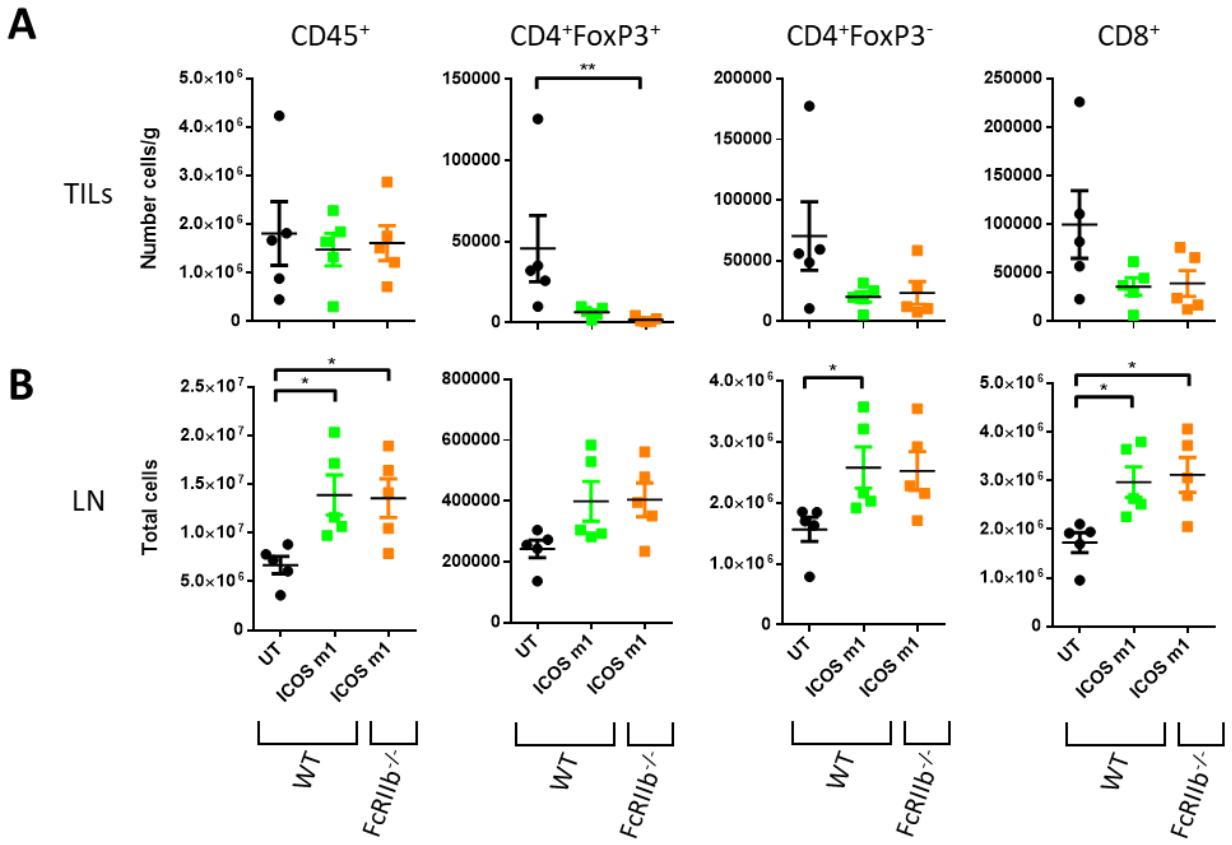

Figure 3.11. Regulatory T-cells are significantly reduced in the tumour after anti-ICOS-mIgG1 mAb treatment in the absence of FcγRIIb.

C57BL/6 and FcγRIIb$^{-/-}$ mice were injected subcutaneously with MCA 205 cells. After the establishment of a solid tumour in the flank, mice were treated with 160 µg anti-ICOS mIgG1 mAb at day 6 and 9. Eleven days after cell injection, a single cell suspension was obtained from draining LNs and tumour-infiltrating lymphocytes (TILs). The cells were stained and evaluated by flow cytometry. **(A)** Number of CD45$^+$ cells, regulatory T-cells, effector CD4$^+$ and CD8$^+$ T-cells normalised to the mass of the tumour (TILs) and **(B)** total number of CD45$^+$ cells, regulatory T-cells, effector CD4$^+$ and CD8$^+$ T-cells in the draining LN. Horizontal bars represent the mean, errors bars shown ± standard error of the mean (SEM). p values were calculated using non-parametrical analysis Kruskal-Wallis test. ns = $p > 0.05$, *$p \leq 0.05$, **$p \leq 0.01$, ***$p \leq 0.001$, **** $P \leq 0.0001$. Results from one experiment with 5 mice per condition.

3.11 Combination of anti-CTLA-4 with anti-ICOS partially impairs the beneficial effect of anti-CTLA-4 therapy *in vivo*

In accordance to our original hypothesis, our data demonstrates that agonistic anti-ICOS antibodies with depleting mIgG2a isotype (equivalent to anti-ICOS hIgG1 mAb used by Jounce and Kymab) fail to drive strong anti-tumour activity *in vivo*, likely due to the elimination of activated effector T cells. This data could provide an explanation to the lack of significant clinical activity reported in the recent ICONIC trial (NCT02904226) sponsored by Jounce Therapeutics. Together the data raises serious concerns regarding the use of anti-ICOS mAbs with depleting activity. The negative effect of depleting isotypes could be amplified in the context of other therapeutic modalities that further upregulate ICOS on effector T-cells or that rely on $ICOS^+$ effector T-cells for their therapeutic efficacy. Amongst these, anti-CTLA-4 antibodies are known to induce ICOS upregulation on activated effector T-cells in the clinic, which correlates with clinical response (Carthon et al., 2010). This has been further supported by experiments in mouse models of cancer demonstrating loss of tumour control in $ICOS^{-/-}$ mice treated by anti-CTLA-4 mAb (Fu et al., 2011).

Of critical relevance, after the release of the initial results of the phase I ICONIC trial (by Jounce Therapeutics) combining anti-ICOS (JTX-2011) mAb and anti-PD-1 mAb, it was announced that an additional arm would evaluate the combination of anti-ICOS with anti-CTLA-4 mAb (Jounce News Release, 2018), following on the initial preclinical data demonstrating that combination of anti-CTLA-4 mAb and ICOSL-expressing tumour cell based vaccines synergised to reject established tumours in mice (Fan et al., 2014).

Based on the above, we next sought to determine whether the combination of anti-CTLA-4 mAb and anti-ICOS mAbs would result in detrimental activity due to depletion of activated effector T-cells.

C57BL/6 mice were challenged with MCA 205 cells in the flank and were treated with three doses of anti-CTLA-4m2a mAb, anti-ICOSm1 mAb, anti-ICOSm2a mAb or a combination of those treatments, and tumour growth and survival was measured. This experimental design was chosen because three doses of anti-CTLA-4m2a mAb are known to drive tumour rejection and long-term survival in this model, as already established by our laboratory, therefore, any decreased survival due to the combination therapy will be easy to detect.

Tumour growth curves in mice left untreated or treated with monotherapy anti-ICOSm1-or anti-ICOSm2a were comparable corroborating the lack of activity of anti-ICOS mAb as single agent in this tumour model. Anti-CTLA-4m2a mAb therapy promoted complete tumour control and long-term survival in all treated mice. As hypothesised, combining anti-CTLA-4 mAb with anti-ICOSm2a mAb lead to a complete loss of tumour rejection driven by anti-CTLA-4 mAb. Interestingly, combination of anti-CTLA-4 mAb plus anti-ICOSm1 mAb lead to a partial tumour control in all mice, in which in half of the mice the tumour has relapsed despite the treatment and in the other half the tumours were rejected (Figure 3.12A). The median survival of untreated, anti-ICOSm1 mAb, anti-ICOSm2a mAb and anti-CTLA-4m2a mAb combined with anti-ICOSm2a mAb groups were 20, 19.5, 21 and 24 days respectively, with no difference between the four groups. In contrast, the median survival of anti-CTLA-4m2a mAb combined with anti-ICOSm1 mAb group was 98 days illustrating a reduction of the survival benefit of anti-CTLA4m2a mAb therapy alone in which all mice survived until end of the experiment (130 days) (Figure 3.12B).

In order to understand the role of T-cell depletion by anti-ICOS mAb in the context of anti-CTLA-4 mAb therapy, mice were challenged with MCA 205 tumour cells, tumours were allowed to grow to a palpable size and then the mice were treated with two doses of anti-ICOSm1 mAb, anti-ICOSm2a mAb, anti-CTLA-4m2a mAb or a combination of anti-CTLA-4m2a with anti-ICOSm1 or anti-ICOSm2a. Draining LNs and TILs were harvested at day 11 post tumour-injection and analysed by flow cytometry. The $CD8^+$/Treg and $CD4^+$effector/Treg ratios were calculated for TILs and draining LNs, and no changes were observed in the LNs. A dramatic increase in the $CD8^+$/Treg ratio was observed with anti-ICOSm2a mAb monotherapy, combination anti-CTLA-4m2a mAb with anti-ICOSm1 mAb and combination anti-CTLA-4m2a mAb with anti-ICOSm2a mAb (Figure 3.13A). It is important to note that anti-CTLA-4m2a mAb therapy alone also increased the $CD8^+$/Treg ratio, but to a lesser extent than the other therapies. Increases in the $CD4^+$effector/Treg ratio were also observed, with significant differences for anti-ICOSm2a mAb, anti-CTLA-4m2a mAb and both combinations of anti-CTLA-4 mAb and anti-ICOS antibodies when compared to untreated mice (Figure 3.13A).

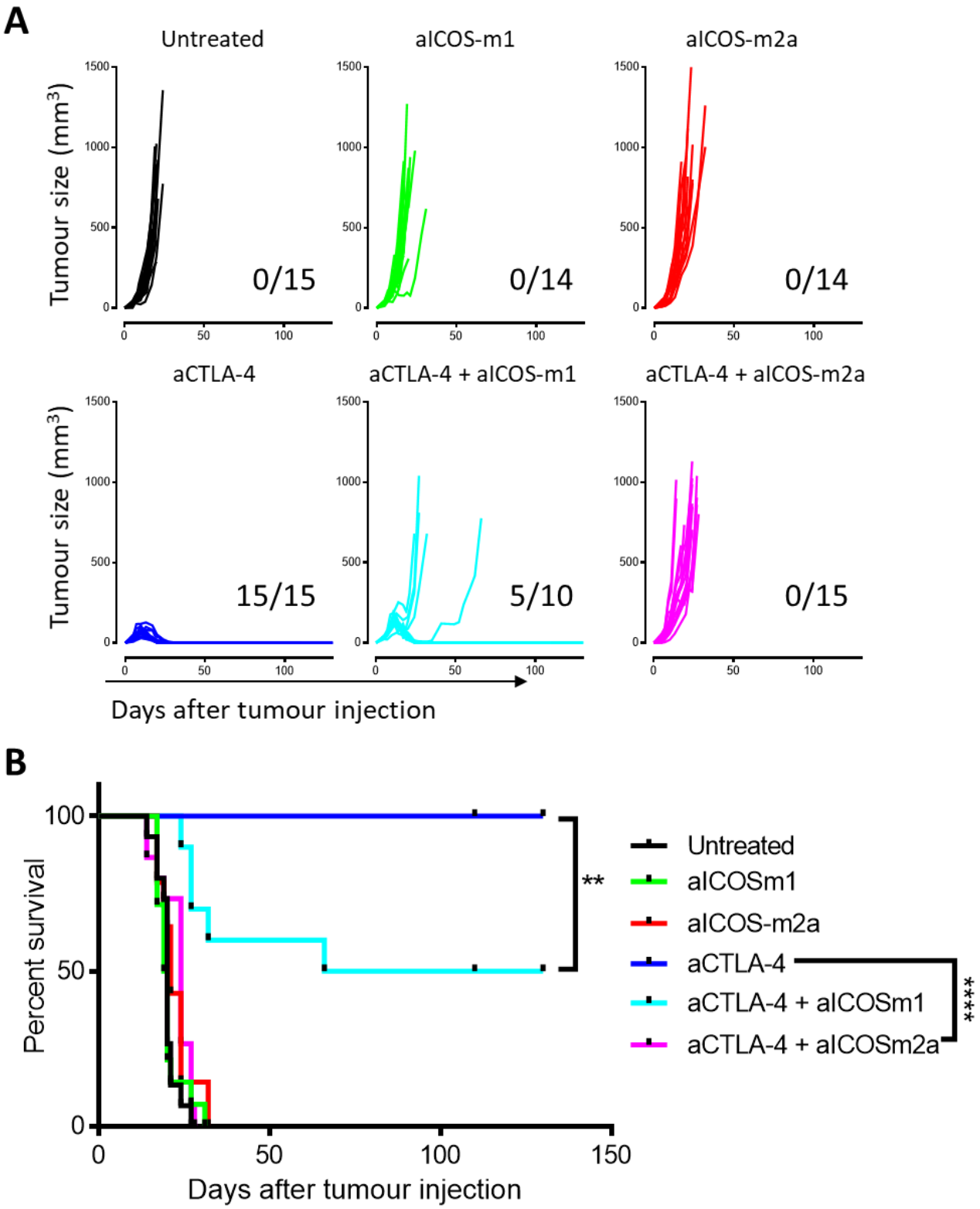
A
Untreated
aICOS-m1
aICOS-m2a
aCTLA-4
aCTLA-4 + aICOS-m1
aCTLA-4 + aICOS-m2a
Tumour size (mm3)
0/15
0/14
0/14
15/15
5/10
0/15
Days after tumour injection
B
Percent survival
Days after tumour injection
Untreated
aICOSm1
aICOS-m2a
aCTLA-4
aCTLA-4 + aICOSm1
aCTLA-4 + aICOSm2a
**
****

Figure 3.12. Combination of anti-CTLA-4 mAb with anti-ICOS mAb impairs the efficacy of anti-CTLA-4 mAb treatment.

C57BL/6 mice were injected subcutaneously with the tumour cells MCA-205. Mice were treated on day 6, 9 and 12 with 100 μg of anti-ICOSm1 mAb, anti-ICOSm2a mAb, anti-CTLA-4m2a mAb or a combination of treatments as indicated. **(A)** MCA-205 tumour growth in individual mice in each group. Numbers show the fraction of mice with complete long-term response. **(B)** Kaplan-Meier curves demonstrating survival of mice that were given different treatment regimens, as described above. ns = $p > 0.05$, *$p \leq 0.05$, **$p \leq 0.01$, ***$p \leq 0.001$, **** $P \leq 0.0001$ log-rank test. Pooled data from two independent experiments.

Whilst the ratios of T-effector/Treg offers insight to the intra-tumour balance between effectors and regulatory T-cells, this indicator fails to provide information on the overall number of cells infiltrating a tumour. Based on this, we next analysed the normalised number of TILs per gram of tumour. Of relevance and in keeping with previous data in this thesis, all treatments reduced the number of Treg cells in the tumour, but the sharpest decreases were caused by anti-ICOSm2a mAb and combinations of anti-CTLA-4 mAb with either anti-ICOS mAb isotypes. Remarkably, anti-CTLA-4m2a mAb injections reduced the number of Treg to a lesser extent when compared with the combination conditions, similarly to anti-ICOSm1 mAb monotherapy (Figure 3.13B). More importantly, the normalised number of $CD4^+$effector and $CD8^+$ T-cells was also reduced in all the conditions when anti-ICOS mAb was administrated, regardless of the isotype of the antibody, with significant reductions when anti-ICOSm2a mAb was given. On the contrary, anti-CTLA-4 mAb was the only condition in which the total number of $CD4^+$effector and $CD8^+$ T-cells remained similar to untreated condition (Figure 3.13B).

Taken together, this data supports the notion that to improve survival it is necessary to increase the $CD8^+$/Treg and $CD4^+$effector/Treg ratios in the tumour as has already been described (Quezada et al., 2006; Bulliard et al., 2013; Selby et al., 2013; Simpson et al., 2013), but it is also necessary to sustain a minimal level of T-cell infiltration and number of effector T-cells within the tumour.

Based on the drastic reduction in the number of effector $CD4^+$ and $CD8^+$ T-cells post therapeutic intervention, we next sought to determine which specific subset of effector T-cells were being eliminated in response to mono- and combination-therapy with anti-ICOS antibodies.

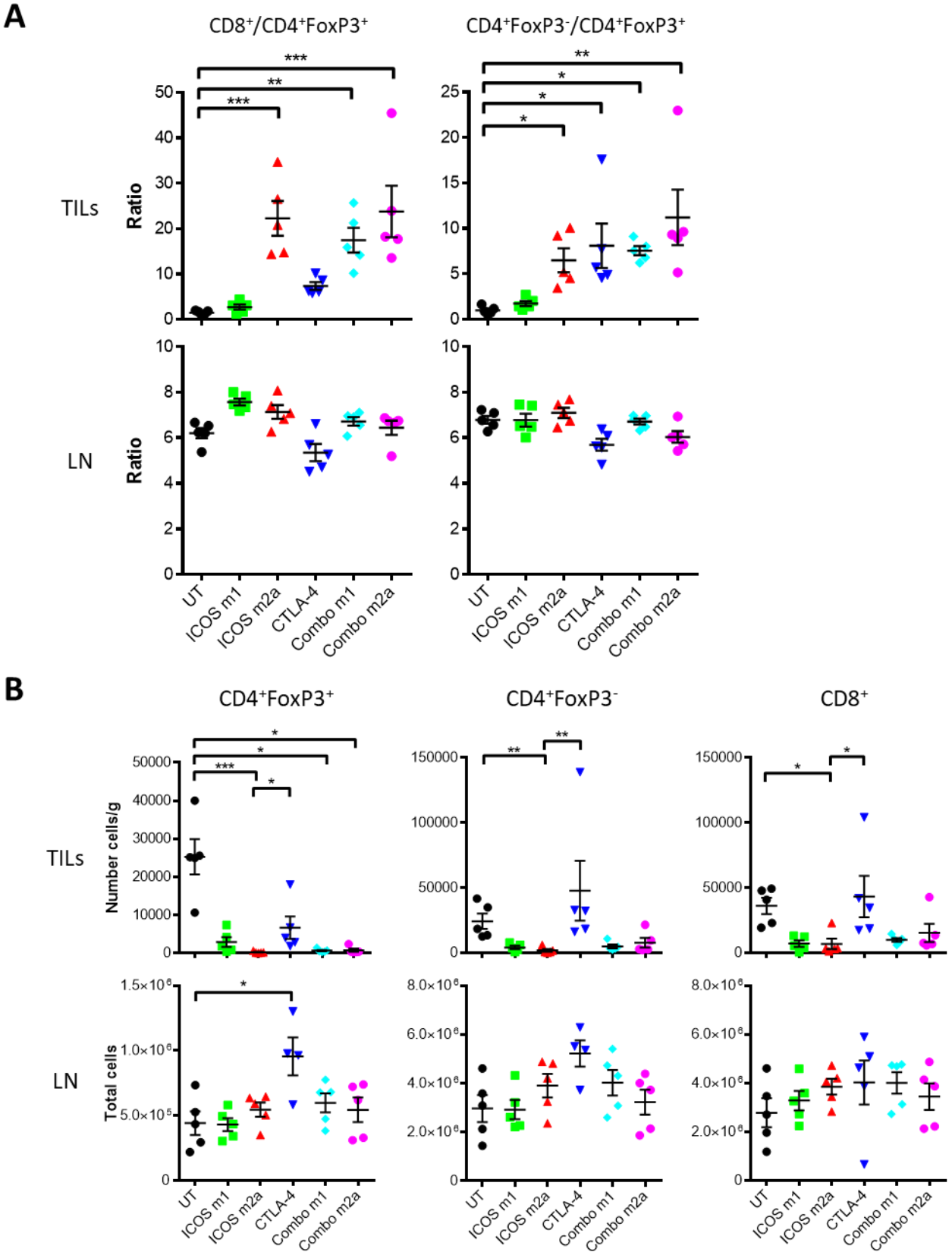
A
CD8+/CD4+FoxP3+
CD4+FoxP3-/CD4+FoxP3+
TILs
LN
Ratio
UT
ICOS m1
ICOS m2a
CTLA-4
Combo m1
Combo m2a
B
CD4+FoxP3+
CD4+FoxP3-
CD8+
Number cells/g
Total cells

Figure 3.13. Combination of anti-CTLA-4 mAb with anti-ICOS mAb diminishes the total number of T-cells in the tumour.

C57BL/6 mice were injected subcutaneously with the tumour cell MCA-205 and were treated with two doses of 100 µg of anti-ICOSm1 mAb, anti-ICOSm2a mAb, anti-CTLA-4m2a mAb or a combination of treatments on days 6 and 8. Ten days after cell injection, tumour-infiltrating lymphocytes (TILs) and draining LN were collected. Cells were stained and evaluated by flow cytometry. **(A)** Ratio between $CD8^+$ T-cells or $CD4^+$ effector T-cells relative to regulatory T-cells in the tumour (TILs) and draining LNs. **(B)** Total number of regulatory $CD4^+FoxP3^+$ T-cells, $CD4^+FoxP3^-$ effector T-cells and $CD8^+$ T-cells found in the tumour (TILs) and draining LN. Horizontal bars represent the mean, errors bars shown ± standard error of the mean (SEM). p values were calculated using non-parametrical analysis Kruskal-Wallis test. ns = $p > 0.05$, *$p \leq 0.05$, **$p \leq 0.01$, ***$p \leq 0.001$, **** $P \leq 0.0001$. Results from one experiment with 5 mice per condition.

3.12 Activated GITR$^+$PD-1$^+$CD4$^+$ cells are eliminated by both isotypes of anti-ICOS mAb

To have a better understanding of the T-cell populations eliminated by both isotypes of anti-ICOS mAb in the context of anti-CTLA-4m2a mAb therapy, a dimensional reduction analysis (t-SNE) (Van Der Maaten and Hinton, 2008) was applied to the immune-modulatory molecule expression data obtained by flow cytometry. Even though the samples were also stained for ICOS expression, this parameter was excluded due to the fact that the therapeutic 37A10 anti-ICOS mAb blocked the staining with the detection anti-ICOS mAb (Supplementary figure 7.1B). The concatenated data of all the samples in the experiment gated by CD45$^+$CD3$^+$ cells are shown in Figure 3.14A. Data shows that CD4$^+$ cells clustered mostly in the areas assigned by polygons 1 and 2, and that CD8$^+$ cells clustered separately in polygons 3 and 4 (Figure 3.14A). FoxP3 and CD25 expression were delimited by area 1, also expressing CD4. Therefore, polygon 1 correspond to Treg, polygon 2 refers to effector CD4$^+$ cells meanwhile the assigned polygons 3 and 4 show the different clusters of CD8$^+$ cells. Higher GITR expression was allocated mostly to Treg cells but was also expressed by CD4$^+$effector and CD8$^+$ T-cells. Similarly, PD-1 expression was narrowed to the T-cell populations with the higher expression on CD8$^+$ T-cells. Granzyme B (GzmB) was restricted to the CD8$^+$ cells and the proliferation marker was mostly allocated to both effector CD4$^+$ and CD8$^+$ cells (Figure 3.14A).

Importantly, when we compared the concatenated data for each group, we observed that in all the treatments there is elimination of the regulatory T-cells present in the untreated (grey) condition, as described before in this work (Figure 3.14B). Furthermore, CD4$^+$effector cells (polygon 2) are also mostly eliminated in all groups receiving any of the isotypes of anti-ICOS mAb but are mainly maintained in the anti-CTLA-4 mAb group. Similarly, for CD8$^+$ cells expressing GITR, PD-1 and GzmB (polygon 3) disappeared in most of the anti-ICOS mAb conditions, except for combination anti-CTLA-4 mAb plus anti-ICOSm1 mAb and anti-CTLA-4 mAb monotherapy, the two conditions with higher median survival (Figure 3.14B).

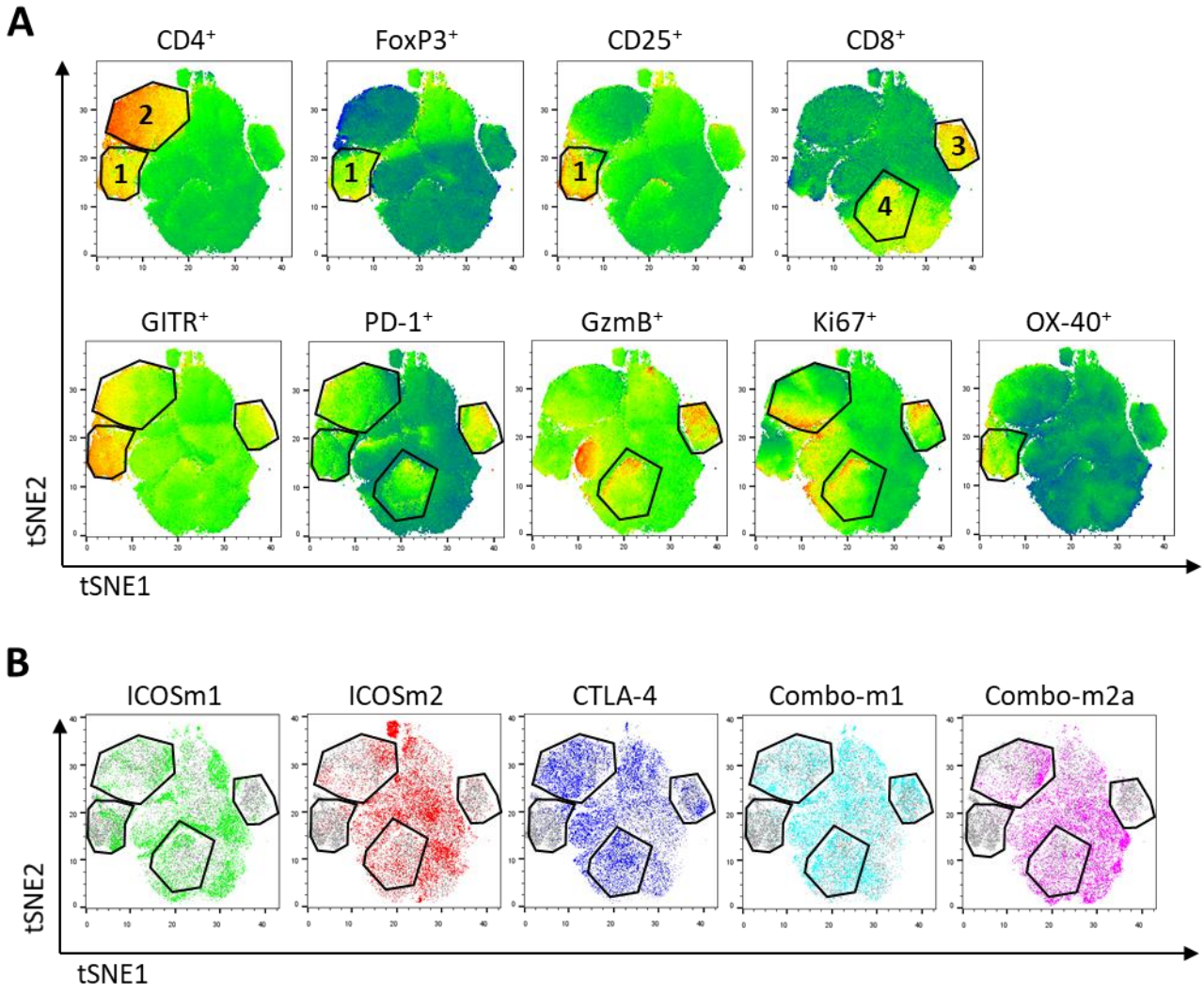

Figure 3.14. Combination of anti-CTLA-4 mAb with anti-ICOS mAb diminishes the frequency of regulatory and activated effector T-cells in the tumour.

C57BL/6 mice were injected subcutaneously with MCA-205 cells and treated with 100 µg of anti-ICOSm1 mAb, anti-ICOSm2a mAb, anti-CTLA-4m2a mAb or a combination of treatments on days 6 and 8. Ten days after cell injection, tumour-infiltrating lymphocytes were collected, stained and evaluated by flow cytometry. Data were analysed using the pipeline Cytofpipev0.2, which apply the PhenoGraph algorithm in its clustering command. Visualisation by tSNE parameters. Polygons indicating clusters of interest are shown. Polygon 1 refers to regulatory T-cells, polygon 2 indicates effector $CD4^+$ T-cells and polygons 3 and 4 correspond to $CD8^+$ T-cells. **(A)** Panels indicating the level of expression of different markers, as indicated. **(B)** Comparison between untreated samples (grey) and treated mice (coloured) are shown. Four polygons indicating different T-cell subsets are also highlighted. Treatments corresponding to anti-ICOS-mIgG1 mAb (green), anti-ICOS-mIgG2a mAb (red), anti-CTLA-4-mIgG2a mAb (blue), anti-ICOS-mIgG1 mAb plus anti-CTLA-4-mIgG2a mAb (light blue) and anti-ICOS-mIgG2a mAb plus anti-CTLA-4-mIgG2a mAb (pink).

To better understand the populations of effector T-cells disappearing after anti-ICOS mAb treatments, $GITR^+PD\text{-}1^+$ cells were gated in $CD4^+$effector and $CD8^+$ T-cell populations (Figure 3.15A, B). The frequency of $CD4^+FoxP3^-GITR^+PD\text{-}1^+$ remained similar between untreated, anti-CTLA-4 mAb and anti-ICOSm1 mAb groups, with a slight decrease in combination anti-CTLA-4 mAb and anti-ICOSm1 mAb group and a decrease (from 60% to 20%) in both conditions treated with anti-ICOSm2a mAb (Figure 3.15A).

A different trend was observed for $CD8^+GITR^+PD\text{-}1^+$ in which frequency was reduced with anti-ICOSm1 mAb, anti-CTLA-4 mAb and the combination of both antibodies, but interestingly the sharpest decrease was observed in the group treated with anti-ICOSm2a mAb alone (Figure 3.15B). The ratio of these populations to Treg population was calculated, showing increased $CD4^+FoxP3^-GITR^+PD\text{-}1^+$/Treg ratio in all the groups treated with anti-CTLA-4 mAb from an average of 0.5 to 5 (10-fold increase), but when the total normalised number of $CD4^+FoxP3^-GITR^+PD\text{-}1^+$ in the tumour was calculated the only condition that maintained those activated $CD4^+$effector cells was anti-CTLA-4 mAb monotherapy group (Figure 3.15C). Different observations were made for activated $CD8^+GITR^+PD\text{-}1^+$ cells, in which the ratio to Treg cells slightly increased when anti-CTLA-4 mAb was given from 0.5 to 1.5 - 2 (three- to four-fold increase) and a significantly higher ratio was obtained when combining anti-CTLA-4 mAb with anti-ICOSm1 mAb. Nevertheless, when the normalised number of this activated $CD8^+GITR^+PD\text{-}1^+$ cells was calculated, a significant decrease was observed in most of the anti-ICOS-treated conditions and just those mice treated with anti-CTLA-4 mAb alone were able to maintain this population of activated $CD8^+$ T-cells (Figure 3.15D).

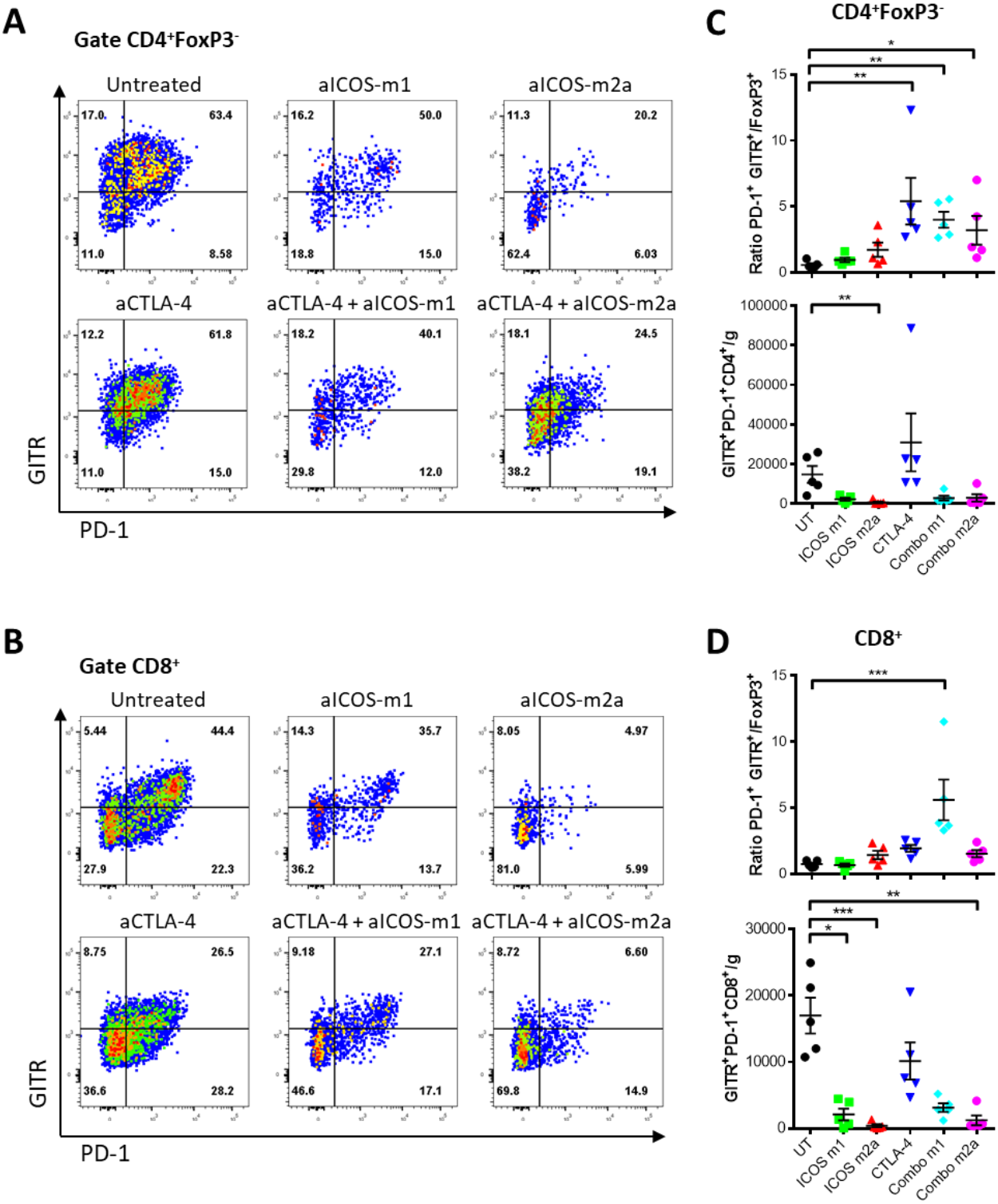

Figure 3.15. The number of activated effector PD-1$^+$ GITR$^+$ cells is reduced with anti-ICOS mAb treatments.

C57BL/6 mice were injected subcutaneously with the tumour cell MCA-205 and were treated with two doses of 100 µg of anti-ICOSm1 mAb, anti-ICOSm2a mAb, anti-CTLA-4m2a mAb or a

combination of treatments on days 6 and 8. At day 10, tumour infiltrating lymphocytes (TILs) were collected and the cell suspension was stained and evaluated by flow cytometry. Representative dot plots showing the frequency of PD-1$^+$ GITR$^+$ are shown for the gates **(A)** CD4$^+$ FoxP3$^-$ effector T-cells and **(B)** CD8$^+$ T-cells. The ratio relative to regulatory T-cells and the total number of activated PD-1$^+$ GITR$^+$ effector cells normalized to the amount of tumour is shown for **(C)** CD4$^+$ FoxP3$^-$ T-cells and **(D)** CD8$^+$ T-cells. Horizontal bars represent the mean, errors bars shown ± standard error of the mean (SEM). p values were calculated using non-parametrical analysis Kruskal-Wallis test. ns = $p > 0.05$, *$p \leq 0.05$, **$p \leq 0.01$, ***$p \leq 0.001$, **** $P \leq 0.0001$. Results from one experiment with 5 mice per condition.

The expression of ICOS and Granzyme B was evaluated in concatenated samples of untreated and anti-CTLA-4 mAb treated mice. Anti-ICOS mAb groups were excluded of this analysis due to the blocking of ICOS staining by 37A10 anti-ICOS mAb treatment.

Figure 3.16A shows that in untreated mice the majority of CD4$^+$effector cells are ICOS$^+$ and GzmB$^-$ or GzmB^{lo} and when the CD4$^+$FoxP3$^-$GITR$^+$PD-1$^+$ population is selected, there is no changes in that distribution. As the majority of CD4$^+$FoxP3$^-$ cells are ICOS$^+$, when anti-ICOS mAb therapy is used most of these CD4$^+$ effector cells, and particularly the activated CD4$^+$FoxP3$^-$GITR$^+$PD-1$^+$ population, can be targeted and depleted. When anti-CTLA-4 mAb is given to the mice, the majority of CD4$^+$effector cells upregulated GzmB$^+$ production, becoming ICOS$^+$GzmB$^+$ - including CD4$^+$FoxP3$^-$GITR$^+$PD-1$^+$ cells – pointing to this population as one key target for anti-ICOS mAb when combination therapy was given (Figure 3.16A).

Similar analysis was carried out for CD8$^+$ cells. In untreated mice, the expression of ICOS and GzmB was restricted to a fraction of all CD8$^+$ T-cells, but when CD8$^+$GITR$^+$PD-1$^+$ cells were gated, the majority of the cells also expressed ICOS and/or GzmB (Figure 3.16A). After

anti-CTLA-4 mAb treatment, most of $CD8^+$ T-cells upregulated GzmB production, and the majority of activated $CD8^+GITR^+PD\text{-}1^+$ cells co-expressed ICOS cells (Figure 3.16A). For this reason, combination of anti-CTLA-4 mAb and anti-ICOS mAb therapy could lead to the elimination of most of the activated $CD8^+GITR^+PD\text{-}1^+GzmB^+$ T-cell pool, which may be driving the undesired outcome of decreased efficacy of anti-CTLA4 mAb therapy upon combining with anti-ICOS mAbs previously described in this work.

For a better visualization of the expression of different molecules on T-cells, SPICE (Simplified Presentation of Incredibly Complex Evaluations) pie charts were made. In the $CD4^+$effector population ICOS was expressed with a high frequency but was also normally co-expressed with at least one of the markers previously evaluated: PD-1 and GITR (Figure 3.16B). In general, there is no differences in the distribution of the different $CD4^+ICOS^+$ population between untreated and anti-CTLA-4-treated groups. Similar scenario is observed for $CD8^+$ in which ICOS is mainly co-expressed with GITR and/or PD-1 in untreated mice. After anti-CTLA-4 mAb therapy, even though the frequency of $CD8^+ICOS^+$ remains similar, the pattern data shows a reduction in the levels of co-expression with GITR (Figure 3.16B).

Importantly, in effector $CD4^+$ and $CD8^+$ T-cells, $ICOS^+$ cells have an activated phenotype, defined by the upregulation of different immune-modulatory molecules on their surface and the production of granzyme B.

Taken all these results together, we concluded that in the context of cancer immunotherapy, targeting ICOS with anti-ICOS monoclonal antibodies may not promote a clinical benefit due to the risk of elimination of important activated effector T-cell compartments as shown in this work using mouse models. Whilst it is clear that anti-ICOS mouse IgG2a drives ADCC of effector T-cells and activated regulatory T-cells, the mechanism underpinning elimination of both subsets by the mouse IgG1 isotype remains elusive and will be discussed later in this thesis.

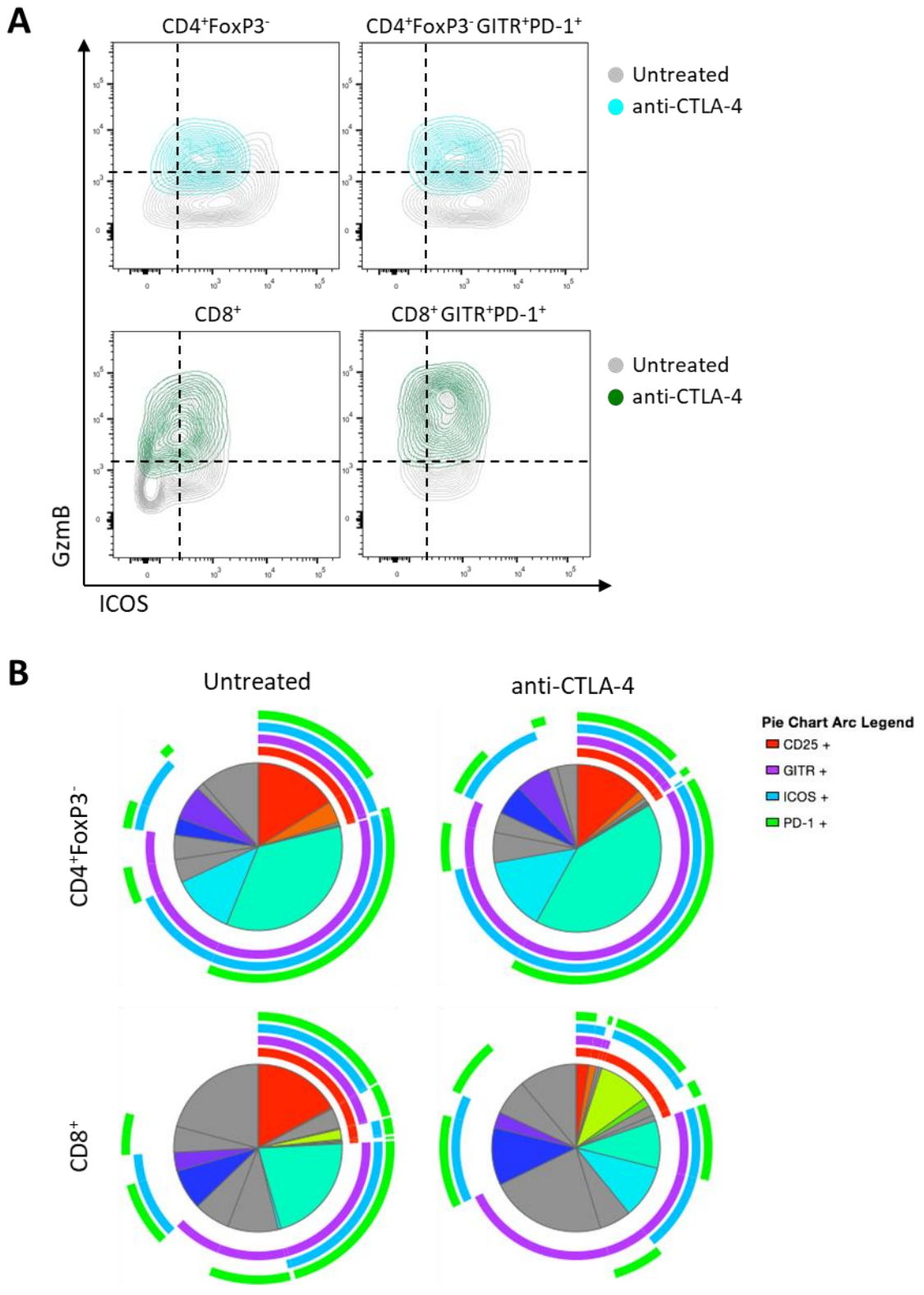

Figure 3.16. ICOS is co-expressed with PD-1 and GITR on effector T-cells activated by anti-CTLA-4, making activated T-cells a target of anti-ICOS mAb therapy.

C57BL/6 mice were injected subcutaneously with the tumour cell MCA-205 and were treated on day 6 and 8 with 100 µg of anti-CTLA-4m2a mAb. At day 10, tumour-infiltrating lymphocytes (TILs) were collected and the cell suspension was stained and evaluated by flow

cytometry. **(A)** Contour plots showing the expression of ICOS and Granzyme B (GzmB) of concatenated untreated and anti-CTLA-4 mAb treated samples. **(B)** SPICE pie charts showing the average expression of CD25, GITR, ICOS and PD-1 on CD4+FoxP3- effector and CD8+ T-cells in untreated and anti-CTLA-4 mAb treated mice.

3.13 Humanised hIgG1 and hIgG4 anti-mICOS antibodies promote depletion of effector and regulatory T-cells in mice bearing human FcγRs

To test the effect of anti-ICOS antibodies with human IgGs in the context of human FcγRs (hFcγRs), a mouse model that recapitulate hFcγR structural and functional diversity was used (Smith et al., 2012). The variable region of anti-ICOS 37A10 mAb was engineered in two human IgG isotypes, the depleting human IgG1 (h1) and non-depleting human IgG4 (h4). As before, mice were injected with MCA 205 cells and treated with two doses of 50 µg anti-ICOS hIgG1 mAb or anti-ICOS hIgG4 mAb on day six and nine after tumour challenge, and after 48 hours of the last dose of antibody tumours and draining LN were recovered and analysed. When the frequency of regulatory T-cells from total $CD3^+$ cells was evaluated, both human IgG isotypes replicated the depletion observed in their equivalent mouse IgGs. In the tumour, the frequency of Treg diminished from an average of 15% to a 4% for anti-ICOSh1 mAb and to 5% for anti-ICOSh4 mAb (Figure 3.17A). The frequency of effector $CD4^+$ and $CD8^+$ from total $CD3^+$ remained comparable between both anti-ICOS isotypes and untreated samples in the tumour, and as described with mouse IgGs, no differences were observed in the draining LN for any of the T-cell subsets (Figure 3.17A). Consequently, the ratios to Treg cells also increased in the tumour with both isotypes of anti-ICOS mAb, whilst a minor decrease in the $CD8^+$/Treg ratio was obtained in the draining LN (Figure 3.17B). Replicating what was

observed previously with mouse IgGs, both human isotypes of anti-ICOS mAbs lead to a statistically significant reduction in the number of Treg cells infiltrating the tumour (Figure 3.17C). Additionally, a not significant trend toward reduced number of effector $CD4^+$ T-cells was also observed in the tumour with both isotypes of the anti-ICOS mAb, whilst the number of tumour infiltrating $CD8^+$ T-cells was significantly lower with the hIgG1 isotype and trended to a lower number with the non-depleting hIgG4 isotype. No differences in the numbers of T-cells from the draining LNs were detected (Figure 3.17C). In general, the data generated with hFcγR mice suggest that anti-ICOS hIgG4 mAb could be the preferred isotype to be used in the clinic, as no statistically significant reduction of effector $CD4^+$ and $CD8^+$ T-cells was observed. However, this isotype trended toward reduced numbers and the experiments with mouse IgGs demonstrated a detrimental ADCC-independent elimination of effector T-cells.

In summary, all the preclinical studies done in this work provide strong evidence regarding a potential deleterious effect of the use of agonistic anti-ICOS antibodies in the clinic for the treatment of cancer.

Even though the exact mechanism by which the elimination of different T-cell subsets is still unknown, this work demonstrated that this elimination is independent of FcγR-engagement, at least in the mouse model. The use of the hFcγR mouse model provided further evidence that the described T-cell elimination in this work is not an effect restricted to mouse IgG/mouse FcγR interaction, and therefore targeting ICOS for antibody therapy in the clinic should be put on hold until safer strategies are available.

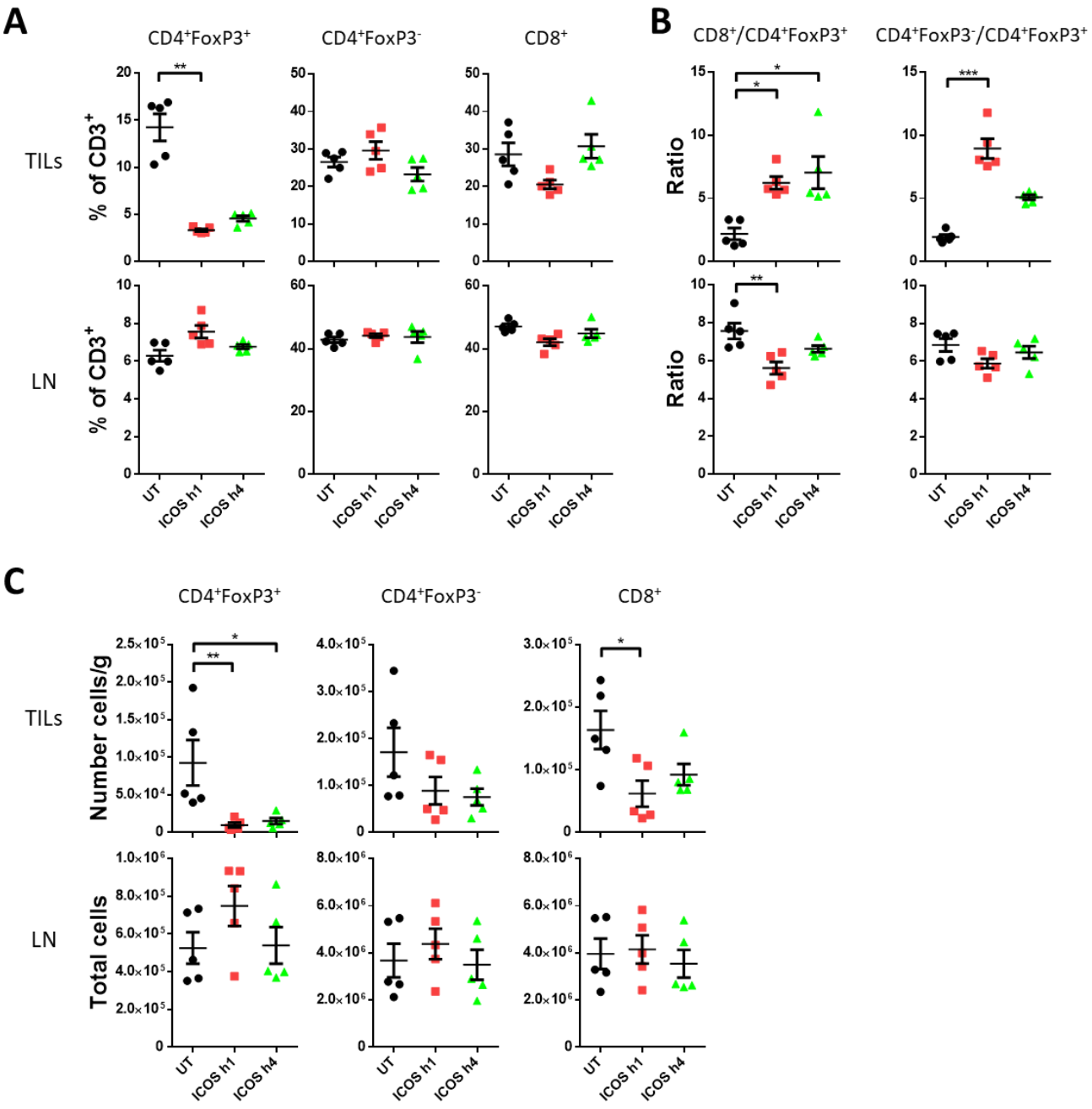

Figure 3.17. Engineered anti-ICOS antibody with human IgGs depletes T-cells in the tumour.

hFcγR mice (C57BL/6 background) were injected subcutaneously with MCA-205 cells and were treated with two doses of 50 µg of anti-ICOSh1 mAb or anti-ICOSh4 mAb on days six and eight. Ten days after cell injection, tumour-infiltrating lymphocytes (TILs) and draining LN were collected. Cells were stained and evaluated by flow cytometry. **(A)** Frequency of regulatory, effector $CD4^+$ and $CD8^+$ T-cells from total CD3+ cells found in the tumour (TILs) and draining LNs. **(B)** Ratio between $CD8^+$ T-cells or $CD4^+$ effector T-cells relative to regulatory

T-cells in the tumour and in the draining LNs. **(C)** Total number of T-cells found in the tumour, normalised to the mass of the tumour. Horizontal bars represent the mean, errors bars shown ± standard error of the mean (SEM). p values were calculated using non-parametrical analysis Kruskal-Wallis test. ns = $p > 0.05$, *$p \leq 0.05$, **$p \leq 0.01$, ***$p \leq 0.001$, **** $P \leq 0.0001$. Results from one experiment with 5 mice per condition.

4 Results: Deciphering the immune tumour microenvironment in mouse models of lung cancer to inform the development of novel therapeutic interventions

4.1 Introduction

As discussed in Chapter 1, lung cancer remains the malignancy with the highest mortality in the world, with just slight improvement in the survival of patients in the last 40 years (Cancer Research UK, 2018a).

It has been reported that NSCLC patients who developed tertiary lymphoid structures within the tumour have improved long-term survival (Dieu-Nosjean et al., 2008). The study identified mature DCs as the best predictor for improved outcome, proposing that the priming of $CD4^+$ Th1 cells by DCs was responsible for the improved survival (Dieu-Nosjean et al., 2008). Similarly, when samples from NSCLC patients were evaluated, a higher number of infiltrating $CD8^+$ T-cells correlated with patient-survival (Zhuang et al., 2010).

Stage III and IV NSCLC patients treated with ipilimumab combined with chemotherapy have also shown improved survival comparing to chemotherapy alone. In the trial, paclitaxel and carboplatin chemotherapies were given in a phased schedule with ipilimumab (anti-CTLA-4 mAb). Compared with chemotherapy alone, the combination of ipilimumab plus chemotherapy increased the immune related overall response almost 2-fold (Lynch et al., 2012). Nivolumab (anti-PD-1 mAb) was also tested in advanced and metastatic NSCLC patients. The group of patients receiving nivolumab had an increased overall survival when compared to patients treated with docetaxel (Borghaei et al., 2015).

Altogether, the data suggest that immunotherapies aiming at activating T-cell function within the tumour bear some activity against lung cancer but also underscores the need for better and more potent therapeutic interventions. We believe that for being able to propose new and rational therapies for lung cancer we also need to develop and characterise novel

mouse models of lung cancer that better represent the immune microenvironment of human lung cancer.

For the purpose of reference, the samples from NSCLC patients were collected and analysed in the laboratory by Dr Andrew Furness. Preliminary data generated from mouse models of lung cancer is also shown as a comparison (Supporting figure 4.1A), which shows that the frequency of regulatory T-cells between NSCLC samples and two mouse models of lung cancer, KPB6.F1 and CMT-167, are similarly low. Additionally, the frequency of expression of different co-stimulatory and co-inhibitory molecules is shown as a reference for the data that will be presented in this chapter (Supporting figure 4.1B).

4.2 Rationale and aims

In order to develop new therapies for lung cancer that promote effector T-cell activation, it is necessary to gain better understanding of the dynamics between the tumour and its immune microenvironment in mouse models of lung cancer.

The main objectives of the work presented in this chapter were:

1. To establish mouse models of lung cancer and characterise their immune landscape with a focus on T-cell infiltrates and the expression of potentially targetable immune modulatory receptors.
2. To evaluate the impact of chemotherapy and radiotherapy in immune infiltration and the expression of immune-regulatory molecules to inform the rational development of combination therapies.
3. Based on the above, propose and test new rational designed immunotherapies in mouse models of lung cancer.
4. To evaluate the impact of antibody-based immunotherapies on the immune microenvironment of mouse models of lung cancer.

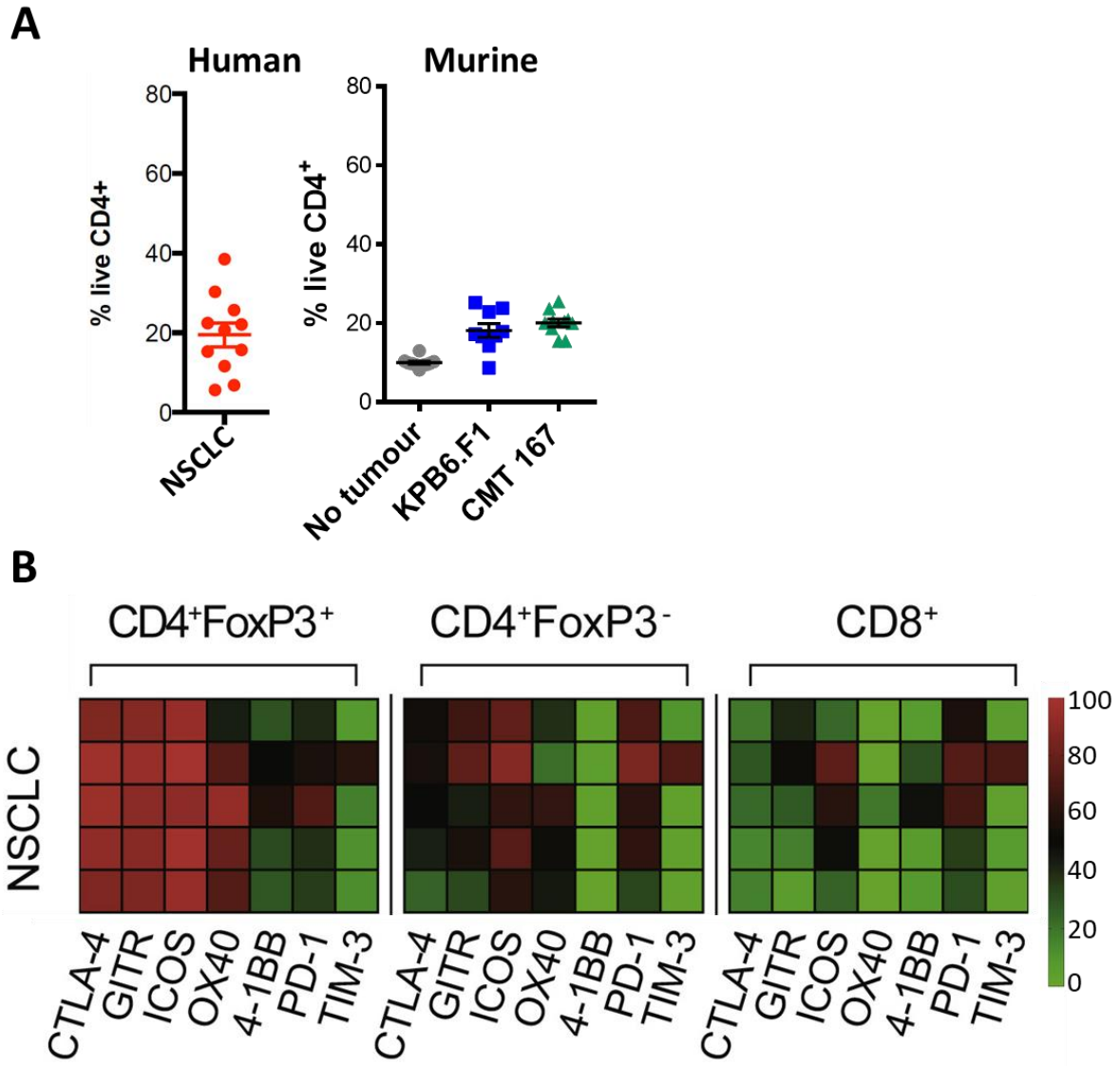

Supporting figure 4.1. Characterisation of the checkpoint landscape on tumour infiltrating T-cells in NSCLC patients.

(A) Frequency of FoxP3$^+$ (Treg) cells from total CD4$^+$ in NSCLC and two mouse models of lung cancer: KPB6.F1 and CMT-167. **(B)** Heatmap demonstrating the frequency of expression of different co-stimulatory and co-inhibitory molecules on the surface of regulatory, effector CD4$^+$ and CD8$^+$ T-cells. Credit human data: Dr Andrew Furness. Modified from (Arce Vargas et al., 2018). Image reproduced with permission of the rights holder, Elsevier.

4.3 Establishment and characterisation of two lung cancer models KPB6.F1 and CMT-167

4.3.1 Establishment of the models

As the main objective of this work was to define and characterise the immune microenvironment of different mouse models of lung cancer, the first step was to find optimal conditions for the growth of tumours in the lung after intravenous injection whilst maintaining the welfare of the animals. For this purpose, a titration of the numbers of cells injected was made for two lung cancer cell lines: KPB6.F1 and CMT-167.

The KPB6.F1 line was derived from lung tumours induced in $Kras^{LSL/G12D}$ $Trp53^{flox/flox}$ mice, as described in Chapter 2. The CMT-167 cell line, a subclone from the mouse lung carcinoma CMT-64, was purchased from Sigma Aldrich, as described in Chapter 2.

Establishing an *in vivo* tumour model can be challenging. It is essential to determine the number of cells needed to be injected in order for the tumour to grow, whilst at the same time the tumour burden cannot be too high leading in premature deaths, or animals needing to be euthanised due to ethical reasons. Titration experiments were carried out as described in Chapter 2, and it was determined that the optimal number of cells to be injected were 80,000 for KPB6.F2 cell line and 300,000 for the CMT-167 cell line (Supplementary figure 7.2).

4.3.2 Tumour infiltrating lymphocytes from the KPB6.F1 and CMT-167 models have a "cold" immune phenotype.

To study the basic biology of the immune populations in the lung tumour microenvironment of both models, mice were injected intravenously with the cell lines KPB6.F1 or CMT-167 and compared with non-tumour bearing mice. The lungs were harvested for each condition - a representative picture is shown in Figure 4.1A. Intravenous injection produced many different tumour nodules in the lungs of the mice; therefore, the quantification of the tumour burden is difficult when avoiding the expression of exogenous proteins such as GFP or luciferase. The use of GFP- or luciferase-expressing tumour cell lines was discarded to avoid adding external immunogenicity to the cell lines, as was observed

previously in this project, which may affect the immune signature of the studied TILs (Supplementary Figure 7.6). For this reason, the weight of the lungs was used as a surrogate measure of the tumour burden in the mice, indicating the development of tumours (Figure 4.1B). In both models we observed a higher frequency of regulatory T-cells (Treg) (out of the total $CD3^+$ compartment) compared to a healthy lung and a trend towards a lower frequency of infiltrating $CD8^+$ T-cells, as observed in other mouse models presented before in this work in Chapter 3 (Figure 4.1C) (Arce Vargas et al., 2017). As shown before, the relative amount of Treg, and therefore effector $CD4^+$, is similar between both mouse models and samples from NSCLC patients (Supporting figure 4.1A). The frequency of NK cells ($NK1.1^+$ cells) was also evaluated in healthy and tumour-bearing lungs, and the percentage of NK cells diminished within both tumour types compared to normal lungs (Figure 4.1D). Interestingly, for the KPB6.F1 model this reduction of NK cells correlated with increased tumour burden (Figure 4.1). The ratio of $CD8^+$ T-cells, $CD4^+$ effector NKs relative to Treg cells was also calculated as shown in Figure 4.1E. The ratio of $CD8^+$, effector $CD4^+$ and NK cells, to Treg cells is decreased in tumour-bearing mice, suggesting an important role of these cells in the evaluated models.

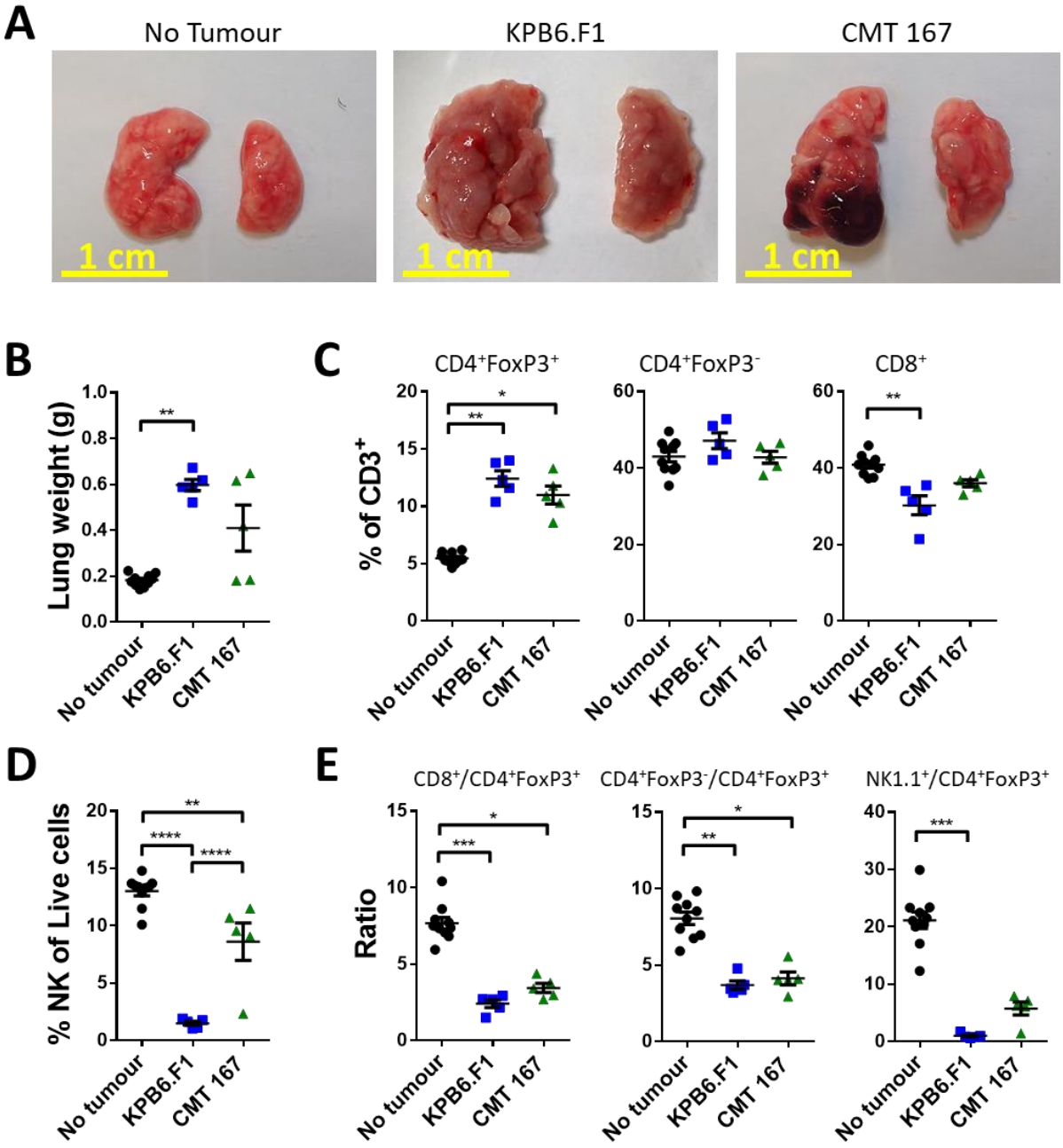

Figure 4.1. Tumour-bearing lungs have an increased frequency of regulatory T-cells when compared to lungs from control mice.

C57BL/6 mice were left untreated or injected intravenously with the tumour cell lines KPB6.F1 or CMT-167. After 20 days the tumour-bearing lungs were collected, and a single cell suspension was generated. Tumour infiltrating lymphocytes were stained and evaluated by flow cytometry. **(A)** Representative pictures of lung from non-tumour bearing mouse (No tumour), KPB6.F1 bearing mouse and CMT-167 bearing mouse. **(B)** Total weight of the lungs for each condition. **(C)** Frequency of regulatory, effector $CD4^+$ and $CD8^+$ T-cells from total $CD3^+$ in the lung. **(D)** Frequency of $NK1.1^+$ cells from total live cells. **(E)** Ratio between $CD8^+$ T-cells,

$CD4^+$ effector T-cells or NK cells relative to regulatory T-cells in the tumour-bearing lungs. Horizontal bars represent the mean, errors bars shown ± standard error of the mean (SEM). p values were calculated using non-parametrical analysis Kruskal-Wallis test. ns = $p > 0.05$, *$p \leq 0.05$, **$p \leq 0.01$, ***$p \leq 0.001$, **** $P \leq 0.0001$. Results from one experiment with 5 mice per condition.

To gain better understanding of the tumour microenvironment, the expression of different co-stimulatory and co-inhibitory molecules was evaluated on the three T-cell compartments by flow cytometry (Figure 4.2A and B). We observed that the frequency of positive cells for each protein was low on $CD4^+$ and $CD8^+$ T-cells, and only Treg cells expressed most of the receptors on their surface. As a reference, T-cells from healthy ("no tumour") mice were also evaluated. Tumour infiltrating Treg cells from both mouse models express more 4-1BB, ICOS, OX-40, CTLA-4, PD-1 and TIGIT when compared to Treg from healthy ("no tumour") mice. Additionally, $CD4^+$ effector and $CD8^+$ T-cells also increased the expression of GITR when compared with their no-tumour counterparts. With the aim to visualise better the tumour microenvironment of both models, a heatmap was produced showing the frequency of cells expressing the different modulatory molecules on the surface of total Treg, $CD4^+$ effector and $CD8^+$ T-cells for five individual mice (Figure 4.2C).

KPB6.F1 and CMT-167 models express a higher frequency of immune modulatory molecules on their $FoxP3^+$ $CD4^+$ cells compared with Treg cells from mice without tumours ("no tumour"). Moreover, $CD4^+$ effector and $CD8^+$ T-cells have a very low frequency of activated T-cells, with a slight increase in the expression of GITR, ICOS and PD-1 when compared to T-cells from healthy mice ("no tumour") (Figure 4.2C).

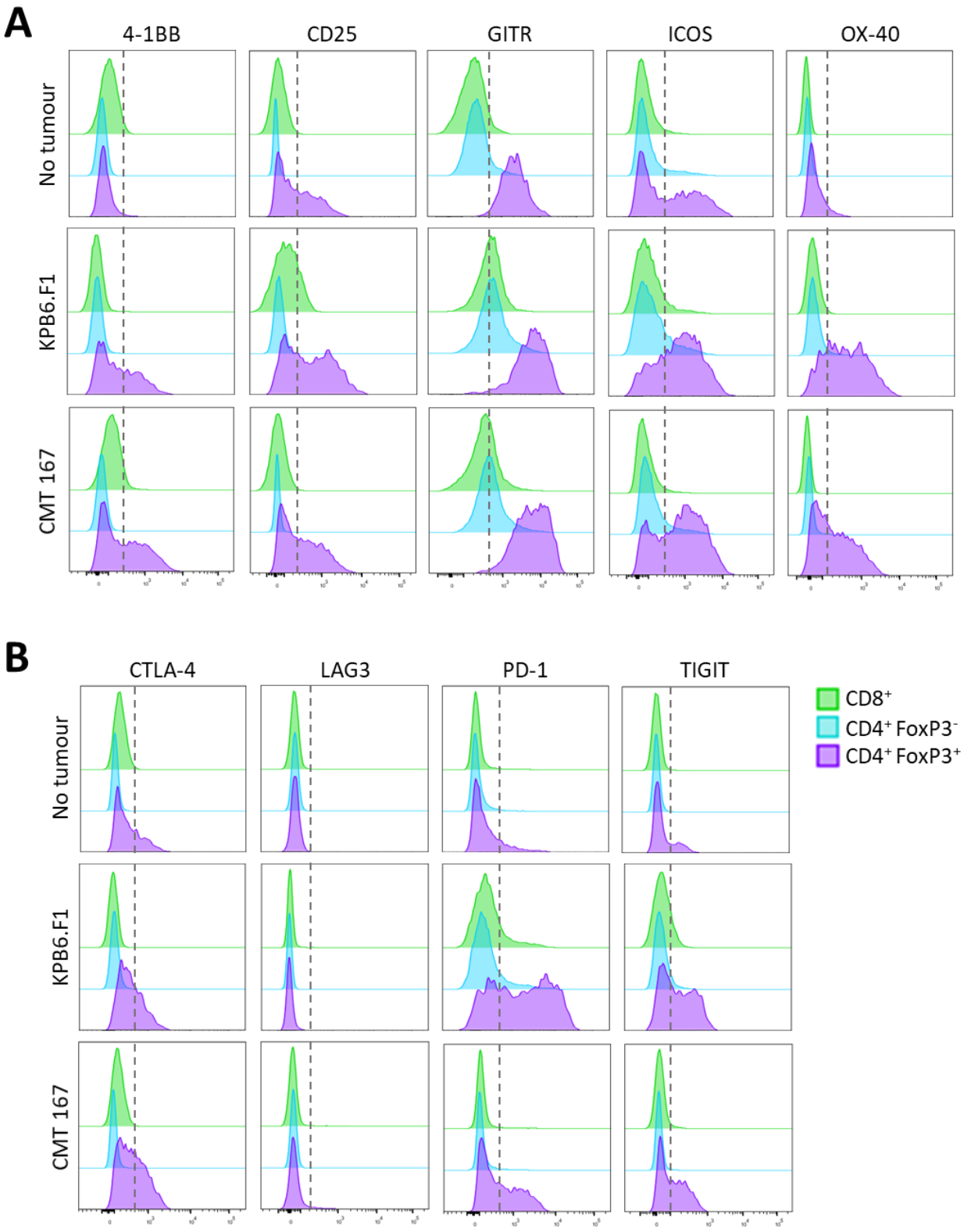
A
4-1BB
CD25
GITR
ICOS
OX-40
No tumour
KPB6.F1
CMT 167
B
CTLA-4
LAG3
PD-1
TIGIT
No tumour
KPB6.F1
CMT 167
CD8+
CD4+ FoxP3-
CD4+ FoxP3+

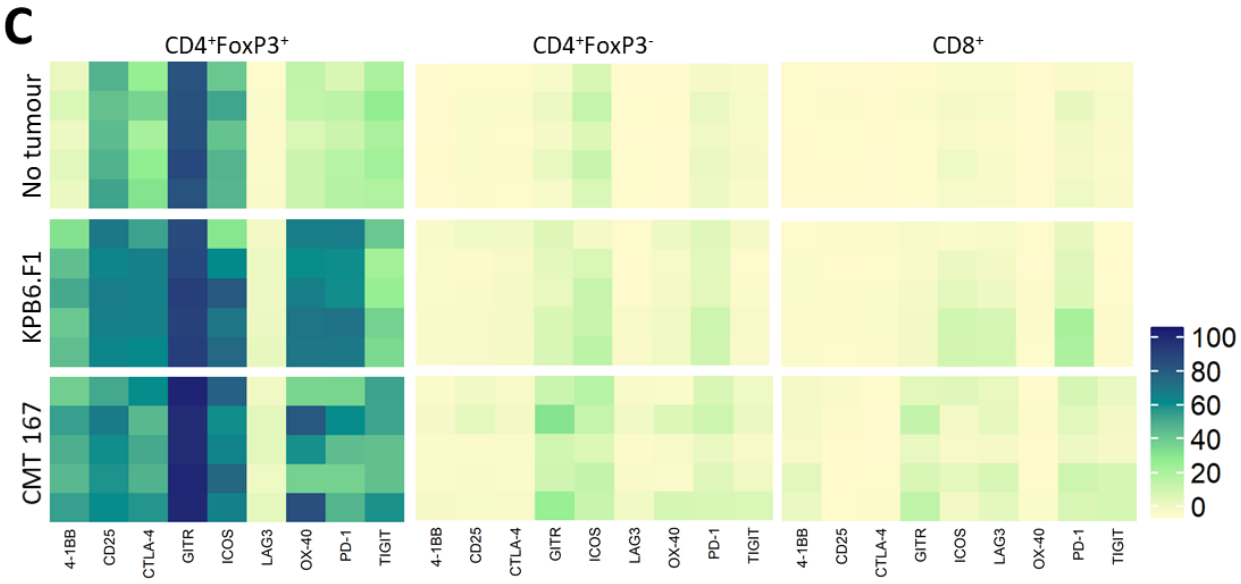

Figure 4.2. KPB6.F1 and CMT-167 mouse models of lung cancer have a cold immune phenotype.

C57BL/6 mice were injected intravenously with the tumour cell lines KPB6.F1 or CMT-167 and lungs were processed as before. Tumour infiltrating lymphocytes were stained and evaluated by flow cytometry. Representative histograms showing the expression of **(A)** co-stimulatory and **(B)** co-inhibitory molecules on regulatory, $CD4^+$ effector and $CD8^+$ T-cells are shown. **(C)** Heatmap showing the frequency of co-inhibitory and co-stimulatory molecules expressed by three different T-cells subsets in the tumour-bearing mice. Results from one experiment with 5 mice per condition.

This expression pattern of co-modulatory molecules on TILs from mouse models of lung cancer resembles the frequency of expression in samples of NSCLC patients (Supporting figure 4.1B).

Therefore, here we demonstrate that the KPB6.F1 and CMT-167 tumour cell lines effectively generate tumours in the lung when injected intravenously. The tumour microenvironment of those models was evaluated, and low expression of activation markers was observed on $CD4^+$ effector and $CD8^+$ T-cells, a classic signature of a "cold" tumour. Additionally, both models have similar frequency of expression of co-modulatory molecules on the surface of infiltrating T-cells to previously described samples of NSCLC patients.

4.4 Localised radiotherapy does not modify the tumour microenvironment of the KPB6.F1 model

As mentioned in Chapter 1, radiotherapy is one of the current standard treatment in lung cancer. The main purpose of radiotherapy is normally to target the tumour burden itself promoting its elimination by radiation-induced apoptosis. However, in the last two decades new insights into the mechanism of action of radiotherapy and its effect on tumour microenvironment have been obtained (Barker et al., 2015). It has been described in multiple mouse models that after radiotherapy there is an accumulation of immune-suppressive cells, such as tumour-associated macrophages (TAMs), Treg cells and myeloid-derived suppressor cells (MDSC) (Laoui et al., 2014; Kachikwu et al., 2011). On the other hand, increased antigen availability and recruitment of circulating immune cells has been proposed to promote a more efficient immune response (Barker et al., 2015). Therefore, the effects of radiotherapy in the activation of different T-cell subsets should be investigated further.

In order to test the effect of radiation in the tumour microenvironment of a murine model of lung, the KPB6.F1-bearing mice were given directed irradiation targeting the right lung. The aim of this evaluation is to develop mouse models which could be used to study combination therapies that entail irradiation as means to activate T-cells. Mice received either one single dose of 8 Gy in the right lung, or 3 x 8Gy fractions delivered with 48 hours between treatments. To assure a thorough data collection that describes the effects of radiotherapy in

the tumour microenvironment, lungs were recovered three and seven days after the last dose received for both radiation schedules. The right and left lungs were analysed separately, to compare local and global effect in the same individual. As a control, mice that did not receive any radiation were also analysed. Figure 4.3A is a scheme showing all the different schedules evaluated.

The frequency of Treg, $CD4^+$ effector and $CD8^+$ T-cells from total $CD3^+$ T-cells was first evaluated, and no differences were found when mice received one dose of radiation at any time evaluated after radiation was received, when compared with untreated (UT) mice. Furthermore, no differences were observed between right and left lung after one dose of 8Gy radiation (Figure 4.3B). Similarly, no differences were observed in the frequency of $CD4^+$ effector and $CD8^+$ T-cells after fractioned 3x8Gy radiation between irradiated right lung or untreated left lung, at any time point evaluated. Although a trend towards an increased frequency of Treg cells from total $CD3^+$ cells after 3x8Gy radiation was observed in the right and left lung when compared with untreated mice, it was not significant (Figure 4.3B). The frequency of NK cells from total $CD45^+$ cells was also evaluated, and no differences were found (Figure 4.3C). Furthermore, the different ratios to Treg cells were calculated for each condition and no differences were found after radiation for $CD8^+$/Treg and $CD4^+$ effector/Treg ratios.

Even though not significant, a trend towards lower NK/Treg ratio was observed after radiation in both lungs. No differences between right and left lung were observed (Figure 4.3D).

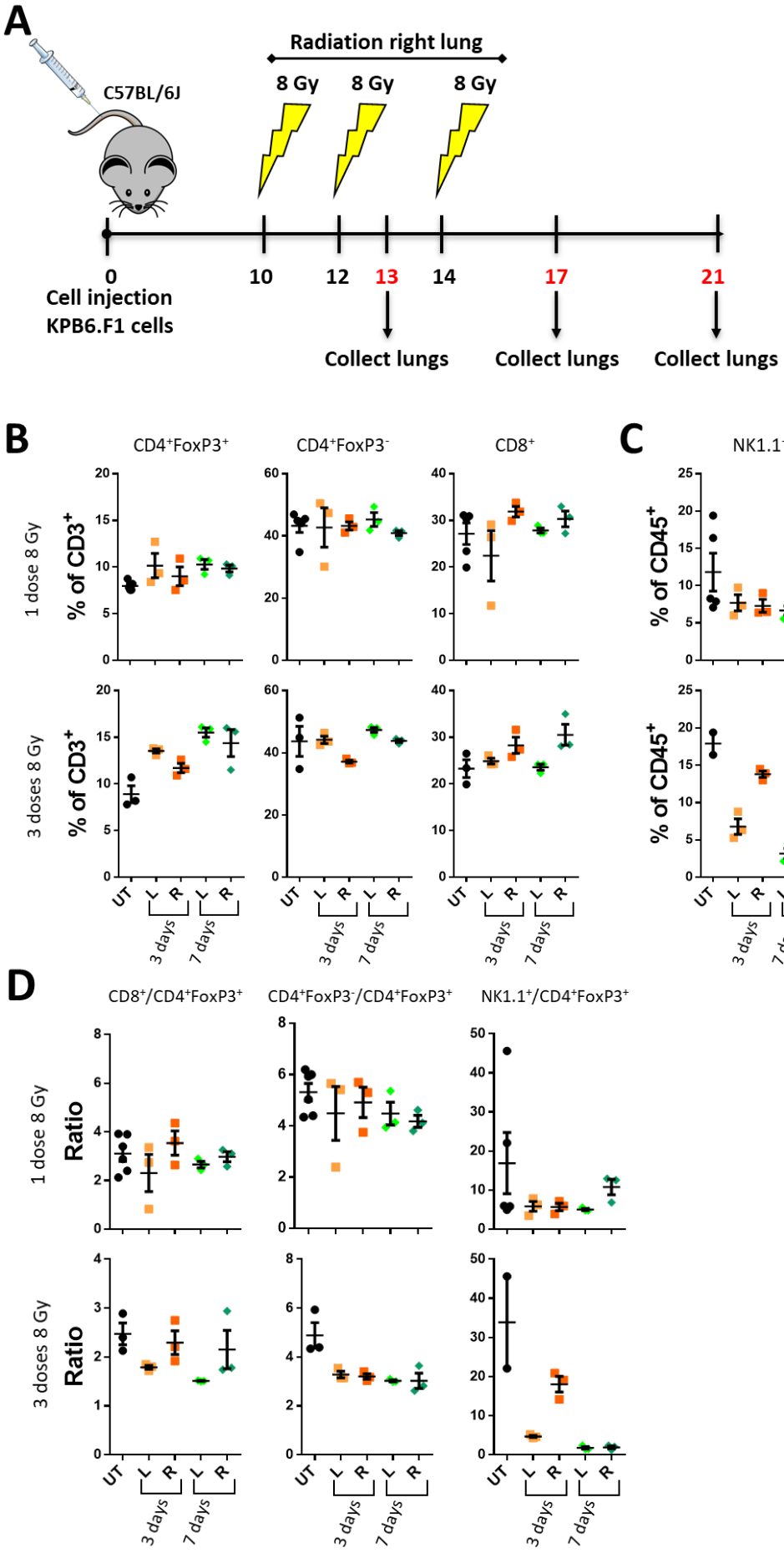
A
Radiation right lung
8 Gy
8 Gy
8 Gy
C57BL/6J
0
Cell injection
KPB6.F1 cells
10
12
13
14
17
21
Collect lungs
Collect lungs
Collect lungs
B
CD4+FoxP3+
CD4+FoxP3-
CD8+
1 dose 8 Gy
3 doses 8 Gy
% of CD3+
C
NK1.1+
% of CD45+
UT
L
R
3 days
7 days
D
CD8+/CD4+FoxP3+
CD4+FoxP3-/CD4+FoxP3+
NK1.1+/CD4+FoxP3+
Ratio

Figure 4.3. Radiotherapy to the right lung maintain T-cell frequencies and ratios unaltered.

C57BL/6 mice were injected intravenously with KPB6.F1 cells. Mice were treated with radiotherapy in the right lung on day 10 (1 dose 8 Gy) or on days 10, 12 and 14 (3 doses 8 Gy) post cell injection. Tumour-bearing lungs were collected three and seven days after the last dose of radiotherapy for both therapy regimen described. single cell suspensions of tumour infiltrating lymphocytes were stained and evaluated by flow cytometry. **(A)** Scheme of radiotherapy doses given to mice and the end points for each dose schedule. **(B)** Frequency of regulatory, effector $CD4^+$ and $CD8^+$ T-cells from total $CD3^+$ in the left (L) and right (R) lung. **(C)** Frequency of $NK1.1^+$ cells from total $CD45^+$ cells. **(D)** Ratio between $CD8^+$ T-cells, $CD4^+$ effector T-cells or NK cells relative to regulatory T-cells in the tumour-bearing lungs. Horizontal bars represent the mean, errors bars shown ± standard error of the mean (SEM). p values were calculated using non-parametrical analysis Kruskal-Wallis test. ns = $p > 0.05$, *$p \leq 0.05$, **$p \leq 0.01$, ***$p \leq 0.001$, **** $P \leq 0.0001$. Results from one experiment with at least 3 mice per condition.

As no significant differences were found in the frequency and ratios of T-cell populations and NK cells when radiation therapy was administrated, the immune phenotype of those populations was evaluated by measuring the expression of co-modulatory molecules on the surface of those cells. The frequency of expression of different co-modulatory proteins for individual mice was plotted as a heatmap for clarity purposes. It was observed that no major changes in the expression of any of the markers was observed for all the populations tested (Figure 4.4).

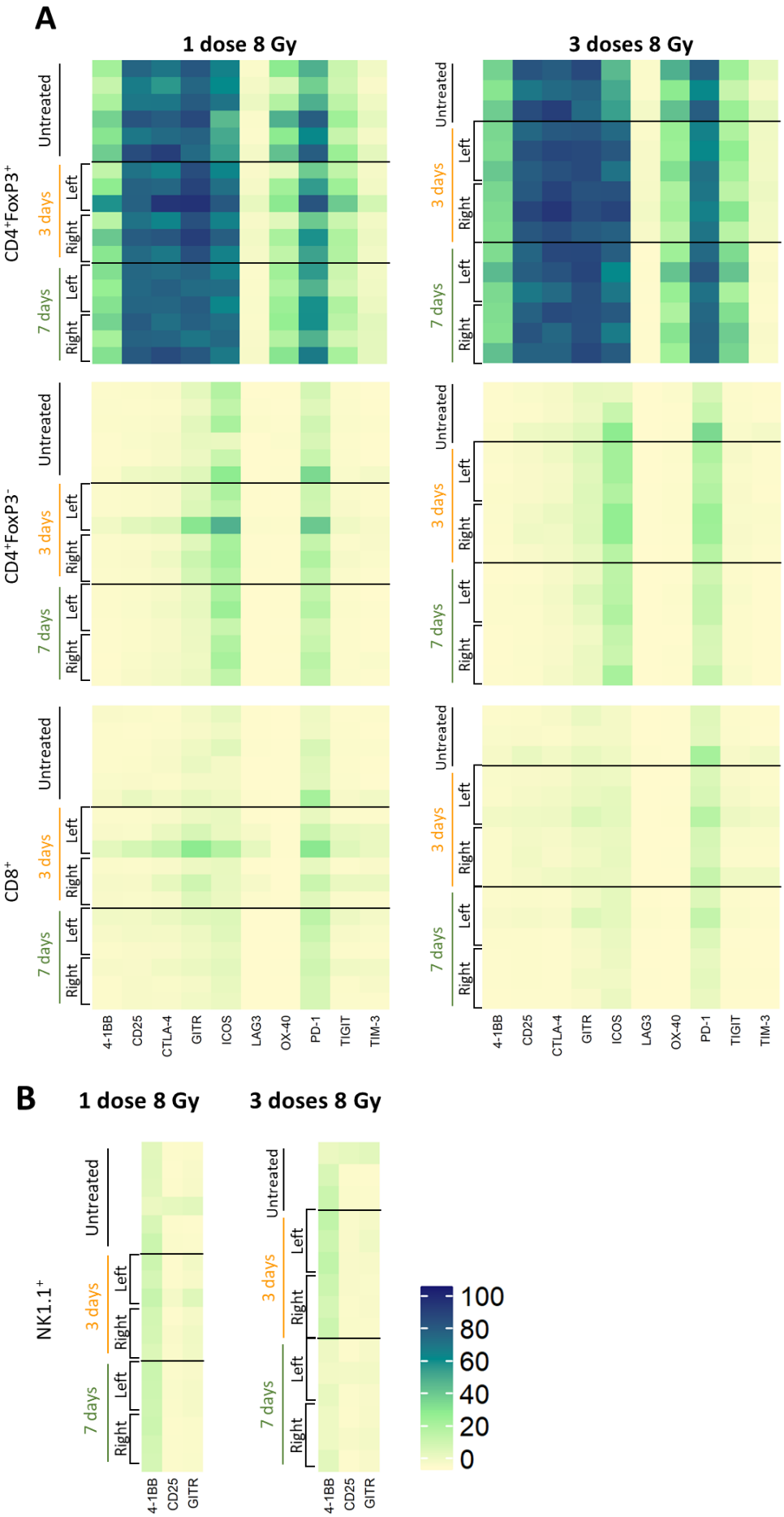
A
1 dose 8 Gy
3 doses 8 Gy
CD4+FoxP3+
CD4+FoxP3-
CD8+
Untreated
3 days
Left
Right
7 days
Left
Right
4-1BB
CD25
CTLA-4
GITR
ICOS
LAG3
OX-40
PD-1
TIGIT
TIM-3
B
1 dose 8 Gy
3 doses 8 Gy
NK1.1+
100
80
60
40
20
0

Figure 4.4. Radiotherapy is unable to modify the activation phenotype of infiltrating T-cells in the KPB6.F1 mouse model of lung cancer.

C57BL/6 mice were injected intravenously with KPB6.F1 cells and treated with localized radiotherapy in the right lung as described above. Tumour infiltrating lymphocytes were stained and evaluated by flow cytometry. Heatmap showing the frequency of co-inhibitory and co-stimulatory molecules expressed by **(A)** three different T-cells subsets and **(B)** NK cells in the tumour-bearing lungs. Results from one experiment with at least 3 mice per condition.

These results indicate that radiotherapy was ineffective in promoting a further activation of TILs found in the lungs of mice carrying KPB6.F1 tumour. Interestingly, for all T-cells compartments no differences were observed between untreated mice and radiotherapy-treated mice, in both irradiated (right) and non-irradiated (left) lung. In the case of NK cells, even though a trend toward reduction of the ratios was observed in radiotherapy-treated mice, this may be attributed to variations between mice rather than radiation itself.

Taking these observations together, irradiation therapy failed to activate the immune cells in the KPB6.F1-derived tumours, possibly by the low immunogenicity of the model.

Initial results of a clinical trial described longer overall survival and progression free-survival after pembrolizumab treatment in NSCLC patients pre-treated with radiotherapy, when compared with patients receiving pembrolizumab without previous radiotherapy (Shaverdian et al., 2017). This benefit associated to the combination of radiotherapy and pembrolizumab was observed regardless pre-treatment levels of PD-L1 expression, indicating that radiotherapy promoted the patient's response to immunotherapy (Shaverdian et al., 2017). Unfortunately, no other immunomodulatory molecules were evaluated in the study. In another phase I trial evaluating treatments for metastatic solid tumours, clinical benefit from combination of ipilimumab and radiotherapy was correlated to increased $CD8^{+}4$-

1BB^{+}PD-1^{+} cells in the periphery, observed in irradiated liver but not in irradiated lungs (Tang et al., 2017).

Thus, as some clinical data suggest benefit of combination of radiotherapy and checkpoint blockade, this is still restricted to a fraction of patients and no data from other immunomodulatory molecules has been generated for NSCLC. Therefore, the KPB6.F1 tumour could be a good model to study types of lung cancer that not benefit from combination of radiotherapy and checkpoints inhibitors, providing strategies to help the development of treatments for this population of patients. Dozens of clinical trials phase I and II are currently evaluating the combination of radiotherapy with checkpoint blockade (NIH - clinicaltrials.gov, 2018), which will provide more important information to compare with murine models.

Given difficulties encountered with accessing a functional irradiator of desired properties, this part of the project has been put on hold and studies in CMT-167 model are yet to be carried out. Furthermore, a comparison to the clinical samples from lung cancer patients treated with irradiation would be of interest.

4.5 Chemotherapy failed to induce activation of TILs in the KPB6.F1 model

In addition to radiotherapy, another therapeutic intervention thought to impact the TME within tumours is chemotherapy, hence we next sought to determine whether chemotherapy could sensitise the tumour to immunotherapy by increasing the activation status of tumour infiltrating T-cells in mice bearing KPB6.F1 tumours. In addition, to counteract the potential accumulation of regulatory T-cells, an anti-CD25 mAb was tested alone as an immunotherapy strategy for Treg depletion. The feasibility of targeting CD25 expressed on Treg cells through a depleting antibody has already been demonstrated by our laboratory with promising therapeutic outcomes in different immunogenic mouse models of fibrosarcoma and colorectal cancer (Arce Vargas et al., 2017).

The role of chemotherapy as a mean to sensitise tumours to antibody immunotherapy has been widely described (Bracci et al., 2014). In the context of mouse models of lung cancer,

Pfirschke and collaborators (Pfirschke et al., 2016) showed that the combination of cyclophosphamide and oxaliplatin in another model of lung cancer derived from the $Kras^{LSL/G12D}$ $Trp53^{flox/flox}$ mice induced the tumours to respond to combination therapy targeting anti-PD-1 mAb plus anti-CTLA-4 mAb, promoting the infiltration of $CD8^+$ into the adenocarcinoma nodules. For this reason, a single dose of both chemotherapies, cyclophosphamide and oxaliplatin, alone and combined, and anti-CD25 mIgG2a mAb were evaluated as different strategies to target regulatory T-cells and induce activation of infiltrating effector $CD4^+$ and cytotoxic T-cells.

As a measure of the tumour burden the weight of the lungs was first evaluated, showing that both chemotherapies (alone and together) induced a slight (although not significant) increase in tumour burden. The same trend was observed between untreated and anti-CD25 mAb treated mice (Figure 4.5A).

The number of T-cells and NK cells normalised to the weight of the lung was also calculated. Whilst the number of effectors $CD4^+$ and $CD8^+$ T-cells remained similar for all the tested conditions, the number or Treg trended towards a reduction when compared to untreated mice, especially when anti-CD25 mAb was used (Figure 4.5B). Furthermore, the number of NK cells infiltrating the lungs was reduced in all the tumour-bearing mice when compared with healthy lungs, with significant difference when cyclophosphamide was administrated (Figure 4.5B). The $CD8^+$/Treg and $CD4^+$effector/Treg ratios also increased, with significant differences when combination of cyclophosphamide and oxaliplatin and anti-CD25-m2a mAb were given, showing the relative reduction of regulatory T-cells in the tumour. On the contrary, the NK/Treg ratio remained similar within all tumour-bearing mice (Figure 4.5C). The proliferation, measured as Ki67 expression, and Granzyme B production were also diminished in all T-cell subsets and NK cells, which correlated with the tumour burden of the treated mice (Figure 4.5D). To determine if chemotherapy in the KPB6.F1 model was capable of increasing susceptibility of the tumour to immunotherapy, the expression of immune modulatory molecules was evaluated on T-cells. NK cells were excluded from the analysis due the low number of cells in the tumour-bearing samples that resulted in misleading frequencies. The frequency of Treg cells expressing 4-1BB, CD25, GITR and OX-40 remained similar in all tumour bearing mice, but the frequency of $ICOS^+$ Treg cells decreased when chemotherapy was given (Figure 4.6). Chemotherapy increased the frequency of

effector T-cells expressing the activation markers 4-1BB, CD25 and GITR whilst a trend towards a reduction in the frequency of $ICOS^{+}CD8^{+}$ cells was also observed (Figure 4.6 A, B, C and D).

The frequency of expression of immune checkpoints CTLA-4, LAG3 and PD-1 were also evaluated on effector and regulatory T-cells with no significant differences after chemotherapy or anti-CD25m2a mAb treatment (Figure 4.7).

Even though some differences in the frequency of modulatory receptors expressed on effector $CD4^{+}$ and $CD8^{+}$ T-cells were observed, the reduction in proliferation suggests that chemotherapy is not promoting the activation of these $CD4^{+}$ and $CD8^{+}$ T-cells. Therefore, we hypothesised that chemotherapy does not sensitise KPB6.F1 tumours to respond to antibody immunotherapies, considering the lack of upregulation of immunomodulatory targets and impaired proliferation. Further experiments are needed to test this hypothesis.

Considering the difficulty of induce the activation of TILs in the KPB6.F1 model by radiotherapy and chemotherapy, and the observation that NK cell presence in the tumour microenvironment had an inverse correlation with the tumour burden, the next strategy was to potentiate the activation of NK and T-cells through anti-4-1BB mAb treatment combined with Treg depletion.

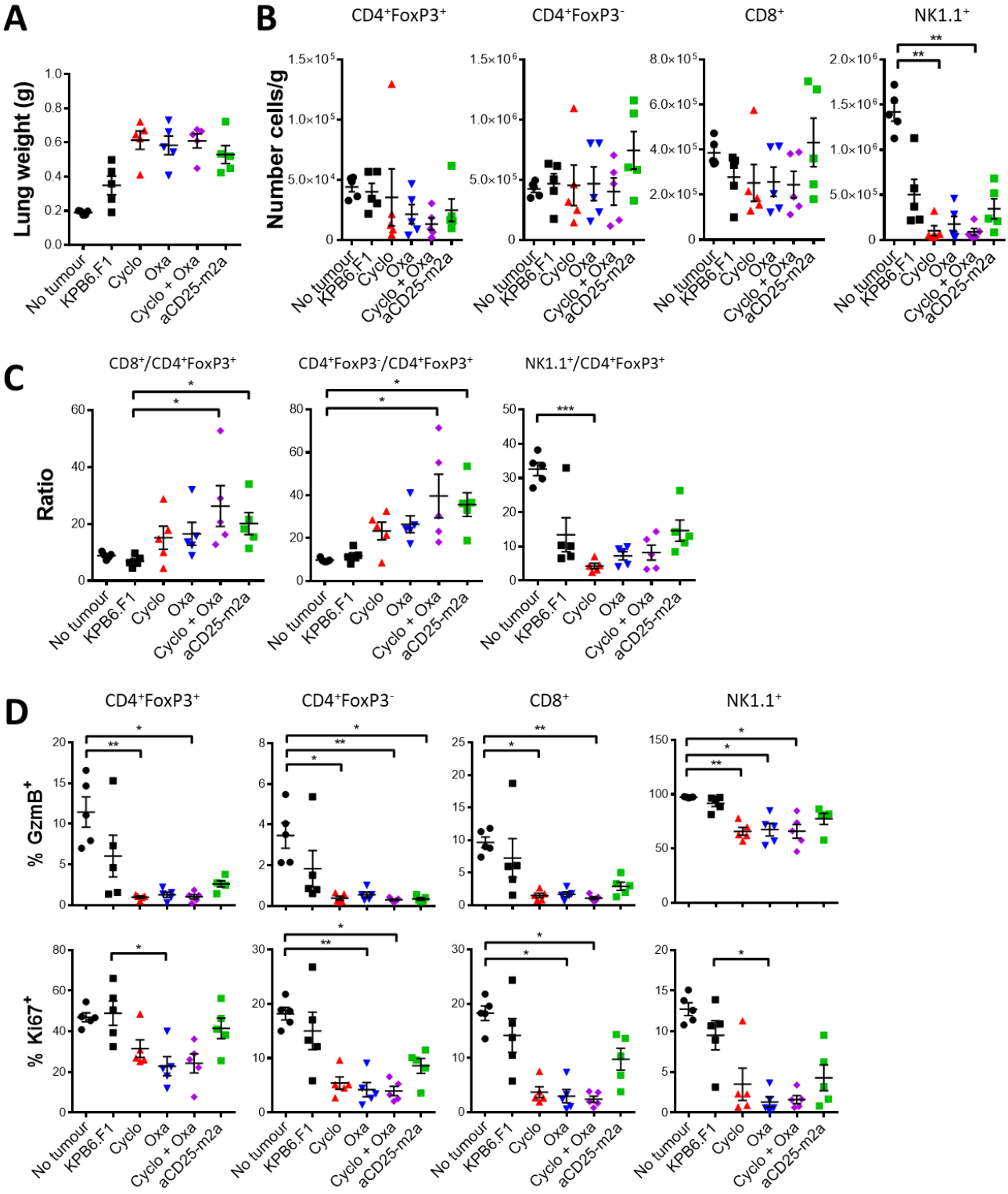
A
Lung weight (g)
B
CD4+FoxP3+
CD4+FoxP3-
CD8+
NK1.1+
Number cells/g
C
CD8+/CD4+FoxP3+
CD4+FoxP3-/CD4+FoxP3+
NK1.1+/CD4+FoxP3+
Ratio
D
CD4+FoxP3+
CD4+FoxP3-
CD8+
NK1.1+
% GzmB+
% Ki67+
No tumour
KPB6.F1
Cyclo
Oxa
Cyclo + Oxa
aCD25-m2a

Figure 4.5. Tumour-bearing mice treated with chemotherapy that developed more tumours are correlated with reduced proliferation and Granzyme B production.

C57BL/6 mice were left untreated or injected intravenously with KPB6.F1 cells. Ten days later, mice received 50 mg/Kg of cyclophosphamide (Cyclo), 2.5 mg/Kg of oxaliplatin (Oxa), a combination of 50 mg/Kg cyclophosphamide plus 2.5 mg/Kg oxaliplatin (Cyclo + Oxa) or 200 µg of anti-CD25 mAb (clone PC61, mouse IgG2a). At day 21 mice were euthanized and lungs were recovered, and a single cell suspension was stained and analysed by flow cytometry. **(A)** Total weight of the lungs for each condition. **(B)** Normalised number of regulatory T-cell, $CD4^+$ effector, $CD8^+$ T-cells and NK cells found in tumour bearing lungs. **(C)** Ratio between $CD8^+$ T-cells, $CD4^+$ effector T-cells and NK cells relative to regulatory T-cells in the tumour-bearing lungs. **(D)** Frequency of Granzyme B ($GzmB^+$) and $Ki67^+$ cells from regulatory, $CD4^+$ effector, $CD8^+$ T-cells and NK cells. Horizontal bars represent the mean, errors bars shown ± standard error of the mean (SEM). p values were calculated using non-parametrical analysis Kruskal-Wallis test. ns = $p > 0.05$, *$p \leq 0.05$, **$p \leq 0.01$, ***$p \leq 0.001$, **** $P \leq 0.0001$. Results from one experiment with 5 mice per condition.

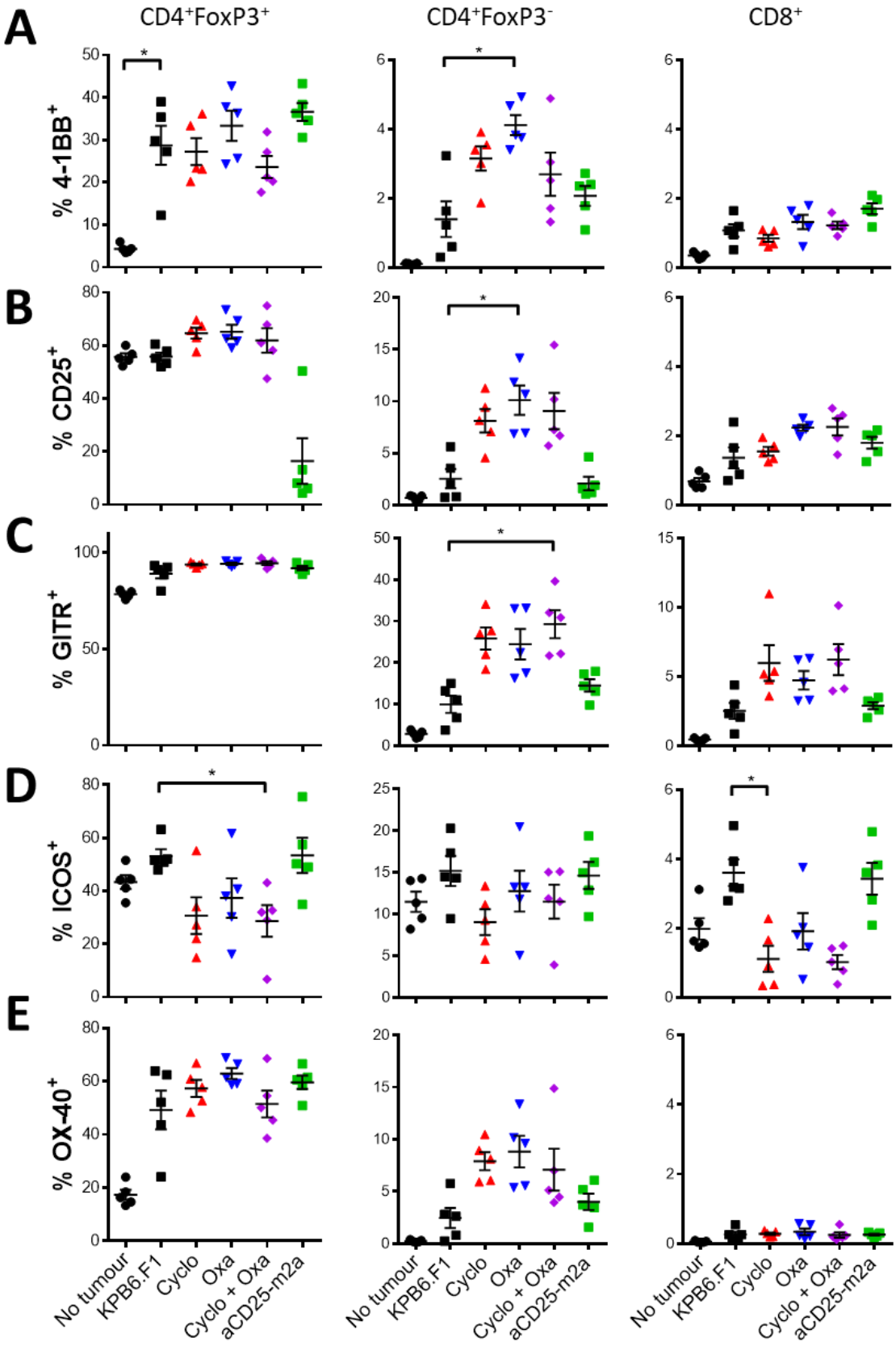
A
B
C
D
E
CD4+FoxP3+
CD4+FoxP3-
CD8+
% 4-1BB+
% CD25+
% GITR+
% ICOS+
% OX-40+
No tumour
KPB6.F1
Cyclo
Oxa
Cyclo + Oxa
aCD25-m2a

Figure 4.6. Chemotherapy treatment increased the frequency of 4-1BB, CD25 and GITR on effector $CD4^+$ T-cells.

C57BL/6 mice were left untreated or injected intravenously with KPB6.F1 cells and treated with chemotherapy or anti-CD25 mAb as explained in the previous figure. At day 21 mice were euthanised, lungs were recovered, and a single cell suspension was stained and analysed by flow cytometry. Graphs summarising the frequency from regulatory T-cells ($CD4^+FoxP3^+$), effector $CD4^+$ ($CD4^+FoxP3^-$), and $CD8^+$ T-cells was determined for **(A)** 4-1BB, **(B)** CD25, **(C)** GITR, **(D)** ICOS and **(E)** OX-40. Horizontal bars represent the mean, errors bars shown ± standard error of the mean (SEM). p values were calculated using non-parametrical analysis Kruskal-Wallis test. ns = $p > 0.05$, *$p \leq 0.05$, **$p \leq 0.01$, ***$p \leq 0.001$, **** $P \leq 0.0001$. Results from one experiment with 5 mice per condition.

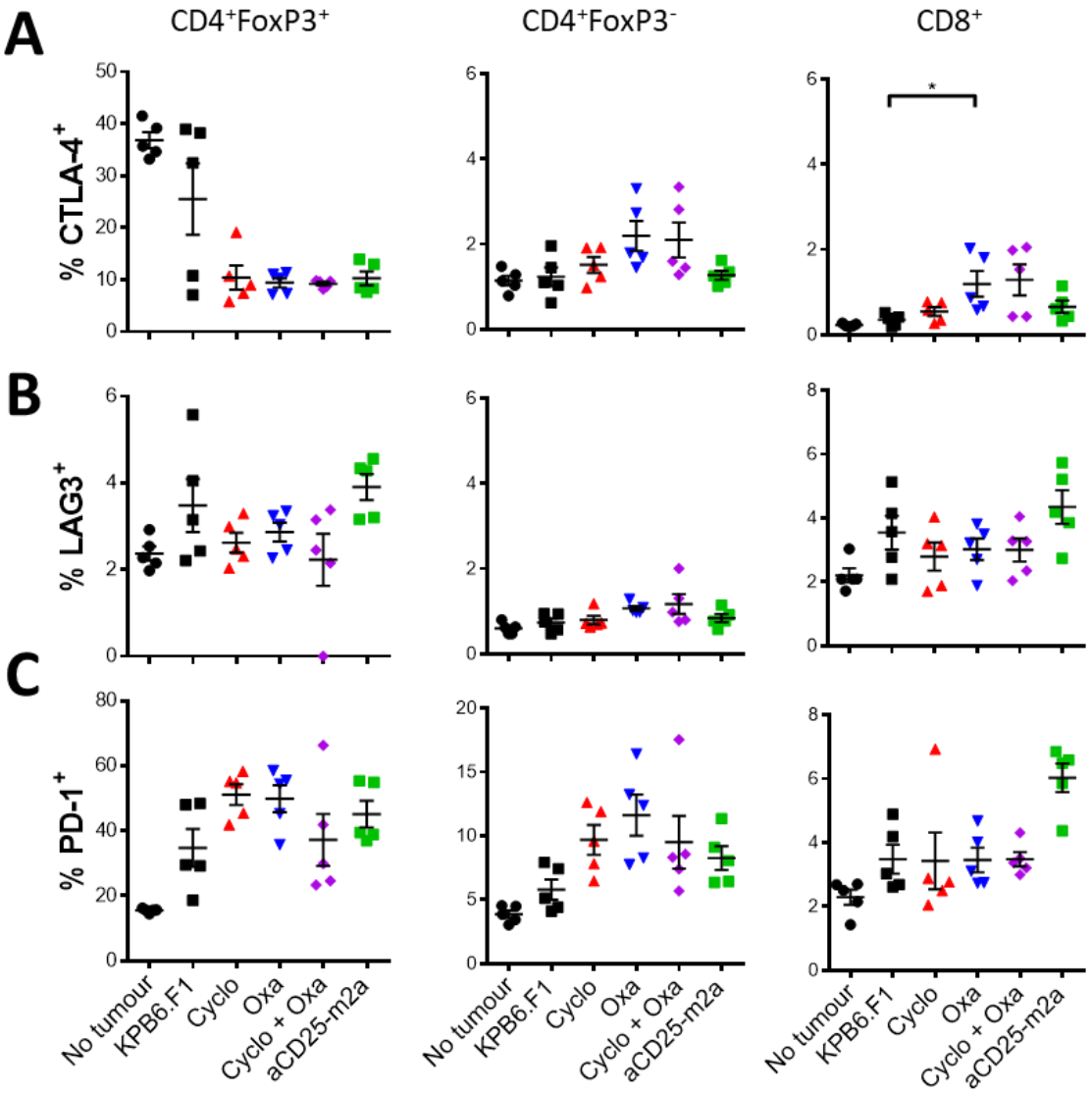

Figure 4.7. Chemotherapy treatment had no effect in frequency of expression of CTLA-4, LAG3 and PD-1 on T-cells.

C57BL/6 mice were left untreated or injected intravenously with KPB6.F1 cells and treated with chemotherapy or anti-CD25 mAb as explained before. At day 21 mice were euthanised, lungs were recovered, and a single cell suspension was stained and analysed by flow cytometry. Graphs summarising the frequency of expression of co-inhibitory checkpoints from regulatory T-cells ($CD4^+FoxP3^+$), effector $CD4^+$ ($CD4^+FoxP3^-$), and $CD8^+$ T-cells was determined for **(A)** CTLA-4, **(B)** LAG3 and **(C)** PD-1. Horizontal bars represent the mean, errors bars shown ± standard error of the mean (SEM). p values were calculated using non-parametrical analysis Kruskal-Wallis test. ns = $p > 0.05$, *$p \leq 0.05$, **$p \leq 0.01$, ***$p \leq 0.001$, **** $P \leq 0.0001$. Results from one experiment with 5 mice per condition.

4.6 Anti-4-1BB mAb therapy promotes proliferation and activation of T-cells in the KPB6.F1 model

As mentioned, radiotherapy and chemotherapy failed to promote activation of infiltrating T-cells. For this reason, according with the aims of this project, it was hypothesised that anti-4-1BB mAb therapy may promote activation of infiltrating T-cells and NK cells in the KPB6.F1 model of lung cancer. In order to avoid Treg suppression activity triggered by anti-4-1BB mAb therapy, anti-CD25 mAb Treg depleting therapy was also evaluated in this context.

4-1BB is a co-stimulatory molecule member of the TNFR family normally upregulated upon T-cell activation and associated to the stable generation of memory $CD8^+$ T-cells. It is also expressed by other activated T-cells, NK cells and NKT cells (Kobayashi et al., 2015; Weigelin et al., 2015; Willoughby et al., 2014; Moran et al., 2013). It has been described that agonistic antibodies targeting 4-1BB lead to increased survival, proliferation and accumulation of GzmB and perforin by $CD8^+$ T-cells, preventing also the anergy of those cells (Wilcox et al., 2002; Hernandez-Chacon et al., 2011). Therefore, in the context of a cold tumour microenvironment such as the KPB6.F1 model where minimal T-cell and NK cell activity is observed, we hypothesised that agonistic antibodies against 4-1BB could drive activation and function of both T-cells and NK cells compartments.

To test if an anti-4-1BB mAb strategy would be successful in activating T-cells and promoting also NK function in the tumour, mice were treated with three doses of an agonistic anti-4-1BB mAb (clone LOB12.3). A group of mice also received anti-CD25m2a mAb 24 hours prior anti-4-1BB mAb treatment, to deplete regulatory T-cells as these cells could reduce the potential *in vivo* activity of anti-4-1BB mAb. The tumour burden in the lungs was evaluated by measuring the weight of the lungs, and no significant differences between the tested conditions were observed (Figure 4.8A). The effectivity of anti-CD25m2a mAb in depleting Treg cells in the lung was confirmed by the lower frequency and total number of Treg cells observed in treated mice (Figure 4.8B and C). Whilst the total number of effectors $CD4^+$ T-cells was not affected by anti-4-1BB mAb treatment, the antibody induced an increase in the frequency and number of $CD8^+$ T-cells in the tumour (Figure 4.8B and C).

The reduction in the frequency of $CD4^+$ effector from total $CD3^+$ cells in anti-4-1BB mAb treatment reflects an increased total $CD3^+$ driven by the increase in $CD3^+CD8^+$ cells

rather than a reduction of $CD3^+CD4^+FoxP3^-$ cells. On the other hand, NK cells significantly decreased after anti-4-1BB mAb therapy (Figure 4.8B).

In order to evaluate the balance between effector and suppressive Treg cells, the ratios were calculated for every condition, showing that combination of Treg depletion by anti-CD25 mAb together with stimulation of T-cells by anti-4-1BB mAb gave the most increased $CD8^+$/Treg and $CD4^+$ effector/Treg ratios (Figure 4.8D). Due to the reduction of NK cells after anti-4-1BB mAb treatment, the NK/Treg ratio just increased when anti-CD25 mAb was given as monotherapy (Figure 4.8D).

Given the increased number of $CD8^+$ T-cells, proliferation was also evaluated. The agonistic anti-4-1BB antibody was effective at promoting the proliferation of all T-cell subsets, with higher increases in $CD4^+$ effector (from 20 to 50% of $Ki67^+$ cells) and $CD8^+$ T-cells, going from 20 to 80% of $CD8^+$ cells expressing Ki67 (Figure 4.9B). Granzyme B production, by $CD4^+$ and $CD8^+$ T-cells was also significantly increased by anti-4-1BB mAb by at least 5-fold (Figure 4.9A). On the contrary, proliferation of Treg was only slightly increased by anti-4-1BB mAb, indicating a shift towards a less immunosuppressive microenvironment after the therapy (Figure 4.9B). The increase in Ki67 expression by NK cells may suggest the start of repopulation in the tumour by those cells after the treatment, but that remains to be confirmed (Figure 4.9B).

The activation phenotype of the cells was also evaluated. In general, the frequency of expression of co-stimulatory molecules on Treg cells remained similar between the three treatment conditions and untreated mice (Figure 4.10). Effector $CD4^+$ and $CD8^+$ T-cells increased the frequency of $ICOS^+$ cells after receiving anti-4-1BB mAb, without changes in the frequency of expression of 4-1BB, CD25, GITR and OX-40 on those effector T-cells (Figure 4.10). We also evaluated the expression of co-inhibitory checkpoints on T-cells. Following anti-4-1BB mAb treatment, we observed an increase in the frequency of $TIGIT^+$ Treg cells, whilst no changes in the frequency of Treg cells expressing CTLA-4, LAG3 or PD-1 was observed (Figure 4.11). On the contrary, significant increases in the frequency of expression of LAG3, PD-1 and TIGIT were observed in $CD4^+FoxP3^-$ and $CD8^+$ T-cells after anti-4-1BB mAb immunotherapy, demonstrating the activation of both T-cell subsets by the therapy, which was correlated to increased GzmB production (Figure 4.11). The percentage of CTLA-4 expressing $CD4^+$ and $CD8^+$ T-cells also increased, but to a lower extend (Figure 4.11).

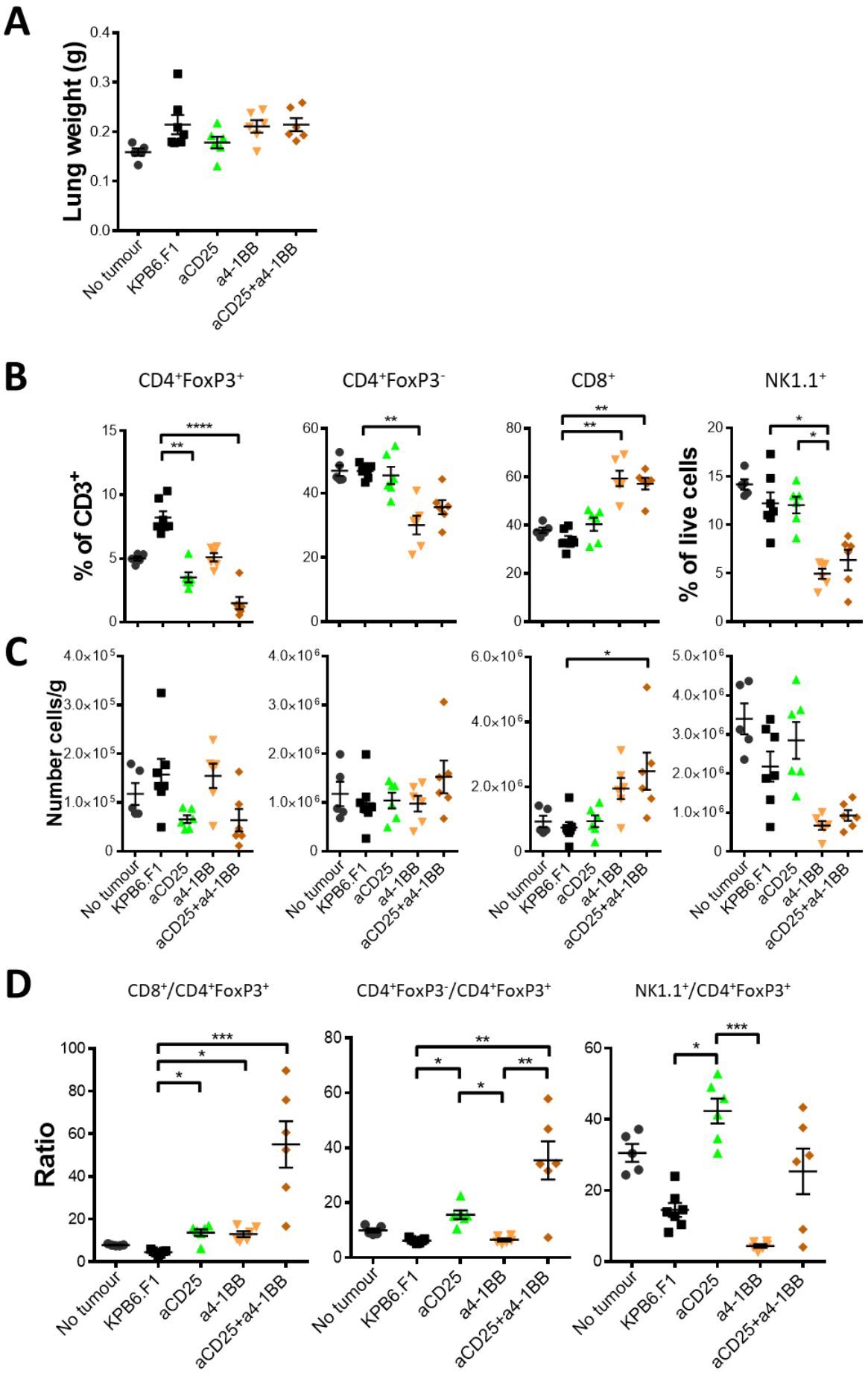
A
Lung weight (g)
0.4
0.3
0.2
0.1
0.0
No tumour
KPB6.F1
aCD25
a4-1BB
aCD25+a4-1BB
B
CD4+FoxP3+
CD4+FoxP3-
CD8+
NK1.1+
% of CD3+
% of live cells
C
Number cells/g
D
CD8+/CD4+FoxP3+
CD4+FoxP3-/CD4+FoxP3+
NK1.1+/CD4+FoxP3+
Ratio

Figure 4.8. Anti-4-1BB mAb treatment promotes higher frequency and number of $CD8^+$ T-cells and increased ratios in tumour-bearing lungs.

C57BL/6 mice were left untreated or injected intravenously with KPB6.F1 cells. Six days after, a group of mice received one dose of 200 μg of anti-CD25 mAb (clone PC61, mouse IgG2a) and later, mice were treated with 200 μg of anti-4-1BB mAb (clone LOB12.3 rat IgG1) on days 7, 10 and 13. At day 17 mice were euthanized and lungs were recovered. Lungs were processed, and a single cell suspension was stained and analysed by flow cytometry. **(A)** Total weight of the lungs for each condition. **(B)** Frequency of regulatory, $CD4^+$ effector and $CD8^+$ T-cells from $CD3^+$ gate and frequency of $NK1.1^+$ from total live cells. **(C)** Total number normalised to the weight of the lungs of regulatory, $CD4^+$ effector, $CD8^+$ T-cells and NK cells. **(D)** Ratio between $CD8^+$ T-cells, $CD4^+$ effector T-cells and NK cells relative to regulatory T-cells in the tumour-bearing lungs. Horizontal bars represent the mean, errors bars shown ± standard error of the mean (SEM). p values were calculated using non-parametrical analysis Kruskal-Wallis test. ns = $p > 0.05$, *$p \leq 0.05$, **$p \leq 0.01$, ***$p \leq 0.001$, **** $P \leq 0.0001$. Results from one experiment with 5 mice per condition.

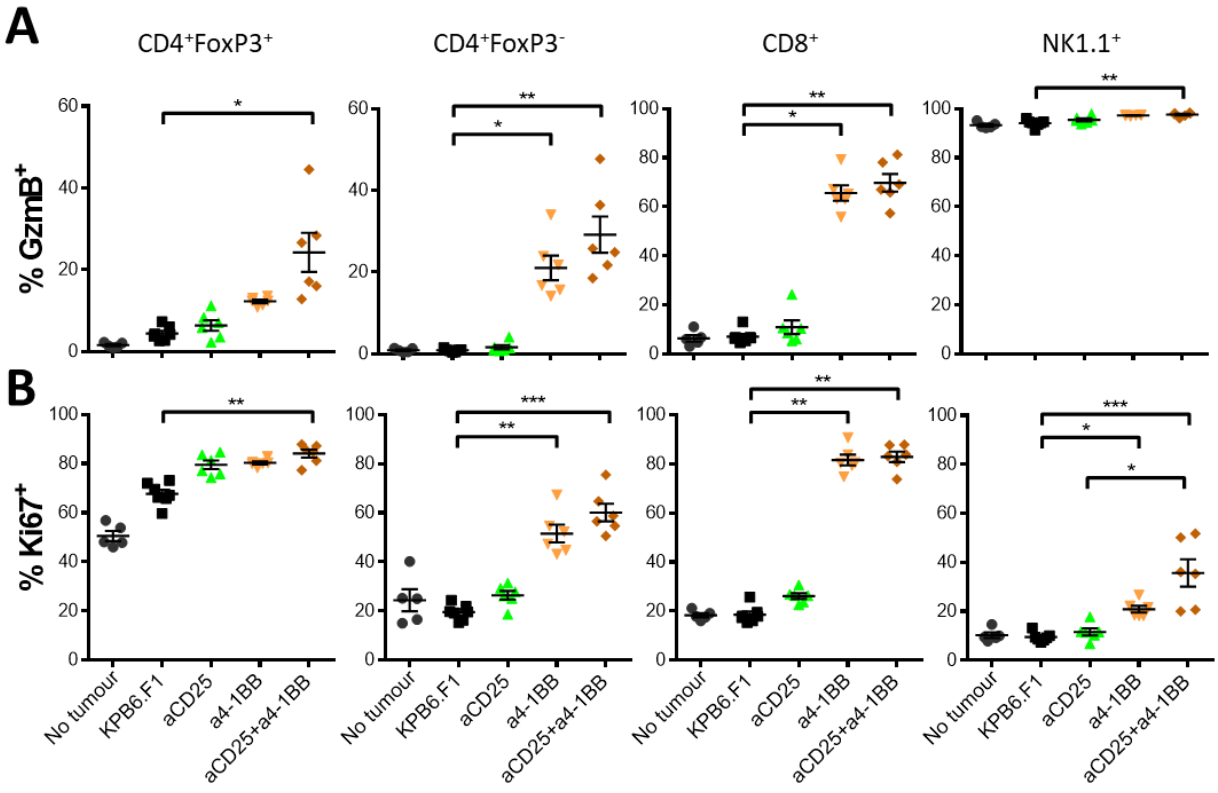

Figure 4.9. Anti-4-1BB mAb treatment promotes Granzyme B production and proliferation in tumour-bearing lungs.

C57BL/6 mice were left untreated or injected intravenously with KPB6.F1 cells. Mice received one dose of 200 µg of anti-CD25 mAb (clone PC61, mouse IgG2a) at day 6 and later were treated with 200 µg of anti-4-1BB mAb (clone LOB12.3 rat IgG1) on days 7, 10 and 13. At day 17 mice were euthanized and lungs were recovered. Lungs were processed, and a single cell suspension was stained and analysed by flow cytometry. Frequency of **(A)** Granzyme B ($GzmB^+$) and **(B)** $Ki67^+$ cells from regulatory, $CD4^+$ effector, $CD8^+$ T-cells and NK cells. Horizontal bars represent the mean, errors bars shown ± standard error of the mean (SEM). p values were calculated using non-parametrical analysis Kruskal-Wallis test. ns = $p > 0.05$, *$p \leq 0.05$, **$p \leq 0.01$, ***$p \leq 0.001$, **** $P \leq 0.0001$. Results from one experiment with 5 mice per condition.

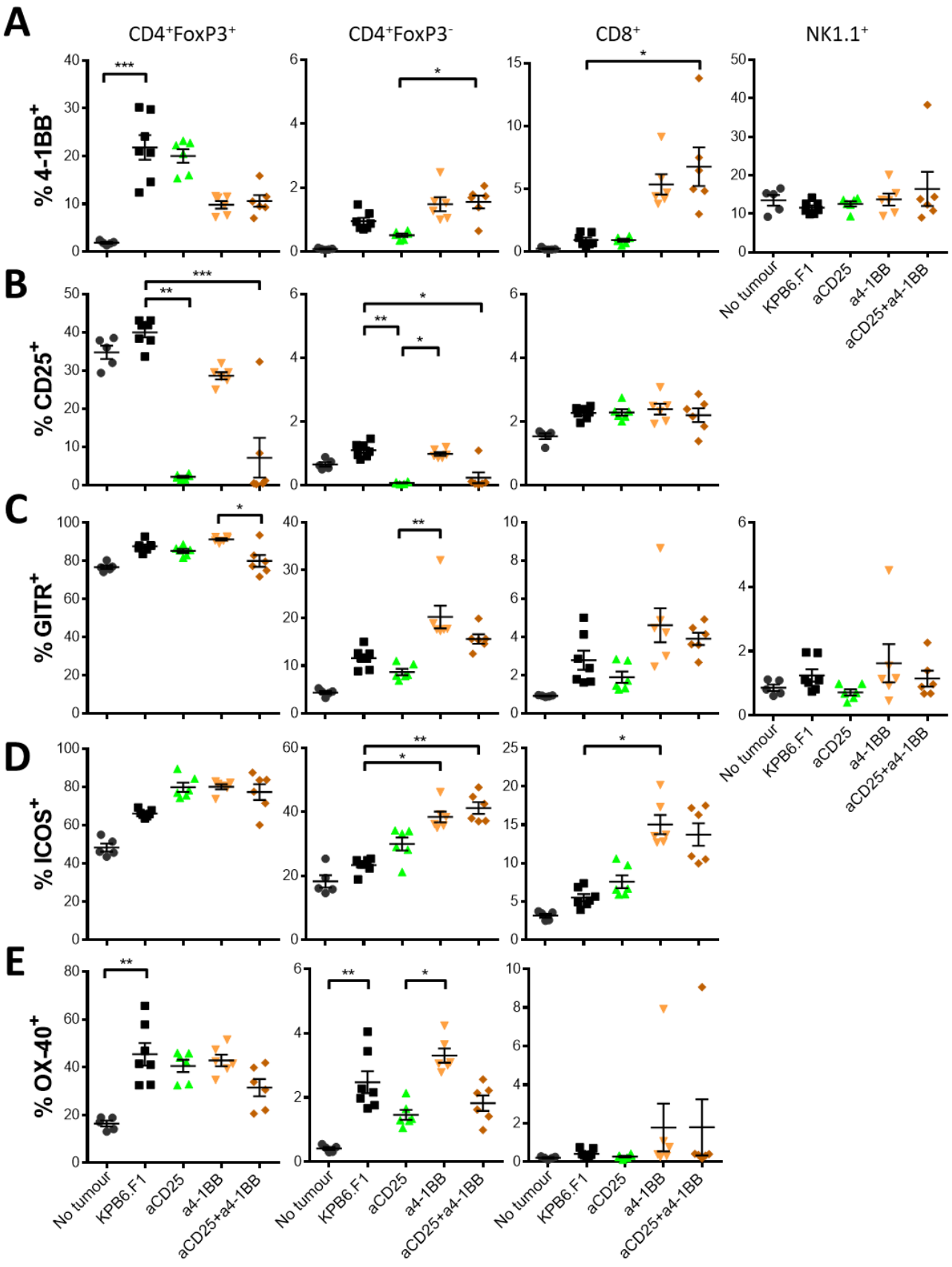
A
B
C
D
E
CD4+FoxP3+
CD4+FoxP3-
CD8+
NK1.1+
% 4-1BB+
% CD25+
% GITR+
% ICOS+
% OX-40+
No tumour
KPB6.F1
aCD25
a4-1BB
aCD25+a4-1BB

Figure 4.10. Immunotherapy with agonistic anti-4-1BB mAb increased 4-1BB, GITR and ICOS expression on $CD4^+$ T-cells.

C57BL/6 mice were left untreated or injected intravenously with KPB6.F1 cells and treated anti-CD25 mAb and anti-4-1BB mAb as explained before. At day 21 mice were euthanised, lungs were recovered, and a single cell suspension was stained and analysed by flow cytometry. Graphs summarising the frequency from regulatory T-cells ($CD4^+FoxP3^+$), effector $CD4^+$ T-cells ($CD4^+FoxP3^-$), $CD8^+$ T-cells and NK cells was determined for **(A)** 4-1BB, **(B)** CD25, **(C)** GITR, **(D)** ICOS and **(E)** OX-40. Horizontal bars represent the mean, errors bars shown ± standard error of the mean (SEM). p values were calculated using non-parametrical analysis Kruskal-Wallis test. ns = $p > 0.05$, *$p \leq 0.05$, **$p \leq 0.01$, ***$p \leq 0.001$, **** $P \leq 0.0001$. Results from one experiment with 5 mice per condition.

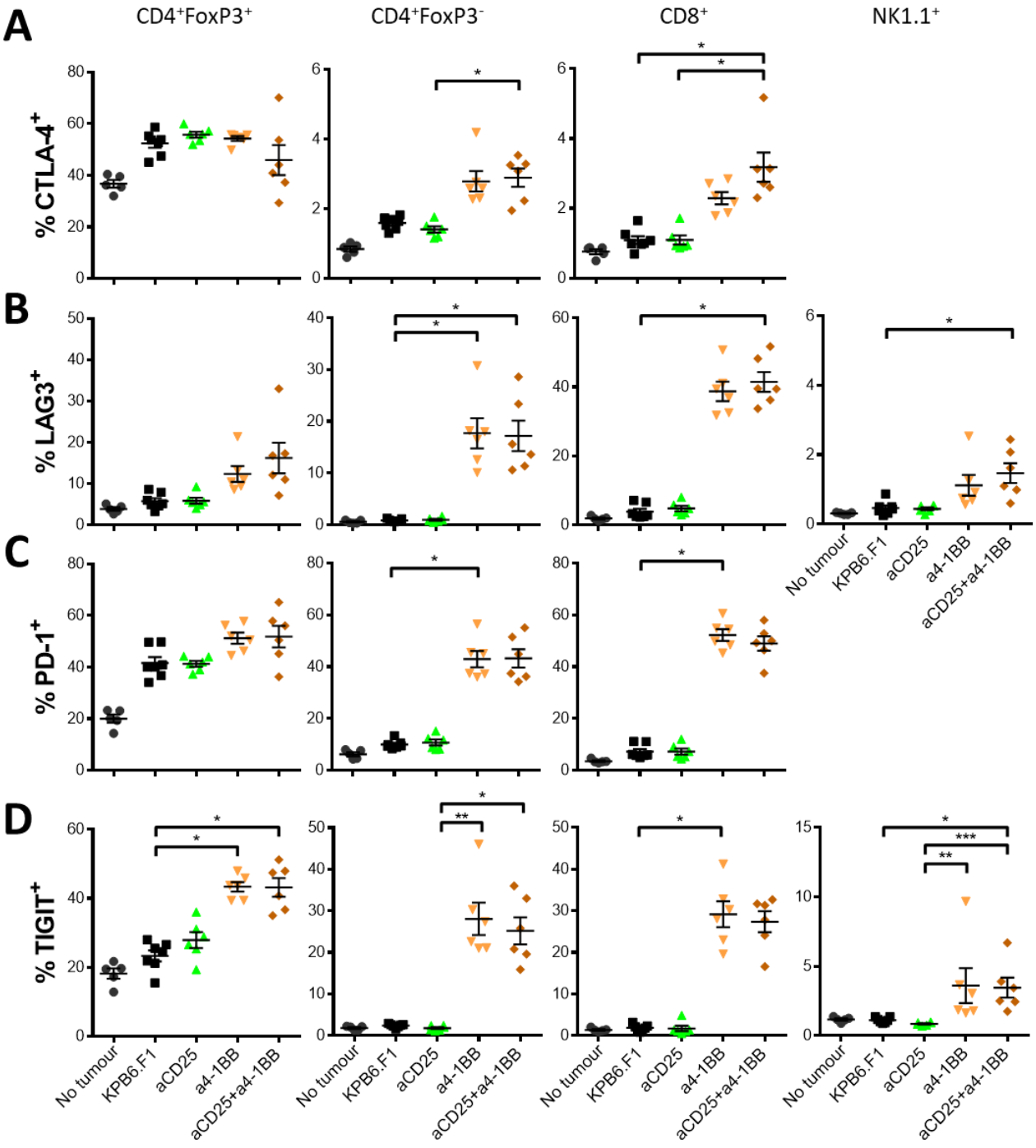

Figure 4.11. Immunotherapy with anti-4-1BB mAb increased the frequency of expression of the inhibitory checkpoints CTLA-4, LAG3, PD-1 and TIGIT on CD4$^+$ and CD8$^+$ T-cells.

C57BL/6 mice were left untreated or injected intravenously with KPB6.F1 cells and treated with anti-CD25 mAb and anti-4-1BB mAb as explained before. After 21 days mice were euthanised and a single cell suspension from the lungs was analysed by flow cytometry. Graphs summarising the frequency from regulatory T-cells (CD4$^+$FoxP3$^+$), effector CD4$^+$ T-cells (CD4$^+$FoxP3$^-$), CD8$^+$ T-cells and NK cells was determined for **(A)** CTLA-4, **(B)** LAG3, **(C)** PD-1 and

(D) TIGIT. Horizontal bars represent the mean, errors bars shown ± standard error of the mean (SEM). p values were calculated using non-parametrical analysis Kruskal-Wallis test. ns = $p > 0.05$, *$p \leq 0.05$, **$p \leq 0.01$, ***$p \leq 0.001$, **** $P \leq 0.0001$. Results from one experiment with 5 mice per condition.

NK cells also slightly increased the expression of LAG3 and TIGIT after the treatment, without statistically significant changes in the expression of the other proteins evaluated (Figure 4.10 and 4.11).

In summary, anti-4-1BB agonistic mAb promoted the proliferation, Granzyme B production and the upregulation of ICOS, LAG3, PD-1 and TIGIT on $CD4^+$ effector and $CD8^+$ T-cells, without significant activation of regulatory T-cells. When combined with Treg depletion, anti-4-1BB mAb plus anti-CD25 mAb therapy significantly increased the $CD8^+$/Treg, $CD4^+$ effector/Treg and NK/Treg ratios in the tumour, showing a signature of an active immune response in the tumour microenvironment of the KPB6.F1 model, which was described previously as a cold tumour. Nevertheless, no differences in the tumour burden were observed despite the shift in the immune cell balance driven by the treatment. Based on the above described data, a combination of anti-4-1BB mAb with antibodies targeting the co-inhibitory receptors upregulated in response to anti-4-1BB (anti-LAG3 mAb or anti-TIGIT mAb) were evaluated in the KPB6.F1 model in order to determine whether those pathways were negatively controlling tumour rejection.

4.7 Combination therapy of anti-4-1BB mAb with checkpoint blockade failed to control tumour burden of the KPB6.F1 model

Considering the sharp rise in the frequency of expression of the checkpoints PD-1, TIGIT and LAG3 after anti-4-1BB mAb therapy on $CD8^+$ T-cells, the combination of anti-4-1BB mAb with blocking antibodies targeting TIGIT or LAG3 were tested in the KPB6.F1 model of lung

cancer. As a dramatic increase in the activation of T-cells by anti-4-1BB mAb therapy was observed, the dose of anti-4-1BB mAb given to the mice was decreased from 200 µg to 100 µg per injection. To promote higher $CD8^+$/Treg, $CD4^+$ effector/Treg and NK/Treg ratios, a single dose of anti-CD25 mAb was also given to a group of mice one day before starting the combination therapy, to deplete Treg cells.

When the tumour burden was evaluated, no statistically significant differences were observed between the treatments, even though a trend toward less weight of the lungs was observed with the combination of anti-4-1BB mAb and anti-TIGIT mAb (Figure 4.12A). Representative images are also shown to illustrate the tumour nodules in the lungs (Figure 4.12B). To check if the effects already described for anti-4-1BB mAb alone in this model were replicated in the combination, the frequency and normalised number of the main T-cell subsets and NK cells were calculated. The effect of anti-CD25 mAb was confirmed with the reduction of the frequency of Treg cells from total $CD3^+$ cells and the normalised number of Treg to the mass of the tissue (Figure 4.12C and D). Additionally, the frequency of $CD3^+CD8^+$ also increased in all treatments with anti-4-1BB mAb when compared with untreated mice (Figure 4.12C and D). Correlated with the high tumour burden observed in the lungs, a lower number of NK cells were observed in all tumour bearing mice (Figure 4.12D). As described before, the $CD8^+$/Treg ratio and $CD4^+$effector/Treg ratio also increased with anti-4-1BB mAb, with ratios being higher upon anti-CD25 mAb treatment (Figure 4.12E). In accordance to lower NK cells, NK/Treg also decreased (Figure 4.12E). Granzyme B production and proliferation of effector $CD4^+$ and $CD8^+$ T-cells were also increased by the combination therapies as before with anti-4-1BB mAb alone, indicating that cytotoxic function of $CD8^+$ T-cells was not promoted further by anti-TIGIT mAb or anti-LAG3 mAb blocking function (Figure 4.13A and B). Also, a small increase in $GzmB^+$ Treg cells was observed in mice treated with anti-4-1BB mAb combined with anti-TIGIT mAb, recovering the frequency observed in healthy mice (Figure 4.13). Due to Treg depletion, the significant increase of the fraction of $GzmB^+$ Treg cells may be considered biologically irrelevant (Figure 4.13A).

Interestingly, NK cells from all treated group also increased their proliferation when compared with untreated mice, indicating anti-4-1BB mAb is promoting the repopulation of these cells in the tumour microenvironment, as observed previously with anti-4-1BB mAb alone (Figure 4.13B).

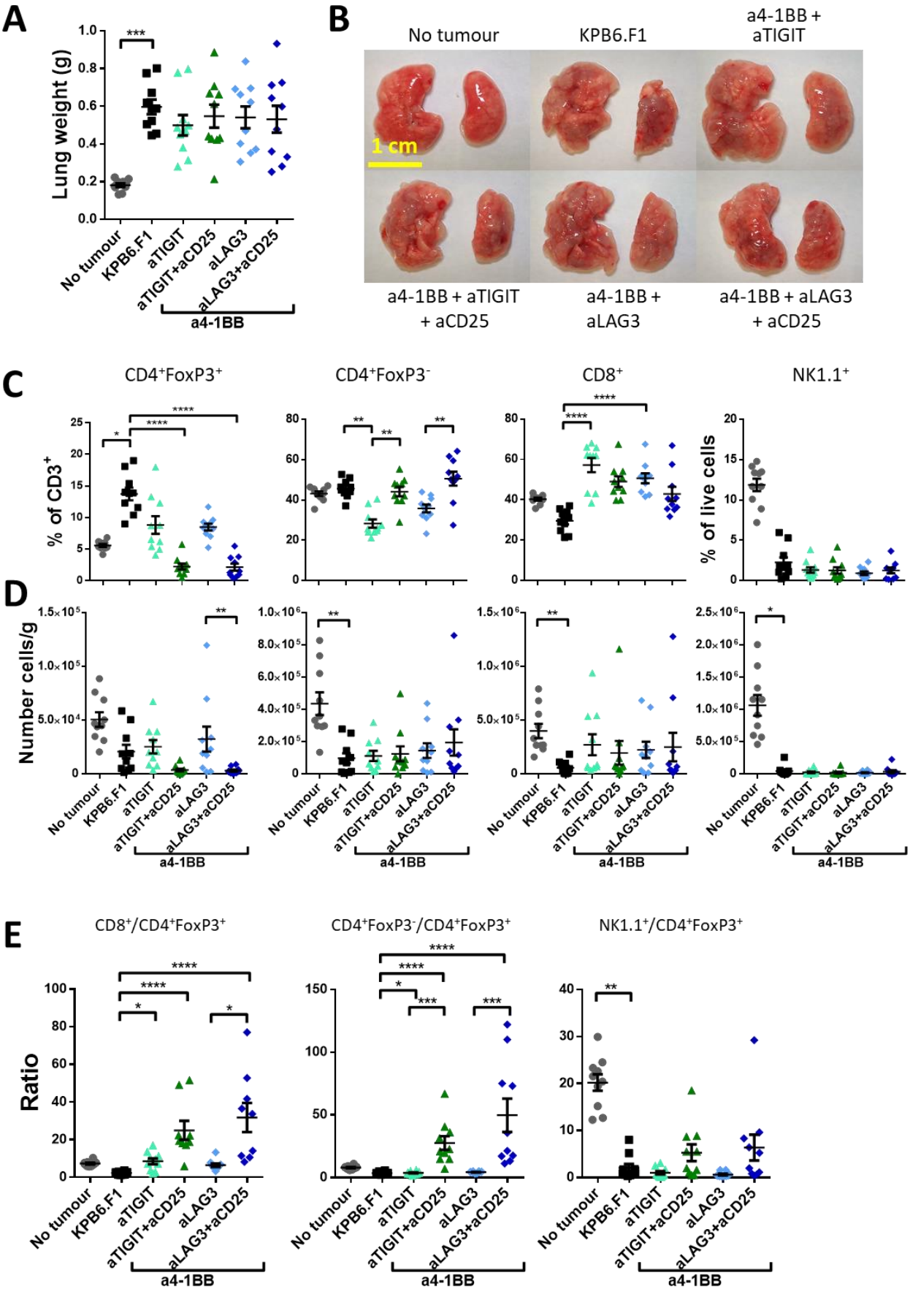
A
Lung weight (g)
No tumour
KPB6.F1
aTIGIT
aTIGIT+aCD25
aLAG3
aLAG3+aCD25
a4-1BB
B
No tumour
KPB6.F1
a4-1BB + aTIGIT
1 cm
a4-1BB + aTIGIT + aCD25
a4-1BB + aLAG3
a4-1BB + aLAG3 + aCD25
C
CD4+FoxP3+
CD4+FoxP3-
CD8+
NK1.1+
% of CD3+
% of live cells
D
Number cells/g
E
CD8+/CD4+FoxP3+
CD4+FoxP3-/CD4+FoxP3+
NK1.1+/CD4+FoxP3+
Ratio

Figure 4.12. Combination therapy with anti-4-1BB mAb and anti-TIGIT mAb or anti-LAG3 mAb promotes higher frequency of $CD8^+$ T-cells and T-effector/Treg ratios in tumour-bearing lungs.

C57BL/6 mice were left untreated or injected intravenously with KPB6.F1 cells. Six days later, some mice received one dose of 200 µg of anti-CD25 mAb (clone PC61, mouse IgG2a) and later, mice were treated concomitantly with 100 µg of anti-4-1BB mAb (clone LOB12.3 rat IgG1) plus 200 µg anti-TIGIT mAb (clone 1G9, mouse IgG1) or 200 µg anti-LAG3 mAb (clone C9B7W, rat IgG1) on days 7, 10 and 13. At day 17 mice were euthanized and lungs were recovered. Lungs were processed, and a single cell suspension was stained and analysed by flow cytometry. **(A)** Total weight of the lungs for each condition. **(B)** Representative pictures for each condition **(C)** Frequency of regulatory, $CD4^+$ effector and $CD8^+$ T-cells from $CD3^+$ gate and frequency of $NK1.1^+$ from total live cells. **(D)** Total number normalised to mass of tissue of regulatory, $CD4^+$ effector, $CD8^+$ T-cells and NK cells. **(E)** Ratio between $CD8^+$ T-cells, $CD4^+$ effector T-cells and NK cells relative to regulatory T-cells in the tumour-bearing lungs. Horizontal bars represent the mean, errors bars shown ± standard error of the mean (SEM). p values were calculated using non-parametrical analysis Kruskal-Wallis test. ns = $p > 0.05$, *$p \leq 0.05$, **$p \leq 0.01$, ***$p \leq 0.001$, **** $P \leq 0.0001$. Combined results from two experiments with 5 mice per condition each.

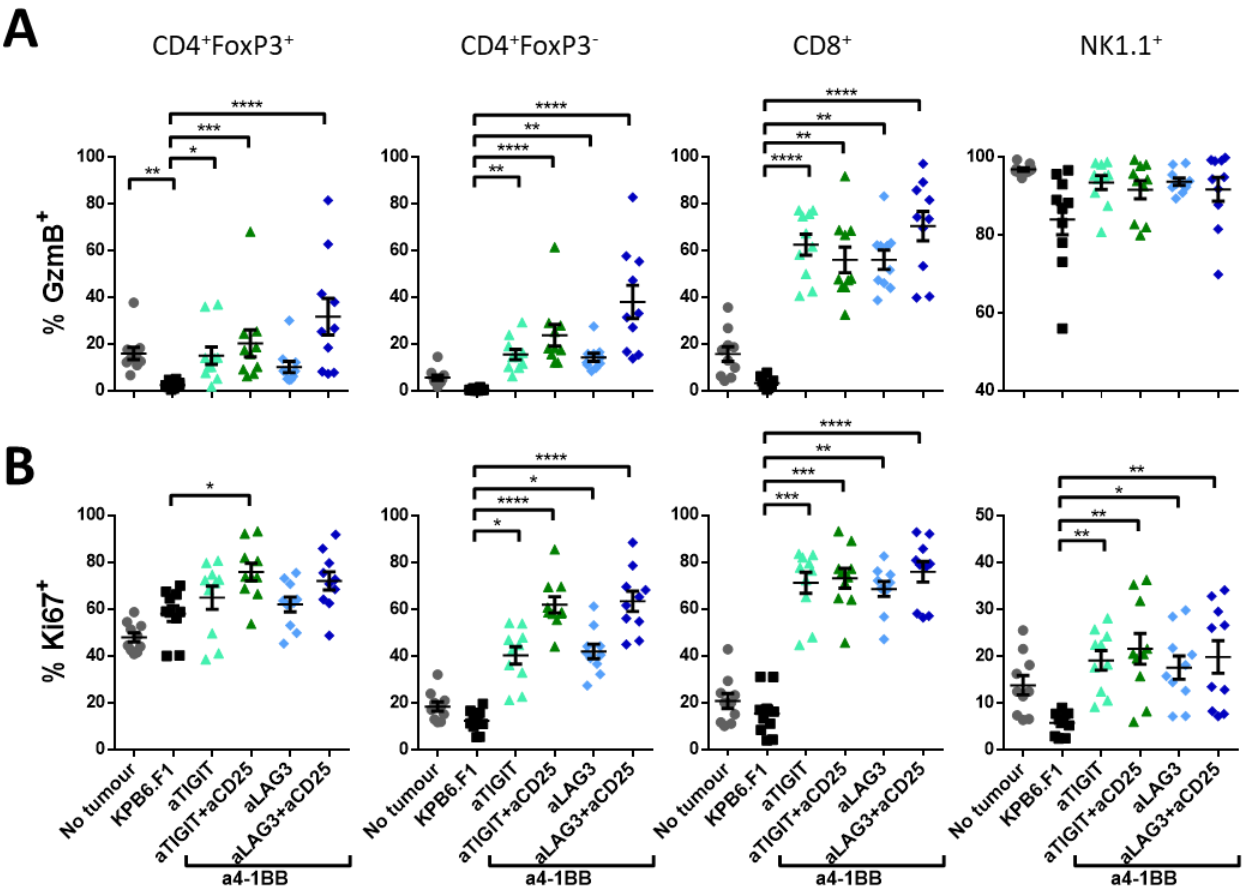

Figure 4.13. Anti-4-1BB mAb treatment in combination with anti-TIGIT mAb or anti-LAG3 mAb keeps its ability to promote Granzyme B production and proliferation in TILs from tumour-bearing lungs.

C57BL/6 mice were left untreated or injected intravenously with KPB6.F1 cells. Mice received one dose of 200 µg of anti-CD25 mAb at day 6 and later were treated concomitantly with 100 µg of anti-4-1BB mAb combined with 200 µg of anti-TIGIT mAb or 200 µg of anti-LAG3 mAb on days 7, 10 and 13. At day 17 mice were euthanized, lungs were processed, and a single cell suspension was stained and analysed by flow cytometry. Frequency of **(A)** Granzyme B ($GzmB^+$) and **(B)** $Ki67^+$ cells from regulatory, $CD4^+$ effector, $CD8^+$ T-cells and NK cells. Horizontal bars represent the mean, errors bars shown ± standard error of the mean (SEM). p values were calculated using non-parametrical analysis Kruskal-Wallis test. ns = $p > 0.05$, *$p \leq 0.05$, **$p \leq 0.01$, ***$p \leq 0.001$, **** $P \leq 0.0001$. Combined results from two experiments with 5 mice per condition each.

As the frequency of the T-cell subsets and NK compartments in the tumour microenvironment remained unchanged between anti-4-1BB mAb monotherapy and the combination therapies when antibody checkpoint blockade was used, the expression of immunomodulatory molecules was evaluated. Similar as upon anti-4-1BB mAb alone treatment, the combination of anti-4-1BB mAb with anti-TIGIT mAb or anti-LAG3 mAb increased the expression of ICOS and 4-1BB on the surface of $CD8^+$ T-cells, with increased ICOS expression also on Treg and $CD4^+$ effector cells (Figure 4.14). More importantly, when co-inhibitory checkpoints were evaluated, the frequency of expression of LAG3, PD-1 and TIGIT remained high on $CD8^+$ T-cells and $CD4^+$ effectors when combined therapy was given. The activation of those T-cells resembles the effects of anti-4-1BB mAb alone (Figure 4.15). It is important to notice that the antibodies for staining LAG3 and TIGIT were partially blocked by the therapeutic antibodies administered before, therefore detected low frequencies of TIGIT expression in the samples from anti-TIGIT mAb treated mice is not reflecting the actual cells expressing TIGIT. Similarly, frequency of $LAG3^+CD8^+$ were masked due to a competition for the antigen between the same clone used for treatment and staining (Figure 4.15A and C). There were not significant differences in the expression of CTLA-4, GITR and OX-40 between treated and untreated mice on all T-cell subsets evaluated (Supplementary Figure 7.7).

In summary, finding the right combination therapy based on the scientific evidence (rational combination immunotherapy) in the KPB6.F1 model was unsuccessful. Even though T-cell activation was promoted by anti-4-1BB mAb therapy, which lead to increased granzyme B production, proliferation and the expression of different activation markers, no tumour growth control upon treatment with any of the above described combinations was observed. When specific checkpoints upregulated by anti-4-1BB mAb such as LAG3 and TIGIT were concomitantly blocked by antibody therapy, no improvement was observed. One possibility is that due to its poor mutational burden, the KPB6.F1 model is poorly immunogenic and lacks the capacity to deliver signal 1 (TCR recognition of the peptide/MHC complex) to effector T-cells from TILs, and that the activation we observed is bystander non-tumour reactive T-cells within the tumour. Future experiments will address the combination of radiation therapy and anti-4-1BB with the aim to increase antigen release and presentation prior to anti-4-1BB co-stimulation.

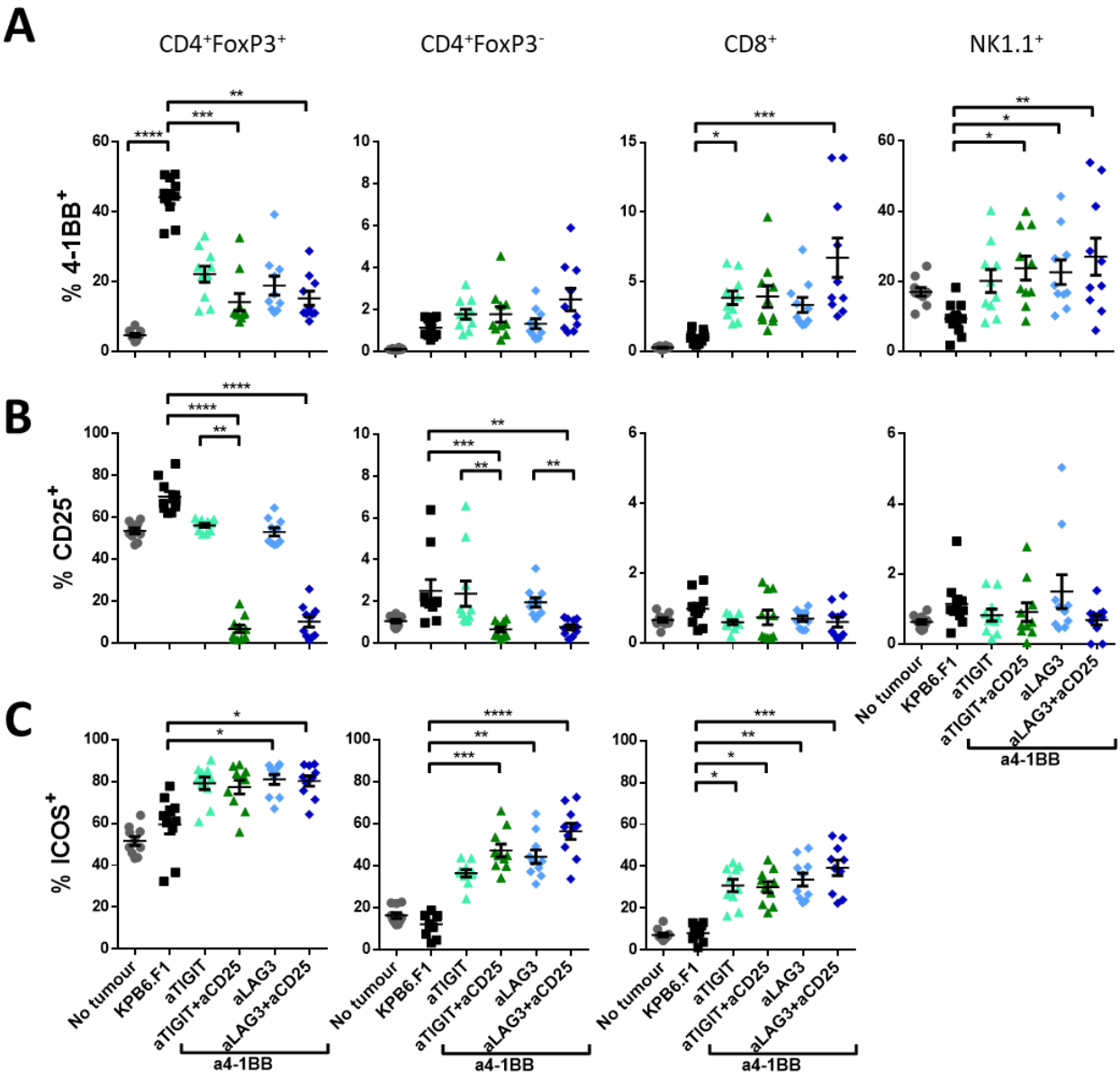

Figure 4.14. Treatment with anti-4-1BB mAb combined with anti-TIGIT mAb or anti-LAG3 mAb promoted increased frequency of ICOS expression on CD4⁺ and CD8⁺ T-cells.

C57BL/6 mice were left untreated or injected with KPB6.F1 cells. Later, mice were treated with anti-CD25 mAb and concomitant doses of anti-4-1BB mAb plus anti-TIGIT mAb or anti-LAG3 mAb, and samples were analysed as explained before. Graphs summarising the frequency from regulatory T-cells ($CD4^+FoxP3^+$), effector $CD4^+$ T-cells ($CD4^+FoxP3^-$), $CD8^+$ T-cells and NK cells was determined for **(A)** 4-1BB, **(B)** CD25 and **(C)** ICOS are shown. Horizontal bars represent the mean, errors bars shown ± standard error of the mean (SEM). p values were calculated using non-parametrical analysis Kruskal-Wallis test. ns = $p > 0.05$, *$p \leq 0.05$, **$p \leq 0.01$, ***$p \leq 0.001$, **** $P \leq 0.0001$. Combined results from two experiments with 5 mice per condition each.

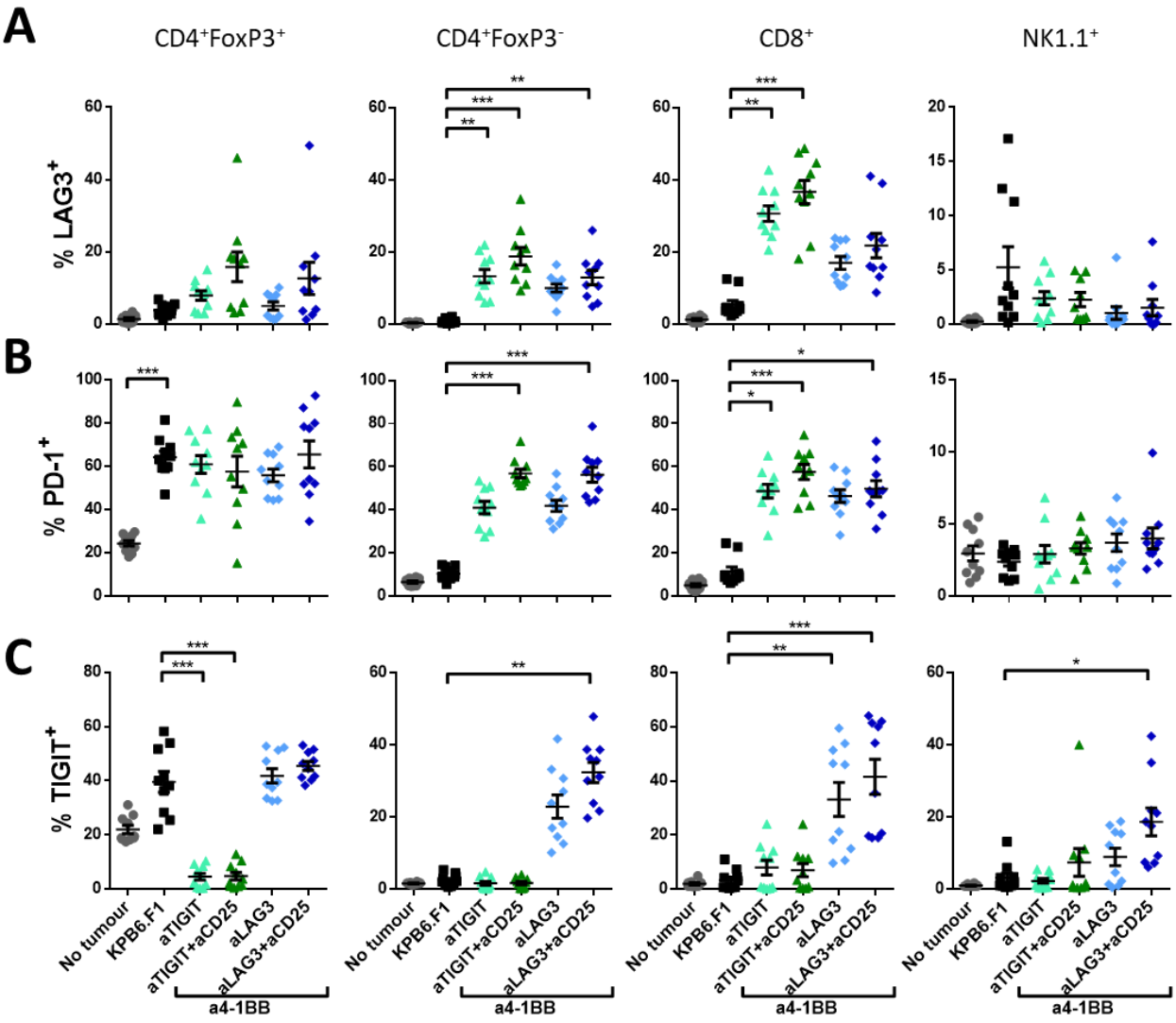

Figure 4.15. Combination therapy with anti-4-1BB mAb plus anti-TIGIT mAb or anti-LAG3 mAb increased the frequency of CD4$^+$ and CD8$^+$ T-cells expressing the inhibitory checkpoints LAG3, PD-1 and TIGIT.

C57BL/6 mice were left untreated or injected with KPB6.F1 cells. Later, mice were treated with anti-CD25 mAb and concomitant doses of anti-4-1BB mAb plus anti-TIGIT mAb or anti-LAG3 mAb and samples were analysed as explained before. Graphs showing the frequency from regulatory T-cells (CD4$^+$FoxP3$^+$), effector CD4$^+$ T-cells (CD4$^+$FoxP3$^-$), CD8$^+$ T-cells and NK cells was determined for **(A)** LAG3, **(B)** PD-1 and **(C)** TIGIT. Horizontal bars represent the mean, errors bars shown ± standard error of the mean (SEM). p values were calculated using non-parametrical analysis Kruskal-Wallis test. ns = $p > 0.05$, *$p \leq 0.05$, **$p \leq 0.01$, ***$p \leq 0.001$, **** $P \leq 0.0001$. Combined results from two experiments with 5 mice per condition each.

4.8 Combination of anti-4-1BB mAb and anti-CD25 mAb promotes tumour reduction in the CMT-167 model

Considering the effectivity of anti-4-1BB mAb therapy in promoting a wide activation of TILs in the mouse model of lung cancer KPB6.F1, the same rationale was tested in the CMT-167 mouse model of lung cancer. As shown previously in this work, the KPB6.F1 and CMT-167 models of lung cancer show similar ratios and level of activation markers on T-cells (Figure 4.1 and 4.2). CMT-167 is a metastatic model of lung cancer that has previously shown partial sensitivity to anti-PD-1 mAb and anti-PD-L1 mAb therapy, when the CMT-167 cell line constitutively expressed luciferase (Li et al., 2017a). Therefore, if the activation driven by anti-4-1BB mAb previously seen in the KPB6.F1 model can be replicated in the CMT-167 model and translated into effective tumour control, we will be able to compare the mechanisms defining the responsiveness to anti-41BB therapy.

Mice were injected intravenously with CMT-167 cells and were treated with three doses of an agonistic anti-4-1BB mAb (clone 3H3, mouse IgG1, 50 µg per dose). As before, some mice received one dose of a depleting anti-CD25 mAb (TUSKC22, mouse IgG2a) to eliminate regulatory T-cells. The mice that received anti-CD25 mAb or anti-4-1BB mAb alone had slightly smaller lung weight than the untreated group suggesting lesser tumour growth, although the differences were not statistically significant (Figure 4.16A). When combination therapy anti-CD25 mAb and anti-4-1BB mAb was given, the weight of the lungs decreased further when compared to untreated mice, however this trend to lesser tumour burden was not statistically significant (Figure 4.16A). Another way to measure tumour burden in mouse models of cancer is through the metastasis index. Briefly, tumour slides are recovered and haematoxylin and eosin (H&E) staining, then the total metastasis volume is normalised to the lung volume (Qian et al., 2009). The metastasis index was calculated for all tumour-bearing left lungs, and even though no significant differences were observed, the metastasis index clearly replicated the trend towards lower metastasis in those mice treated with the combination therapy (Figure 4.16 B).

The composition of T-cell subsets was also evaluated. The frequency of Treg and effector $CD4^+$ cells from total $CD3^+$ cells was reduced in mice receiving combination of anti-4-1BB mAb plus anti-CD25 mAb, which was driven mostly by a sharp increase of $CD8^+$ T-cells

(Figure 4.16C and D). The frequency and total number of NK cells was dramatically reduced by anti-4-1BB mAb therapy, interestingly not correlated with the tumour burden of the lungs as observed previously in the KPB6.F1 model (Figure 4.16 C and D).

The ratios were calculated, re-confirming the importance of Treg depletion to promote higher frequency of $CD4^+$ and $CD8^+$ cells in relation to Treg cells present in the tumour (Figure 4.16E). As observed previously in the KPB6.F1 model, anti-4-1BB mAb agonistic antibody promoted granzyme B production by almost all $CD8^+$ and the totality of $CD4^+$ $FoxP3^-$ cells when combined with anti-CD25 mAb depleting antibody (Figure 4.17A). Proliferation was also significantly augmented in all three T-cell subsets and NK cells after anti-4-1BB mAb therapy (Figure 4.17B). Even though a trend towards increased frequency of ICOS was observed on all T-cells subsets, those were no significant, indicating another difference with the KPB6.F1 model (Figure 4.18B).

Another effect of anti-4-1BB mAb therapy was the increase in the frequency of 4-$1BB^+CD4^+$ T-cells, from 10% to 30% after treatment (Figure 4.18A) whilst no difference of CD25, GITR and OX-40 on all T-cells populations was observed (Supplementary figure 7.8).

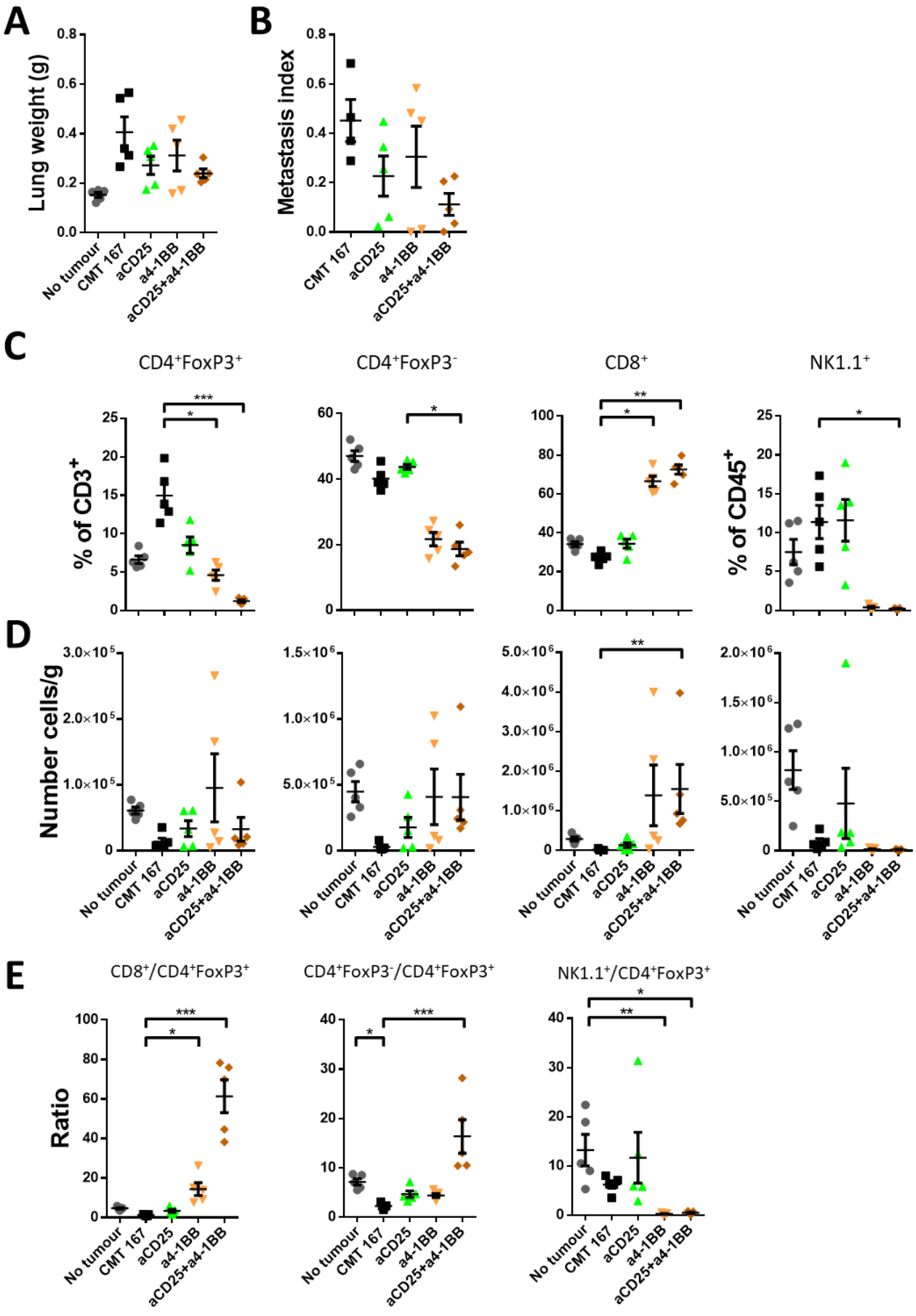
A
Lung weight (g)
0.0
0.2
0.4
0.6
0.8
No tumour
CMT 167
aCD25
a4-1BB
aCD25+a4-1BB
B
Metastasis index
0.0
0.2
0.4
0.6
0.8
CMT 167
aCD25
a4-1BB
aCD25+a4-1BB
C
CD4+FoxP3+
CD4+FoxP3-
CD8+
NK1.1+
% of CD3+
% of CD45+
D
Number cells/g
E
CD8+/CD4+FoxP3+
CD4+FoxP3-/CD4+FoxP3+
NK1.1+/CD4+FoxP3+
Ratio

Figure 4.16. Anti-4-1BB mAb treatment promotes higher frequency and number of $CD8^+$ T-cells and increased ratios in tumour-bearing lungs.

C57BL/6 mice were left untreated or injected intravenously with CMT-167 cells. Five days later, some mice received one dose of 200 µg of anti-CD25 mAb (TUSKC22, mouse IgG2a) and later, mice were treated with 50 µg of anti-4-1BB mAb (clone 3H3 mouse IgG1) on days 6, 9 and 12. At day 19 mice were euthanized and lungs were recovered. Lungs were processed, and a single cell suspension was stained and analysed by flow cytometry. **(A)** Total weight of the lungs for each tested condition. **(B)** Metastasis index obtained from quantification of H&E slides from the left lung of the mice. **(C)** Frequency of regulatory T-cells, $CD4^+$ effector and $CD8^+$ T-cells from $CD3^+$ gate and frequency of $NK1.1^+$ from $CD45^+$ gated cells. **(D)** Total number normalized to mass of tissue of regulatory, $CD4^+$ effector, $CD8^+$ T-cells and NK cells. **(E)** Ratio between $CD8^+$ T-cells, $CD4^+$ effector T-cells and NK cells relative to regulatory T-cells in the tumour-bearing lungs. Horizontal bars represent the mean, errors bars shown ± standard error of the mean (SEM). p values were calculated using non-parametrical analysis Kruskal-Wallis test. ns = $p > 0.05$, *$p \leq 0.05$, **$p \leq 0.01$, ***$p \leq 0.001$, **** $P \leq 0.0001$. Results from one experiment with 5 mice per condition.

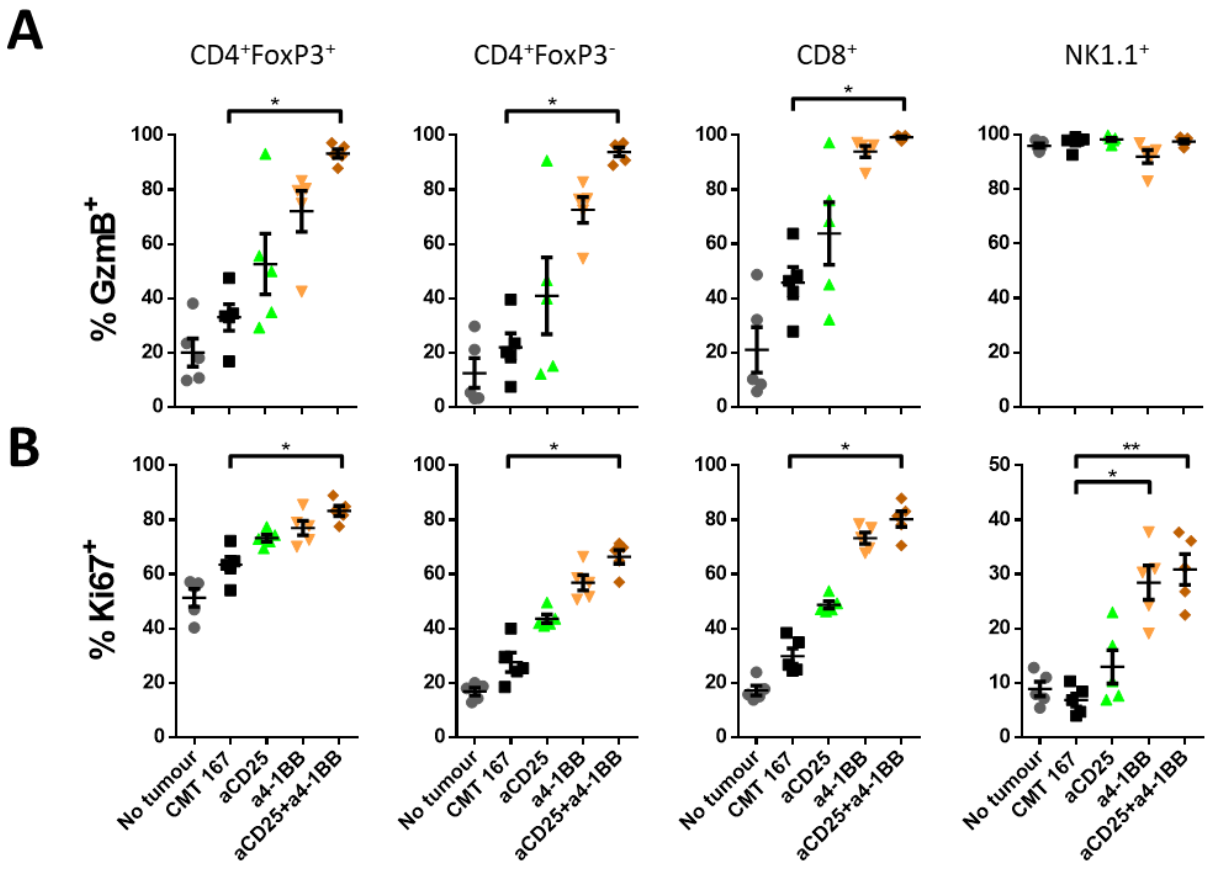

Figure 4.17. Anti-4-1BB mAb treatment promotes Granzyme B production and proliferation in the CMT-167 model of lung cancer.

C57BL/6 mice were left untreated or injected intravenously with CMT-167 cells. Mice received one dose of 200 µg of anti-CD25 mAb (TUSKC22) at day 5 and then they were treated with 50 µg of anti-4-1BB mAb on days 6, 9 and 12, as described above. At day 19 lungs were recovered and the single cell suspension was stained and analysed by flow cytometry. Frequency of **(A)** Granzyme B ($GzmB^+$) and **(B)** $Ki67^+$ cells from regulatory, $CD4^+$ effector, $CD8^+$ T-cells and NK cells are shown. Horizontal bars represent the mean, errors bars shown ± standard error of the mean (SEM). p values were calculated using non-parametrical analysis Kruskal-Wallis test. ns = $p > 0.05$, *$p \leq 0.05$, **$p \leq 0.01$, ***$p \leq 0.001$, **** $P \leq 0.0001$. Results from one experiment with 5 mice per condition.

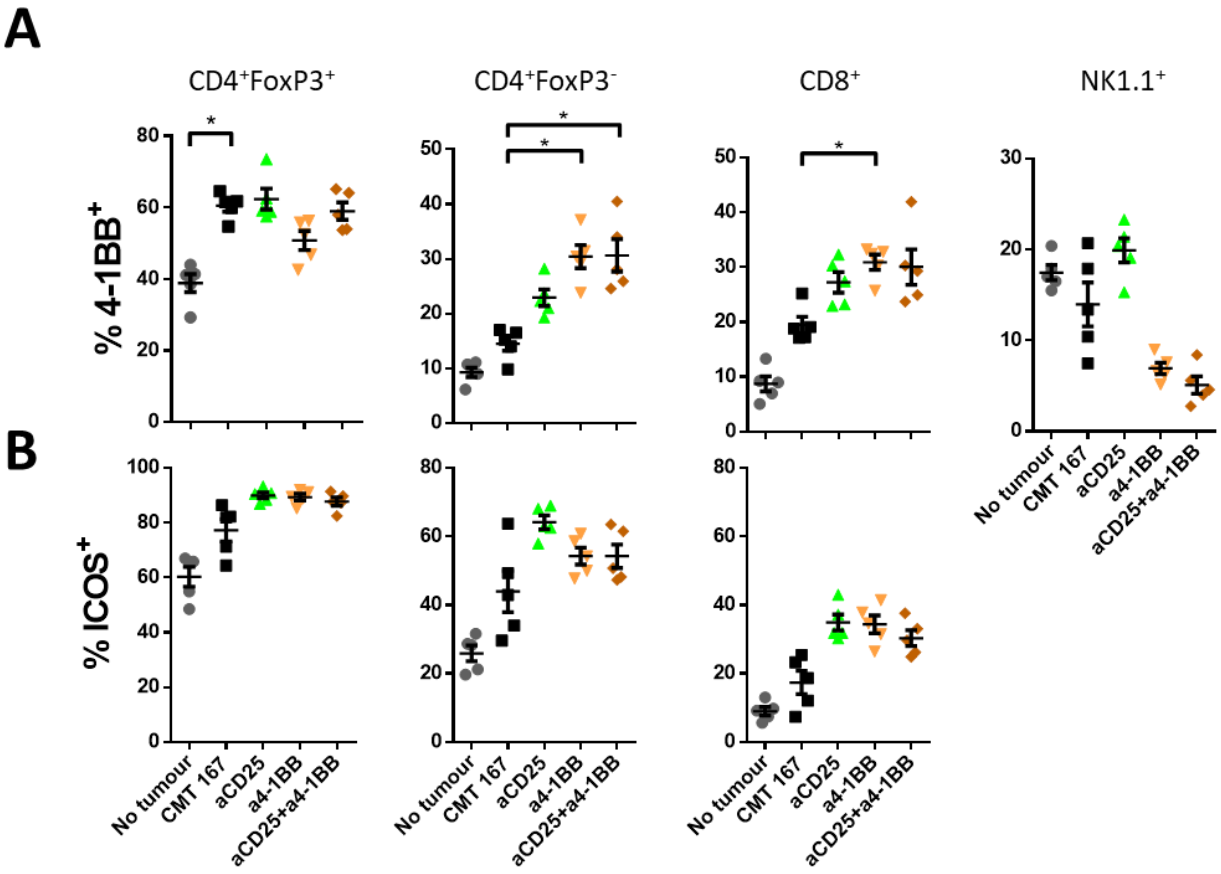

Figure 4.18. Anti-4-1BB mAb treatment increased the frequency of 4-1BB$^+$ and ICOS$^+$ T-cells in the CMT-167 model of lung cancer.

C57BL/6 mice were left untreated or injected intravenously with CMT-167 cells. Mice were treated with one dose of 200 µg of anti-CD25 mAb at day 5 and with three doses of 50 µg of anti-4-1BB mAb on days 6, 9 and 12, as described above. At day 19 lungs were recovered and the single cell suspension was stained and analysed by flow cytometry. Frequency of the co-stimulatory molecules **(A)** 4-1BB and **(B)** ICOS expressed on regulatory T-cells, CD4$^+$ effector, CD8$^+$ T-cells and NK cells are shown. Horizontal bars represent the mean, errors bars shown ± standard error of the mean (SEM). p values were calculated using non-parametrical analysis Kruskal-Wallis test. ns = $p > 0.05$, *$p \leq 0.05$, **$p \leq 0.01$, ***$p \leq 0.001$, **** $P \leq 0.0001$. Results from one experiment with 5 mice per condition.

Interestingly, when inhibitory checkpoints were evaluated in the tumour microenvironment of the CMT-167 model, it was found that the drastic increase in the frequency of expression of LAG3 and TIGIT observed in KPB6.F1 tumours was not replicated (Figure 4.19). For example, the percentage of $LAG3^{+}CD8^{+}$ cells remained similar between all the CMT-167 tumour-bearing mice, in contrast to the 8-fold increase detected in the KPB6.F1 model (Figure 4.19A). On the other hand, $LAG3^{+}CD4^{+}$ effector cells frequency rose from 6% to 20% in the CMT-167 model, whilst the rise in KPB6.F1 tumours was steeper, from 1% to 20% in average, reaching both models around 20% expression LAG3 on effector T-cells (Figure 4.19A). As KPB6.F1-derived TILs had very low frequency of TIGIT expression, anti-4-1BB mAb treatment increased the $TIGIT^{+}$ population of $CD8^{+}$ and effector $CD4^{+}$ from 5% to 50% (Figure 4.11D). In contrast, in the CMT-167 model TIGIT frequency increased on effector $CD4^{+}$ T-cells, from average 10% to 30%, remaining without changes on $CD8^{+}$ after anti-4-1BB mAb (Figure 4.19C). The frequency of expression of the immune checkpoint protein PD-1 was increased on effector $CD4^{+}$ and $CD8^{+}$ T-cells in both models of lung cancer after anti-4-1BB mAb treatment. Whilst in the KPB6.F1 tumours PD-1 expression rose from 5% to 50% on effector $CD4^{+}$ and $CD8^{+}$ T-cells (Figure 4.11C), in the CMT-167 model the frequency augmented from 35% to 75% in average for those T-cell populations (Figure 4.19B). Interestingly, the frequency of $CD8^{+}PD\text{-}1^{+}$ cells remained similar between untreated and combination treated groups with anti-4-1BB mAb and anti-CD25 mAb in the CMT-167 model. The frequency of PD-1 on Treg diminished upon treatment with the combination (Figure 4.19B), different to what was observed in the KPB6.F1 model. The frequency of expression of the co-inhibitory molecule TIM-3 also rose on all T-cell subsets and NK cells, with significant differences just on NK cells (Figure 4.19D). The levels of CTLA-4 expression remained unchanged in all treatment groups, like in the KPB6.F1 model (Supplementary figure 7.8).

In general, the rationale-based combination immunotherapy of anti-4-1BB mAb together with anti-CD25 mAb proved to be a good strategy for treatment of mice bearing CMT-167 lung cancer tumours as observed by the weight of the lungs and metastasis index; despite that the KPB6.F1 lung tumour did not responded to the same therapy.

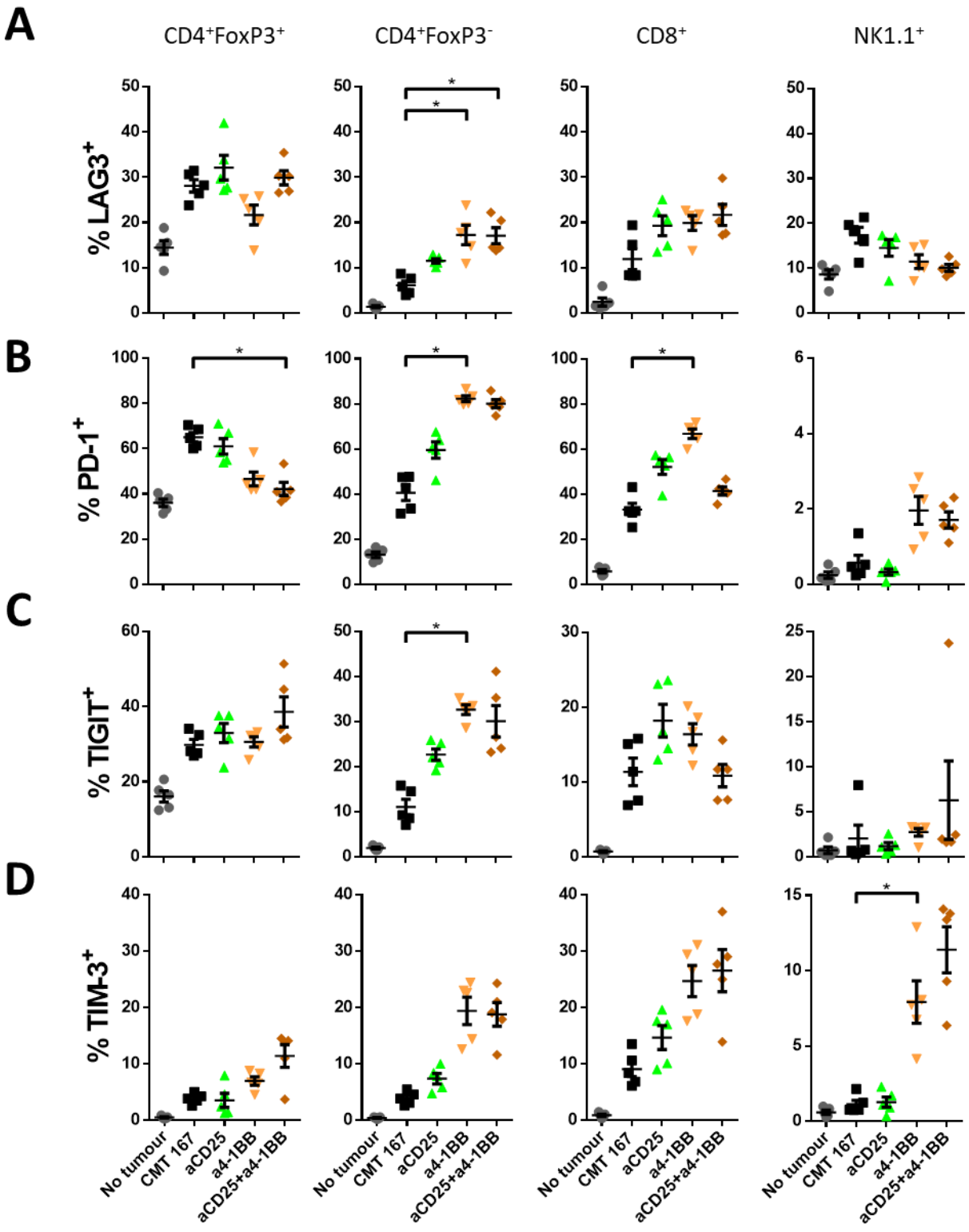

Figure 4.19. Increased expression frequency of checkpoints after anti-4-1BB mAb treatment in the CMT-167 model of lung cancer.

C57BL/6 mice were left untreated or injected intravenously with CMT-167 cells. Mice were treated with one dose of 200 µg of anti-CD25 mAb at day 5 and with three doses of 50 µg of

anti-4-1BB mAb on days 6, 9 and 12, as described above. At day 19 lungs were recovered and the single cell suspension was stained and analysed by flow cytometry. Graphs indicating the expression frequency of the co-inhibitory checkpoints **(A)** LAG3, **(B)** PD-1, **(C)** TIGIT and **(D)** TIM-3 on regulatory T-cells, $CD4^+$ effector, $CD8^+$ T-cells and NK cells are shown. Horizontal bars represent the mean, errors bars shown ± standard error of the mean (SEM). p values were calculated using non-parametrical analysis Kruskal-Wallis test. ns = $p > 0.05$, *$p \leq 0.05$, **$p \leq 0.01$, ***$p \leq 0.001$, **** $P \leq 0.0001$. Results from one experiment with 5 mice per condition.

Considering that for some checkpoints as TIGIT and LAG3, higher frequency of expression of $CD8^+$ and $CD4^+$ effector cells was observed in the non-responder KPB6.F1 model after therapy, it is clear that co-activation (by agonistic antibodies as anti-4-1BB mAb) and the blocking of inhibitory signals by immunotherapy can only be translated in tumour control benefit when a certain degree of T-cell activation is already present in the tumour microenvironment. Possibly, the slightly higher levels of PD-1, TIGIT and LAG3 in untreated mice bearing CMT-167 tumours when compared with KPB6.F1 bearing mice suggest a degree of initial activation in absence of therapy. This initial activation may be due to tumour recognition by the tumour-infiltrating T-cells in the sample or by the lack of other immunosuppressive signals present in others tumour microenvironments, for example the KPB6.F1 model.

5 General Discussion

Checkpoint inhibitor-based immunotherapy has proven to be an effective anti-tumour strategy, resulting in long lasting responses in a restricted group of patients (McDermott et al., 2013). Therefore, the need to develop new and more effective therapies, in order to achieve complete responses in more patients, is urgently needed.

In the course of the research presented in this thesis, with the help of mouse models, we undertook the challenge of a rational design of new immunotherapies from two different perspectives:

1. The first approach entailed targeting the tumour-infiltrating T-cells by an antibody specific to a co-stimulatory molecule highly expressed in the tumour microenvironment (ICOS), which has been suggested to have an important role in tumour control and testing it *in vivo*. We showed preclinical evidence that ICOS, currently intensively investigated in clinical development, may be inefficient in eliminating tumours as monotherapy and in combination with two checkpoint inhibitors (CTLA-4 and PD-1) already approved by regulatory bodies, such as FDA and its equivalents in other countries.
2. With the development of two mouse models of lung cancer, we were able to propose and test different treatment strategies, based on the data of the frequency of expression of co-modulatory molecules in the tumour-infiltrating lymphocytes from untreated and treated mice. In this way, changes in the tumour microenvironment drove the proposal of new treatments that may be later translated to the clinic.

Both approaches in the design and proposal of therapies had their own challenges. For ICOS, we described an unexpected effect of the antibody in the number of T-cells infiltrating the tumour microenvironment. On the other hand, for models of lung cancer and the testing of new combination therapies, we described different approaches that failed to promote an activation of infiltrating T-cells in the KPB6.F1 model. This was evident when comparing the response to anti-4-1BB mAb plus anti-CD25 mAb therapy between both models.

This work showed that even slight differences in the expression levels of immunomodulatory molecules on T-cells could determine the efficacy of the treatment in the

clinic. Furthermore, the field requires further research into discovery of novel biomarkers that would reliably predict the probability of the patient responding to the treatment. Small differences in level of expression can be an unreliable strategy leading to patients receiving inappropriate treatments.

5.1 Anti-ICOS agonistic antibody promoted the elimination of T-cells in the tumour, leading to negative outcomes in preclinical tumour models.

The data presented in this thesis shows that the use of an agonistic anti-ICOS mAb as an anti-tumour therapy in mouse models of cancer did not improve survival of mice. We used the 37A10 anti-ICOS mAb clone, which is a mouse and human cross-reactive antibody according to its description in a public available patent (Sazinsky et al., 2016). We evaluated the correct binding of the antibody in mouse (Figure 3.1B) and human cells (Supplementary figure 7.1B) and tested its agonistic activity *in vitro* by an assay designed during this study (Figure 3.1C), before producing two different mouse isotypes of that antibody.

It was hypothesised at the beginning of this project, that the best potential strategy to create an anti-ICOS antibody with good tumour-eliminating properties would be designing it so that it is agonistic and of a non-depleting isotype. It was speculated that such properties would promote the function of activated T-cells that have upregulated ICOS expression as a result of other therapies, such as anti-CTLA-4 mAb blockade (Carthon et al., 2010; Di Giacomo et al., 2013). This hypothesis was in opposition to the approach taken by Jounce and its ICONIC trial (NCT02904226) that is currently evaluating the clinical efficacy of an anti-ICOS mAb human IgG1 (depleting) isotype as monotherapy and in combination with nivolumab (an anti-PD-1 mAb). Our experiments, in a variety of mouse models, showed clearly that there was no benefit in the survival of the mice compared to the control group for an anti-ICOS m2a mAb (depleting) isotype as a monotherapy nor in combination with PD-1 (Figure 3.3). These findings were consistent with the first reports of the ICONIC trial presented in ASCO 2018 where the clinical benefit of combination therapy was mild, without benefit of anti-ICOS mAb treatment alone (Yap et al., 2018). Therefore, it was hypothesised that mice treated with combination therapy of anti-PD-1 mAb and anti-ICOS mIgG1 mAb, to avoid T-cell depletion,

should bring survival benefit in the CT26 mouse model over the untreated group (Figure 3.4 and 3.5). Unexpectedly, no survival benefit with the non-depleting mIgG1 isotype of anti-ICOS mAb combined with anti-PD-1 mAb or anti-ICOSm1 mAb as monotherapy was observed. The failure of anti-ICOSm1 mAb as monotherapy to promote tumour control or survival benefit in treated mice gave some evidence of a lack of agonistic function *in vivo*. Furthermore, the absence of survival benefit between mice that received anti-PD-1 mAb alone and mice treated with anti-ICOSm1 mAb combined with anti-PD-1 mAb also suggested a missing agonistic function. Additionally, even though significant differences in the survival curves were observed between both combination therapies (anti-PD-1 mAb combined with anti-ICOSm1 mAb versus combination with anti-ICOSm2a mAb, Figure 3.5), we believe the difference observed was mostly due to the effective depletion of activated T-cells driven by anti-ICOSm2a mAb therapy rather than the agonistic function promoted by anti-ICOSm1 mAb in combination setting.

Moreover, when a functional assay comparing the effect in the tumour microenvironment of both isotypes was run, it became apparent that no agonistic function could be clearly attributed to the anti-ICOSm1 mAb due to elimination of T-cells in the tumour microenvironment by both isotypes (Figure 3.6). No significant differences were observed in the frequency and number of cells after either isotype of the anti-ICOS mAb in draining LNs (Figure 3.6). Even though the elimination of tumour-infiltrating T-cells was predicted for anti-ICOSm2a mAb, the elimination of T-cells by anti-ICOSm1 mAb, to a lesser degree than mIgG2a isotype, was striking. By using a mouse model lacking activating FcγRs and a blocking anti-CD16/CD32 mAb, to block Fc engagement by FcγRIIb, it has been demonstrated that the elimination of T-cells driven by anti-ICOSm1 mAb was independent of FcγR-engagement (Figure 3.9). In this setting, even though the frequency of Treg, $CD4^+$ effector and $CD8^+$ T-cells was similar compared to untreated wild-type mice, when the number of tumour-infiltrating T-cells normalised to the weight of the tumour was calculated, they were equally reduced – as in anti-ICOSm1-treated wild-type mice (Figure 3.8 and 3.9). Interestingly, when $FcγRIIb^{-/-}$ mice were treated with anti-ICOSm1 mAb, a reduction in the percentage of Tregs from total $CD3^+$ cells was observed from an average 15% in untreated WT mice, to 7% in WT mice treated with anti-ICOSm1 mAb and 1% in $FcγRIIb^{-/-}$ mice treated with anti-ICOSm1 mAb (Figure 3.10). Subsequently, the total normalised number of infiltrating T-cells also decreased (Figure 3.11).

This is consistent to previous observations that in the absence of the inhibitory FcγRIIb, a mIgG1 increases its A:I ratio favouring depletion of cells expressing the antigen by binding to the activating FcγRIII (Nimmerjahn et al., 2005). This experiment also confirmed the preferred engagement of the anti-ICOSm1 mAb to the FcγRIIb and the effective inhibitory signalling triggered by the engagement of the mIgG1 fraction of the anti-ICOSm1 mAb by the FcγRIIb.

The most important confirmation that anti-ICOS mAb may not provide any demonstrable clinical benefit was obtained when hFcγR mice were used. Anti-ICOS mAbs with human IgGs were tested in the mouse model that recapitulates human FcγRs (Smith et al., 2012), to generate evidence for T-cell elimination in a human-like context. The data clearly showed reduced frequency of Tregs upon treatment with either of the isotypes, hIgG1 and hIgG4, similarly to what was described for mouse IgGs previously in this work (Figure 3.17). Even though no significant reduction in the frequency of effector $CD4^+$ and $CD8^+$ T-cells was observed, the numbers of cells trended toward a reduction in all T-cell subsets, with no statistical significance for both isotypes. These results provide a plausible explanation of the mechanism of action behind the unsatisfactory results of tumour growth control observed so far in the clinical trial ICONIC (Yap et al., 2018) and predicts an unfavourable outcome of the INDUCE-1 trial (by GSK, NCT02723955), which tests anti-ICOS hIgG4 mAb isotype. Interestingly, as the observation of T-cell elimination is restricted to the tumour in the mouse models, the blood immunophenotyping planned for patients on these trials may not be able to detect the intra-tumoral T-cell elimination.

Considering the relationship between anti-CTLA-4 mAb therapy and the upregulation of ICOS by T-cells described before (Carthon et al., 2010; Di Giacomo et al., 2013), the combination of anti-CTLA-4 mAb with both anti-ICOS mAb isotypes was evaluated. Clear negative survival effect was observed in mice treated with either anti-CTLA-4 mAb and anti-ICOSm1 mAb, and anti-CTLA-4 mAb combined with anti-ICOSm2a mAb (Figure 3.12 and 3.13). The level of Treg depletion in mice treated with either anti-ICOS mAb isotype or anti-CTLA-4 mAb alone was compared. Anti-ICOSm2a mAb monotherapy depleted Treg to a greater extent than anti-CTLA-4m2a, however without survival benefit. The lack of beneficial outcome was attributed to the elimination, not only of Treg cells, but also of infiltrating $CD4^+$ effector and $CD8^+$ T-cells by the anti-ICOS mAb therapy. These activated T-cells were absent in all anti-ICOS mAb treated groups but remained in the group treated with anti-CTLA-4 mAb

alone (Figure 3.13 and 3.14). The importance of a high T effector to Treg ratio for cancer immunotherapy to be effective in tumour growth control and for a good survival prognosis has been investigated in the past and is widely accepted (Quezada et al., 2006; Hodi et al., 2008; Shang et al., 2015). This work on the mechanism of action of anti-ICOS mAb therapy demonstrates that not only increased ratios of $CD4^+$ effector/Treg and $CD8^+$/Treg ratios but also sufficient number of effector and cytotoxic cells capable to execute an effective immune response against the tumour is required (Figure 3.13 and 3.15). This logical observation might be difficult to assess in the context of clinical trials as peripheral blood does not always reflect the dynamics of the tumour microenvironment. This work on anti-ICOS mAb therapy in mouse models, showed that the T-cell elimination was restricted to the tumour microenvironment and no differences were observed in the draining lymph nodes (Figure 3.6 to 3.11).

Further work contemplates an evaluation of the combination therapy with anti-CTLA-4 hIgG1 mAb and both human isotypes of anti-ICOS mAb in hFcγR mice, to replicate the observed effects when mouse IgGs are used.

Although experiments presented in this thesis show that the elimination of T-cells by anti-ICOS mAbs occurred in an FcγR-independent manner, further work should be carried out to elicit the mechanism that drives T-cell elimination by targeting ICOS with antibodies. One possibility may be the induction of T-cell apoptosis by AICD in the tumour, triggered by ICOS-stimulation through the agonistic function of the anti-ICOS mAbs. To test this hypothesis, further experiments combining anti-ICOSm1 mAb with blocking of CD95L signalling will be performed.

An alternative explanation for the elimination of T-cells subsets in the tumour after anti-ICOS mAb treatment could be the lack of co-stimulation by the blocking of the interaction between ICOS and ICOSL by the antibody. It has been described that the 37A10 anti-ICOS mAb blocks the ICOS/ICOSL interaction, promoting an agonistic signal *in vitro* (Figure 3.1) (Sazinsky et al., 2016). The data generated during this thesis suggest that the 37A10 anti-ICOS mAb lacks agonistic function *in vivo*, that may block pro-survival signals in T-cells mediated by ICOSL in the tumour. If the T-cell elimination in the tumour observed after 37A10 anti-ICOS mAb therapy is caused by lack of co-stimulation and agonistic function *in vivo*, this may be replicated using antagonistic anti-ICOS mAb and anti-ICOSL mAb in further experiments.

The importance of a functioning ICOS/ICOSL pathway in the context of anti-CTLA-4 mAb therapy has been widely suggested by clinical and preclinical data and reviewed at the beginning of Chapter 3 (Fan et al., 2014; Fu et al., 2011; Di Giacomo et al., 2013). Work presented in this thesis has shown that agonistic anti-ICOS antibodies are not the best approach to target and potentiate this pathway. A blocking or an antagonistic anti-ICOS mAb is also unlikely to provide the ICOS/ICOSL pathway function expected, therefore the use of antagonistic anti-ICOS antibodies for the treatment of solid tumours will block co-stimulatory signals and further effector and cytotoxic T-cell function. Moreover, as human-ICOSL can interact with CD28 and CTLA-4 (Yao et al., 2011), the development of a soluble form of the ligand may be detrimental. Additionally, this interaction (ICOSL binding CD28 and CTLA-4) does not exist in the murine context (Yao et al., 2011), therefore no pre-clinical data can be generated to describe the possible mechanism in the human setting.

Bispecific antibodies targeting ICOS and PD-L1 are also under investigation, like the bi-specific anti-ICOS and anti-PD-L1 hIgG1 KY1055, by Kymab (Sainson et al., 2018b). The data presented in this work is unable to support the rationale behind the design of this molecule, as the exact mechanism of action of KY0155 hIgG1 has not been defined. Using mouse models, the authors claimed that KY1055 effectively depletes Treg cells and increases the Teff/Treg ratio in the tumour, without informing if effector T-cells were also depleted by the use of a hIgG1 (depleting isotype). The data presented in this project shows that depleting isotypes of the anti-ICOS mAb (mIgG2a and hIgG1) increased $CD8^+$/Treg and $CD4^+$effector/Treg ratios despite eliminating $CD8^+$ and $CD4^+$ effector cells (Figure 3.6). Given that the data (Section 3.9, Chapter 3) suggest that anti-ICOS mAb induced elimination of all T-cell populations independent of the FcγR engagement, changes in the Fc portion of the antibody should not potentiate any change. On the other hand, if the elimination of T-cell is dependent on the interaction of both paratopes to the epitope of ICOS, a benefit may be observed. In any scenario, this should be thoroughly studied in preclinical *in vivo* models before translating to the clinic.

5.2 Challenges in modifying the tumour immune microenvironment

5.2.1 Chemotherapy fails to increase tumour infiltration in the context of non-immunogenic tumours as demonstrated by KPB6.F1 model

To study the possibility of discovering a novel approach to treat poorly immunogenic tumours by promoting the changes in the tumour microenvironment, two different chemotherapies (oxaliplatin and cyclophosphamide) were tested in the KPB6.F1 mouse model of non-immunogenic lung cancer. Even though these chemotherapies are not currently the standard of care for the treatment of lung cancer, as explained in the introduction (Chapter 1), they were chosen for their speculated potential effect on promoting infiltration of $CD8^+$ T-cells whilst at the same time depleting Tregs in the tumour. As described previously by Pfirschke et al., the use of a combination of oxaliplatin and cyclophosphamide promotes sensitivity to combination therapy of anti-PD-1 mAb and anti-CTLA-4 mAb in other poorly-immunogenic models of lung cancer (Pfirschke et al., 2016). According to the authors, the combination chemotherapy promoted the sensitivity of lung tumours to respond to checkpoint blockade by promoting $CD8^+$ T-cells infiltration into the tumour (Pfirschke et al., 2016). On the contrary to the data presented in this publication, in the KPB6.F1 model of lung cancer a trend towards increased tumour burden was observed without increased number of infiltrating $CD8^+$ T-cells or modifications in the expression of immuno-modulatory molecules (Figure 4.5A). Moreover, proliferation (as expression of Ki67) and, to a lesser extent, granzyme B production were reduced after treatment with this combination of chemotherapies in KPB6.F1 model, suggesting poor $CD8^+$ T-cell activation as the mechanism behind the failure to reduce the tumour burden of chemotherapy-treated mice (Figure 4.5D).

The following points should be taken into consideration when attempting to reconcile the divergent observations between the KPB6.F1 model and the work by Pfirshcke. Firstly, Pfirschke et al. used the genetic model $Kras^{LSL\text{-}G12D/+}$ $Trp53^{flox/flox}$ and induced tumour development in the lung by administration of adenovirus expressing Cre-recombinase intra-tracheally. In this model, the development of tumours required several weeks, and untreated mice could survive a median of 100 days, indicating a very slow kinetic model (Pfirschke et al.,

2016). In the KPB6.F1 model, the number of cells injected intravenously were adjusted to secure the survival of mice for 21 days, with a high tumour burden. Therefore, the difference in kinetics between the models suggests there is a window of opportunity to provide the combination chemotherapy to promote response. Pfirschke et al. also used a cell line (KP1.9) derived from $Kras^{LSL\text{-}G12D/+}$ $Trp53^{flox/flox}$ nodules. The KP1.9 cell line was injected orthotopically and generated tumours in the lung of C57BL/6 mice that were analysed 19 days after (Pfirschke et al., 2016) with a tumour burden similar to the one observed in the KPB6.F1 model. Even though similarities between the KP1.9 (orthotopically injected) and the KPB6.F1 (intravenously injected) models in kinetics and tumour burden do exist, no similarities in the response to oxaliplatin were observed. Pfirschke et al. tested combination chemotherapy of oxaliplatin plus masfosfamide in the KP1.9 (orthotopically injected) model, with a significant reduction in the weight of the lungs when compared to untreated mice. In this model, no significant survival benefit was observed between combination of oxaliplatin and cyclophosphamide treated mice and the untreated mice (Pfirschke et al., 2016). In contrast, the KPB6.F1 model shows a trend towards increased tumour burden upon treatment with oxaliplatin and combination of oxaliplatin and cyclophosphamide (Figure 4.5A). The authors also tested the KP1.9 cell line injected intravenously, recovering the tissues after 42 days. In this setting, reduction of the tumour burden was observed when combination of oxaliplatin and cyclophosphamide was given (Pfirschke et al., 2016).

Altogether, the differences in response to combination chemotherapy (oxaliplatin plus cyclophosphamide) between the KPB6.F1 model and the published models observed in this work could indicate that:

1. The KPB6.F1 model is highly aggressive, as high tumour burden is achieved with low numbers of cells injected intravenously, with a rapid kinetic in the development of tumour;
2. The lack of $CD8^+$ infiltration by oxaliplatin and cyclophosphamide combination chemotherapy in the KPB6.F1 model may be related to different kinetics of tumour development between the models;
3. The KPB6.F1 model has one extra passage *in vivo* than the KP1.9 (and both were generated from $Kras^{LSL\text{-}G12D/+}$ $Trp53^{flox/flox}$ mice), therefore the extra

immunoediting possibly gave this model more resilience to chemotherapy, either intrinsic to the tumour or related to the modulation of the TME.

As mentioned in Chapter 2 and shown in the supplementary data (Supplementary Figure 7.3), two cell lines derived from $Kras^{LSL\text{-}G12D/+}$ $Trp53^{flox/flox}$ mice after *in vivo* passages (the KPB6.F1 and KPB6.F2) were tested. The KPB6.F1 was generated after recovery and culture of the lungs harvested from WT mice that were injected with KPB6.F0, the cell line obtained directly from the nodules of tumour-bearing $Kras^{LSL\text{-}G12D/+}$ $Trp53^{flox/flox}$ mice. Similarly, the KPB6.F2 was obtained after recovering lungs of WT mice previously injected intravenously with the KPB6.F1 cell line. Both cell lines, KPB6.F1 and KPB6.F2, developed similar tumour burden and TME, and the decision to continue working with the KPB6.F1 cell line was made based on avoiding contamination with *Mycoplasma sp.* (Supplementary Figure 7.3 to 7.5).

Considering the differences in the response to chemotherapy observed between KPB6.F1 and KP1.9 tumours, it can be hypothesised that one *in vivo* passage in WT mice provided the KPB6.F1 cell line with an extra immunoediting process that promoted resistance to chemotherapy.

In general, more chemotherapies could be tested in the future to better understand the role of chemotherapy and its potential synergy or lack thereof in combination with immunotherapy in non-immunogenic tumours.

5.2.2 Radiotherapy fails to increase tumour infiltration in the context of non-immunogenic tumours as demonstrated by KPB6.F1 model

Apart from decreasing the tumour burden, radiotherapy is thought to exert its effect via so called immunogenic cell death which entails the release of tumour antigens that may promote recognition of the tumour by the immune system, and the subsequent sensitisation of the tumour to antibody immunotherapy (Barker et al., 2015).

It was hypothesised that radiotherapy could be an effective approach to tackle tumours with low immunogenicity such as KPB6.F1 model. To that end, radiotherapy was tested in the KPB6.F1 model with two different schedules: 1 dose of 8Gy or 3x8Gy fractions

directly in the right lung of the mice (Figure 4.3 and 4.4). The exclusive targeting of the right lung of the mice required a 3D image reconstruction for each individual mouse prior to treatment planning, imposing time constraints for these experiments. For this reason, only 3 mice per condition were studied. The rationale behind choosing to deliver the localised radiation to the right lung only, was to study, in the same individual, changes in the TME due to direct radiation, as well as the abscopal effect, together with the influence of fractionation of doses of radiotherapy. However, no significant differences were observed between the left and right lung of the same mouse, between fractioning of radiation or between different time points after the last dose of radiation was received (Figure 4.3 and 4.4). Even though only a few mice could be analysed for each condition, this experiment suggests that radiotherapy alone cannot promote TILs-activation in the KPB6.F1 model, at least as concluded based on the immunomodulatory molecules evaluated.

As mentioned before in Chapter 4.1, radiotherapy has also been linked to increased numbers of immunosuppressive cells in the tumour (Laoui et al., 2014; Kachikwu et al., 2011). Even though no differences were observed in the frequency or activation of regulatory T-cells in the tumour, the frequency of other suppressive compartments as TAM and MDSC remains to be evaluated. The lack of response upon radiotherapy strongly suggest that the KPB6.F1 is highly immunosuppressed, and further studies are needed to better understand the changes in the dynamic between various immune populations of KPB6.F1 tumours upon irradiation.

The data presented in this thesis suggest that the CMT-167 model of lung cancer, although similar in its immune signature to KPB6.F1, is more sensitive, than KPB6.F1, to immunotherapy treatments such as anti-4-1BB mAb. Accordingly, further work testing fractionated radiotherapy combined with anti-4-1BB mAb has been planned, to evaluate if increased antigen recognition by radiotherapy could trigger more precise anti-4-1BB-expansion of tumour-reactive TILs.

5.2.3 Targeting depletion of regulatory T-cells in lung cancer

To explore further the potential treatment avenues for lung cancers that are non-immunogenic and do not respond to checkpoint blockade inhibitors, such as ipilimumab or nivolumab, a combination of chemotherapies and anti-CD25 mIgG2a mAb treatment were

tested. The rationale behind this combination entailed elimination of Treg cells in the tumour based on previous research undertaken in the laboratory and hence promoting an effective immune response (Arce Vargas et al., 2017). Even though anti-CD25 mIgG2a mAb alone has shown tumour-reduction and survival of mice in the CT26 model and combination of anti-CD25m2a mAb and anti-PD-1 mAb has improved survival in the subcutaneous models MCA205 and MC38 (Arce Vargas et al., 2017), in the KPB6.F1 model no differences were observed in the tumour burden upon treatment with anti-CD25m2a mAb or combination anti-CD25m2a mAb and anti-4-1BB mAb (Figure 4.5A and 4.8A). Even though efficient Treg depletion could be observed up to 11 days after anti-CD25m2a mAb injection, this only resulted in a marginal and non-statistically significant increase in the frequency of $CD8^+$ $PD\text{-}1^+$ cells (Figure 4.7C).

Importantly, anti-CD25m2a mAb maintained proliferation of $CD8^+$ T-cells, and therefore, it was the therapy chosen for continuation of exploration of combinations that would effectively reduce tumour burden in the KPB6.F1 mouse model (Figure 4.5D). In further experiments testing anti-CD25m2a mAb and anti-4-1BB mAb, anti-CD25m2a mAb antibody effect was mainly limited to reducing the frequency of infiltrating Tregs, whilst anti-4-1BB provided overall activation of all T-cell subsets (Figures 4.8 to 4.15). When triple-combination was tested, anti-CD25m2a mAb plus anti-4-1BB mAb together with either anti-LAG3 mAb or anti-TIGIT mAb, anti-CD25m2a mAb promoted Treg depletion and increased ratios but not significant differences in the expression of activation markers when compared with mice treated without anti-CD25m2a mAb (Figures 4.12 and 4.15).

Unfortunately, neither therapy promoted tumour rejection in the KPB6.F1 model. But when the CMT-167 model was treated with anti-CD25m2a mAb plus anti-4-1BB mAb, the trend towards less tumour burden in the combination group versus anti-4-1BB mAb group, even though non-significant, suggested the important contribution of Treg cells in promoting tumour growth in this model (Figure 4.16A and B). In the CMT-167 model, T-cell activation by anti-4-1BB mAb is not enough to promote tumour regression, and Treg depletion is necessary to allow effective functionality of effector $CD4^+$ and $CD8^+$ T-cells in the tumour.

Altogether, the results presented in this thesis suggest that although the two studied lung cancer models, KPB6.F1 and CMT-167, appear to have similar frequency of regulatory T-cell in the TME, the contribution of Treg depletion to the tumour rejection cannot be

predicted based only on the frequency of Tregs. Clearly, in the KPB6.F1 model, other strong immunosuppressive strategies are exploited by the tumour to escape treatment. The evaluation of other classic immunosuppressive populations, such as MDSC and TAM, in the TME of both models, will improve the understanding of which treatments could effectively eliminate tumours with low immunogenicity. Such mouse model data may potentially hold significant value for the development of rational combination therapy against cancer in the clinic.

5.2.4 Potential and challenges of anti-4-1BB therapy

It has been largely described that targeting 4-1BB promotes proliferation, activation and survival of NK and T-cells, breaking the anergy of cytotoxic T-cells. There are also multiple studies showing anti-tumour response after anti-4-1BB mAb therapy in various models of cancer (Chester et al., 2017; Melero et al., 1997; Vinay et al., 2015; Palazón et al., 2011).

The work presented in this thesis provides promising new combination therapies to be studied further. It has been shown that anti-4-1BBm1 mAb agonistic antibody promotes tumour-reduction in the presence of anti-CD25m2a mAb in the CMT-167 model. During this project, the dose of anti-4-1BB mAb given was reduced from 200 µg to 50 µg without losing the increased proliferation and activation of T-cells in the tumour. Therefore, it is possible that the clinical doses of anti-4-1BB mAb could be further lowered in order to prevent hepatotoxicity, without losing the effectivity of anti-4-1BB mAb therapy (Chester et al., 2017).

The importance of developing mouse models that reproduce key features of human malignancies resistant to the currently available treatments is undeniable. Advanced NSCLC is generally difficult to treat, with a 3-year overall survival of 17% in patients treated with nivolumab, an improvement of the 8% 3-years overall survival of docetaxel (Vokes et al., 2018). Improved survival of NSCLC patients has been observed in patients with high infiltration of NK cells in the stroma (Al-Shibli et al., 2009; Jin et al., 2014). In both models of lung cancer investigated in this project, NK elimination correlated with increased tumour-burden in the lungs. Therefore, anti-4-1BB mAb therapy was tested to promote NK cell activation in the lung TME. The NK population dropped in all experiments after anti-4-1BB mAb therapy (Figures 4.8, 4.12 and 4.16). This result was unexpected, but interestingly

highlighted the role of T-cell response in the tumour control observed in the CMT-167. As discussed below, it is hypothesised that the activation and proliferation of $CD8^+$ $PD\text{-}1^+$ cells after therapy is important for the reduction in tumour burden. Considering that a minority of patients (10%) have high levels of expression of CD56 (NK cell marker) (Al-Shibli et al., 2009), both mouse models resemble features similar to the general NSCLC patient population.

5.2.5 Differences between models of lung cancer

During the project presented in this thesis, the T-cell immune phenotypes from two different mouse models of lung cancer, KPB6.F1 and CMT-167, were characterised. Different aspects including tumour burden, infiltration, relative amount and expression of co-modulatory markers were compared (Figures 4.1 and 4.2).

In general, the frequency of the T-cell compartments and T-cell ratios were similar between both models. Moreover, the expression of co-modulatory molecules on the surface of the three T-cell subsets was similar, although not identical, between the models. Interestingly, when both models were tested for combination immunotherapy with anti-CD25 mAb plus anti-4-1BB mAb, both models showed increased $CD8^+$ activation and proliferation, but just the CMT-167 showed a trend towards lesser tumour burden (Figure 4.16B).

As mentioned in the previous chapter, CMT-167 tumour-bearing mice showed higher frequencies of expression of PD-1, LAG3 and TIGIT on $CD4^+$ effector and $CD8^+$ when compared to untreated KPB6.F1-bearing mice. It has been extensively described that for human cancer the selection of $CD8^+$ $PD\text{-}1^+$ T-cells enriches for tumour-reactive $CD8^+$ T-cells (Inozume et al., 2010; Gros et al., 2014; Ahmadzadeh et al., 2009; Ye et al., 2014). Therefore, the difference in the frequency of expression of PD-1 by $CD8^+$ T-cells between the models evaluated suggest more infiltration of tumour-reactive cells in the CMT-167 model. Consistent with this hypothesis, $PD\text{-}1^+$ expression in the KPB6.F1 model did no significantly change when radiotherapy or chemotherapy were tested.

In this regard, anti-4-1BB mAb therapy potentiated a strong T-cell activation in all T-cell compartments in both models. Depletion of regulatory T-cells by anti-CD25 mIgG2a mAb 24 hours before anti-4-1BB mAb treatment directed the T-cell activation to effector $CD4^+$ and $CD8^+$ T-cells. Additionally, anti-CD25 mAb administration is thought to prevent (by the

depletion of Treg cells) the potential suppressive effects in the TME after Treg activation mediated by anti-4-1BB mAb therapy (Zhang et al., 2007), changing the balance in the TME towards an efficient immune response after combination therapy. Even though both models showed increased proliferation and granzyme B production after the treatment with the combination immunotherapy (anti-CD25 mAb plus anti-4-1BB mAb), we hypothesized that the presence of tumour-reactive TILs in the CMT-167 model was decisive in the outcome of the mice after therapy. In the CMT-167 model, anti-4-1BB mAb therapy is thought to promote the proliferation of tumour reactive T-cells, among other T-cell populations, generating an anti-tumour response. On the contrary, in the KPB6.F1 model, less tumour-reactive TILs are available, and the proliferation of T-cells becomes unspecific, without preferential enrichment of tumour-reactive TILs.

Moreover, different expression frequency of 4-1BB on $CD8^+$ T-cells was observed between both models. Even though both models upregulated 4-1BB on $CD8^+$ T-cells comparing to $CD8^+$ T-cells from the lungs of healthy mice, only the CMT-167 model had an average of 15% of 4-$1BB^+$ cells in untreated conditions (versus an average of 2% for the KPB6.F1 model). Therefore, these models of lung cancer differ in the frequency of $CD8^+$ 4-$1BB^+$ T-cells that are able to bind anti-4-1BB mAb and be activated by the agonistic function of the antibody, promoting activation, survival and proliferation of these $CD8^+$ T-cells. In the CMT-167, these $CD8^+$4-$1BB^+$ cells (15% of total $CD8^+$) are capable of both proliferation and activation following the first dose of treatment, whilst for T-cells from KPB6.F1 tumours this can be achieved only in a very small population. It has been described that a portion of $CD8^+$ PD-1^+ tumour-reactive cells express 4-1BB (Gros et al., 2014). Moreover, the upregulation of 4-1BB on TILs and peripheral $CD8^+$ in melanoma patients has been defined as an activation marker associated with recognition of neoantigens (Ye et al., 2014; Gros et al., 2014, 2016). If the expression of 4-1BB by $CD8^+$ T-cells is also indicative of tumour-reactive T-cells, then tumour-recognition initial difference can translate to tumour-control or escape after anti-4-1BB mAb therapy. Importantly, a trend of tumour-burden control was observed only after Treg depletion, promoting a less immunosuppressive function.

Future work will focus on describing the mechanism underlying the differential response to immunomodulatory antibody therapy of CMT-167 model when compared to the unresponsive KPB6.F1 model. If both mouse models are differentially recognised by the

immune system, as defined by the frequency and number of tumour reactive T-cells, this could be tested by an IFNγ ELIspot. Moreover, analysis of TCR clonality might also provide further evidence; if clonal expansion of some TCR is found in the tumour that are not present in draining LN or spleen, this could indicate infiltration of reactive T-cells.

If the hypothesis that CMT-167 have more tumour-reactive TILs than the KPB6.F1 model is corroborated, then:

1. The CMT-167 tumour cell line could also be used to establish a mouse model for adenocarcinomas with reactive TILs that are suppressed in their function. Assessment of exhaustion of those T-cells will be necessary and will provide evidence of anti-CD25 mAb combined with anti-4-1BB mAb as a strategy to overcome dysfunctionality (or "exhaustion");

2. The KPB6.F1 tumour could be further studied as a model of NSCLC adenocarcinomas with poorly infiltrating reactive T-cells. The evaluation of tumour-antigens and neoantigens within the tumour will test if a lack of tumour antigens is correlated with the limited reactive TILs. In this scenario, another possibility may be the presence of non-infiltrating reactive T-cells (for example, in the draining LN), and the study of immunotherapies that can overcome the mechanisms that avoid T-cell infiltration into the tumour;

3. On the contrary, if KPB6.F1 and CMT-167 models have a similar frequency of reactive TILs, both models could be used to compare effectivity of a given therapy in different tumour microenvironments with similar recognition by T-cells. After therapy, the differences in the non-T-cell TME could be compared. In this case, evaluation of myeloid markers will be crucial.

In general, the description of the TME and the effect of different therapies in both models showed slight differences that eventually had an important impact on the acquisition of tolerance or effective immune response upon administration of the same therapy. Therefore, comparison between both models subjected to the same therapy could describe critical markers, predicting reduced or increased sensitisation to the aforementioned therapy.

5.2.6 Concluding Remarks

Since discovery of ipilimumab, the field of immunotherapy has grown exponentially, seeing approval of not only anti-CTLA4 mAb but also various anti-PD-1 and anti-PD-L1 mAb therapies. While immunotherapy is a very promising way of treating cancer and has proved to be effective for many patients who would not survive the disease with standard of care anti-cancer therapy, a large population of patients do not respond to immunotherapy either. There are multiple reasons for that, primarily due to the cross talk between various immune pathways and a multitude of so-called immune escape mechanisms (Sharma et al., 2017) that allow the tumour to continue growing. To that end multiple medical centres in collaboration with pharmaceutical industry have embarked on testing combination treatments to address such escape mechanisms. The past 3 years have seen an incredible boom in such studies, however, sometimes with not necessarily well thought through scientific rationale nor in-depth and robust preclinical studies. For instance, Incyte's IDO-inhibitor epacadostat failed in the clinic despite promising pre-clinical data (NCT02752074) (Long et al., 2018). Another clinical trial that may follow Incyte's fate, sponsored by Jounce Therapeutics (NCT02904226, ICONIC trial), is evaluating anti-ICOS hIgG1 JTX-2011 mAb alone and in combination with anti-PD-1 mAb or anti-CTLA-4 mAb. Data presented in this thesis address the mechanism of action of various isotypes of ICOS antibodies and hopefully will be used in the future to improve existing therapies.

To further understand why certain patients "fail" to respond to certain immunotherapies, while others go into full remission, further studies of animal models of resistant cancers are required. The deeper understanding of the interplay between tumours and their microenvironment, including the immune system, is absolutely crucial in designing novel therapies as well as predicting which patients should be given which therapy. The second part of work presented in this thesis shows how miniscule differences in the TME can affect therapeutic outcomes and attempts to determine what treatments should be further evaluated to treat NSCLC non-responding patients. One of the proposed avenues entails combining anti-4-1BB mAb with anti-CD25 mAb for patient subgroups with $CD8^{+}PD\text{-}1^{+}4\text{-}1BB^{+}$ cells present in the tumour microenvironment, including discussing relevance of dose adjustment in the clinic.

While cancer is still a disease with significant high unmet medical need, immunotherapy brings hope for treatment to certain groups of patients. Further robust research into its underlying mechanism of action will assist the development of more clinically effective treatments that will hopefully improve complete remission rates or lead to durable responses and thus improved overall survival of patients.

6 Bibliography

Ahmadzadeh, M., L.A. Johnson, B. Heemskerk, J.R. Wunderlich, M.E. Dudley, D.E. White, and S.A. Rosenberg. 2009. Tumor antigen–specific CD8 T cells infiltrating the tumor express high levels of PD-1 and are functionally impaired. *Blood*. 114:1537 LP-1544.

Aida, K., R. Miyakawa, K. Suzuki, K. Narumi, T. Udagawa, Y. Yamamoto, T. Chikaraishi, T. Yoshida, and K. Aoki. 2014. Suppression of Tregs by anti-glucocorticoid induced TNF receptor antibody enhances the antitumor immunity of interferon-α gene therapy for pancreatic cancer. *Cancer Sci*. 105:159–167. doi:10.1111/cas.12332.

Al-Shibli, K., S. Al-Saad, T. Donnem, M. Persson, R.M. Bremnes, and L.-T. Busund. 2009. The prognostic value of intraepithelial and stromal innate immune system cells in non-small cell lung carcinoma. *Histopathology*. 55:301–312. doi:10.1111/j.1365-2559.2009.03379.x.

Alspach, E., D.M. Lussier, and R.D. Schreiber. 2018. Interferon γ and Its Important Roles in Promoting and Inhibiting Spontaneous and Therapeutic Cancer Immunity. *Cold Spring Harb Perspect Biol* . doi:10.1101/cshperspect.a028480.

Amatore, F., L. Gorvel, and D. Olive. 2018. Inducible Co-Stimulator (ICOS) as a potential therapeutic target for anti-cancer therapy. *Expert Opin Ther Targets*. 22:1–9. doi:10.1080/14728222.2018.1444753.

Angevin, E., M.S. Barnette, T.M. Bauer, D.C. Cho, C.E. Ellis, H.K. Gan, A.R. Hansen, A. Hoos, R.C. Jewell, J. Katz, J. Martin-Liberal, M. Maio, P.A. Mayes, M. Millward, V. Moreno, A.J. Olszanski, D. Rischin, J.H.M. Schellens, S. Yadavilli, and H. Zhou. 2017. INDUCE-1: A phase I open-label study of GSK3359609, an ICOS agonist antibody, administered alone and in combination with pembrolizumab in patients with advanced solid tumors. *J Clin Oncol*. 35:TPS3113-TPS3113. doi:10.1200/JCO.2017.35.15_suppl.TPS3113.

Apetoh, L., F. Ghiringhelli, A. Tesniere, M. Obeid, C. Ortiz, A. Criollo, G. Mignot, M.C. Maiuri, E. Ullrich, P. Saulnier, H. Yang, S. Amigorena, B. Ryffel, F.J. Barrat, P. Saftig, F. Levi, R. Lidereau, C. Nogues, J.-P. Mira, A. Chompret, V. Joulin, F. Clavel-Chapelon, J. Bourhis, F. André, S. Delaloge, T. Tursz, G. Kroemer, and L. Zitvogel. 2007. Toll-like receptor 4–dependent contribution of the immune system to anticancer chemotherapy and

radiotherapy. *Nat Med*. 13:1050.

Arce Vargas, F., A.J.S. Furness, K. Litchfield, K. Joshi, R. Rosenthal, E. Ghorani, I. Solomon, M.H. Lesko, N. Ruef, C. Roddie, J.Y. Henry, L. Spain, A. Ben Aissa, A. Georgiou, Y.N.S. Wong, M. Smith, D. Strauss, A. Hayes, D. Nicol, T. O'Brien, L. Mårtensson, A. Ljungars, I. Teige, B. Frendéus, K. Harrington, A. Melcher, A. Wotherspoon, N. Francis, B. Challacombe, A. Fernando, S. Hazell, A. Chandra, L. Pickering, J. Lynch, S. Rudman, S. Chowdhury, K. Harrison-Phipps, M. Varia, C. Horsfield, A. Polson, G. Stamp, M. O'Donnell, W. Drake, P. Hill, D. Hrouda, E. Mayer, J. Olsburgh, G. Kooiman, K. O'Connor, G. Stewart, M. Aitchison, M. Tran, N. Fotiadis, H. Verma, J. Lopez, J. Lester, F. Morgan, M. Kornaszewska, R. Attanoos, H. Adams, H. Davies, D. Fennell, J. Shaw, J. Le Quesne, A. Nakas, S. Rathinam, W. Monteiro, H. Marshall, L. Nelson, J. Bennett, J. Riley, L. Primrose, L. Martinson, G. Anand, S. Khan, M. Nicolson, K. Kerr, S. Palmer, H. Remmen, J. Miller, K. Buchan, M. Chetty, L. Gomersall, S. Lock, B. Naidu, G. Langman, S. Trotter, M. Bellamy, H. Bancroft, A. Kerr, S. Kadiri, J. Webb, G. Middleton, M. Djearaman, Y. Summers, R. Califano, P. Taylor, R. Shah, et al. 2018. Fc Effector Function Contributes to the Activity of Human Anti-CTLA-4 Antibodies. *Cancer Cell*. 33:649–663.e4. doi:10.1016/j.ccell.2018.02.010.

Arce Vargas, F., A.J.S. Furness, I. Solomon, K. Joshi, L. Mekkaoui, M.H. Lesko, E. Miranda Rota, R. Dahan, A. Georgiou, A. Sledzinska, A. Ben Aissa, D. Franz, M. Werner Sunderland, Y.N.S. Wong, J.Y. Henry, T. O'Brien, D. Nicol, B. Challacombe, S.A. Beers, L. Spain, A. Wotherspoon, N. Francis, M. Smith, D. Strauss, A. Hayes, A. Soultati, M. Stares, L. Spain, J. Lynch, N. Fotiadis, A. Fernando, S. Hazell, A. Chandra, L. Pickering, S. Rudman, S. Chowdhury, C. Swanton, M. Jamal-Hanjani, S. Veeriah, S. Shafi, J. Czyzewska-Khan, D. Johnson, J. Laycock, L. Bosshard-Carter, G. Goh, R. Rosenthal, P. Gorman, N. Murugaesu, R.E. Hynds, G. Wilson, N.J. Birkbak, T.B.K. Watkins, N. McGranahan, S. Horswell, R. Mitter, M. Escudero, A. Stewart, P. Van Loo, A. Rowan, H. Xu, S. Turajlic, C. Hiley, C. Abbosh, J. Goldman, R.K. Stone, T. Denner, N. Matthews, G. Elgar, S. Ward, J. Biggs, M. Costa, S. Begum, B. Phillimore, T. Chambers, E. Nye, S. Graca, M. Al Bakir, J.A. Hartley, H.L. Lowe, J. Herrero, D. Lawrence, M. Hayward, N. Panagiotopoulos, S. Kolvekar, M. Falzon, E. Borg, C. Simeon, G. Hector, A. Smith, M. Aranda, M. Novelli, D. Oukrif, S.M. Janes, R. Thakrar, M. Forster, T. Ahmad, S.M. Lee, D. Papadatos-Pastos, et al. 2017. Fc-Optimized Anti-CD25 Depletes Tumor-Infiltrating Regulatory T Cells and Synergizes with

PD-1 Blockade to Eradicate Established Tumors. *Immunity*. 46:577–586. doi:10.1016/j.immuni.2017.03.013.

Assarsson, E., T. Kambayashi, C.M. Persson, B.J. Chambers, and H.-G. Ljunggren. 2005. 2B4/CD48-Mediated Regulation of Lymphocyte Activation and Function. *J Immunol*. 175:2045 LP-2049.

Avice, M.-N., M. Sarfati, F. Triebel, G. Delespesse, and C.E. Demeure. 1999. Lymphocyte Activation Gene-3, a MHC Class II Ligand Expressed on Activated T Cells, Stimulates TNF-α and IL-12 Production by Monocytes and Dendritic Cells. *J Immunol*. 162:2748 LP-2753.

Bansal-Pakala, P., B.S. Halteman, M.H.-Y. Cheng, and M. Croft. 2004. Costimulation of CD8 T Cell Responses by OX40. *J Immunol*. 172:4821 LP-4825.

Barker, H.E., J.T.E. Paget, A.A. Khan, and K.J. Harrington. 2015. The tumour microenvironment after radiotherapy: Mechanisms of resistance and recurrence. *Nat Rev Cancer*. 15:409–425. doi:10.1038/nrc3958.

Barok, M., J. Isola, Z. Pályi-Krekk, P. Nagy, I. Juhász, G. Vereb, P. Kauraniemi, A. Kapanen, M. Tanner, G. Vereb, and J. Szöllösi. 2007. Trastuzumab causes antibody-dependent cellular cytotoxicity–mediated growth inhibition of submacroscopic JIMT-1 breast cancer xenografts despite intrinsic drug resistance. *Mol Cancer Ther*. 6:2065 LP-2072.

Barry, M., and R.C. Bleackley. 2002. Cytotoxic T lymphocytes: all roads lead to death. *Nat Rev Immunol*. 2:401.

Bartkowiak, T., A.R. Jaiswal, C.R. Ager, R. Chin, C.-H. Chen, P. Budhani, M. Ai, M.J. Reilley, M.M. Sebastian, D.S. Hong, and M.A. Curran. 2018. Activation of 4-1BB on Liver Myeloid Cells Triggers Hepatitis via an Interleukin-27–Dependent Pathway. *Clin Cancer Res*. 24:1138 LP-1151.

Baum, P.R., R.B. Gayle, F. Ramsdell, S. Srinivasan, R.A. Sorensen, M.L. Watson, M.F. Seldin, E. Baker, G.R. Sutherland, and K.N. Clifford. 1994. Molecular characterization of murine and human OX40/OX40 ligand systems: identification of a human OX40 ligand as the HTLV-1-regulated protein gp34. *EMBO J*. 13:3992–4001. doi:10.1002/j.1460-2075.1994.tb06715.x.

Beers, S.A., M.J. Glennie, and A.L. White. 2016. Influence of immunoglobulin isotype on therapeutic antibody function. *Blood*. 127:1097–1101. doi:10.1182/blood-2015-09-625343.

Bell, R.B., R.S. Leidner, R.A. Duhen, C. Ballesteros-Merino, Z. Feng, Y. Koguchi, C.B. Bifulco, B.D. Curti, W.J. Urba, B.A. Fox, and A.D. Weinberg. 2017. Abstract 37: Anti-OX40 (MEDI6469) prior to definitive surgical resection in patients with head and neck squamous cell carcinoma. *Clin Cancer Res*. 23:37 LP-37.

Bender, E. 2014. Epidemiology: The dominant malignancy. *Nature*. 513:2011–2012. doi:10.1038/513S2a.

Bernal, M., F. Ruiz-Cabello, A. Concha, A. Paschen, and F. Garrido. 2012. Implication of the β2-microglobulin gene in the generation of tumor escape phenotypes. *Cancer Immunol Immunother*. 61:1359–1371. doi:10.1007/s00262-012-1321-6.

Birkeland, S.A., H.H. Storm, L.U. Lamm, L. Barlow, I. Blohmé, B. Forsberg, B. Eklund, O. Fjeldborg, M. Friedberg, L. Frödin, E. Glattre, S. Halvorsen, N. V Holm, A. Jakobsen, H.E. Jorgensen, J. Ladefoged, T. Lindholm, G. Lundgren, and E. Pukkala. 1995. Cancer risk after renal transplantation in the nordic countries, 1964–1986. *Int J Cancer*. 60:183–189. doi:10.1002/ijc.2910600209.

Blank, C., I. Brown, A.C. Peterson, T.C.R. Transgenic, C.D.T. Cells, M. Spiotto, Y. Iwai, T. Honjo, and T.F. Gajewski. 2004. PD-L1 / B7H-1 Inhibits the Effector Phase of Tumor Rejection by T Cell Receptor (TCR) Transgenic CD8 + T Cells PD-L1 / B7H-1 Inhibits the Effector Phase of Tumor Rejection by T Cell Receptor. *Cancer Res*. 1140–1145. doi:10.1158/0008-5472.CAN-03-3259.

Borghaei, H., L. Paz-Ares, L. Horn, D.R. Spigel, M. Steins, N.E. Ready, L.Q. Chow, E.E. Vokes, E. Felip, E. Holgado, F. Barlesi, M. Kohlhäufl, O. Arrieta, M.A. Burgio, J. Fayette, H. Lena, E. Poddubskaya, D.E. Gerber, S.N. Gettinger, C.M. Rudin, N. Rizvi, L. Crinò, G.R. Blumenschein, S.J. Antonia, C. Dorange, C.T. Harbison, F. Graf Finckenstein, and J.R. Brahmer. 2015. Nivolumab versus Docetaxel in Advanced Nonsquamous Non–Small-Cell Lung Cancer. *N Engl J Med*. 373:1627–1639. doi:10.1056/NEJMoa1507643.

Boshoff, C., and R. Weiss. 2002. Aids-related malignancies. *Nat Rev Cancer*. 2:373.

Bournazos, S., and J. V. Ravetch. 2017. Fcγ Receptor Function and the Design of Vaccination Strategies. *Immunity*. 47:224–233. doi:10.1016/j.immuni.2017.07.009.

Bracci, L., G. Schiavoni, A. Sistigu, and F. Belardelli. 2014. Immune-based mechanisms of cytotoxic chemotherapy: Implications for the design of novel and rationale-based combined treatments against cancer. *Cell Death Differ*. 21:15–25. doi:10.1038/cdd.2013.67.

Bretscher, P.A. 1999. A two-step, two-signal model for the primary activation of precursor helper T cells. *Proc Natl Acad Sci*. 96:185 LP-190.

Brignone, C., B. Escudier, C. Grygar, M. Marcu, and F. Triebel. 2009. A Phase I Pharmacokinetic and Biological Correlative Study of IMP321, a Novel MHC Class II Agonist, in Patients with Advanced Renal Cell Carcinoma. *Clin Cancer Res*.

Brignone, C., M. Gutierrez, F. Mefti, E. Brain, R. Jarcau, F. Cvitkovic, N. Bousetta, J. Medioni, J. Gligorov, C. Grygar, M. Marcu, and F. Triebel. 2010. First-line chemoimmunotherapy in metastatic breast carcinoma: combination of paclitaxel and IMP321 (LAG-3Ig) enhances immune responses and antitumor activity. *J Transl Med*. 8:71. doi:10.1186/1479-5876-8-71.

van den Broek, M.E., D. Kägi, F. Ossendorp, R. Toes, S. Vamvakas, W.K. Lutz, C.J. Melief, R.M. Zinkernagel, and H. Hengartner. 1996. Decreased tumor surveillance in perforin-deficient mice. *J Exp Med*. 184:1781 LP-1790.

Bulliard, Y., R. Jolicoeur, M. Windman, S.M. Rue, S. Ettenberg, D.A. Knee, N.S. Wilson, G. Dranoff, and J.L. Brogdon. 2013. Activating Fc γ receptors contribute to the antitumor activities of immunoregulatory receptor-targeting antibodies. *J Exp Med*. 210:1685 LP-1693.

Bulliard, Y., R. Jolicoeur, J. Zhang, G. Dranoff, N.S. Wilson, and J.L. Brogdon. 2014. OX40 engagement depletes intratumoral Tregs via activating FcγRs, leading to antitumor efficacy. *Immunol Cell Biol*. 92:475–480. doi:10.1038/icb.2014.26.

Burmeister, Y., T. Lischke, A.C. Dahler, H.W. Mages, K.-P. Lam, A.J. Coyle, R.A. Kroczek, and A. Hutloff. 2008. ICOS Controls the Pool Size of Effector-Memory and Regulatory T Cells. *J Immunol*. 180:774–782. doi:10.4049/jimmunol.180.2.774.

Burugu, S., A.R. Dancsok, and T.O. Nielsen. 2017. Emerging targets in cancer immunotherapy. *Semin Cancer Biol*. 0–1. doi:10.1016/j.semcancer.2017.10.001.

Cancer Research UK. 2018a. Lung cancer statistics | Cancer Research UK. Accesed 21-07-2018. *Cancer Res UK*. doi:http://www.cancerresearchuk.org/health-professional/cancer-statistics/statistics-by-cancer-type/lung-cancer#heading-Zero.

Cancer Research UK. 2018b. Treatment for non small cell lung cancer (NSCLC). Accesed 27-07-2018. doi:https://www.cancerresearchuk.org/about-cancer/lung-cancer/treatment/non-small-cell-lung-cancer.

Carthon, B.C., J.D. Wolchok, J. Yuan, A. Kamat, D.S. Ng Tang, J. Sun, G. Ku, P. Troncoso, C.J. Logothetis, J.P. Allison, and P. Sharma. 2010. Preoperative CTLA-4 blockade: Tolerability and immune monitoring in the setting of a presurgical clinical trial. *Clin Cancer Res*. 16:2861–2871. doi:10.1158/1078-0432.CCR-10-0569.

Chan, I.H., M.-H. Xie, A. Lam, F.T. Axelrod, J. Elechko, A.I. Park, and A. Gurney. 2018. Abstract 2726: In vitro functional activity of OMP-336B11, a GITRL-Fc fusion protein, on primary human immune cells. *Cancer Res*. 78:2726 LP-2726.

Chang, W.-C., C.-H. Li, S.-C. Huang, D.-Y. Chang, L.-Y. Chou, and B.-C. Sheu. 2010. Clinical significance of regulatory T cells and CD8+ effector populations in patients with human endometrial carcinoma. *Cancer*. 116:5777–5788. doi:10.1002/cncr.25371.

Chauvin, J., A.J. Korman, H.M. Zarour, J. Chauvin, O. Pagliano, J. Fourcade, Z. Sun, H. Wang, C. Sander, J.M. Kirkwood, T.T. Chen, M. Maurer, A.J. Korman, and H.M. Zarour. 2015. TIGIT and PD-1 impair tumor antigen–specific CD8+ T cells in melanoma patients. *J Clin Invest*. 125:2046–2058. doi:10.1172/JCI80445.

Chen, D.S., and I. Mellman. 2013. Oncology Meets Immunology: The Cancer-Immunity Cycle. *Immunity*. 39:1–10. doi:10.1016/j.immuni.2013.07.012.

Chen, W., R. Zheng, P.D. Baade, S. Zhang, H. Zeng, F. Bray, A. Jemal, X.Q. Yu, and J. He. 2016. Cancer Statistics in China. *CA Cancer J Clin*. 66:115–132. doi:10.3322/caac.21338.

Chester, C., M.F. Sanmamed, J. Wang, and I. Melero. 2017. Immunotherapy targeting 4-1BB: mechanistic rationale, clinical results, and future strategies. *Blood*. 131:49–57.

doi:10.1182/blood-2017-06-741041.

Chinai, J.M., M. Janakiram, F. Chen, W. Chen, M. Kaplan, and X. Zang. 2015. New immunotherapies targeting the PD-1 pathway. *Trends Pharmacol Sci*. 36:587–595. doi:https://doi.org/10.1016/j.tips.2015.06.005.

Choi, B.K., S.C. Lee, M.J. Lee, Y.H. Kim, Y.-W. Kim, K.-W. Ryu, J.-H. Lee, S.M. Shin, S.-H. Lee, S. Suzuki, H.S. Oh, C.H. Kim, D.G. Lee, S.H. Hwang, E.-M. Yu, I.O. Lee, and B.S. Kwon. 2014. 4-1BB-based Isolation and Expansion of CD8+ T Cells Specific for Self-Tumor and Non–Self-Tumor Antigens for Adoptive T-cell Therapy. *J Immunother*. 37.

Clark Wallace H., J., D.E. Elder, I. V Guerry DuPont, L.E. Braitman, B.J. Trock, D. Schultz, M. Synnestvedt, and A.C. Halpern. 1989. Model Predicting Survival in Stage I Melanoma Based on Tumor Progression. *JNCI J Natl Cancer Inst*. 81:1893–1904.

Clouthier, D.L., and T.H. Watts. 2014. Cell-specific and context-dependent effects of GITR in cancer, autoimmunity, and infection. *Cytokine Growth Factor Rev*. 25:91–106. doi:10.1016/j.cytogfr.2013.12.003.

Clynes, R.A., T.L. Towers, L.G. Presta, and J. V Ravetch. 2000. Inhibitory Fc receptors modulate in vivo cytoxicity against tumor targets. *Nat Med*. 6:443.

Coe, D., S. Begom, C. Addey, M. White, J. Dyson, and J.-G. Chai. 2010. Depletion of regulatory T cells by anti-GITR mAb as a novel mechanism for cancer immunotherapy. *Cancer Immunol Immunother*. 59:1367–1377. doi:10.1007/s00262-010-0866-5.

Crespo, J., H. Sun, T.H. Welling, Z. Tian, and W. Zou. 2013. T cell anergy, exhaustion, senescence, and stemness in the tumor microenvironment. *Curr Opin Immunol*. 25:214–221. doi:10.1016/j.coi.2012.12.003.

Curran, M.A., W. Montalvo, H. Yagita, and J.P. Allison. 2010. PD-1 and CTLA-4 combination blockade expands infiltrating T cells and reduces regulatory T and myeloid cells within B16 melanoma tumors. *Proc Natl Acad Sci*. 107:4275–4280. doi:10.1073/pnas.0915174107.

Curti, B.D., M. Kovacsovics-Bankowski, N. Morris, E. Walker, L. Chisholm, K. Floyd, J. Walker, I. Gonzalez, T. Meeuwsen, B.A. Fox, T. Moudgil, W. Miller, D. Haley, T. Coffey, B. Fisher,

L. Delanty-Miller, N. Rymarchyk, T. Kelly, T. Crocenzi, E. Bernstein, R. Sanborn, W.J. Urba, and A.D. Weinberg. 2013. OX40 is a potent immune stimulating target in late stage cancer patients. *Cancer Res*. 73:7189–7198. doi:10.1158/0008-5472.CAN-12-4174.

Dariavach, P., M.-G. Mattéi, P. Golstein, and M.-P. Lefranc. 2018. Human Ig superfamily CTLA-4 gene: chromosomal localization and identity of protein sequence between murine and human CTLA-4 cytoplasmic domains. *Eur J Immunol*. 18:1901–1905. doi:10.1002/eji.1830181206.

Demeure, C.., J. Wolfers, N. Martin-Garcia, P. Gaulard, and F. Triebel. 2001. T Lymphocytes infiltrating various tumour types express the MHC class II ligand lymphocyte activation gene-3 (LAG-3): role of LAG-3/MHC class II interactions in cell–cell contacts. *Eur J Cancer*. 37:1709–1718. doi:10.1016/S0959-8049(01)00184-8.

Dempke, W.C.M., K. Fenchel, P. Uciechowski, and S.P. Dale. 2017. Second- and third-generation drugs for immuno-oncology treatment—The more the better? *Eur J Cancer*. 74:55–72. doi:10.1016/j.ejca.2017.01.001.

Detterbeck, F.C. 2018. The eighth edition TNM stage classification for lung cancer: What does it mean on main street? *J Thorac Cardiovasc Surg*. 155:356–359. doi:10.1016/j.jtcvs.2017.08.138.

Detterbeck, F.C., D.J. Boffa, A.W. Kim, and L.T. Tanoue. 2017. The Eighth Edition Lung Cancer Stage Classification. *Chest*. 151:193–203. doi:10.1016/j.chest.2016.10.010.

Deuss, F.A., B.S. Gully, J. Rossjohn, and R. Berry. 2017. Recognition of nectin-2 by the natural killer cell receptor T cell immunoglobulin and ITIM domain (TIGIT). *J Biol Chem*. 292:11413–11422. doi:10.1074/jbc.M117.786483.

Dieu-Nosjean, M.-C., M. Antoine, C. Danel, D. Heudes, M. Wislez, V. Poulot, N. Rabbe, L. Laurans, E. Tartour, L. de Chaisemartin, S. Lebecque, W.-H. Fridman, and J. Cadranel. 2008. Long-Term Survival for Patients With Non–Small-Cell Lung Cancer With Intratumoral Lymphoid Structures. *J Clin Oncol*. 26:4410–4417. doi:10.1200/JCO.2007.15.0284.

Dighe, A.S., E. Richards, L.J. Old, and R.D. Schreiber. 1994. Enhanced in vivo growth and resistance to rejection of tumor cells expressing dominant negative IFNγ receptors.

Immunity. 1:447–456. doi:https://doi.org/10.1016/1074-7613(94)90087-6.

Dougall, W.C., S. Kurtulus, M.J. Smyth, and A.C. Anderson. 2017. TIGIT and CD96: new checkpoint receptor targets for cancer immunotherapy. *Immunol Rev*. 276:112–120. doi:10.1111/imr.12518.

Du, X., F. Tang, M. Liu, J. Su, Y. Zhang, W. Wu, M. Devenport, C.A. Lazarski, P. Zhang, X. Wang, P. Ye, C. Wang, E. Hwang, T. Zhu, T. Xu, P. Zheng, and Y. Liu. 2018. A reappraisal of CTLA-4 checkpoint blockade in cancer immunotherapy. *Cell Res*. 28:416–432. doi:10.1038/s41422-018-0011-0.

Duan, F., Y. Lin, C. Liu, M.E. Engelhorn, A.D. Cohen, M. Curran, S. Sakaguchi, T. Merghoub, S. Terzulli, J.D. Wolchok, and A.N. Houghton. 2009. Immune Rejection of Mouse Tumors Expressing Mutated Self. *Cancer Res*.

Duffy, A.G., O. V Makarova-Rusher, D. Pratt, D.E. Kleiner, S. Fioravanti, M. Walker, S. Carey, W.D. Figg, S.M. Steinberg, V. Anderson, E. Levy, V. Krishnasamy, B.J. Wood, J. Jones, D.E. Citrin, and T.F. Greten. 2016. A pilot study of AMP-224, a PD-L2 Fc fusion protein, in combination with stereotactic body radiation therapy (SBRT) in patients with metastatic colorectal cancer. *J Clin Oncol*. 34:560. doi:10.1200/jco.2016.34.4_suppl.560.

Dunn, G.P., A.T. Bruce, H. Ikeda, L.J. Old, and R.D. Schreiber. 2002. Cancer immunoediting : from immuno- surveillance to tumor escape. *Nat Immunol*. 3:991–998. doi:10.1038/ni1102-991.

Dunn, G.P., L.J. Old, and R.D. Schreiber. 2003. The Three Es of Cancer Immunoediting. *Annu Rev Immunol*. 22:329–360. doi:10.1146/annurev.immunol.22.012703.104803.

DuPage, M., A.L. Dooley, and T. Jacks. 2009. Conditional mouse lung cancer models using adenoviral or lentiviral delivery of Cre recombinase. *Nat Protoc*. 4:1064.

Eggermont, A.M.M., V. Chiarion-Sileni, J.-J. Grob, R. Dummer, J.D. Wolchok, H. Schmidt, O. Hamid, C. Robert, P.A. Ascierto, J.M. Richards, C. Lebbé, V. Ferraresi, M. Smylie, J.S. Weber, M. Maio, L. Bastholt, L. Mortier, L. Thomas, S. Tahir, A. Hauschild, J.C. Hassel, F.S. Hodi, C. Taitt, V. de Pril, G. de Schaetzen, S. Suciu, and A. Testori. 2016. Prolonged Survival in Stage III Melanoma with Ipilimumab Adjuvant Therapy. *N Engl J Med*. 375:1845–1855. doi:10.1056/NEJMoa1611299.

van Elsas, A., A.A. Hurwitz, and J.P. Allison. 1999. Combination Immunotherapy of B16 Melanoma Using Anti–Cytotoxic T Lymphocyte–Associated Antigen 4 (Ctla-4) and Granulocyte/Macrophage Colony-Stimulating Factor (Gm-Csf)-Producing Vaccines Induces Rejection of Subcutaneous and Metastatic Tumors Accompanied . *J Exp Med*. 190:355 LP-366.

Faget, J., N. Bendriss-Vermare, M. Gobert, I. Durand, D. Olive, C. Biota, T. Bachelot, I. Treilleux, S. Goddard-Leon, E. Lavergne, S. Chabaud, J.Y. Blay, C. Caux, and C. Meńétrier-Caux. 2012. ICOS-ligand expression on plasmacytoid dendritic cells supports breast cancer progression by promoting the accumulation of immunosuppressive CD4 + T cells. *Cancer Res*. 72:6130–6141. doi:10.1158/0008-5472.CAN-12-2409.

Faget, J., V. Sisirak, J.-Y. Blay, C. Caux, N. Bendriss-Vermare, and C. Ménétrier-Caux. 2013. ICOS is associated with poor prognosis in breast cancer as it promotes the amplification of immunosuppressive CD4 $^{+}$ T cells by plasmacytoid dendritic cells. *Oncoimmunology*. 2:e23185. doi:10.4161/onci.23185.

Fan, X., S.A. Quezada, M.A. Sepulveda, P. Sharma, and J.P. Allison. 2014. Engagement of the ICOS pathway markedly enhances efficacy of CTLA-4 blockade in cancer immunotherapy. *J Exp Med*. 211:715–725. doi:10.1084/jem.20130590.

FDA website, oficial. 2018. Approved Drugs>Hematology/Oncology (Cancer) Approvals & Safety Notifications. Accesed 16-08-2018. doi:https://www.fda.gov/drugs/informationondrugs/approveddrugs/ucm279174.htm.

Fourcade, J., Z. Sun, M. Benallaoua, P. Guillaume, I.F. Luescher, C. Sander, J.M. Kirkwood, V. Kuchroo, and H.M. Zarour. 2010. Upregulation of Tim-3 and PD-1 expression is associated with tumor antigen–specific CD8+ T cell dysfunction in melanoma patients. *J Exp Med*. 207:2175 LP-2186.

Francisco, L.M., V.H. Salinas, K.E. Brown, V.K. Vanguri, G.J. Freeman, V.K. Kuchroo, and A.H. Sharpe. 2009. PD-L1 regulates the development, maintenance, and function of induced regulatory T cells. *J Exp Med*. 206:3015 LP-3029.

Fu, T., Q. He, and P. Sharma. 2011. The ICOS/ICOSL pathway is required for optimal antitumor responses mediated by anti-CTLA-4 therapy. *Cancer Res*. 71:5445–5454.

doi:10.1158/0008-5472.CAN-11-1138.

Fuertes Marraco, S.A., N.J. Neubert, G. Verdeil, and D.E. Speiser. 2015. Inhibitory receptors beyond T cell exhaustion. *Front Immunol*. 6:1–14. doi:10.3389/fimmu.2015.00310.

Furness, A.J.S., F.A. Vargas, K.S. Peggs, and S.A. Quezada. 2014. Impact of tumour microenvironment and Fc receptors on the activity of immunomodulatory antibodies. *Trends Immunol*. 35:290–298. doi:10.1016/j.it.2014.05.002.

Gabrilovich, D.I., and S. Nagaraj. 2009. Myeloid-derived suppressor cells as regulators of the immune system. *Nat Rev Immunol*. 9:162–174. doi:10.1038/nri2506.

Gautron, A.-S., M. Dominguez-Villar, M. Marcken, and D.A. Hafler. 2014. Enhanced suppressor function of TIM-3+FoxP3+ regulatory T cells. *Eur J Immunol*. 44:2703–2711. doi:10.1002/eji.201344392.

Di Giacomo, A.M., L. Calabrò, R. Danielli, E. Fonsatti, E. Bertocci, I. Pesce, C. Fazio, O. Cutaia, D. Giannarelli, C. Miracco, M. Biagioli, M. Altomonte, and M. Maio. 2013. Long-term survival and immunological parameters in metastatic melanoma patients who responded to ipilimumab 10 mg/kg within an expanded access programme. *Cancer Immunol Immunother*. 62:1021–1028. doi:10.1007/s00262-013-1418-6.

Godfrey, W.R., F.F. Fagnoni, M.A. Harara, D. Buck, and E.G. Engleman. 1994. Identification of a human OX-40 ligand, a costimulator of CD4+ T cells with homology to tumor necrosis factor. *J Exp Med*. 180:757 LP-762.

Golay, J., C. Cortiana, M. Manganini, G. Cazzaniga, A. Salvi, O. Spinelli, R. Bassan, T. Barbui, A. Biondi, A. Rambaldi, and M. Introna. 2006. The sensitivity of acute lymphoblastic leukemia cells carrying the t(12;21) translocation to campath-1H-mediated cell lysis. *Haematologica*. 91:322 LP-330.

Golden-Mason, L., B.E. Palmer, N. Kassam, L. Townshend-Bulson, S. Livingston, B.J. McMahon, N. Castelblanco, V. Kuchroo, D.R. Gretch, and H.R. Rosen. 2009. Negative Immune Regulator Tim-3 Is Overexpressed on T Cells in Hepatitis C Virus Infection and Its Blockade Rescues Dysfunctional CD4⁺ and CD8⁺ T Cells. *J Virol*. 83:9122 LP-9130.

Goldstraw, P., K. Chansky, J. Crowley, R. Rami-Porta, H. Asamura, W.E.E. Eberhardt, A.G. Nicholson, P. Groome, A. Mitchell, V. Bolejack, D. Ball, D.G. Beer, R. Beyruti, F. Detterbeck, W.E.E. Eberhardt, J. Edwards, F. Galateau-Sallé, D. Giroux, F. Gleeson, J. Huang, C. Kennedy, J. Kim, Y.T. Kim, L. Kingsbury, H. Kondo, M. Krasnik, K. Kubota, A. Lerut, G. Lyons, M. Marino, E.M. Marom, J. Van Meerbeeck, T. Nakano, A. Nowak, M. Peake, T. Rice, K. Rosenzweig, E. Ruffini, V. Rusch, N. Saijo, P. Van Schil, J.P. Sculier, L. Shemanski, K. Stratton, K. Suzuki, Y. Tachimori, C.F. Thomas, W. Travis, M.S. Tsao, A. Turrisi, J. Vansteenkiste, H. Watanabe, Y.L. Wu, P. Baas, J. Erasmus, S. Hasegawa, K. Inai, K. Kernstine, H. Kindler, L. Krug, K. Nackaerts, H. Pass, D. Rice, C. Falkson, P.L. Filosso, G. Giaccone, K. Kondo, M. Lucchi, M. Okumura, E. Blackstone, F. Abad Cavaco, E. Ansótegui Barrera, J. Abal Arca, I. Parente Lamelas, A. Arnau Obrer, R. Guijarro Jorge, G.K. Bascom, A.I. Blanco Orozco, M. González Castro, M.G. Blum, D. Chimondeguy, V. Cvijanovic, S. Defranchi, B. De Olaiz Navarro, I. Escobar Campuzano, I. Macía Vidueira, E. Fernández Araujo, F. Andreo García, K.M. Fong, G. Francisco Corral, S. Cerezo González, J. Freixinet Gilart, L. García Arangüena, S. García Barajas, P. Girard, T. Goksel, M.T. González Budiño, G. González Casaurrán, et al. 2016. The IASLC lung cancer staging project: Proposals for revision of the TNM stage groupings in the forthcoming (eighth) edition of the TNM Classification for lung cancer. *J Thorac Oncol*. 11:39–51. doi:10.1016/j.jtho.2015.09.009.

Goodwin, R.G., W.S. Din, T. Davis-Smith, D.M. Anderson, S.D. Gimpel, T.A. Sato, C.R. Maliszewski, C.I. Brannan, N.G. Copeland, N.A. Jenkins, T. Farrah, R.J. Armitage, W.C. Fanslow, and C.A. Smith. 1993. Molecular cloning of a ligand for the inducible T cell gene 4-1BB: a member of an emerging family of cytokines with homology to tumor necrosis factor. *Eur J Immunol*. 23:2631–2641. doi:10.1002/eji.1830231037.

Gopal, A.K., N.L. Bartlett, R. Levy, R. Houot, S.D. Smith, N.H. Segal, A.D. Thall, G. Mugundu, B. Huang, C. Davis, and H.E. Kohrt. 2015. A phase I study of PF-05082566 (anti-4-1BB) + rituximab in patients with CD20+ NHL. *J Clin Oncol*. 33:3004. doi:10.1200/jco.2015.33.15_suppl.3004.

Govindan, R., A. Szczesna, M.-J. Ahn, C.-P. Schneider, P.F. Gonzalez Mella, F. Barlesi, B. Han, D.E. Ganea, J. Von Pawel, V. Vladimirov, N. Fadeeva, K.H. Lee, T. Kurata, L. Zhang, T. Tamura, P.E. Postmus, J. Jassem, K. O'Byrne, J. Kopit, M. Li, M. Tschaika, and M. Reck. 2017. Phase III Trial of Ipilimumab Combined With Paclitaxel and Carboplatin in

Advanced Squamous Non–Small-Cell Lung Cancer. *J Clin Oncol*. 35:3449–3457. doi:10.1200/JCO.2016.71.7629.

Gramaglia, I., A. Jember, S.D. Pippig, A.D. Weinberg, N. Killeen, and M. Croft. 2000. The OX40 Costimulatory Receptor Determines the Development of CD4 Memory by Regulating Primary Clonal Expansion. *J Immunol*. 165:3043 LP-3050.

Greene, J.L., G.M. Leytze, J. Emswiler, R. Peach, W. Cosand, and P.S. Linsley. 1996. Covalent Dimerization of CD28 / CTLA-4 and Oligomerization of CD80 / CD86 Regulate T Cell Costimulatory Interactions. *J Biol Chem*. 271:26762–26771. doi:10.1074/jbc.271.43.26762.

Gros, A., M.R. Parkhurst, E. Tran, A. Pasetto, P.F. Robbins, S. Ilyas, T.D. Prickett, J.J. Gartner, J.S. Crystal, I.M. Roberts, K. Trebska-McGowan, J.R. Wunderlich, J.C. Yang, and S.A. Rosenberg. 2016. Prospective identification of neoantigen-specific lymphocytes in the peripheral blood of melanoma patients. *Nat Med*. 22:433.

Gros, A., P.F. Robbins, X. Yao, Y.F. Li, S. Turcotte, E. Tran, J.R. Wunderlich, A. Mixon, S. Farid, M.E. Dudley, K. Hanada, J.R. Almeida, S. Darko, D.C. Douek, J.C. Yang, and S.A. Rosenberg. 2014. PD-1 identifies the patient-specific CD8+ tumor-reactive repertoire infiltrating human tumors. *J Clin Invest*. 124:2246–2259. doi:10.1172/JCI73639.

Guo, Z., X. Wang, D. Cheng, Z. Xia, M. Luan, and S. Zhang. 2014. PD-1 blockade and OX40 triggering synergistically protects against tumor growth in a murine model of ovarian cancer. *PLoS One*. 9. doi:10.1371/journal.pone.0089350.

Gupta, S., T.B. Thornley, W. Gao, R. Larocca, L.A. Turka, V.K. Kuchroo, and T.B. Strom. 2012. Allograft rejection is restrained by short-lived TIM-3+PD-1+Foxp3+ Tregs. *J Clin Invest*. 122:2395–2404. doi:10.1172/JCI45138.

Hamaguchi, Y., Y. Xiu, K. Komura, F. Nimmerjahn, and T.F. Tedder. 2006. Antibody isotype-specific engagement of Fcγ receptors regulates B lymphocyte depletion during CD20 immunotherapy. *J Exp Med*. 203:743 LP-753.

Hanson, D.C., P.C. Canniff, M.J. Primiano, C.B. Donovan, J.P. Gardner, E.J. Natoli, R.W. Morgan, R.J. Mather, D.H. Singleton, P.A. Hermes, M.J. Neveu, G.C. Andrews, C.D. Castro, E.A. Elliott, and V. Bedian. 2004. Preclinical in vitro characterization

of anti-CTLA4 therapeutic antibody CP-675,206. *Cancer Res*. 64:877 LP-877.

Hara, M., H. Nakanishi, K. Tsujimura, M. Matsui, Y. Yatabe, T. Manabe, and M. Tatematsu. 2008. Interleukin-2 potentiation of cetuximab antitumor activity for epidermal growth factor receptor-overexpressing gastric cancer xenografts through antibody-dependent cellular cytotoxicity. *Cancer Sci*. 99:1471–1478. doi:10.1111/j.1349-7006.2008.00821.x.

Harrington, K.J., L.J. Billingham, T.B. Brunner, N.G. Burnet, C.S. Chan, P. Hoskin, R.I. Mackay, T.S. Maughan, J. Macdougall, W.G. Mckenna, C.M. Nutting, A. Oliver, R. Plummer, I.J. Stratford, and T. Illidge. 2011. Guidelines for preclinical and early phase clinical assessment of novel radiosensitisers. *Br J Cancer*. 105:628–639.

He, J., Y. Hu, M. Hu, and B. Li. 2015. Development of PD-1/PD-L1 Pathway in Tumor Immune Microenvironment and Treatment for Non-Small Cell Lung Cancer. *Sci Rep*. 5:1–9. doi:10.1038/srep13110.

Hellmann, M.D., T.-E. Ciuleanu, A. Pluzanski, J.S. Lee, G.A. Otterson, C. Audigier-Valette, E. Minenza, H. Linardou, S. Burgers, P. Salman, H. Borghaei, S.S. Ramalingam, J. Brahmer, M. Reck, K.J. O'Byrne, W.J. Geese, G. Green, H. Chang, J. Szustakowski, P. Bhagavatheeswaran, D. Healey, Y. Fu, F. Nathan, and L. Paz-Ares. 2018. Nivolumab plus Ipilimumab in Lung Cancer with a High Tumor Mutational Burden. *N Engl J Med*. 378:2093–2104. doi:10.1056/NEJMoa1801946.

Hemon, P., F. Jean-Louis, K. Ramgolam, C. Brignone, M. Viguier, H. Bachelez, F. Triebel, D. Charron, F. Aoudjit, R. Al-Daccak, and L. Michel. 2011. MHC Class II Engagement by Its Ligand LAG-3 (CD223) Contributes to Melanoma Resistance to Apoptosis. *J Immunol*. 186:5173–5183. doi:10.4049/jimmunol.1002050.

Hernandez-Chacon, J.A., Y. Li, R.C. Wu, C. Bernatchez, Y. Wang, J.S. Weber, P. Hwu, and L.G. Radvanyi. 2011. Costimulation Through the CD137/4-1BB Pathway Protects Human Melanoma Tumor-infiltrating Lymphocytes From Activation-induced Cell Death and Enhances Antitumor Effector Function. *J Immunother*. 34.

Hodi, F.S., M. Butler, D.A. Oble, M. V. Seiden, F.G. Haluska, A. Kruse, S. MacRae, M. Nelson, C. Canning, I. Lowy, A. Korman, D. Lautz, S. Russell, M.T. Jaklitsch, N. Ramaiya, T.C. Chen, D. Neuberg, J.P. Allison, M.C. Mihm, and G. Dranoff. 2008. Immunologic and clinical effects

of antibody blockade of cytotoxic T lymphocyte-associated antigen 4 in previously vaccinated cancer patients. *Proc Natl Acad Sci*. 105:3005–3010. doi:10.1073/pnas.0712237105.

Hodi, F.S., J. Chesney, A.C. Pavlick, C. Robert, K.F. Grossmann, D.F. McDermott, G.P. Linette, N. Meyer, J.K. Giguere, S.S. Agarwala, M. Shaheen, M.S. Ernstoff, D.R. Minor, A.K. Salama, M.H. Taylor, P.A. Ott, C. Horak, P. Gagnier, J. Jiang, J.D. Wolchok, and M.A. Postow. 2016. Combined nivolumab and ipilimumab versus ipilimumab alone in patients with advanced melanoma: 2-year overall survival outcomes in a multicentre, randomised, controlled, phase 2 trial. *Lancet Oncol*. 17:1558–1568. doi:10.1016/S1470-2045(16)30366-7.

Hodi, F.S., S.J. O'Day, D.F. McDermott, R.W. Weber, J.A. Sosman, J.B. Haanen, R. Gonzalez, C. Robert, D. Schadendorf, J.C. Hassel, W. Akerley, A.J.M. van den Eertwegh, J. Lutzky, P. Lorigan, J.M. Vaubel, G.P. Linette, D. Hogg, C.H. Ottensmeier, C. Lebbé, C. Peschel, I. Quirt, J.I. Clark, J.D. Wolchok, J.S. Weber, J. Tian, M.J. Yellin, G.M. Nichol, A. Hoos, and W.J. Urba. 2010. Improved Survival with Ipilimumab in Patients with Metastatic Melanoma. *N Engl J Med*. 363:711–723. doi:10.1056/NEJMoa1003466.

Houot, R., M.J. Goldstein, H.E. Kohrt, J.H. Myklebust, A.A. Alizadeh, J.T. Lin, J.M. Irish, J.A. Torchia, A. Kolstad, L. Chen, and R. Levy. 2009. Therapeutic effect of CD137 immunomodulation in lymphoma and its enhancement by T_{reg} depletion. *Blood*. 114:3431 LP-3438.

Huang, C.-T.T., C.J. Workman, D. Flies, X. Pan, A.L. Marson, G. Zhou, E.L. Hipkiss, S. Ravi, J. Kowalski, H.I. Levitsky, J.D. Powell, D.M. Pardoll, C.G. Drake, and D.A.A. Vignali. 2004. Role of LAG-3 in regulatory T cells. *Immunity*. 21:503–513. doi:10.1016/j.immuni.2004.08.010.

Huang, R.-Y., C. Eppolito, S. Lele, P. Shrikant, J. Matsuzaki, and K. Odunsi. 2015. LAG3 and PD1 co-inhibitory molecules collaborate to limit CD8⁺ T cell signaling and dampen antitumor immunity in a murine ovarian cancer model. *Oncotarget*. 6:27359–27377. doi:10.18632/oncotarget.4751.

Huard, B., P. Prigent, M. Tournier, D. Bruniquel, and F. Triebel. 1995. CD4/major histocompatibility complex class II interaction analyzed with CD4-and lymphocyte

activation gene-3 (LAG-3)-Ig fusion proteins. *Eur J Immunol*. 25:2718–2721.

Hui, L., and Y. Chen. 2015. Tumor microenvironment: Sanctuary of the devil. *Cancer Lett*. 368:7–13. doi:10.1016/J.CANLET.2015.07.039.

Hurtado, J.C., S.H. Kim, K.E. Pollok, Z.H. Lee, and B.S. Kwon. 1995. Potential role of 4-1BB in T cell activation. Comparison with the costimulatory molecule CD28. *J Immunol*. 155:3360 LP-3367.

Hurtado, J.C., Y.J. Kim, and B.S. Kwon. 1997. Signals through 4-1BB are costimulatory to previously activated splenic T cells and inhibit activation-induced cell death. *J Immunol*. 158:2600 LP-2609.

Hutloff, A., A.M. Dittrich, K.C. Beier, B. Eljaschewitsch, R. Kraft, I. Anagnostopoulos, and R.A. Kroczek. 1999. ICOS is an inducible T-cell co-stimulator structurally and functionally related to CD28. *Nature*. 397:263–266. doi:10.1038/16717.

Immutep. 2018. ASX/Media Release. IMMUTEP ENTERS INTO CLINICAL TRIAL COLLABORATION AND SUPPLY AGREEMENT WITH MERCK KGAA, DARMSTADT, GERMANY, AND PFIZER. Accessed 25-09-2018. *http://www.immutep.com/files/content/investor/press-release/2018/1847468.pdf*.

Inozume, T., K. Hanada, Q.J. Wang, M. Ahmadzadeh, J.R. Wunderlich, S.A. Rosenberg, and J.C. Yang. 2010. Selection of CD8+PD-1+ Lymphocytes in Fresh Human Melanomas Enriches for Tumor-reactive T Cells. *J Immunother*. 33.

Ishida, Y., Y. Agata, K. Shibahara, and T. Honjo. 1992. Induced expression of PD-1, a novel member of the immunoglobulin gene superfamily, upon programmed cell death. *EMBO J*. 11:3887–95. doi:10.1128/MCB.25.21.9543.

Ishigami, S., S. Natsugoe, K. Tokuda, A. Nakajo, X. Che, H. Iwashige, K. Aridome, S. Hokita, and T. Aikou. 2000. Prognostic value of intratumoral natural killer cells in gastric carcinoma. *Cancer*. 88:577–583. doi:10.1002/(SICI)1097-0142(20000201)88:3<577::AID-CNCR13>3.0.CO;2-V.

Jin, H.-T., A.C. Anderson, W.G. Tan, E.E. West, S.-J. Ha, K. Araki, G.J. Freeman, V.K. Kuchroo, and R. Ahmed. 2010. Cooperation of Tim-3 and PD-1 in CD8 T-cell exhaustion during

chronic viral infection. *Proc Natl Acad Sci*. 107:14733 LP-14738.

Jin, S., Y. Deng, J.-W. Hao, Y. Li, B. Liu, Y. Yu, F.-D. Shi, and Q.-H. Zhou. 2014. NK Cell Phenotypic Modulation in Lung Cancer Environment. *PLoS One*. 9:e109976.

Johnson, P., and M. Glennie. 2003. The mechanisms of action of rituximab in the elimination of tumor cells. *Semin Oncol*. 30:3–8. doi:10.1053/sonc.2003.50025.

Johnston, R.J., L. Comps-Agrar, J. Hackney, X. Yu, M. Huseni, Y. Yang, S. Park, V. Javinal, H. Chiu, B. Irving, D.L. Eaton, and J.L. Grogan. 2014. The Immunoreceptor TIGIT Regulates Antitumor and Antiviral CD8+ T Cell Effector Function. *Cancer Cell*. 26:923–937. doi:10.1016/J.CCELL.2014.10.018.

Jones, R.B., L.C. Ndhlovu, J.D. Barbour, P.M. Sheth, A.R. Jha, B.R. Long, J.C. Wong, M. Satkunarajah, M. Schweneker, J.M. Chapman, G. Gyenes, B. Vali, M.D. Hyrcza, F.Y. Yue, C. Kovacs, A. Sassi, M. Loutfy, R. Halpenny, D. Persad, G. Spotts, F.M. Hecht, T.-W. Chun, J.M. McCune, R. Kaul, J.M. Rini, D.F. Nixon, and M.A. Ostrowski. 2008. Tim-3 expression defines a novel population of dysfunctional T cells with highly elevated frequencies in progressive HIV-1 infection. *J Exp Med*. 205:2763 LP-2779.

Jounce News Release. 2018. Jounce Therapeutics Presents Preliminary Efficacy Data from Ongoing Phase 1/2 ICONIC Trial of JTX-2011 in Patients with Advanced Cancers. Accessed 14-07-2018. *http://ir.jouncetx.com/phoenix.zhtml?c=254289&p=irol-newsArticle_print&ID=2352867*.

Kachikwu, E.L., K.S. Iwamoto, Y.P. Liao, J.J. Demarco, N. Agazaryan, J.S. Economou, W.H. McBride, and D. Schaue. 2011. Radiation enhances regulatory T cell representation. *Int J Radiat Oncol Biol Phys*. 81:1128–1135. doi:10.1016/j.ijrobp.2010.09.034.

Kaufman, H.L., J. Russell, O. Hamid, S. Bhatia, P. Terheyden, S.P. D'Angelo, K.C. Shih, C. Lebbé, G.P. Linette, M. Milella, I. Brownell, K.D. Lewis, J.H. Lorch, K. Chin, L. Mahnke, A. von Heydebreck, J.-M. Cuillerot, and P. Nghiem. 2016. Avelumab in patients with chemotherapy-refractory metastatic Merkel cell carcinoma: a multicentre, single-group, open-label, phase 2 trial. *Lancet Oncol*. 17:1374–1385. doi:10.1016/S1470-2045(16)30364-3.

Keir, M.E., M.J. Butte, G.J. Freeman, and A.H. Sharpe. 2008. PD-1 and Its Ligands in Tolerance

and Immunity. *Annu Rev Immunol*. 26:677–704. doi:10.1146/annurev.immunol.26.021607.090331.

Khalil, D.N., E.L. Smith, R.J. Brentjens, and J.D. Wolchok. 2016. The future of cancer treatment: Immunomodulation, CARs and combination immunotherapy. *Nat Rev Clin Oncol*. 13:273–290. doi:10.1038/nrclinonc.2016.25.

Khayyamian, S., A. Hutloff, K. Büchner, M. Gräfe, V. Henn, R.A. Kroczek, and H.W. Mages. 2002. ICOS-ligand, expressed on human endothelial cells, costimulates Th1 and Th2 cytokine secretion by memory CD4+ T cells. *Proc Natl Acad Sci U S A*. 99:6198–203. doi:10.1073/pnas.092576699.

Knee, D.A., B. Hewes, and J.L. Brogdon. 2016. Rationale for anti-GITR cancer immunotherapy. *Eur J Cancer*. 67:1–10. doi:10.1016/J.EJCA.2016.06.028.

Ko, H.-J., Y.-J. Kim, Y.-S. Kim, W.-S. Chang, S.-Y. Ko, S.-Y. Chang, S. Sakaguchi, and C.-Y. Kang. 2007. A Combination of Chemoimmunotherapies Can Efficiently Break Self-Tolerance and Induce Antitumor Immunity in a Tolerogenic Murine Tumor Model. *Cancer Res*. 67:7477 LP-7486.

Kobayashi, T., B.L. Doff, R.C. Rearden, G.R. Leggatt, and S.R. Mattarollo. 2015. NKT cell-targeted vaccination plus anti-4–1BB antibody generates persistent CD8 T cell immunity against B cell lymphoma. *Oncoimmunology*. 4:1–11. doi:10.4161/2162402X.2014.990793.

Koon, H.B., D.R. Shepard, T. Merghoub, D.A. Schaer, C.A. Sirard, and J.D. Wolchok. 2016. First-in-human phase 1 single-dose study of TRX-518, an anti-human glucocorticoid-induced tumor necrosis factor receptor (GITR) monoclonal antibody in adults with advanced solid tumors. *J Clin Oncol*. 34:3017. doi:10.1200/JCO.2016.34.15_suppl.3017.

Krausz, L.T., E. Fischer-Fodor, Z.Z. Major, and B. Fetica. 2012. Gitr-Expressing Regulatory T-Cell Subsets are Increased in Tumor-Positive Lymph Nodes from Advanced Breast Cancer Patients as Compared to Tumor-Negative Lymph Nodes. *Int J Immunopathol Pharmacol*. 25:59–66. doi:10.1177/039463201202500108.

Kroemer, G., L. Galluzzi, O. Kepp, and L. Zitvogel. 2013. Immunogenic Cell Death in Cancer Therapy. *Annu Rev Immunol*. 31:51–72. doi:10.1146/annurev-immunol-032712-100008.

Kurtulus, S., K. Sakuishi, S.-F. Ngiow, N. Joller, D.J. Tan, M.W.L. Teng, M.J. Smyth, V.K. Kuchroo, and A.C. Anderson. 2015. TIGIT predominantly regulates the immune response via regulatory T cells. *J Clin Invest*. 125:4053–4062. doi:10.1172/JCI81187.

Kwon, E.D., C.G. Drake, H.I. Scher, K. Fizazi, A. Bossi, A.J.M. van den Eertwegh, M. Krainer, N. Houede, R. Santos, H. Mahammedi, S. Ng, M. Maio, F.A. Franke, S. Sundar, N. Agarwal, A.M. Bergman, T.E. Ciuleanu, E. Korbenfeld, L. Sengeløv, S. Hansen, C. Logothetis, T.M. Beer, M.B. McHenry, P. Gagnier, D. Liu, and W.R. Gerritsen. 2014. Ipilimumab versus placebo after radiotherapy in patients with metastatic castration-resistant prostate cancer that had progressed after docetaxel chemotherapy (CA184-043): a multicentre, randomised, double-blind, phase 3 trial. *Lancet Oncol*. 15:700–712. doi:10.1016/S1470-2045(14)70189-5.

Kwon, E.D., A.A. Hurwitz, B.A. Foster, C. Madias, A.L. Feldhaus, N.M. Greenberg, M.B. Burg, and J.P. Allison. 1997. Manipulation of T cell costimulatory and inhibitory signals for immunotherapy of prostate cancer. *Proc Natl Acad Sci*. 94:8099 LP-8103.

Kymab News Release. 2018. Kymab Announces Agreement to Evaluate KY1044, its Novel Antibody Targeting ICOS, and Anti-PD-L1 Immunotherapy for testing in Multiple Solid Tumors. Accessed 15-07-2018. *https://www.kymab.com/media/uploads/files/28_Jun_2018_Kymab_agreement_Roche_evaluate_anti-ICOS_KY1044_EaEZqcv.pdf*.

Laoui, D., E. Van Overmeire, P. De Baetselier, J.A. Van Ginderachter, and G. Raes. 2014. Functional Relationship between Tumor-Associated Macrophages and Macrophage Colony-Stimulating Factor as Contributors to Cancer Progression . *Front Immunol* . 5:489.

Larkin, J., V. Chiarion-Sileni, R. Gonzalez, J.J. Grob, C.L. Cowey, C.D. Lao, D. Schadendorf, R. Dummer, M. Smylie, P. Rutkowski, P.F. Ferrucci, A. Hill, J. Wagstaff, M.S. Carlino, J.B. Haanen, M. Maio, I. Marquez-Rodas, G.A. McArthur, P.A. Ascierto, G. V Long, M.K. Callahan, M.A. Postow, K. Grossmann, M. Sznol, B. Dreno, L. Bastholt, A. Yang, L.M. Rollin, C. Horak, F.S. Hodi, and J.D. Wolchok. 2015. Combined Nivolumab and Ipilimumab or Monotherapy in Untreated Melanoma. *N Engl J Med*. 373:23–34. doi:10.1056/NEJMoa1504030.

Latchman, Y., C.R. Wood, T. Chernova, D. Chaudhary, M. Borde, I. Chernova, Y. Iwai, A.J. Long, J.A. Brown, R. Nunes, E.A. Greenfield, K. Bourque, V.A. Boussiotis, L.L. Carter, B.M. Carreno, N. Malenkovich, H. Nishimura, T. Okazaki, T. Honjo, A.H. Sharpe, and G.J. Freeman. 2001. PD-L2 is a second ligand for PD-1 and inhibits T cell activation. *Nat Immunol*. 2:261.

Leach, D.R., M.F. Krummel, and J.P. Allison. 1996. Enhancement of Antitumor Immunity by CTLA-4 Blockade. *Science (80-)*. 271:1734 LP-1736.

Levin, S.D., D.W. Taft, C.S. Brandt, C. Bucher, E.D. Howard, E.M. Chadwick, J. Johnston, A. Hammond, K. Bontadelli, D. Ardourel, L. Hebb, A. Wolf, T.R. Bukowski, M.W. Rixon, J.L. Kuijper, C.D. Ostrander, J.W. West, J. Bilsborough, B. Fox, Z. Gao, W. Xu, F. Ramsdell, B.R. Blazar, and K.E. Lewis. 2011. Vstm3 is a member of the CD28 family and an important modulator of T-cell function. *Eur J Immunol*. 41:902–915. doi:10.1002/eji.201041136.

Li, C.-H., W.-H. Kuo, W.-C. Chang, S.-C. Huang, K.-J. Chang, and B.-C. Sheu. 2011. Activation of regulatory T cells instigates functional down-regulation of cytotoxic T lymphocytes in human breast cancer. *Immunol Res*. 51:71. doi:10.1007/s12026-011-8242-x.

Li, F., and J. V Ravetch. 2011. Inhibitory Fcγ Receptor Engagement Drives Adjuvant and Anti-Tumor Activities of Agonistic CD40 Antibodies. *Science (80-)*. 333:1030 LP-1034.

Li, H.Y., M. V McSharry, B. Bullock, T.T. Nguyen, J. Kwak, J.M. Poczobutt, T.R. Sippel, L.E. Heasley, M.C. Weiser-Evans, E.T. Clambey, and R.A. Nemenoff. 2017a. The Tumor Microenvironment Regulates Sensitivity of Murine Lung Tumors to PD-1/PDL1 Antibody Blockade. *Cancer Immunol Res*. canimm.0365.2016. doi:10.1158/2326-6066.CIR-16-0365.

Li, S., K.R. Schmitz, P.D. Jeffrey, J.J.W. Wiltzius, P. Kussie, and K.M. Ferguson. 2005. Structural basis for inhibition of the epidermal growth factor receptor by cetuximab. *Cancer Cell*. 7:301–311. doi:10.1016/j.ccr.2005.03.003.

Li, Z., X. Liu, R. Guo, and P. Wang. 2017b. TIM-3 plays a more important role than PD-1 in the functional impairments of cytotoxic T cells of malignant Schwannomas. *Tumor Biol*. 39:1010428317698352. doi:10.1177/1010428317698352.

Liakou, C.I., A. Kamat, D.N. Tang, H. Chen, J. Sun, P. Troncoso, C. Logothetis, and P. Sharma.

2008. CTLA-4 blockade increases IFN -producing CD4+ICOShi cells to shift the ratio of effector to regulatory T cells in cancer patients. *Proc Natl Acad Sci*. 105:14987–14992. doi:10.1073/pnas.0806075105.

Linedale, R., C. Schmidt, B.T. King, A.G. Ganko, F. Simpson, B.J. Panizza, and G.R. Leggatt. 2017. Elevated frequencies of CD8 T cells expressing PD-1, CTLA-4 and Tim-3 within tumour from perineural squamous cell carcinoma patients. *PLoS One*. 12:e0175755.

Long, G. V, R. Dummer, O. Hamid, T. Gajewski, C. Caglevic, S. Dalle, A. Arance, M.S. Carlino, J.-J. Grob, T.M. Kim, L. V Demidov, C. Robert, J.M.G. Larkin, J. Anderson, J.E. Maleski, M.M. Jones, S.J. Diede, and T.C. Mitchell. 2018. Epacadostat (E) plus pembrolizumab (P) versus pembrolizumab alone in patients (pts) with unresectable or metastatic melanoma: Results of the phase 3 ECHO-301/KEYNOTE-252 study. *J Clin Oncol*. 36:108. doi:10.1200/JCO.2018.36.15_suppl.108.

Lu, L., X. Xu, B. Zhang, R. Zhang, H. Ji, and X. Wang. 2014. Combined PD-1 blockade and GITR triggering induce a potent antitumor immunity in murine cancer models and synergizes with chemotherapeutic drugs. *J Transl Med*. 12:36. doi:10.1186/1479-5876-12-36.

Lu, X., L. Yang, D. Yao, X. Wu, J. Li, X. Liu, L. Deng, C. Huang, Y. Wang, D. Li, and J. Liu. 2017. Tumor antigen-specific CD8+ T cells are negatively regulated by PD-1 and Tim-3 in human gastric cancer. *Cell Immunol*. 313:43–51. doi:10.1016/J.CELLIMM.2017.01.001.

Lynch, T.J., I. Bondarenko, A. Luft, P. Serwatowski, F. Barlesi, R. Chacko, M. Sebastian, J. Neal, H. Lu, J.-M. Cuillerot, and M. Reck. 2012. Ipilimumab in Combination With Paclitaxel and Carboplatin As First-Line Treatment in Stage IIIB/IV Non–Small-Cell Lung Cancer: Results From a Randomized, Double-Blind, Multicenter Phase II Study. *J Clin Oncol*. 30:2046–2054. doi:10.1200/JCO.2011.38.4032.

Van Der Maaten, L.J.P., and G.E. Hinton. 2008. Visualizing high-dimensional data using t-sne. *J Mach Learn Res*. 9:2579–2605. doi:10.1007/s10479-011-0841-3.

Malvezzi, M., P. Bertuccio, T. Rosso, M. Rota, F. Levi, C. La Vecchia, and E. Negri. 2015. European cancer mortality predictions for the year 2015: Does lung cancer have the highest death rate in EU women? *Ann Oncol*. 26:779–786. doi:10.1093/annonc/mdv001.

Marabelle, A., H. Kohrt, I. Sagiv-Barfi, B. Ajami, R.C. Axtell, G. Zhou, R. Rajapaksa, M.R. Green,

J. Torchia, J. Brody, R. Luong, M.D. Rosenblum, L. Steinman, H.I. Levitsky, V. Tse, and R. Levy. 2013. Depleting tumor-specific Tregs at a single site eradicates disseminated tumors. *J Clin Invest*. 123:2447–2463. doi:10.1172/JCI64859.

Margolin, K., M.S. Ernstoff, O. Hamid, D. Lawrence, D. McDermott, I. Puzanov, J.D. Wolchok, J.I. Clark, M. Sznol, T.F. Logan, J. Richards, T. Michener, A. Balogh, K.N. Heller, and F.S. Hodi. 2012. Ipilimumab in patients with melanoma and brain metastases: an open-label, phase 2 trial. *Lancet Oncol*. 13:459–465. doi:10.1016/S1470-2045(12)70090-6.

Martin-Orozco, N., Y. Li, Y. Wang, S. Liu, P. Hwu, Y.J. Liu, C. Dong, and L. Radvanyi. 2010. Melanoma cells express ICOS ligand to promote the activation and expansion of T-regulatory cells. *Cancer Res*. 70:9581–9590. doi:10.1158/0008-5472.CAN-10-1379.

McAdam, A.J., R.J. Greenwald, M.A. Levin, T. Chernova, N. Malenkovich, V. Ling, G.J. Freeman, and A.H. Sharpe. 2001. Icos is critical for CD40-mediated antibody class switching. *Nature*. 409:102–105. doi:10.1038/35051107.

McDermott, D., J. Haanen, T.-T. Chen, P. Lorigan, S. O'Day, and for the M.-20 investigators. 2013. Efficacy and safety of ipilimumab in metastatic melanoma patients surviving more than 2 years following treatment in a phase III trial (MDX010-20). *Ann Oncol*. 24:2694–2698.

Melero, I., W.W. Shuford, S.A. Newby, A. Aruffo, J.A. Ledbetter, K.E. Hellström, R.S. Mittler, and L. Chen. 1997. Monoclonal antibodies against the 4-1BB T-cell activation molecule eradicate established tumors. *Nat Med*. 3:682–685. doi:10.1038/nm0697-682.

Messal, N., N.-E. Serriari, S. Pastor, J.A. Nunès, and D. Olive. 2011. PD-L2 is expressed on activated human T cells and regulates their function. *Mol Immunol*. 48:2214–2219. doi:10.1016/J.MOLIMM.2011.06.436.

Mihm, M.C., C.G. Clemente, and N. Cascinelli. 1996. Tumor infiltrating lymphocytes in lymph node melanoma metastases: a histopathologic prognostic indicator and an expression of local immune response. *Lab Invest*. 74:43—47.

Miyazaki, T., A. Dierich, C. Benoist, and D. Mathis. 1996. LAG-3 is not responsible for selecting T helper cells in CD4-deficient mice. *Int Immunol*. 8:725–729.

Molina, J.R., P. Yang, S.D. Cassivi, S.E. Schild, and A.A. Adjei. 2008. Non–Small Cell Lung Cancer: Epidemiology, Risk Factors, Treatment, and Survivorship. *Mayo Clin Proc*. 83:584–594.

Monteiro, I.D.P., R. Califano, G. Mountzios, and R.A. De Mello. 2016. Immunotherapy with checkpoint inhibitors for lung cancer: Novel agents, biomarkers and paradigms. *Futur Oncol*. 12:551–564. doi:10.2217/fon.15.309.

Moran, A.E., M. Kovacsovics-Bankowski, and A.D. Weinberg. 2013. The TNFRs OX40, 4-1BB, and CD40 as targets for cancer immunotherapy. *Curr Opin Immunol*. 25:230–237. doi:10.1016/j.coi.2013.01.004.

Morvan, M.G., and L.L. Lanier. 2016. NK cells and cancer: You can teach innate cells new tricks. *Nat Rev Cancer*. 16:7–19. doi:10.1038/nrc.2015.5.

Mountain, C.F. 1997. Revisions in the International System for Staging Lung Cancer. *Chest*. 111:1710–1717. doi:10.1378/chest.111.6.1710.

Mozayen, M., M. Alsharedi, I. Mehmi, T.W. Gress, M. Tria, T. Md, J.C. Edwards, T. Gress, M.T. Tirona, and M. Triatirona. 2016. Delaying Chemotherapy in the Treatment of Stage IV Non-Small Cell Lung Cancer Does Not Adversely Affect Survival Outcome. *Virginia Med J*. 112:34–37.

Murphy, K., and C. Weaver. 2017. Janeway's Immunobiology.

Nagase, H., T. Takeoka, S. Urakawa, A. Morimoto-Okazawa, A. Kawashima, K. Iwahori, S. Takiguchi, H. Nishikawa, E. Sato, S. Sakaguchi, M. Mori, Y. Doki, and H. Wada. 2016. ICOS+ Foxp3+ TILs in gastric cancer are prognostic markers and effector regulatory T cells associated with Helicobacter pylori. *Int J Cancer*. 140:686–695. doi:10.1002/ijc.30475.

Naito, Y., K. Saito, K. Shiiba, A. Ohuchi, K. Saigenji, H. Nagura, and H. Ohtani. 1998. CD8+ T Cells Infiltrated within Cancer Cell Nests as a Prognostic Factor in Human Colorectal Cancer. *Cancer Res*. 58:3491 LP-3494.

Ng Tang, D., Y. Shen, J. Sun, S. Wen, J.D. Wolchok, J. Yuan, J.P. Allison, and P. Sharma. 2013. Increased Frequency of ICOS+ CD4 T Cells as a Pharmacodynamic Biomarker for Anti-CTLA-4 Therapy. *Cancer Immunol Res*. 1:229–234. doi:10.1158/2326-6066.CIR-13-0020.

NICE. 2017. Pembrolizumab for treating PD-L1-positive non-small-cell lung cancer after

chemotherapy.

Nicholson, S.M., G. Carlesso, L.I. Cheng, H. Cook, K. DaCosta, J. Leininger, K. McKeever, S. (Weasel) Scott, D. Taylor, K. Streicher, S. Eck, M. Reed, R. Faggioni, R. Herbst, R. Dixit, and P.C. Ryan. 2017. Effects of ICOS+ T cell depletion via afucosylated monoclonal antibody MEDI-570 on pregnant cynomolgus monkeys and the developing offspring. *Reprod Toxicol*. 74:116–133. doi:10.1016/j.reprotox.2017.08.018.

NIH - clinicaltrials.gov. 2018. Home - ClinicalTrials.gov. Accesed 22-08-2018. *https://www.clinicaltrials.gov/*.

NIH - clinicaltrials.gov. 2019. Home - ClinicalTrials.gov. *https://www.clinicaltrials.gov/*.

Nimmerjahn, F., P. Bruhns, K. Horiuchi, and J. V. Ravetch. 2005. FcγRIV: A Novel FcR with Distinct IgG Subclass Specificity. *Immunity*. 23:41–51. doi:10.1016/J.IMMUNI.2005.05.010.

Nimmerjahn, F., and J. V. Ravetch. 2006. Fcγ Receptors: Old Friends and New Family Members. *Immunity*. 24:19–28. doi:10.1016/J.IMMUNI.2005.11.010.

Nishimura H, Nose M, Hiai H, Minato N, H.T. 1999. Development of lupus-like autoimmune diseases by dis- ruption of the PD-1 gene encoding an ITIM motif-car- rying immunoreceptor. *Immunity*. 11:141–151.

Nishimura, H., T. Okazaki, Y. Tanaka, K. Nakatani, M. Hara, A. Matsumori, S. Sasayama, A. Mizoguchi, H. Hiai, N. Minato, and T. Honjo. 2001. Autoimmune Dilated Cardiomyopathy in PD-1 Receptor-Deficient Mice. *Science (80-)*. 291:319 LP-322.

Noman, M.Z., M. Hasmim, Y. Messai, S. Terry, C. Kieda, B. Janji, and S. Chouaib. 2015. Hypoxia: a key player in antitumor immune response. A Review in the Theme: Cellular Responses to Hypoxia. *Am J Physiol Physiol*. 309:C569–C579. doi:10.1152/ajpcell.00207.2015.

Overman, M.J., S. Lonardi, K.Y.M. Wong, H.-J. Lenz, F. Gelsomino, M. Aglietta, M.A. Morse, E. Van Cutsem, R. McDermott, A. Hill, M.B. Sawyer, A. Hendlisz, B. Neyns, M. Svrcek, R.A. Moss, J.-M. Ledeine, Z.A. Cao, S. Kamble, S. Kopetz, and T. André. 2018. Durable Clinical Benefit With Nivolumab Plus Ipilimumab in DNA Mismatch Repair–Deficient/Microsatellite Instability–High Metastatic Colorectal Cancer. *J Clin Oncol*.

36:773–779. doi:10.1200/JCO.2017.76.9901.

Palazón, A., A. Teijeira, I. Martínez-Forero, S. Hervás-Stubbs, C. Roncal, I. Peñuelas, J. Dubrot, A. Morales-Kastresana, J.L. Pérez-Gracia, M.C. Ochoa, L. Ochoa-Callejero, A. Martínez, A. Luque, J. Dinchuk, A. Rouzaut, M. Jure-Kunkel, and I. Melero. 2011. Agonist Anti-CD137 mAb Act on Tumor Endothelial Cells to Enhance Recruitment of Activated T Lymphocytes. *Cancer Res*.

Pallasch, C.P., I. Leskov, C.J. Braun, D. Vorholt, A. Drake, Y.M. Soto-Feliciano, E.H. Bent, J. Schwamb, B. Iliopoulou, N. Kutsch, N. van Rooijen, L.P. Frenzel, C.M. Wendtner, L. Heukamp, K.A. Kreuzer, M. Hallek, J. Chen, and M.T. Hemann. 2014. Sensitizing Protective Tumor Microenvironments to Antibody-Mediated Therapy. *Cell*. 156:590–602. doi:10.1016/J.CELL.2013.12.041.

Paris, F., Z. Fuks, A. Kang, P. Capodieci, G. Juan, D. Ehleiter, A. Haimovitz-Friedman, C. Cordon-Cardo, and R. Kolesnick. 2001. Endothelial Apoptosis as the Primary Lesion Initiating Intestinal Radiation Damage in Mice. *Science (80-)*. 293:293 LP-297.

Pedroza-Gonzalez, A., G. Zhou, S.P. Singh, P.P.C. Boor, Q. Pan, D. Grunhagen, J. de Jonge, T.C.K. Tran, C. Verhoef, J.N.M. IJzermans, H.L.A. Janssen, K. Biermann, J. Kwekkeboom, and D. Sprengers. 2015. GITR engagement in combination with CTLA-4 blockade completely abrogates immunosuppression mediated by human liver tumor-derived regulatory T cells ex vivo. *Oncoimmunology*. 4:e1051297. doi:10.1080/2162402X.2015.1051297.

Penn, I. 1996. MALIGNANT MELANOMA IN ORGAN ALLOGRAFT RECIPIENTS1,2. *Transplantation*. 61.

Penn, I., and T.E. Starzl. 1972. Malignant Tumors Arising De Novo in Immunosuppressed Organ Transplant Recipients. *Transplantation*. 14:407–417.

Pfirschke, C., C. Engblom, S. Rickelt, V. Cortez-Retamozo, C. Garris, F. Pucci, T. Yamazaki, V. Poirier-Colame, A. Newton, Y. Redouane, Y.J. Lin, G. Wojtkiewicz, Y. Iwamoto, M. Mino-Kenudson, T.G. Huynh, R.O. Hynes, G.J. Freeman, G. Kroemer, L. Zitvogel, R. Weissleder, and M.J. Pittet. 2016. Immunogenic Chemotherapy Sensitizes Tumors to Checkpoint Blockade Therapy. *Immunity*. 44:343–354. doi:10.1016/j.immuni.2015.11.024.

Pham, S.M., R.L. Kormos, R.J. Landreneau, A. Kawai, I. Gonzalez-Cancel, R.L. Hardesty, B.G. Hattler, and B.P. Griffith. 1995. Solid tumors after heart transplantation: Lethality of lung cancer. *Ann Thorac Surg*. 60:1623–1626. doi:10.1016/0003-4975(95)00120-4.

Piconese, S., E. Timperi, I. Pacella, V. Schinzari, C. Tripodo, M. Rossi, N. Guglielmo, G. Mennini, G.L. Grazi, S. Di Filippo, S. Brozzetti, K. Fazzi, G. Antonelli, M.A. Lozzi, M. Sanchez, and V. Barnaba. 2014. Human OX40 tunes the function of regulatory T cells in tumor and nontumor areas of hepatitis C virus–infected liver tissue. *Hepatology*. 60:1494–1507. doi:10.1002/hep.27188.

Piconese, S., B. Valzasina, and M.P. Colombo. 2008. OX40 triggering blocks suppression by regulatory T cells and facilitates tumor rejection. *J Exp Med*. 205:825 LP-839.

Postow, M.A., J. Chesney, A.C. Pavlick, C. Robert, K. Grossmann, D. McDermott, G.P. Linette, N. Meyer, J.K. Giguere, S.S. Agarwala, M. Shaheen, M.S. Ernstoff, D. Minor, A.K. Salama, M. Taylor, P.A. Ott, L.M. Rollin, C. Horak, P. Gagnier, J.D. Wolchok, and F.S. Hodi. 2015. Nivolumab and Ipilimumab versus Ipilimumab in Untreated Melanoma. *N Engl J Med*. 372:2006–2017. doi:10.1056/NEJMoa1414428.

Qian, B., Y. Deng, J.H. Im, R.J. Muschel, Y. Zou, J. Li, R.A. Lang, and J.W. Pollard. 2009. A distinct macrophage population mediates metastatic breast cancer cell extravasation, establishment and growth. *PLoS One*. 4. doi:10.1371/journal.pone.0006562.

Qing, J., X. Du, Y. Chen, P. Chan, H. Li, P. Wu, S. Marsters, S. Stawicki, J. Tien, K. Totpal, S. Ross, S. Stinson, D. Dornan, D. French, Q.-R. Wang, J.-P. Stephan, Y. Wu, C. Wiesmann, and A. Ashkenazi. 2009. Antibody-based targeting of FGFR3 in bladder carcinoma and t(4;14)-positive multiple myeloma in mice. *J Clin Invest*. 119:1216–1229. doi:10.1172/JCI38017.

Quezada, S.A., K.S. Peggs, M.A. Curran, and J.P. Allison. 2006. CTLA4 blockade and GM-CSF combination immunotherapy alters the intratumor balance of effector and regulatory T cells. *J Clin Invest*. 116:1935–1945. doi:10.1172/JCI27745.

Ramstad, T., L. Lawnicki, J. Vetto, and A. Weinberg. 2000. Immunohistochemical analysis of primary breast tumors and tumor-draining lymph nodes by means of the T-cell costimulatory molecule OX-40. *Am J Surg*. 179:400–406. doi:10.1016/S0002-9610(00)00361-5.

Redmond, W.L., S.N. Linch, and M.J. Kasiewicz. 2014. Combined Targeting of Costimulatory (OX40) and Coinhibitory (CTLA-4) Pathways Elicits Potent Effector T Cells Capable of Driving Robust Antitumor Immunity. *Cancer Immunol Res*. 2:142–153. doi:10.1158/2326-6066.CIR-13-0031-T.

Redoglia, V., U. Dianzani, J.M. Rojo, P. Portolés, M. Bragardo, H. Wolff, D. Buonfiglio, S. Bonissoni, and C.A. Janeway. 2018. Characterization of H4: a mouse T lymphocyte activation molecule functionally associated with the CD3/T cell receptor. *Eur J Immunol*. 26:2781–2789. doi:10.1002/eji.1830261134.

Ribas, A., R. Kefford, M.A. Marshall, C.J.A. Punt, J.B. Haanen, M. Marmol, C. Garbe, H. Gogas, J. Schachter, G. Linette, P. Lorigan, K.L. Kendra, M. Maio, U. Trefzer, M. Smylie, G.A. McArthur, B. Dreno, P.D. Nathan, J. Mackiewicz, J.M. Kirkwood, J. Gomez-Navarro, B. Huang, D. Pavlov, and A. Hauschild. 2013. Phase III randomized clinical trial comparing tremelimumab with standard-of-care chemotherapy in patients with advanced melanoma. *J Clin Oncol*. 31:616—622. doi:10.1200/JCO.2012.44.6112.

Ritchie, H. 2018. How many people in the world die from cancer?. Accesed 24-07-2018. doi:https://ourworldindata.org/how-many-people-in-the-world-die-from-cancer.

Rittmeyer, A., F. Barlesi, D. Waterkamp, K. Park, F. Ciardiello, J. von Pawel, S.M. Gadgeel, T. Hida, D.M. Kowalski, M.C. Dols, D.L. Cortinovis, J. Leach, J. Polikoff, C. Barrios, F. Kabbinavar, O.A. Frontera, F. De Marinis, H. Turna, J.-S. Lee, M. Ballinger, M. Kowanetz, P. He, D.S. Chen, A. Sandler, and D.R. Gandara. 2017. Atezolizumab versus docetaxel in patients with previously treated non-small-cell lung cancer (OAK): a phase 3, open-label, multicentre randomised controlled trial. *Lancet*. 389:255–265. doi:10.1016/S0140-6736(16)32517-X.

Robert, C., G. V Long, B. Brady, C. Dutriaux, M. Maio, L. Mortier, J.C. Hassel, P. Rutkowski, C. McNeil, E. Kalinka-Warzocha, K.J. Savage, M.M. Hernberg, C. Lebbé, J. Charles, C. Mihalcioiu, V. Chiarion-Sileni, C. Mauch, F. Cognetti, A. Arance, H. Schmidt, D. Schadendorf, H. Gogas, L. Lundgren-Eriksson, C. Horak, B. Sharkey, I.M. Waxman, V. Atkinson, and P.A. Ascierto. 2014. Nivolumab in Previously Untreated Melanoma without BRAF Mutation. *N Engl J Med*. 372:320–330. doi:10.1056/NEJMoa1412082.

Romano, E., M. Kusio-Kobialka, P.G. Foukas, P. Baumgaertner, C. Meyer, P. Ballabeni, O. Michielin, B. Weide, P. Romero, and D.E. Speiser. 2015. Ipilimumab-dependent cell-mediated cytotoxicity of regulatory T cells ex vivo by nonclassical monocytes in melanoma patients. *Proc Natl Acad Sci*. 112:6140 LP-6145.

Ross Sheil, A.G. 1986. Cancer after transplantation. *World J Surg*. 10:389–396. doi:10.1007/BF01655298.

Rudd, C.E., and H. Schneider. 2003. Unifying concepts in CD28, ICOS and CTLA4 co-receptor signalling. *Nat Rev Immunol*. 3:544–556. doi:10.1038/nri1131.

Sainson, R.C., M. McCourt, A. Thotakura, N. Parveen, M. Kismac, G. Borhis, J. Carvalho, T. Myers, R. Rowlands, H. Ali, H. Craig, V. Wong, Q. Liang, and V. Germaschewski. 2018a. Abstract 2792: The combination of immune checkpoint blockers with the anti-ICOS KY1044 antibody results in a strong tumor response. *Cancer Res*. 78:2792 LP-2792.

Sainson, R.C., N. Parveen, G. Borhis, M. Kosmac, T. OKell, E. Taggart, J. Carvalho, M. McCourt, H. Ali, H. Craig, and A. Labokha. 2018b. Abstract LB-153: KY1055, a novel ICOS-PD-L1 bispecific antibody, efficiently enhances T cell activation and delivers a potent anti-tumour response in vivo. *Cancer Res*. 78:LB-153 LP-LB-153.

Sakuishi, K., L. Apetoh, J.M. Sullivan, B.R. Blazar, V.K. Kuchroo, and A.C. Anderson. 2010. Targeting Tim-3 and PD-1 pathways to reverse T cell exhaustion and restore anti-tumor immunity. *J Exp Med*. 207:2187 LP-2194.

Sánchez-Fueyo, A., J. Tian, D. Picarella, C. Domenig, X.X. Zheng, C.A. Sabatos, N. Manlongat, O. Bender, T. Kamradt, V.K. Kuchroo, J.-C. Gutiérrez-Ramos, A.J. Coyle, and T.B. Strom. 2003. Tim-3 inhibits T helper type 1–mediated auto- and alloimmune responses and promotes immunological tolerance. *Nat Immunol*. 4:1093.

Sazinsky, S., J.S. Michaelson, S. Sathyanarayanan, and K.G. Elpek. 2016. US20160304610A1. Antibodies to ICOS. https://patents.google.com/patent/US20160304610A1/.

Scagliotti, G.V., P. Parikh, J. Von Pawel, B. Biesma, J. Vansteenkiste, C. Manegold, P. Serwatowski, U. Gatzemeier, R. Digumarti, M. Zukin, J.S. Lee, A. Mellemgaard, K. Park, S. Patil, J. Rolski, T. Goksel, F. De Marinis, L. Simms, K.P. Sugarman, and D. Gandara. 2008. Phase III study comparing cisplatin plus gemcitabine with cisplatin plus pemetrexed in

chemotherapy-naive patients with advanced-stage non-small-cell lung cancer. *J Clin Oncol*. 26:3543–3551. doi:10.1200/JCO.2007.15.0375.

Schadendorf, D., F.S. Hodi, C. Robert, J.S. Weber, K. Margolin, O. Hamid, D. Patt, T.-T. Chen, D.M. Berman, and J.D. Wolchok. 2015. Pooled Analysis of Long-Term Survival Data From Phase II and Phase III Trials of Ipilimumab in Unresectable or Metastatic Melanoma. *J Clin Oncol*. 33:1889–1894. doi:10.1200/JCO.2014.56.2736.

Schreiber, R.D., L.J. Old, and M.J. Smyth. 2011. Cancer immunoediting: Integrating immunity's roles in cancer suppression and promotion. *Science (80-)*. 331:1565–1570. doi:10.1126/science.1203486.

Schumacher, K., W. Haensch, C. Röefzaad, and P.M. Schlag. 2001. Prognostic Significance of Activated CD8+ T Cell Infiltrations within Esophageal Carcinomas. *Cancer Res*. 61:3932 LP-3936.

Segal, N.H., A.K. Gopal, S. Bhatia, H.E. Kohrt, R. Levy, M.J. Pishvaian, R. Houot, N. Bartlett, P. Nghiem, S.A. Kronenberg, A.D. Thall, G. Mugundu, B. Huang, and C. Davis. 2014. A phase 1 study of PF-05082566 (anti-4-1BB) in patients with advanced cancer. *J Clin Oncol*. 32:3007. doi:10.1200/jco.2014.32.15_suppl.3007.

Segal, N.H., T.F. Logan, F.S. Hodi, D. McDermott, I. Melero, O. Hamid, H. Schmidt, C. Robert, V. Chiarion-Sileni, P.A. Ascierto, M. Maio, W.J. Urba, T.C. Gangadhar, S. Suryawanshi, J. Neely, M. Jure-Kunkel, S. Krishnan, H. Kohrt, M. Sznol, and R. Levy. 2017. Results from an Integrated Safety Analysis of Urelumab, an Agonist Anti-CD137 Monoclonal Antibody. *Clin Cancer Res*. 23:1929 LP-1936.

Selby, M.J., J.J. Engelhardt, M. Quigley, K.A. Henning, T. Chen, M. Srinivasan, and A.J. Korman. 2013. Anti-CTLA-4 Antibodies of IgG2a Isotype Enhance Antitumor Activity through Reduction of Intratumoral Regulatory T Cells. *Cancer Immunol Res*.

Shang, B., Y. Liu, S. Jiang, and Y. Liu. 2015. Prognostic value of tumor-infiltrating FoxP3+ regulatory T cells in cancers: a systematic review and meta-analysis. *Sci Rep*. 5:15179.

Sharma, P., S. Hu-Lieskovan, J.A. Wargo, and A. Ribas. 2017. Primary, Adaptive, and Acquired Resistance to Cancer Immunotherapy. *Cell*. 168:707–723. doi:10.1016/j.cell.2017.01.017.

Shaverdian, N., A.E. Lisberg, K. Bornazyan, D. Veruttipong, J.W. Goldman, S.C. Formenti, E.B. Garon, and P. Lee. 2017. Previous radiotherapy and the clinical activity and toxicity of pembrolizumab in the treatment of non-small-cell lung cancer: a secondary analysis of the KEYNOTE-001 phase 1 trial. *Lancet Oncol*. 18:895–903. doi:10.1016/S1470-2045(17)30380-7.

Shayan, G., R. Srivastava, J. Li, N. Schmitt, L.P. Kane, and R.L. Ferris. 2017. Adaptive resistance to anti-PD1 therapy by Tim-3 upregulation is mediated by the PI3K-Akt pathway in head and neck cancer. *Oncoimmunology*. 6:e1261779. doi:10.1080/2162402X.2016.1261779.

Shimizu, J., S. Yamazaki, T. Takahashi, Y. Ishida, and S. Sakaguchi. 2002. Stimulation of CD25+CD4+regulatory T cells through GITR breaks immunological self-tolerance. *Nat Immunol*. 3:135–142. doi:10.1038/ni759.

Shuford, W.W., K. Klussman, D.D. Tritchler, D.T. Loo, J. Chalupny, A.W. Siadak, T.J. Brown, J. Emswiler, H. Raecho, C.P. Larsen, T.C. Pearson, J.A. Ledbetter, A. Aruffo, and R.S. Mittler. 1997. 4-1BB Costimulatory Signals Preferentially Induce CD8⁺ T Cell Proliferation and Lead to the Amplification In Vivo of Cytotoxic T Cell Responses. *J Exp Med*. 186:47 LP-55.

Siegel, R., K.D. Miller, and J. Ahmedin. 2017. Cancer Statistics. *Ca Cancer J*. 67:7–30. doi:10.3322/caac.21387.

Sim, G.C., N. Martin-Orozco, L. Jin, Y. Yang, S. Wu, E. Washington, D. Sanders, C. Lacey, Y. Wang, L. Vence, P. Hwu, and L. Radvanyi. 2014. IL-2 therapy promotes suppressive ICOS+ Treg expansion in melanoma patients. *J Clin Invest*. 124:99–110. doi:10.1172/JCI46266.

Simpson, T.R., F. Li, W. Montalvo-Ortiz, M.A. Sepulveda, K. Bergerhoff, F. Arce, C. Roddie, J.Y. Henry, H. Yagita, J.D. Wolchok, K.S. Peggs, J. V. Ravetch, J.P. Allison, and S.A. Quezada. 2013. Fc-dependent depletion of tumor-infiltrating regulatory T cells co-defines the efficacy of anti–CTLA-4 therapy against melanoma. *J Exp Med*. 210:1695–1710. doi:10.1084/jem.20130579.

Śledzińska, A., L. Menger, K. Bergerhoff, K.S. Peggs, and S.A. Quezada. 2015. Negative immune checkpoints on T lymphocytes and their relevance to cancer immunotherapy. *Mol Oncol*. 9:1936–1965. doi:10.1016/j.molonc.2015.10.008.

Smith, P., D.J. DiLillo, S. Bournazos, F. Li, and J. V. Ravetch. 2012. Mouse model recapitulating human Fc receptor structural and functional diversity. *Proc Natl Acad Sci*. 109:6181–6186. doi:10.1073/pnas.1203954109.

Spiro, S.G., R.M. Rudd, R.L. Souhami, J. Brown, D.J. Fairlamb, N.H. Gower, L. Maslove, R. Milroy, V. Napp, M.K.B. Parmar, M.D. Peake, R.J. Stephens, H. Thorpe, D.A. Waller, and P. West. 2004. Chemotherapy versus supportive care in advanced non-small cell lung cancer: Improved survival without detriment to quality of life. *Thorax*. 59:828–836. doi:10.1136/thx.2003.020164.

Strauss, L., C. Bergmann, M.J. Szczepanski, S. Lang, J.M. Kirkwood, and T.L. Whiteside. 2008. Expression of ICOS on Human Melanoma-Infiltrating CD4+CD25highFoxp3+ T Regulatory Cells: Implications and Impact on Tumor-Mediated Immune Suppression. *J Immunol*. 180:2967–2980. doi:10.4049/jimmunol.180.5.2967.

Strome, S.E., H. Dong, H. Tamura, S.G. Voss, D.B. Flies, K. Tamada, D. Salomao, J. Cheville, F. Hirano, W. Lin, J.L. Kasperbauer, K. V Ballman, and L. Chen. 2003. B7-H1 Blockade Augments Adoptive T-Cell Immunotherapy for Squamous Cell Carcinoma. *Cancer Res*. 63:6501 LP-6505.

Sundar, R., R. Soong, B.C. Cho, J.R. Brahmer, and R.A. Soo. 2014. Immunotherapy in the treatment of non-small cell lung cancer. *Lung Cancer*. 85:101–109. doi:10.1016/j.lungcan.2014.05.005.

Takahashi, T., T. Tagami, S. Yamazaki, T. Uede, J. Shimizu, N. Sakaguchi, T.W. Mak, and S. Sakaguchi. 2000. Regulatory T Cells Constitutively Expressing Cytotoxic T Lymphocyte – associated Antigen 4. *J Exp Med*. 192:303–309. doi:10.1084/jem.192.2.303.

Takai, T., M. Li, D. Sylvestre, R. Clynes, and J. V. Ravetch. 1994. FcR γ chain deletion results in pleiotrophic effector cell defects. *Cell*. 76:519–529. doi:10.1016/0092-8674(94)90115-5.

Takai, T., M. Ono, M. Hikida, H. Ohmori, and J. V Ravetch. 1996. Augmented humoral and anaphylactic responses in FcγRII-deficient mice. *Nature*. 379:346.

Tang, C., J.W. Welsh, P. de Groot, E. Massarelli, J.Y. Chang, K.R. Hess, S. Basu, M.A. Curran, M.E. Cabanillas, V. Subbiah, S. Fu, A.M. Tsimberidou, D. Karp, D.R. Gomez, A. Diab, R. Komaki, J. V Heymach, P. Sharma, A. Naing, and D.S. Hong. 2017. Ipilimumab with

Stereotactic Ablative Radiation Therapy: Phase I Results and Immunologic Correlates from Peripheral T Cells. *Clin Cancer Res*. 23:1388 LP-1396.

Tang, F., X. Du, M. Liu, P. Zheng, and Y. Liu. 2018. Anti-CTLA-4 antibodies in cancer immunotherapy: selective depletion of intratumoral regulatory T cells or checkpoint blockade? *Cell Biosci*. 8:30. doi:10.1186/s13578-018-0229-z.

Tannir, N.M., H.J. Hammers, A. Amin, M.-O. Grimm, B.I. Rini, S. Mekan, M.B. McHenry, and C.K. Kollmannsberger. 2018. Characterization of the benefit-risk profile of nivolumab + ipilimumab (N+I) v sunitinib (S) for treatment-naïve advanced renal cell carcinoma (aRCC; CheckMate 214). *J Clin Oncol*. 36:686. doi:10.1200/JCO.2018.36.6_suppl.686.

Tassi, E., G. Grazia, C. Vegetti, I. Bersani, G. Bertolini, A. Molla, P. Baldassari, F. Andriani, L. Roz, G. Sozzi, U. Pastorino, R. Mortarini, and A. Anichini. 2016. Early effector T lymphocytes coexpress multiple inhibitory receptors in primary non-small cell lung cancer. *Cancer Res*.

Tivol, E.A., F. Borriello, A.N. Schweitzer, W.P. Lynch, J.A. Bluestone, and A.H. Sharpe. 1995. Loss of CTLA-4 leads to massive lymphoproliferation and fatal multiorgan tissue destruction, revealing a critical negative regulatory role of CTLA-4. *Immunity*. 3:541–547. doi:10.1016/1074-7613(95)90125-6.

Torre, L.A., F. Bray, R.L. Siegel, J. Ferlay, J. Lortet-tieulent, and A. Jemal. 2015. Global Cancer Statistics, 2012. *CA a cancer J Clin*. 65:87–108. doi:10.3322/caac.21262.

Triebel, F., K. Hacene, and M.-F. Pichon. 2006. A soluble lymphocyte activation gene-3 (sLAG-3) protein as a prognostic factor in human breast cancer expressing estrogen or progesterone receptors. *Cancer Lett*. 235:147–153. doi:10.1016/J.CANLET.2005.04.015.

Triebel, F., S. Jitsukawa, E. Baixeras, S. Roman-Roman, C. Genevee, E. Viegas-Pequignot, and T. Hercend. 1990. LAG-3, a novel lymphocyte activation gene closely related to CD4. *J Exp Med*. 171:1393 LP-1405.

Trofe, J., T.M. Beebe, J.F. Buell, M.J. Hanaway, M.R. First, R.R. Alloway, T.G. Gross, and E.S. Woodle. 2004. Posttransplant Malignancy. *Prog Transplant*. 14:193–200. doi:10.1177/152692480401400304.

Turley, S.J., V. Cremasco, and J.L. Astarita. 2015. Immunological hallmarks of stromal cells in the tumour microenvironment. *Nat Rev Immunol*. 15:669.

Uchida, J., Y. Hamaguchi, J.A. Oliver, J. V Ravetch, J.C. Poe, K.M. Haas, and T.F. Tedder. 2004. The Innate Mononuclear Phagocyte Network Depletes B Lymphocytes through Fc Receptor–dependent Mechanisms during Anti-CD20 Antibody Immunotherapy. *J Exp Med*. 199:1659 LP-1669.

Umansky, V., C. Blattner, C. Gebhardt, and J. Utikal. 2016. The Role of Myeloid-Derived Suppressor Cells (MDSC) in Cancer Progression. *Vaccines* . 4. doi:10.3390/vaccines4040036.

Vetto, J.T., S. Lum, A. Morris, M. Sicotte, J. Davis, M. Lemon, and A. Weinberg. 1997. Presence of the T-cell activation marker OX-40 on tumor infiltrating lymphocytes and draining lymph node cells from patients with melanoma and head and neck cancers. *Am J Surg*. 174:258–265. doi:10.1016/S0002-9610(97)00139-6.

Vinay, D.S., and B.S. Kwon. 2012. Immunotherapy of Cancer with 4-1BB. *Mol Cancer Ther*.

Vinay, D.S., E.P. Ryan, G. Pawelec, W.H. Talib, J. Stagg, E. Elkord, T. Lichtor, W.K. Decker, R.L. Whelan, H.M.C.S. Kumara, E. Signori, K. Honoki, A.G. Georgakilas, A. Amin, W.G. Helferich, C.S. Boosani, G. Guha, M.R. Ciriolo, S. Chen, S.I. Mohammed, A.S. Azmi, W.N. Keith, A. Bilsland, D. Bhakta, D. Halicka, H. Fujii, K. Aquilano, S.S. Ashraf, S. Nowsheen, X. Yang, B.K. Choi, and B.S. Kwon. 2015. Immune evasion in cancer: Mechanistic basis and therapeutic strategies. *Semin Cancer Biol*. 35:S185–S198. doi:10.1016/j.semcancer.2015.03.004.

Visbal, A.L., N.B. Leighl, R. Feld, and F.A. Shepherd. 2005. Adjuvant Chemotherapy for Early-Stage Non-small Cell Lung Cancer. *Chest*. 128:2933–2943. doi:10.1378/chest.128.4.2933.

Vokes, E.E., N. Ready, E. Felip, L. Horn, M.A. Burgio, S.J. Antonia, O.A. Frontera, S. Gettinger, E. Holgado, D. Spigel, D. Waterhouse, M. Domine, M. Garassino, L.Q.M. Chow, G. Blumenschein, F. Barlesi, B. Coudert, J. Gainor, O. Arrieta, J. Brahmer, C. Butts, M. Steins, W.J. Geese, A. Li, D. Healey, and L. Crinò. 2018. Nivolumab versus docetaxel in previously treated advanced non-small-cell lung cancer (CheckMate 017 and CheckMate 057): 3-year update and outcomes in patients with liver metastases. *Ann Oncol*. 29:959–965.

doi:10.1093/annonc/mdy041.

Vonderheide, R.H., P.M. Lorusso, M. Khalil, E.M. Gartner, D. Khaira, D. Soulieres, P. Dorazio, J.A. Trosko, J. Rüter, G.L. Mariani, T. Usari, and S.M. Domchek. 2010. Tremelimumab in combination with exemestane in patients with advanced breast cancer and treatment-associated modulation of inducible costimulator expression on patient T cells. *Clin Cancer Res*. 16:3485–3494. doi:10.1158/1078-0432.CCR-10-0505.

Waight, J., P. Iyer, E. Breous-Nystrom, C. Riordan, M. Findeis, D. Underwood, J. Connolly, M. Sanicola-Nadel, H. Nastri, P. Scherle, G. Hollis, R. Huber, R. Stein, M. van Dijk, and N.S. Wilson. 2018a. Abstract 3825: INCAGN02390, a novel antagonist antibody that targets the co-inhibitory receptor TIM-3. *Cancer Res*. 78:3825 LP-3825.

Waight, J.D., D. Chand, S. Dietrich, R. Gombos, T. Horn, A.M. Gonzalez, M. Manrique, L. Swiech, B. Morin, C. Brittsan, A. Tanne, B. Akpeng, B.A. Croker, J.S. Buell, R. Stein, D.A. Savitsky, and N.S. Wilson. 2018b. Selective FcγR Co-engagement on APCs Modulates the Activity of Therapeutic Antibodies Targeting T Cell Antigens. *Cancer Cell*. 33:1033–1047.e5. doi:10.1016/j.ccell.2018.05.005.

Walunas, T.L., D.J. Lenschow, C.Y. Bakker, P.S. Linsley, G.J. Freeman, J.M. Green, C.B. Thompson, and J.A. Bluestone. 1994. CTLA-4 can function as a negative regulator of T cell activation. *Immunity*. 1:405–413. doi:10.1016/1074-7613(94)90071-X.

Wang, F., H. Hou, S. Wu, Q. Tang, W. Liu, M. Huang, B. Yin, J. Huang, L. Mao, Y. Lu, and Z. Sun. 2015. TIGIT expression levels on human NK cells correlate with functional heterogeneity among healthy individuals. *Eur J Immunol*. 45:2886–2897. doi:doi:10.1002/eji.201545480.

Wang, J., T. Yoshida, F. Nakaki, H. Hiai, T. Okazaki, and T. Honjo. 2005. Establishment of NOD-Pdcd1-/- mice as an efficient animal model of type I diabetes. *Proc Natl Acad Sci U S A*. 102:11823 LP-11828.

Wang, L., K. Pino-Lagos, V.C. de Vries, I. Guleria, M.H. Sayegh, and R.J. Noelle. 2008. Programmed death 1 ligand signaling regulates the generation of adaptive Foxp3+CD4+ regulatory T cells. *Proc Natl Acad Sci*. 105:9331–9336. doi:10.1073/pnas.0710441105.

Ward-Kavanagh, L.K., W.W. Lin, J.R. Šedý, and C.F. Ware. 2016. The TNF Receptor Superfamily

in Co-stimulating and Co-inhibitory Responses. *Immunity*. 44:1005–1019. doi:10.1016/j.immuni.2016.04.019.

Waterhouse, P., J.M. Penninger, E. Timms, A. Wakeham, A. Shahinian, K.P. Lee, C.B. Thompson, H. Griesser, and T.W. Mak. 1995. Lymphoproliferative Disorders with Early Lethality in Mice Deficient in Ctla-4 *Science (80-)*. 270:985 LP-988.

Weigelin, B., E. Bolaños, A. Teijeira, I. Martinez-Forero, S. Labiano, A. Azpilikueta, A. Morales-Kastresana, J.I. Quetglas, E. Wagena, A.R. Sánchez-Paulete, L. Chen, P. Friedl, and I. Melero. 2015. Focusing and sustaining the antitumor CTL effector killer response by agonist anti-CD137 mAb. *Proc Natl Acad Sci*. 112:7551–7556. doi:10.1073/pnas.1506357112.

Weiner, L.M., R. Surana, and S. Wang. 2010. Monoclonal antibodies: Versatile platforms for cancer immunotherapy. *Nat Rev Immunol*. 10:317–327. doi:10.1038/nri2744.

Wherry, E.J., S.-J. Ha, S.M. Kaech, W.N. Haining, S. Sarkar, V. Kalia, S. Subramaniam, J.N. Blattman, D.L. Barber, and R. Ahmed. 2007. Molecular Signature of CD8+ T Cell Exhaustion during Chronic Viral Infection. *Immunity*. 27:670–684. doi:10.1016/J.IMMUNI.2007.09.006.

White, A.L., H.T.C. Chan, A. Roghanian, R.R. French, C.I. Mockridge, A.L. Tutt, S. V Dixon, D. Ajona, J.S. Verbeek, A. Al-Shamkhani, M.S. Cragg, S.A. Beers, and M.J. Glennie. 2011. Interaction with FcγRIIB Is Critical for the Agonistic Activity of Anti-CD40 Monoclonal Antibody. *J Immunol*.

Wikenheiser, D.J., and J.S. Stumhofer. 2016. ICOS co-stimulation: Friend or foe? *Front Immunol*. 7:1–16. doi:10.3389/fimmu.2016.00304.

Wilcox, R.A., D.B. Flies, G. Zhu, A.J. Johnson, K. Tamada, A.I. Chapoval, S.E. Strome, L.R. Pease, and L. Chen. 2002. Provision of antigen and CD137 signaling breaks immunological ignorance, promoting regression of poorly immunogenic tumors. *J Clin Invest*. 109:651–659. doi:10.1172/JCI0214184.

Williams, J.B., B.L. Horton, Y. Zheng, Y. Duan, J.D. Powell, and T.F. Gajewski. 2017. The EGR2 targets LAG-3 and 4-1BB describe and regulate dysfunctional antigen-specific CD8+ T

cells in the tumor microenvironment. *J Exp Med*. 214:381 LP-400.

Willoughby, J., J. Griffiths, I. Tews, and M.S. Cragg. 2017. OX40: Structure and function – What questions remain? *Mol Immunol*. 83:13–22. doi:10.1016/j.molimm.2017.01.006.

Willoughby, J.E., J.P. Kerr, A. Rogel, V.Y. Taraban, S.L. Buchan, P.W.M. Johnson, and A. Al-Shamkhani. 2014. Differential Impact of CD27 and 4-1BB Costimulation on Effector and Memory CD8 T Cell Generation following Peptide Immunization. *J Immunol*. 193:244–251. doi:10.4049/jimmunol.1301217.

Wing, K., Y. Onishi, P. Prieto-Martin, T. Yamaguchi, M. Miyara, Z. Fehervari, T. Nomura, and S. Sakaguchi. 2008. CTLA-4 Control over Foxp3+ Regulatory T Cell Function. *Science (80-)*. 322:271–275. doi:10.1126/science.1160062.

Woo, S.R., M.E. Turnis, M. V. Goldberg, J. Bankoti, M. Selby, C.J. Nirschl, M.L. Bettini, D.M. Gravano, P. Vogel, C.L. Liu, S. Tangsombatvisit, J.F. Grosso, G. Netto, M.P. Smeltzer, A. Chaux, P.J. Utz, C.J. Workman, D.M. Pardoll, A.J. Korman, C.G. Drake, and D.A.A. Vignali. 2012. Immune inhibitory molecules LAG-3 and PD-1 synergistically regulate T-cell function to promote tumoral immune escape. *Cancer Res*. 72:917–927. doi:10.1158/0008-5472.CAN-11-1620.

Workman, C.J., K.J. Dugger, and D.A.A. Vignali. 2002. Cutting Edge: Molecular Analysis of the Negative Regulatory Function of Lymphocyte Activation Gene-3. *J Immunol*. 169:5392 LP-5395.

Workman, C.J., and D.A.A. Vignali. 2005. Negative Regulation of T Cell Homeostasis by Lymphocyte Activation Gene-3 (CD223). *J Immunol*. 174:688 LP-695.

Wu, T., and Y. Dai. 2017. Tumor microenvironment and therapeutic response. *Cancer Lett*. 387:61–68. doi:10.1016/J.CANLET.2016.01.043.

Wu, Y.-L., S. Lu, Y. Cheng, C. Zhou, J. Wang, T. Mok, L. Zhang, H. Tu, L. Wu, J. Feng, Y. Zhang, A.V. Luft, J. Zhou, Z. Ma, Y. Lu, C. Hu, Y. Shi, C. Baudelet, Z. Li, and J. Chang. 2018. Abstract CT114: Nivolumab versus docetaxel in a predominantly Chinese patient population with previously treated advanced non-small cell lung cancer (NSCLC): results of the phase 3 CheckMate 078 study. *Proc Am Assoc Cancer Res Annu Meet 2018*. 78:CT114. doi:10.1158/1538-7445.AM2018-CT114.

Xia, W., X. Yu, Q. Mao, W. Xia, A. Wang, G. Dong, B. Chen, W. Ma, L. Xu, and F. Jiang. 2017. Improvement of survival for non-small cell lung cancer over time. *Onco Targets Ther*. 10:4295–4303. doi:10.2147/OTT.S145036.

Xie, J., J. Wang, S. Cheng, L. Zheng, F. Ji, L. Yang, Y. Zhang, and H. Ji. 2016. Expression of immune checkpoints in T cells of esophageal cancer patients. *Oncotarget*. 7:63669–63678. doi:10.18632/oncotarget.11611.

Xu, D.-P., B. V Sauter, T.-G. Huang, M. Meseck, S.L.C. Woo, and S.-H. Chen. 2005. The systemic administration of Ig-4-1BB ligand in combination with IL-12 gene transfer eradicates hepatic colon carcinoma. *Gene Ther*. 12:1526.

Yang, Z.-Z., D.M. Grote, S.C. Ziesmer, T. Niki, M. Hirashima, A.J. Novak, T.E. Witzig, and S.M. Ansell. 2012. IL-12 upregulates TIM-3 expression and induces T cell exhaustion in patients with follicular B cell non-Hodgkin lymphoma. *J Clin Invest*. 122:1271–1282. doi:10.1172/JCI59806.

Yao, S., Y. Zhu, G. Zhu, M. Augustine, L. Zheng, D.J. Goode, M. Broadwater, W. Ruff, S. Flies, H. Xu, D. Flies, L. Luo, S. Wang, and L. Chen. 2011. B7-H2 Is a Costimulatory Ligand for CD28 in Human. *Immunity*. 34:729–740. doi:10.1016/j.immuni.2011.03.014.

Yap, T.A., H.A. Burris, S. Kummar, G.S. Falchook, R.K. Pachynski, P. LoRusso, S.S. Tykodi, G.T. Gibney, J.F. Gainor, O.E. Rahma, T.Y. Seiwert, F. Meric-Bernstam, M.A.B. Murphy, J.K. Litton, E.M.D. Hooper, H.A. Hirsch, C. Harvey, M. Clancy, T. McClure, and M.K. Callahan. 2018. ICONIC: Biologic and clinical activity of first in class ICOS agonist antibody JTX-2011 +/- nivolumab (nivo) in patients (pts) with advanced cancers. *ASCO Annu Meet*. 3000.

Ye, Q., D.-G. Song, M. Poussin, T. Yamamoto, A. Best, C. Li, G. Coukos, and D.J. Powell. 2014. CD137 Accurately Identifies and Enriches for Naturally Occurring Tumor-Reactive T Cells in Tumor. *Clin Cancer Res*. 20:44 LP-55.

Yi, J.S., N. Ready, P. Healy, C. Dumbauld, R. Osborne, M. Berry, D. Shoemaker, J. Clarke, J. Crawford, B. Tong, D. Harpole, T.A. D'Amico, F. McSherry, F. Dunphy, S.J. McCall, J.D. Christensen, X. Wang, and K.J. Weinhold. 2017. Immune activation in early-stage non–small cell lung cancer patients receiving neoadjuvant chemotherapy plus ipilimumab. *Clin Cancer Res*. 23:7474–7482. doi:10.1158/1078-0432.CCR-17-2005.

Yokouchi, H., K. Yamazaki, K. Chamoto, E. Kikuchi, N. Shinagawa, S. Oizumi, F. Hommura, T. Nishimura, and M. Nishimura. 2008. Anti-OX40 monoclonal antibody therapy in combination with radiotherapy results in therapeutic antitumor immunity to murine lung cancer. *Cancer Sci*. 99:361–367. doi:10.1111/j.1349-7006.2007.00664.x.

Yu, N., S. Fu, Z. Xu, Y. Liu, J. Hao, A. Zhang, and B. Wang. 2015. Synergistic antitumor responses by combined GITR activation and sunitinib in metastatic renal cell carcinoma. *Int J Cancer*. 138:451–462. doi:10.1002/ijc.29713.

Yu, X., K. Harden, L. C Gonzalez, M. Francesco, E. Chiang, B. Irving, I. Tom, S. Ivelja, C.J. Refino, H. Clark, D. Eaton, and J.L. Grogan. 2008. The surface protein TIGIT suppresses T cell activation by promoting the generation of mature immunoregulatory dendritic cells. *Nat Immunol*. 10:48.

Zappa, C., and S.A. Mousa. 2016. Non-small cell lung cancer: current treatment and future advances. *Transl Lung Cancer Res*. 5:288–300. doi:10.21037/tlcr.2016.06.07.

Zhang, L., J.R. Conejo-Garcia, D. Katsaros, P.A. Gimotty, M. Massobrio, G. Regnani, A. Makrigiannakis, H. Gray, K. Schlienger, M.N. Liebman, S.C. Rubin, and G. Coukos. 2003. Intratumoral T Cells, Recurrence, and Survival in Epithelial Ovarian Cancer. *N Engl J Med*. 348:203–213. doi:10.1056/NEJMoa020177.

Zhang, P., F. Gao, Q. Wang, X. Wang, F. Zhu, C. Ma, W. Sun, and L. Zhang. 2007. Agonistic Anti-4-1BB Antibody Promotes the Expansion of Natural Regulatory T Cells While Maintaining Foxp3 Expression. *Scand J Immunol*. 66:435–440. doi:10.1111/j.1365-3083.2007.01994.x.

Zhang, Q., J. Bi, X. Zheng, Y. Chen, H. Wang, W. Wu, Z. Wang, Q. Wu, H. Peng, H. Wei, R. Sun, and Z. Tian. 2018. Blockade of the checkpoint receptor TIGIT prevents NK cell exhaustion and elicits potent anti-tumor immunity. *Nat Immunol*. 19:723–732. doi:10.1038/s41590-018-0132-0.

Zhang, Y., Y. Luo, S.L. Qin, Y.F. Mu, Y. Qi, M.H. Yu, and M. Zhong. 2016. The clinical impact of ICOS signal in colorectal cancer patients. *Oncoimmunology*. 5:1–9. doi:10.1080/2162402X.2016.1141857.

Zhou, E., Q. Huang, J. Wang, C. Fang, L. Yang, M. Zhu, J. Chen, L. Chen, and M. Dong. 2015.

Up-regulation of Tim-3 is associated with poor prognosis of patients with colon cancer. *Int J Clin Exp Pathol*. 8:8018–8027.

Zhou, P., L. L'italien, D. Hodges, and X.M. Schebye. 2007. Pivotal Roles of CD4+ Effector T cells in Mediating Agonistic Anti-GITR mAb-Induced-Immune Activation and Tumor Immunity in CT26 Tumors. *J Immunol*. 179:7365–7375. doi:10.4049/jimmunol.179.11.7365.

Zhou, P., J. Qiu, L. L'Italien, D. Gu, D. Hodges, C.-C. Chao, and X.M. Schebye. 2010. Mature B Cells Are Critical to T-cell-mediated Tumor Immunity Induced by an Agonist Anti-GITR Monoclonal Antibody. *J Immunother*. 33.

Zhu, C., A.C. Anderson, A. Schubart, H. Xiong, J. Imitola, S.J. Khoury, X.X. Zheng, T.B. Strom, and V.K. Kuchroo. 2005. The Tim-3 ligand galectin-9 negatively regulates T helper type 1 immunity. *Nat Immunol*. 6:1245.

Zhu, L.X., M. Davoodi, M.K. Srivastava, P. Kachroo, J.M. Lee, M. St. John, M. Harris-White, M. Huang, R.M. Strieter, S. Dubinett, and S. Sharma. 2015. GITR agonist enhances vaccination responses in lung cancer. *Oncoimmunology*. 4:e992237. doi:10.4161/2162402X.2014.992237.

Zhuang, X., X. Xia, C. Wang, F. Gao, N. Shan, L. Zhang, and L. Zhang. 2010. A High Number of CD8+ T Cells Infiltrated in NSCLC Tissues is Associated With a Favorable Prognosis. *Appl Immunohistochem Mol Morphol*. 18.

7 Annex

7.1 Supplementary figures

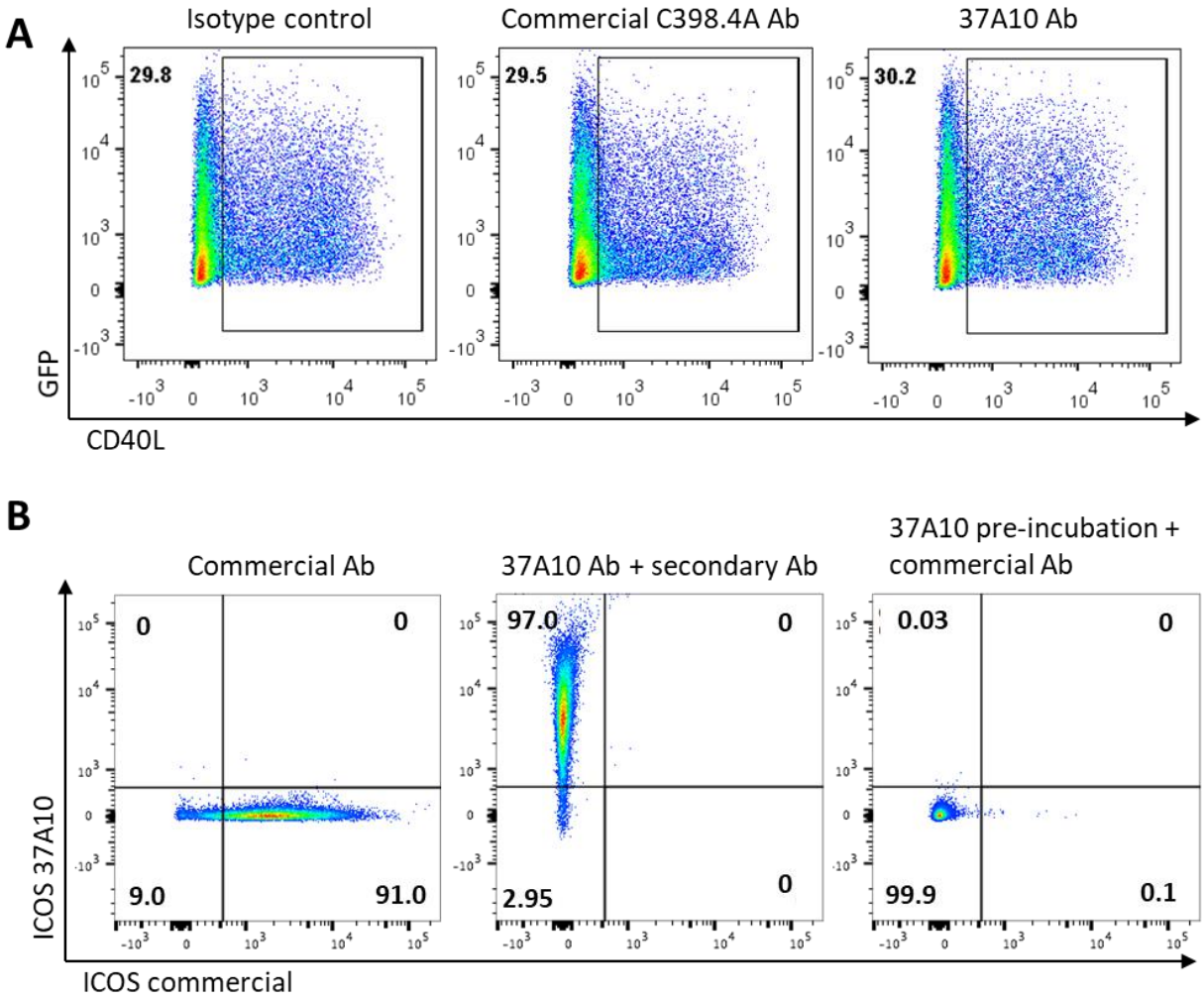

7.1 Supplementary figure 7.1. Anti-ICOS 3710 mAb is cross-reactive and blocks the binding of the anti-ICOS staining mAb.

(A) Jurkat-NFAT.GFP/mICOS cells were activated with plate-bound 250 ng of anti-CD3 clone OKT3 mAb with either 20 µg/mL of soluble isotype control, anti-ICOS (clone C398.4A) mAb or anti-ICOS (clone 37A10) mAb. After 72 hours, cells were stained and the levels of CD40L were measured by flow cytometry. **(B)** Activated PBMC were stained with a commercial (clone C398.4A) mAb or the tested (clone 37A10) anti-ICOS antibody to check the binding of the 37A10 clone to human ICOS. Some PBMC were pre-incubated with the tested (clone 37A10) anti-ICOS antibody, washed and stained with the commercial anti-ICOS (clone C398.4A) mAb, to check blocking of both antibodies.

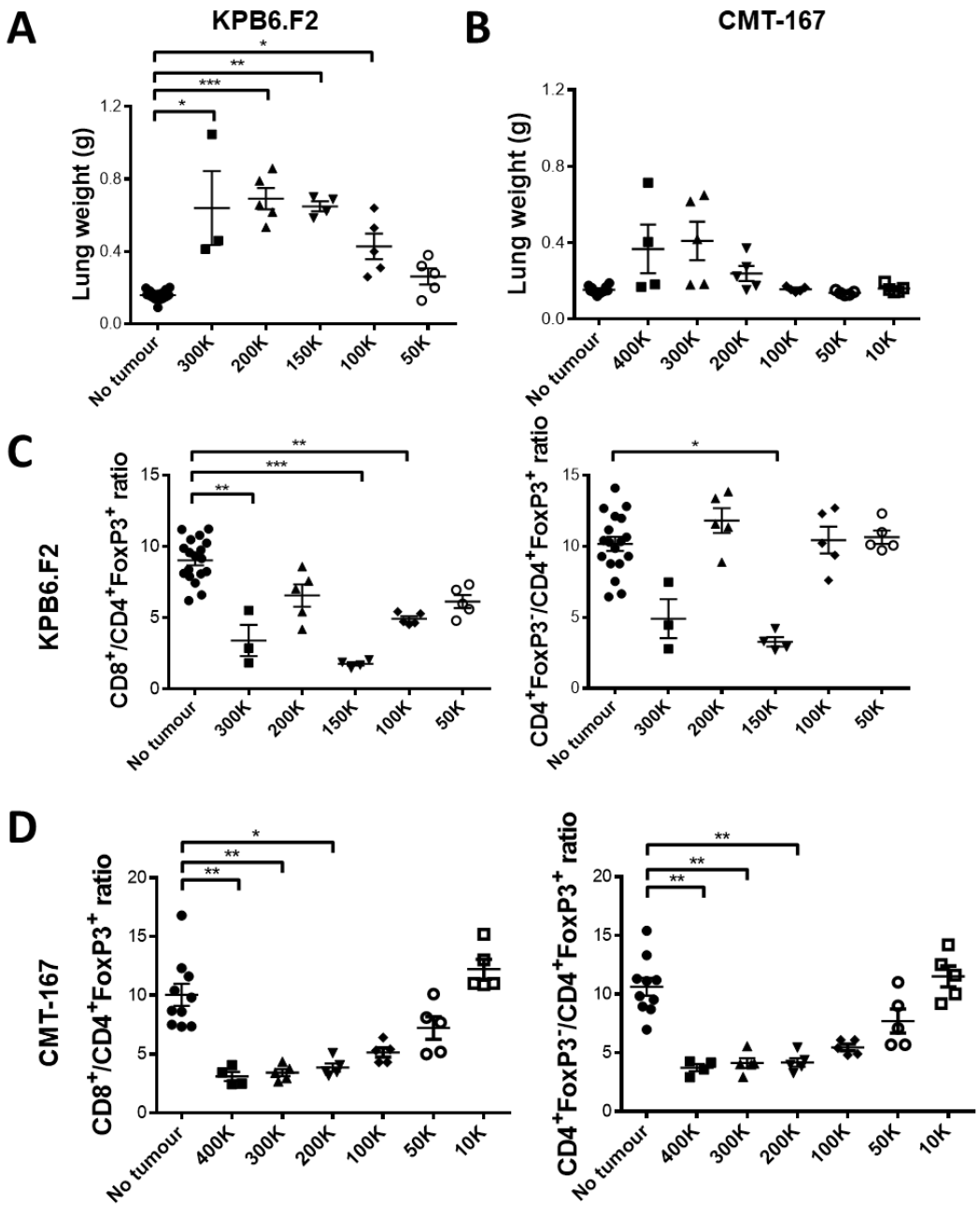

7.2. Supplementary figure 7.2. Titration of the number of KPB6.F2 cells injected into mice to generate lung tumours.

C57BL/6 mice were left untreated or injected intravenously with increasing numbers of KPB6.F2 or CMT-167 cells. At day 21 mice were euthanized and lungs were recovered. Lungs were processed and a single cell suspension was stained and analysed by flow cytometry. **(A)** Lung weight for KPB6.F2-tumour bearing lungs. **(B)** Lung weight for CMT167-tumour bearing lungs. **(C and D)** $CD8^+$/Treg and $CD4^+$effector/Treg ratios for **(C)** KPB6.F2 tumours and **(D)** CMT-167 tumours. Horizontal bars represent the mean, errors bars shown ± standard error of the mean (SEM). p values were calculated using non-parametrical analysis Kruskal-Wallis test. ns = $p > 0.05$, *$p \leq 0.05$, **$p \leq 0.01$, ***$p \leq 0.001$, **** $P \leq 0.0001$.

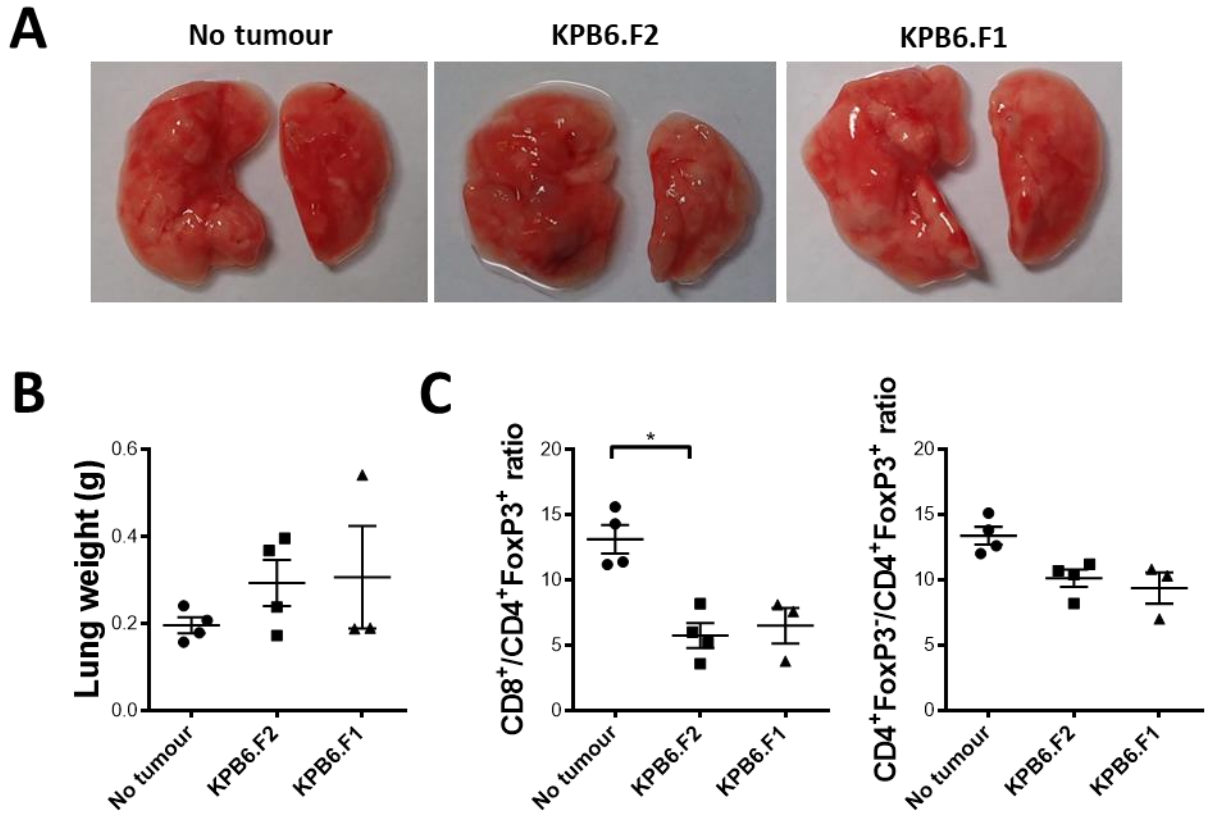

7.3. Supplementary figure 7.3. Mice injected with KPB6.F2 or KPB6.F1 cell line had similar features regarding visible tumour nodules, weight of lungs and $CD8^+$/Treg and Teff/Treg ratios.

C57BL/6 mice were left untreated or injected intravenously with 50,000 cells from either KPB6.F2 or KPB6.F1 cells. After 21 days lungs were recovered for analysis. **(A)** Representative picture of lungs for each condition. **(B)** Lung weight. **(C)** $CD8^+$/Treg and $CD4^+$ effector/Treg ratios. Horizontal bars represent the mean, errors bars shown ± standard error of the mean (SEM). p values were calculated using non-parametrical analysis Kruskal-Wallis test. ns = $p > 0.05$, *$p \leq 0.05$, **$p \leq 0.01$, ***$p \leq 0.001$, **** $P \leq 0.0001$.

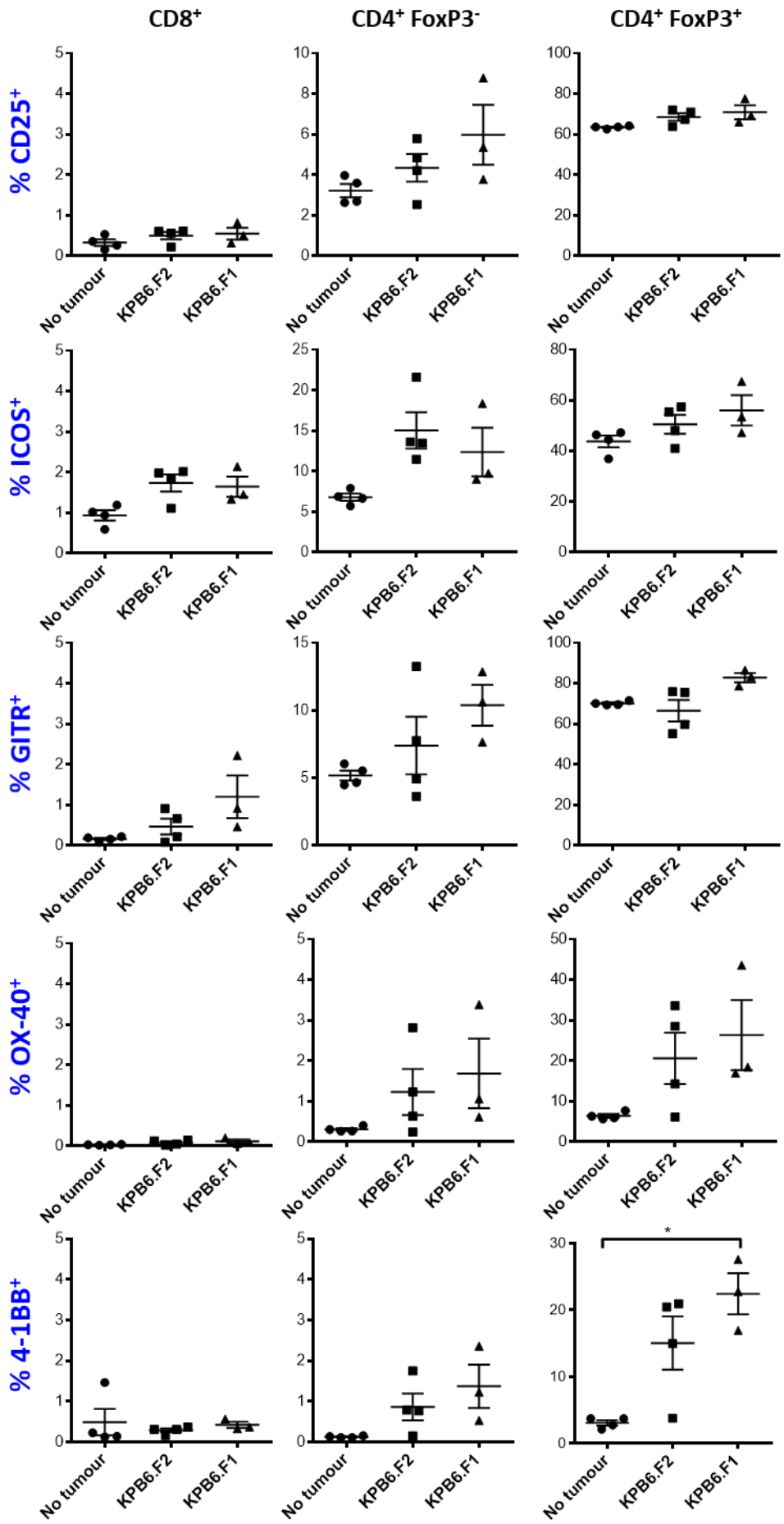
CD8+
CD4+ FoxP3-
CD4+ FoxP3+
% CD25+
% ICOS+
% GITR+
% OX-40+
% 4-1BB+
No tumour
KPB6.F2
KPB6.F1
*

7.4. Supplementary figure 7.4. Mice injected with KPB6.F2 or KPB6.F1 cell line had similar frequency of expression of co-stimulatory molecules.

C57BL/6 mice were left untreated or injected intravenously with 50,000 cells from either KPB6.F2 or KPB6.F1 cell lines. At day 21 mice were euthanised, lungs were recovered, and a single cell suspension was stained and analysed by flow cytometry. Graphs summarising the frequency from regulatory T-cells ($CD4^+FoxP3^+$), effector $CD4^+$ ($CD4^+FoxP3^-$), and $CD8^+$ T-cells was determined for CD25, GITR, ICOS, OX-40 and 4-1BB. Horizontal bars represent the mean, errors bars shown ± standard error of the mean (SEM). p values were calculated using non-parametrical analysis Kruskal-Wallis test. ns = $p > 0.05$, *$p \leq 0.05$, **$p \leq 0.01$, ***$p \leq 0.001$, **** $P \leq 0.0001$.

7.5.

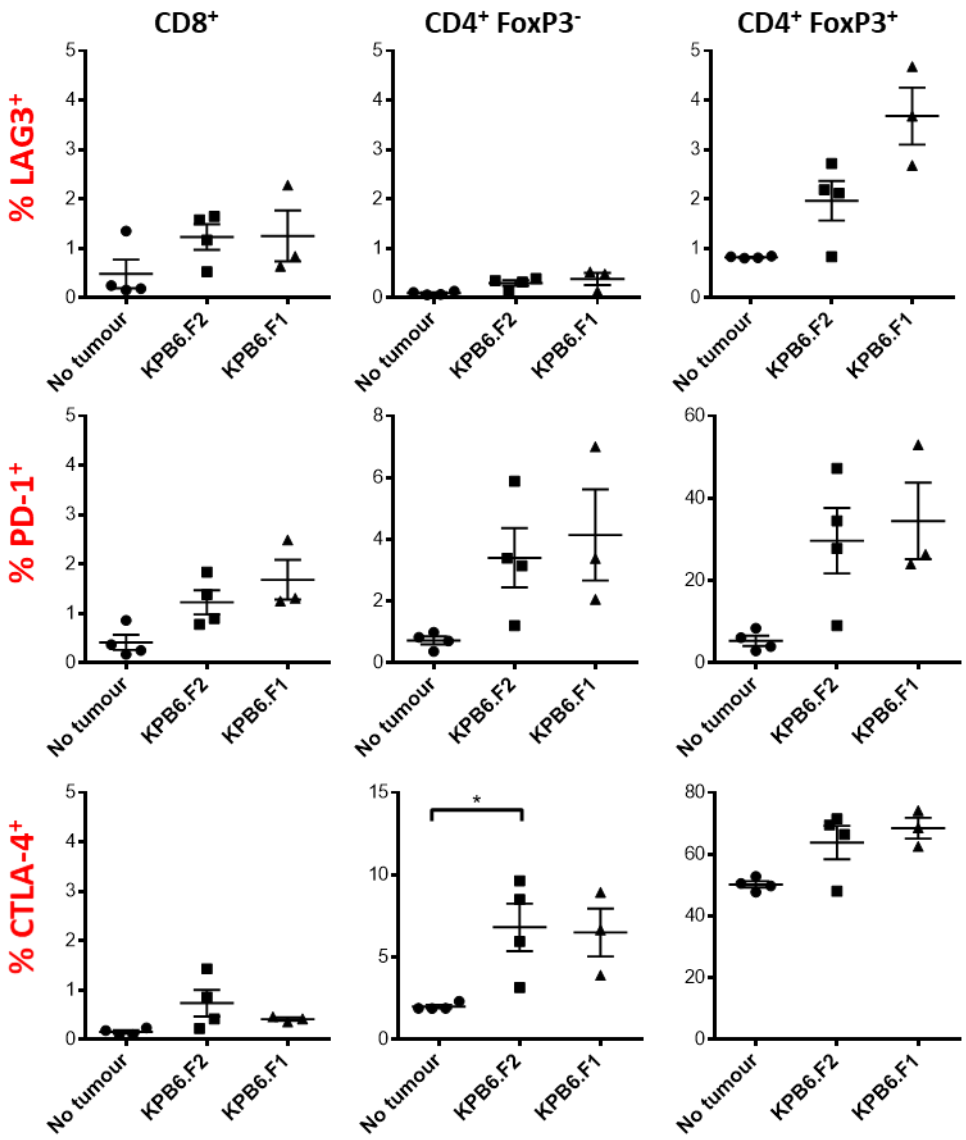

Supplementary figure 7.5. Mice injected with KPB6.F2 or KPB6.F1 cell line had similar frequency of expression of co-inhibitory molecules.

C57BL/6 mice were left untreated or injected intravenously with 50,000 cells from either KPB6.F2 or KPB6.F1 cell lines. At day 21 mice were euthanised, lungs were recovered, and a single cell suspension was stained and analysed by flow cytometry. Graphs summarising the frequency from regulatory T-cells ($CD4^+FoxP3^+$), effector $CD4^+$ ($CD4^+FoxP3^-$), and $CD8^+$ T-cells was determined for LAG3, PD-1 and CTLA-4. Horizontal bars represent the mean, errors bars shown ± standard error of the mean (SEM). p values were calculated using non-parametrical analysis Kruskal-Wallis test. ns = $p > 0.05$, *$p \leq 0.05$, **$p \leq 0.01$, ***$p \leq 0.001$, **** $P \leq 0.0001$.

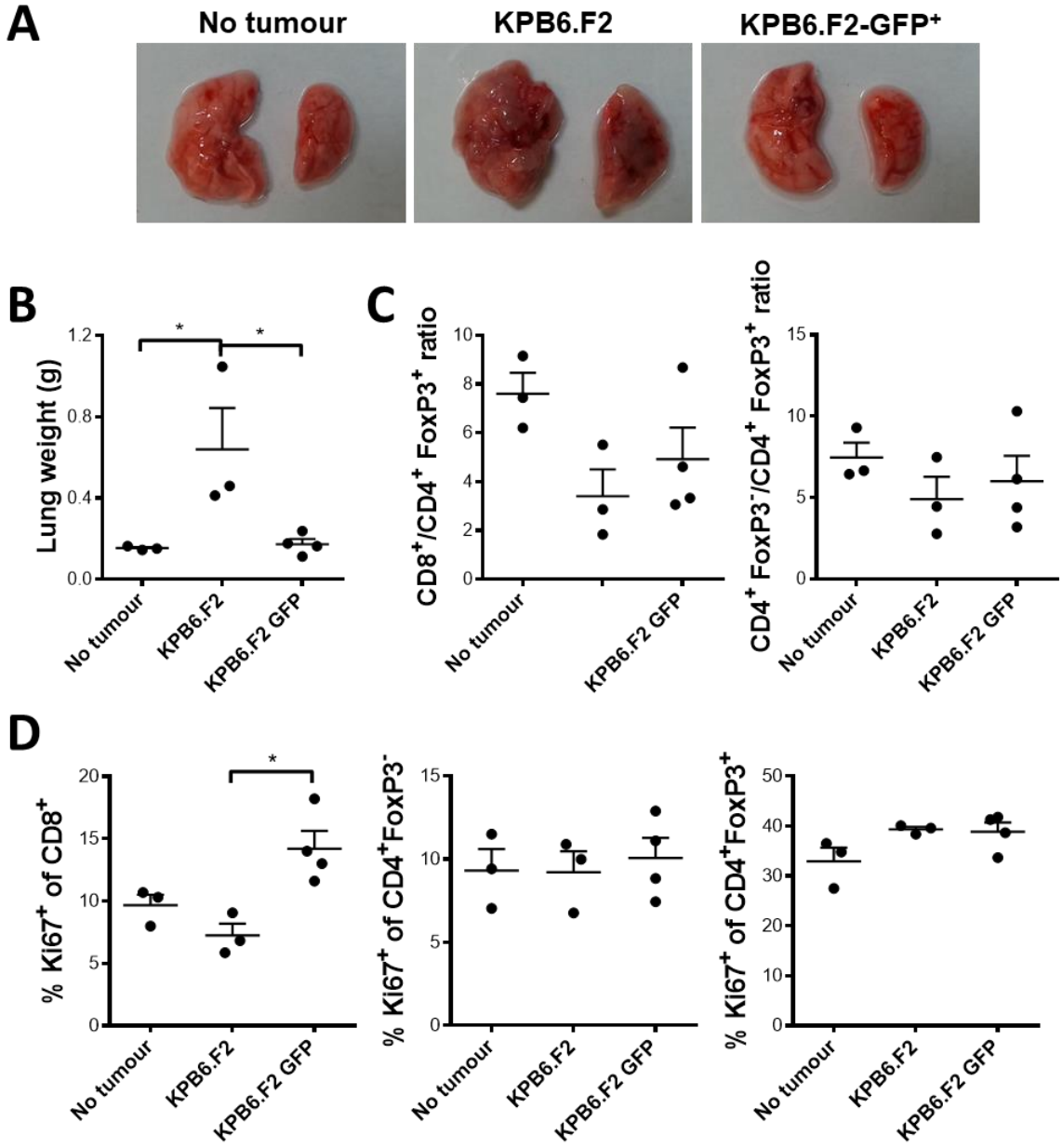

7.6. Supplementary figure 7.6. Mice injected with KPB6F2.GFP$^+$ did not develop visible tumour nodules.

C57BL/6 mice were left untreated or injected intravenously with either 300,000 KPB6.F2 cells or 300,00 KPB6.F2-GFP$^+$ cells. At day 21 mice were euthanized and lungs were recovered. Lungs were processed and a single cell suspension was stained and analysed by flow cytometry. **(A)** Representative picture of lung for each group. **(B)** Lung weight. **(C)** CD8$^+$/Treg and CD4$^+$effector/Treg ratios. **(D)** Percentage of Ki67$^+$ cells gated on CD8$^+$, CD4$^+$ FoxP3$^-$ effectors T-cells and CD4$^+$ FoxP3$^+$ Treg cells, respectively. Horizontal bars represent the mean, errors bars shown ± standard error of the mean (SEM). p values were calculated using non-parametrical analysis Kruskal-Wallis test. ns = $p > 0.05$, *$p \leq 0.05$, **$p \leq 0.01$, ***$p \leq 0.001$, **** $P \leq 0.0001$.

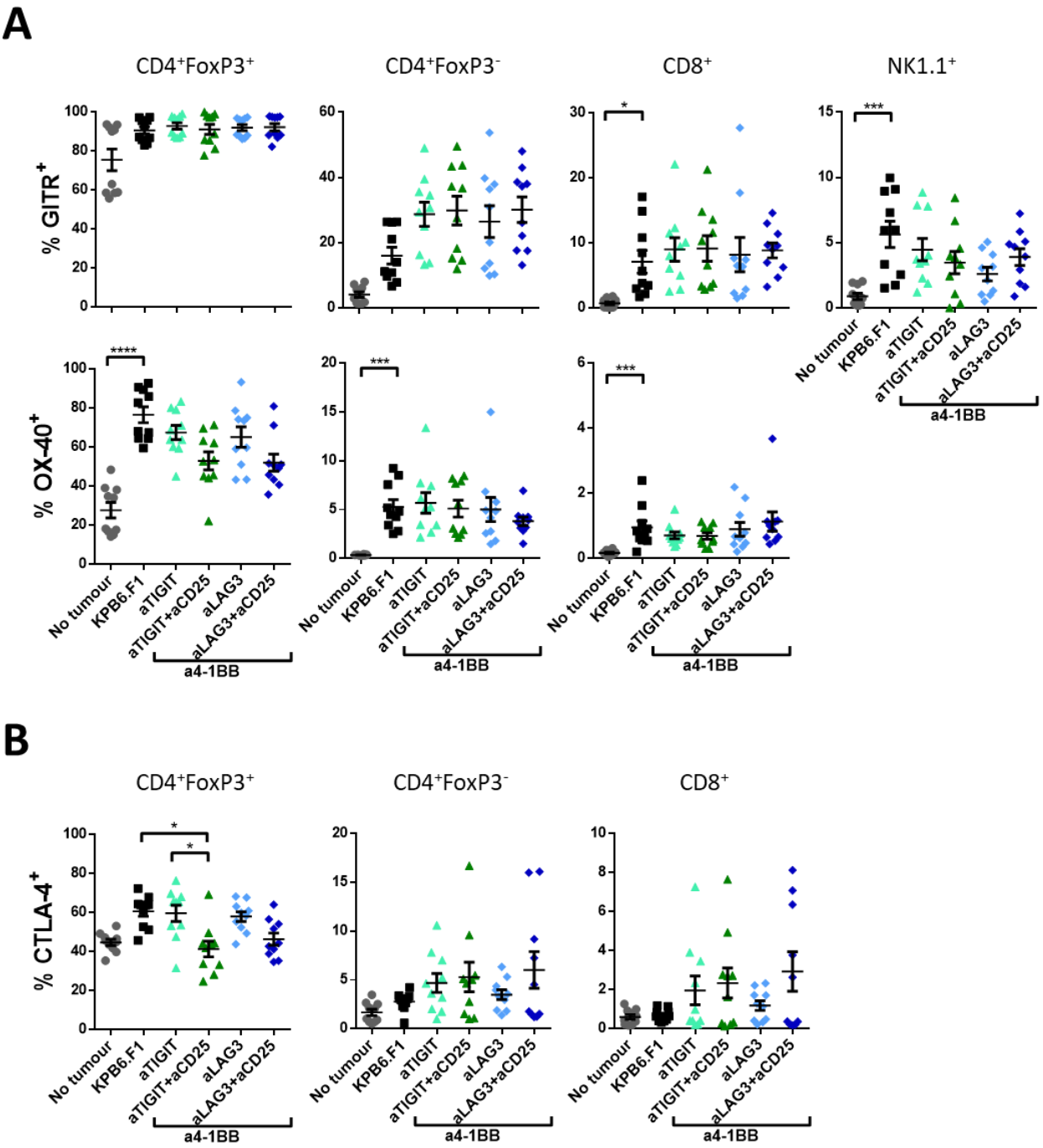

7.7. Supplementary figure 7.7. Combination therapy with anti-4-1BB mAb and anti-TIGIT mAb or anti-LAG3 mAb does not modify the frequency of expression of the immuno-modulatory molecules GITR, OX-40 and CTLA-4 on T-cells from tumour-bearing lungs.

C57BL/6 mice were left untreated or injected intravenously with KPB6.F1 cells. Six days after some mice received one dose of 200 µg of anti-CD25 mAb (clone PC61, mouse IgG2a) and later mice were treated concomitantly with 100 µg of anti-4-1BB mAb (clone LOB12.3 rat IgG1) plus 200 µg anti-TIGIT mAb (clone 1G9, mouse IgG1) or 200 µg anti-LAG3 mAb (clone C9B7W, rat IgG1) on days 7, 10 and 13. At day 17 mice were euthanized and lungs were

recovered. Lungs were processed, and a single cell suspension was stained and analysed by flow cytometry. Graphs featuring the frequency from regulatory T-cells ($CD4^+FoxP3^+$), effector $CD4^+$ T-cells ($CD4^+FoxP3^-$), $CD8^+$ T-cells and NK cells was determined for **(A)** the co-stimulatory molecules GITR and OX-40 and **(B)** the co-inhibitory checkpoint CTLA-4 are shown. Horizontal bars represent the mean, errors bars shown ± standard error of the mean (SEM). p values were calculated using non-parametrical analysis Kruskal-Wallis test. ns = $p > 0.05$, *$p \leq 0.05$, **$p \leq 0.01$, ***$p \leq 0.001$, **** $P \leq 0.0001$.

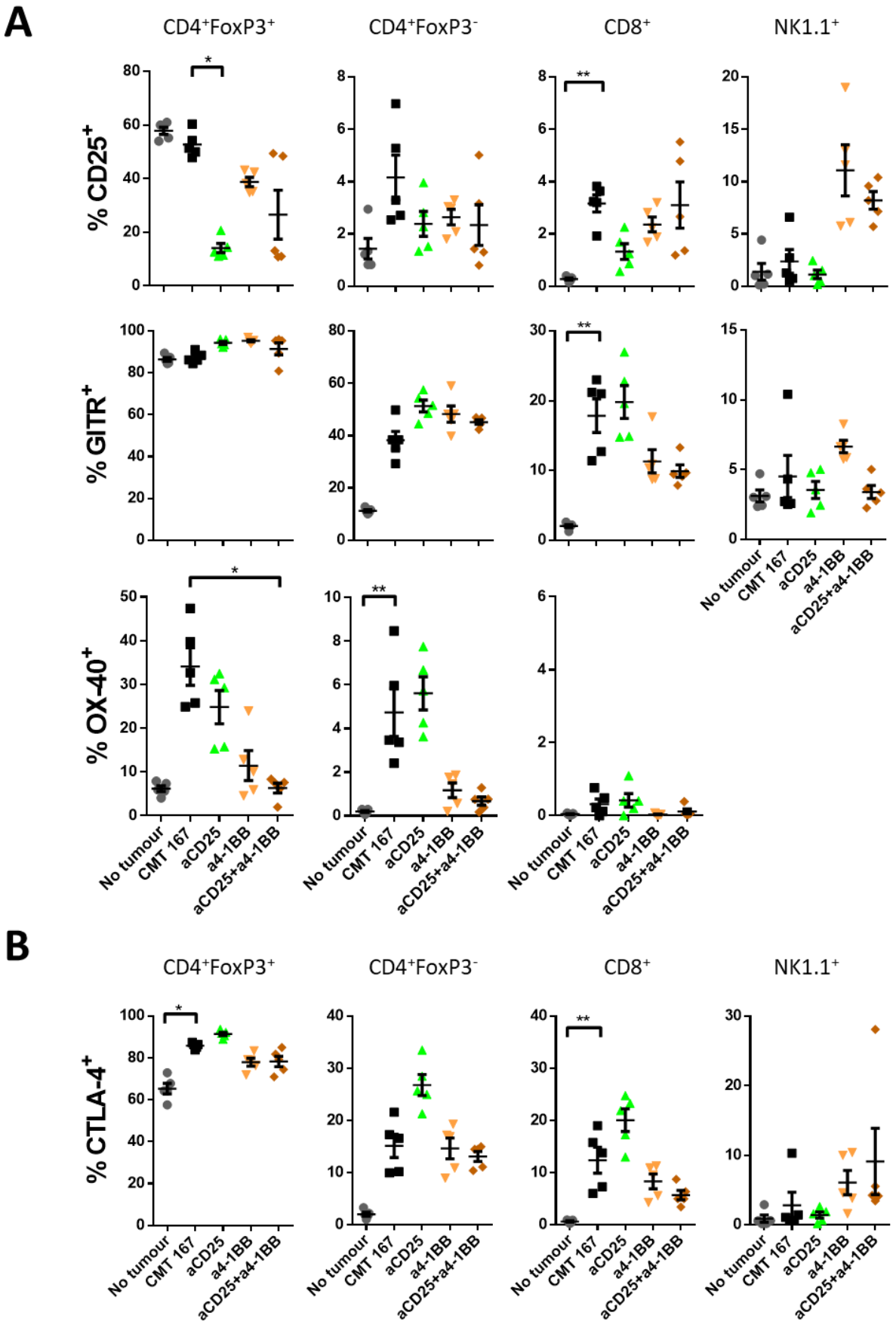
A
CD4+FoxP3+
CD4+FoxP3-
CD8+
NK1.1+
% CD25+
% GITR+
% OX-40+
No tumour
CMT 167
aCD25
a4-1BB
aCD25+a4-1BB
B
CD4+FoxP3+
CD4+FoxP3-
CD8+
NK1.1+
% CTLA-4+
No tumour
CMT 167
aCD25
a4-1BB
aCD25+a4-1BB

7.8. Supplementary figure 7.8. No changes in the frequency of expression of the modulatory proteins CD25, GITR, OX-40 and CTLA-4 by anti-4-1BB mAb treatment in the CMT-167 model of lung cancer.

C57BL/6 mice were left untreated or injected intravenously with CMT-167 cells. Five days after some mice received one dose of 200 µg of anti-CD25 mAb (TUSKC22, mouse IgG2a) and later mice were treated with 50 µg of anti-4-1BB mAb (clone 3H3 mouse IgG1) on days 6, 9 and 12. At day 19 mice were euthanized and lungs were recovered. Lungs were processed, and a single cell suspension was stained and analysed by flow cytometry. Graphs indicating the frequency of the **(A)** co-stimulatory molecules CD25, GITR and OX-40 and **(B)** the co-inhibitory checkpoint CTLA-4 expressed on regulatory T-cells, $CD4^+$ effector, $CD8^+$ T-cells and NK cells are shown. Horizontal bars represent the mean, errors bars shown ± standard error of the mean (SEM). p values were calculated using non-parametrical analysis Kruskal-Wallis test. ns = $p > 0.05$, *$p \leq 0.05$, **$p \leq 0.01$, ***$p \leq 0.001$, **** $P \leq 0.0001$.